IMAGE ANALYSIS OF AIR VOIDS IN AIR-ENTRAINED CONCRETE

BY

GEORGE R. DEWEY

DAVID DARWIN

A Report on Research Sponsored by
AXIM Concrete Technologies, Inc.
(formerly Solvay Construction Materials, Inc.)

UNIVERSITY OF KANSAS
LAWRENCE, KANSAS
AUGUST 1991

ABSTRACT

The application of image analysis techniques to characterize the air-void system in hardened concrete is demonstrated. Both lineal and areal feature analyses are investigated. Feature size distributions and total air contents are obtained using both types of analysis. The areal analyses also include the measurement of individual feature perimeters for use in comparing void shapes. A two phase standard specimen is developed to insure the consistency of measurements and repeatability of results.

Correction methods, based on geometric probability, are developed to remove the distortions in the image analysis data resulting from frame edge effects. Separate methods are presented for lineal and areal analyses. Using discrete class sizes, both correction procedures are expressed in a matrix format. The corrected areal feature distributions are used to obtain volume distributions of spherical air voids using standard stereological procedures.

The procedures are applied to ten concrete specimens, at magnifications of 12x and 30x. The specimens represent concretes made using three different air-entraining admixtures, as well as non-air entrained concrete. Air-void parameters calculated from corrected image analysis results for the ten specimens are compared to results obtained using the modified point count method and to freeze-thaw results obtained from surface scaling tests of companion specimens. The differences in the air-void systems created by the various air-entraining agents are studied by comparing different characteristics including: the Powers spacing factor, the Philleo factor, profile shape, average feature size, numerical density of features, and the cumulative percent of total air versus feature size.

The study demonstrates that image analysis provides a viable alternative to traditional lineal traverse and modified point count methods for characterization of air-void systems in hardened concrete and, in the process, provides significant detail not available with the traditional methods. The study indicates that air-entraining agents produce characteristic air void distributions. Comparisons made in the study show that lineal and areal image analysis techniques provide similar determinations of total air content that are, on average, 1.15 volume percent lower than those obtained from a modified point count analysis. Application of the frame edge effect correction procedures to the lineal data results in an average decrease in the total chord density of 2.3% and 5.0% for magnifications of 12x and 30x, respectively. Application of the frame edge effect correction procedures to the areal data results in an average decrease in the total profile density of 3.3% and 5.9% for magnifications of 12x and 30x, respectively. The accuracy of the analysis decreases if size classes are much greater than 30 μm. Accurate lineal analyses require the class size to be an exact increment of pixel length. A similar requirement does not apply to areal analyses.

ACKNOWLEDGMENTS

This report is based on a thesis presented by George R. Dewey in partial fulfillment of the requirements for the Ph.D. degree. The research was supported by AXIM Concrete Technologies, Inc., formerly Solvay Construction Materials, Inc. Additional support was provided by the University of Kansas Center for Research, Inc. and the Department of Civil Engineering.

Donald R. Lane, President of AXIM Concrete Technologies, Inc., supervised preparation of the concrete test samples described in this report. Professional Services Industries performed manual modified point count analyses of the samples.

Image analyses were performed in the School of Engineering Microanalysis Laboratory. The numerical calculations were performed on Apollo work stations in the Microanalysis Laboratory and in the Civil Engineering Graduate Graphics and Computer Applications Laboratory.

TABLE OF CONTENTS

TABLE OF CONTENTS (continued)

LIST OF TABLES

LIST OF TABLES (continued)

LIST OF TABLES (continued)

LIST OF TABLES (continued)

LIST OF TABLES (continued)

LIST OF TABLES (continued)

LIST OF TABLES (continued)

LIST OF FIGURES

LIST OF FIGURES (continued)

LIST OF FIGURES (continued)

LIST OF FIGURES (continued)

LIST OF FIGURES (continued)

CHAPTER 1

INTRODUCTION

1.1 General

When moist concrete is exposed to alternating cycles of freezing and thawing, internal deterioration can result. This accumulated damage is referred to as freeze-thaw or frost damage. Common examples of concrete routinely exposed to these freezing hazards include: highway pavements, airport runways, dam spillways, sidewalks, foundation walls, and bridge decks.

Perhaps the most profound discovery concerning the resistance of concrete to freeze-thaw damage was that the entrainment of microscopic air voids can vastly improve resistance to such damage. As early as the 1930's, deliberate efforts were made to take advantage of this beneficial use of entrained air (Lawton 1939). Today it is common practice (ACI Committee 201 1977) to intentionally entrain air in concrete that is expected to be subjected to freezing temperatures in the presence of moisture.

In his pioneering efforts to understand the freeze-thaw damage phenomenon, Powers (1945, 1949) proposed a method to quantify the effectiveness of entrained air. He found that the spacing between air-voids, rather than the total volume of entrained air, was the better measure of resistance to freeze-thaw damage. Powers proposed the use of a measure of the average spacing between air voids to determine the extent of frost protection. He developed an expression, now known as the Powers spacing factor, to measure expected freeze-thaw performance. While the Powers spacing factor is not considered to be a truly definitive measure of frost performan-

ce, it is still used as the standard method for quantifying the distribution of entrained air in concrete. Other measures for characterizing entrained air have been proposed, but none have been adopted for general use.

Current techniques for measuring air-void parameters (ASTM C 457-82a) include the examination of polished sections of hardened concrete. The most common technique is the linear traverse method which measures the chord intercepts of air voids. Typical information obtained from a linear traverse analysis includes an average chord intercept length and the number of voids intercepted per unit length of traverse. From this information, the volume percent of air and the Powers spacing factor can be determined. Proposed improvements to this method have included the tabulation of the individual chord lengths to obtain a measure of the size distribution of air-voids. Numerous efforts have also been directed towards automating the linear traverse method.

Since 1977, computer-based image analysis methods have been used to measure air-void chord lengths (Chatterji and Gundmundsson 1977, Houde and Meilleur 1983, Roberts and Scali 1984, MacInnis and Racic 1986). Reasonably good correlation with linear traverse results has been reported. However, typical image analysis techniques underestimate the average chord length and overestimate the number of chords per unit length compared to results obtained using a continuous traverse. This is because some of the chords are truncated by the edges of the finite fields of view, yielding measured lengths that are smaller than the true lengths and an apparent increase in the number of chords per unit length. As a result of this frame edge effect, the calculated value of the spacing factor is reduced and chord length size distributions are skewed toward the smaller sizes. The magnitude of the

frame edge effect is dependent on the size of the discrete frames used, and hence the magnification.

The purpose of the present study is to demonstrate the use of image analysis techniques to measure air-void profiles on polished sections of hardened concrete. Both area equivalent diameters and chord lengths are measured to determine feature size distributions. The results are corrected for frame edge effects using geometric probability. Stereological methods are used to obtain volume size distributions of air voids from the corrected profile size distributions. The results obtained from the proposed techniques are compared with results from traditional analyses.

1.2 Background

To fully understand the role of entrained air voids in providing resistance to freeze-thaw damage, it is important to understand the mechanisms of such damage. The susceptibility of aggregates to frost damage is a separate issue and is not dealt with here.

Frost damage in concrete is considered to result from excess internal pressures resulting from the freezing action of water (Powers 1975). The magnitude of these internal pressures is dependent on the concrete pore structure, moisture content, and rate of freezing. The temperature at which water will freeze is a function of the size of the pore in which it is contained. The smaller the pore size, the lower the temperature required to cause freezing. Cement paste can be protected from damage due to freezing by keeping the internal pore sizes small enough such that freezing will not occur at expected winter temperatures. This is theoretically possible by eliminating the capillary pores. Frost protection can also be achieved by providing an adequate volume and dispersion of entrained air voids.

Pore Structures.– It is generally agreed (Verbeck 1978, Neville 1981, Philleo 1987) that the pore structures in the cement-paste phase of concrete can be classified into three distinct groups: cement gel pores, capillary pores, and air voids. The first two, gel and capillary pores, are initially filled with water. As hydration proceeds, the quantity of hydrated gel increases, expanding into the capillary pore space. At any time during the hydration process, that part of the initial water-filled space not occupied by hydration products is referred to as the capillary pore space. For water/cement ratios (w/c) below about 0.35 by weight, the initial water-filled spaces are small enough so that the hydration products could eventually completely fill them, essentially eliminating the capillary pores. At a w/c above about 0.7, even after complete hydration, an interconnected system of capillary pores will remain. For w/c between 0.35 and 0.7, the resulting network of randomly distributed capillary pore spaces will remain interconnected only through the cement gel pores.

Cement gel is about 28 percent void space by volume (Neville 1981). The size of the interstitial gel pores is believed to be on the order of 2.0×10^{-3} μm (Powers and Brownyard 1947). Their small size is such that water will not freeze in them above –78°C, well below normally expected winter temperatures. The size of the capillary pores is believed (Verbeck 1978) to range from 1.0 μm down to 0.1 μm, depending on the w/c and the degree of hydration. The capillary pores are large enough so that water can freeze in them at or just below 0°C. Thus, the capillary pores represent an important element in determining a concrete's vulnerability to freeze-thaw damage. If the capillary pores could be eliminated, the vulnerability of concrete to frost damage would be greatly reduced. Research efforts with high

strength concretes have been directed toward this objective (Philleo 1987).

By far the largest elements of the pore structure are the air voids. They are generally classified into two groups, intentionally entrained and unintentionally entrapped. The entrained air-voids result from the addition of admixtures that are specifically designed to produce large quantities of microscopic air bubbles when mixed into fresh concrete. Numbers of entrained air-voids range up to tens of billions of bubbles per cubic yard of concrete, depending on the particular air-entraining agent used. The size of entrained air voids ranges from about 10 μm to over 1 mm. Entrapped air-voids are present, to some extent, in all concrete and are due to incomplete consolidation. Entrapped air-voids can range in size from microscopic spaces to honeycombing, often seen in poorly consolidated concrete. While it is virtually impossible to make a clear distinction between entrained and entrapped air-voids, quite often (ASTM C 125-88) voids larger than 1.0 mm in diameter, and irregular in shape, are labeled as entrapped. These larger air-voids contribute significantly to the total air content of concrete, but their contribution to frost resistance is negligible.

Frost Mechanism.– Internal pressures in concrete arising from freezing are considered to be the result of two separate phenomena. In his early efforts to understand freeze-thaw action in concrete, Powers (1945) attributed freeze-thaw damage to excessive hydraulic pressures resulting from the expansion of ice. More recent theories (Powers 1975) consider osmotic potential to be the primary cause of excess pressure.

The temperature at which water will freeze in concrete is a function of the alkali concentration as well as pore size. Freezing will only occur when the

temperature becomes low enough to allow ice formation at the existing alkali concentration.

Because of their relatively large size, air voids become the initial freezing sites. As the solution freezes, only pure water forms the ice. Thus, the remaining unfrozen liquid at the freezing sites becomes a more concentrated alkaline solution. The less concentrated alkaline solution in the surrounding paste is then drawn to the freezing sites in an effort to maintain thermodynamic equilibrium. The driving force for the movement of this solution is a function of the alkali concentration gradient. As the unfrozen solution at the freezing sites is diluted, by the infusion of surrounding water, additional ice growth occurs. This progressive ice formation can occur at any solute concentration including zero (Powers 1956, 1975) and is referred to as ice-accretion. This process continues until either one of two possible conditions prevail. If there exists adequate air-void space, sufficiently distributed throughout the paste, all of the freezable water will eventually diffuse to the freezing sites inside the air voids and reach a state of equilibrium. This is desirable since the resulting absence of freezable water in the surrounding capillary pore spaces will mean that the paste phase is protected from frost damage. The other possible situation is that the air void space is inadequate to accommodate all of the surrounding unfrozen water. If this occurs, osmotic pressures will result due to the remaining differences in alkali concentrations. Pressures that exceed the tensile strength of the hardened cement paste will naturally cause damage. Also, freezable water will remain in the capillary pores if the air-void space is insufficient to accommodate it or if the rate of temperature drop is too fast to allow all of the water to diffuse to the air voids. This freezable water in the capillary pores is susceptible

to ice crystal growth at low enough temperatures. Excessive hydraulic pressures may then result as unfrozen water is forced through the pore structure due to ice expansion.

1.3 Measures of Frost Resistance

Frost protection is often specified in terms of the total volume of entrained air. However, by itself, the total air content is an unreliable measure of freeze-thaw protection. This is because no information is given about the size and spacing of the individual air voids.

The Powers spacing factor is by far the most widely used measure of air-void dispersion in concrete. Powers (1945) proposed that the distance that freezable water must travel before reaching an air-void will determine the possible level of internal pressure resulting from freezing. He developed two expressions for a spacing factor (Powers 1949) to describe this distance. Both expressions require a determination of the total air-void specific surface (the total bubble surface area per unit volume of air). Willis (1949) demonstrated that the total volume of air voids and their total specific surface can be estimated from the mean air-void intercept or chord length obtained from a linear traverse. Assuming all voids to be spherical and using geometric probability concepts, the total specific surface, α, expressed in terms of the average chord length, $\bar{l}$, was shown to be $\alpha = 4/\bar{l}$. Using similar reasoning, Willis (1951) also developed an expression for the total specific surface from an areal analysis as $\alpha = (16/\pi)(\sum n_i y_i / \sum n_i y_i^2)$.

Powers first spacing factor expression was obtained by simply calculating the volume of cement paste per unit area of air-void surface. This is given as

$$\bar{L} = \frac{P}{\alpha A} \qquad (1.1)$$

in which $\bar{L}$ = spacing factor, in units of length

α = total specific surface of the air voids, in consistent units of length^{-1}

P = paste content, in volume percent of concrete

A = total volume of air voids, in volume percent of concrete

His second expression is based on a hypothetical system of uniformly spaced spherical voids of equal size dispersed throughout the paste phase of concrete. The size of each of these hypothetical voids is determined by setting their specific surface (3/R) equal to the total measured specific surface of the true void system and then solving for the resulting sphere radius, R. By making the total air content of the hypothetical system of voids equal to the measured value of air content, the number of hypothetical voids is then determined.

The cubic packing of this hypothetical void system can be visualized as a system of equal size adjoining cubes of cement paste with an internal air-void located at the center of each. The maximum distance from anywhere in such a system to the nearest surface of an air-void is the distance along the cross diagonal from a cube corner to the enclosed void surface. This distance is equal to one-half of the length of the diagonal minus one-half of the sphere diameter. The Powers spacing factor thus obtained is

$$\bar{L} = (3/\alpha)\left[1.4\left((P/A)+1\right)^{\frac{1}{3}} - 1\right] \qquad (1.2)$$

Powers recognized that neither expression for spacing factor provides a true measure of void spacing. Assuming that both expressions overestimate the true average void spacing, he recommended using the smaller spacing value obtained from the two equations. Eq. 1.1 yields a smaller spacing factor for P/A less than 4.33, and Eq. 1.2 gives the smaller value when P/A is greater than 4.33. A spacing factor of less than 0.008 in. (0.20 mm) has come to be accepted (Mielenz et al. 1958) as desirable for a frost resistant concrete.

There have been numerous freeze-thaw studies (Powers 1954, Backstrom et al. 1954, Klieger 1978) that have shown reasonably good correlation between the Powers spacing factor and freeze-thaw durability. There have also been test results (Larson et al. 1967) that have shown less than desirable or inconsistent correlations.

Lord and Willis (1951) suggested that a spacing factor based on average measures of the true void system may serve better than one based on total specific surface. The actual average void diameter, the diameter of a sphere with the average volume, or the diameter of a sphere with an average specific surface were offered as possible examples. To determine these average void measures, it is necessary to know the volume size distribution of the air voids. They developed a graphical method to determine the volume size distribution based on the measured distribution of void chord lengths obtained from a random traverse. Their method is general in nature and applicable to any random dispersal of spheres. The procedure also provides the number of voids per unit volume.

Larger entrapped air voids often comprise a significant portion of the total volume of internal air, but provide relatively little contribution to frost protection.

This is because the influence of these larger voids is concentrated at discrete locations rather than dispersed throughout the paste. Some researchers have chosen to exclude the larger voids from the calculations of the Powers spacing factor. Ignoring the larger voids, however, can often lead to apparently illogical results. In situations when Eq. 1.2 is used, the Powers spacing factor calculated considering only the smaller entrained voids will usually be smaller than that obtained when the larger voids are included. It does not seem reasonable that the average distance between voids should decrease with the removal of a number of large voids from the system. This anomaly occurs because the increase in the calculated total specific surface $\left(\alpha = 4/\bar{l}\right)$ resulting from ignoring the larger chord lengths exerts a greater influence in Eq. 1.2 than does the resulting decrease in air content.

A spacing factor based on the use of only the smaller entrained air voids was proposed by Walker (1980). Noting that frost protection is primarily provided by the small air voids, he developed an expression for a small void spacing factor.

$$\bar{L}_S = \bar{L} + 3/4\left[(A_T/N_T) - (A_S/N_S)\right] \qquad (1.3)$$

in which $\bar{L}_S$ = small void spacing factor, in units of length

$\bar{L}$ = Powers spacing factor, in units of length

A_T = Total length of traverse across voids, in units of length

N_T = Total number of voids encountered

A_S = Length of traverse across small voids, in units of length

N_S = Number of voids defined as small voids

The chord length used to distinguish small voids is arbitrarily defined. Using 1000 μm to define the break between large and small voids, Walker (1984) subsequently analyzed the freeze-thaw test results of 151 concrete mixes. He found that the small void spacing factor did not provide a better correlation with freeze-thaw performance than did the Powers spacing factor.

A spacing factor that is based only on the total void specific surface and volume, without regard to the true number of voids, cannot be a truly definitive parameter. This is because any number of different air-void size distributions can yield the same calculated spacing factor. The same is also true for any average size measure. Recognizing this, Philleo (1983) developed an expression for the maximum distance to the surface of the nearest air void for a given percentage of the paste. This approach has become known as the protected paste volume concept. To calculate this maximum distance, known as the Philleo factor, it is necessary to know the total volume of air and the number of voids per unit volume. An expression for the Philleo factor is given (Philleo 1983) as

$$S = \left(0.62/N^{\frac{1}{3}}\right)\left[\left(\ln(1/(1-A)) + \ln(1/(1-F))\right)^{\frac{1}{3}} - \left(\ln(1/(1-A))\right)^{\frac{1}{3}}\right] \qquad (1.4)$$

in which S = Maximum distance, from within the protected paste volume, to the edge of an air-void, in units of length

N = Number of air voids per unit volume of paste, in consistent units of length^{-3}

F = Fraction of the paste within the protected volume, in percent volume

A = Air content of the paste, in percent volume

For F = 90 percent, Eq. 1.4 reduces to

$$S = \left(0.62/N_3^{\frac{1}{3}}\right)\left[\left(\ln(1/(1-A)) + 2.303\right)^{\frac{1}{3}} - \left(\ln(1/(1-A))\right)^{\frac{1}{3}}\right] \qquad (1.5)$$

Research by Larson et al. (1967) found that the Philleo spacing factor provides a better correlation to freeze-thaw durability than does the Powers spacing factor.

It is clearly necessary to consider the size distribution of air voids in order to completely characterize the dispersion of air in concrete. Typically, a single distribution summary parameter has been used for this purpose. Powers used the total specific surface to develop his spacing factor and Philleo used the total number of voids per unit volume to calculate his void spacing index. Other researchers have attempted to use the chord distribution curve to represent the air void dispersion.

Larson et al. (1967) used an exponential function to fit the measured chord length distributions. Tests of freeze-thaw durability failed to provide a correlation between their calculated distribution parameters and frost performance.

Roberts and Scheiner (1981) used a logarithmic distribution to describe the measured chord distribution. No efforts were reported on correlating the distribution parameters with frost durability. An interesting finding of their research was that the distribution shape parameters were relatively insensitive to the total air content for the particular entraining agent used in their study. In other research concerning the effects of superplasticizers on the air-void system, MacInnis and Racic (1986) also found similarity between chord distribution shapes in concretes

made with the same air entraining agents but containing significantly different air contents.

Gutmann (1988a, 1988b) studied the characteristics of bubbles produced by different air entraining agents in both water and concrete. He noted differences in the resulting air-void shapes and uniformity of dispersion. He speculated that void shape characteristics, along with the degree of void coalescence, were a function of the air-entraining agents and may affect concrete compressive strength.

1.4 Air Measurement

The air content in plastic concrete is typically measured by either the volumetric method (ASTM C 173-78) or the pressure method (ASTM C 231-89a). A high pressure meter (Amsler et al. 1973) has also been successfully used to determine the total air content in hardened concrete. While these methods do provide a measure of the total volume of internal air, they provide no information about the air void sizes or their dispersion. The volume fraction of air voids in hardened concrete can be estimated from information obtained by microscopic examination of a plane surface. This data can be used to determine air-void sizes and their dispersion.

Stereology.—The general mathematical methods used to extrapolate measurements obtained from two-dimensional surfaces to three-dimensional space is known as stereology (Underwood 1970, Weibel 1979, Russ 1986). Volume fraction estimation is one of the most widely used stereological processes. The fundamental relationships of volume fraction estimation depend upon an equivalence between the volume density and the quantities measured on a plane section. These measured quantities may include area, line, or point fractions. The mathematical derivation of volume fraction relationships is presented by Hillard (1968), and an

interesting presentation of their historical development is given by Chayes (1950).

The French geologist, Delesse, is credited with first proposing (Delesse 1848) that the volume per unit volume, V_V, of a component could be directly estimated by measuring the area per unit area, A_A, of that component on a plane surface. He did this by cutting out and weighing the various components from image tracings. Instead of directly measuring the area percent on a plane surface, the area percent can also be estimated using either a linear intercept or a point counting method. The estimation of the area fraction from a linear intercept fraction was first presented by Rosiwal (1898). A linear traverse analysis is still often referred to as a Rosiwal traverse. The linear intercept fraction of a constituent of interest, L_L, provides a direct estimate of that constituent's area fraction, A_A. The area fraction can also be estimated by use of a point counting technique. A systematic grid system is superimposed on the plane surface, and the constituent falling beneath each grid point is identified. The percentage of points falling on each constituent, P_P, provides an estimate of their area fractions, A_A, or lineal fractions, L_L, depending, respectively, on whether a two-dimensional or one-dimensional point grid is used. Thomson (1930) was the first to introduce this point counting technique with a two-dimensional point grid. Glagolev (1933) applied the technique with a one-dimensional point grid system. The method was greatly facilitated by the development of a practical stage by Chayes (1955) for advancing a specimen beneath a microscope in discrete steps.

The general stereological relationships thus obtained are:

$$P_P = L_L = A_A = V_V \qquad (1.5)$$

All three methods of volume fraction estimation have been applied to the measurement of air voids in hardened concrete. The linear traverse and point counting methods have been developed as standard procedures and are detailed in ASTM C 457-82a.

Areal Traverse.– The areal traverse method of measuring air-void characteristics in hardened concrete was first presented by Verbeck (1947). He used the Camera Lucida Method, whereby a planimeter is used to measure the areas of individual air voids on a projected image of the concrete surface. He presented limited data on the total air content, average air-void area, and intercepted area size distribution. Warren (1953) introduced another plane-intercept method of analysis. He measured the air-void profile diameters directly from enlarged photographic images. Assuming the air voids to be spherical, equations were presented relating the measured profile diameters to the average air-void diameter, total specific surface, and the numerical density of air voids. Because of the tediousness of the areal traverse technique, only limited areas of a specimen could be surveyed. The manual nature of data collection prevented these areal traverse techniques from being adopted for general use.

Linear Traverse.– Rexford (1947) described an apparatus he used for performing a Rosiwal type linear traverse analysis on thin sections of concrete mortar. He used a multiple spindle integrating stage to traverse the specimen beneath the cross hairs of a microscope. Different spindles were allocated to the different constituents of the mortar, i.e., voids, paste, and aggregate. While viewing the specimen through the microscope, the separate spindles were used to advance the specimen across their respective constituent. At the end of a traverse, the calibrated

spindles provide the accumulated total linear intercepts of each constituent. The percentage traversed across each constituent provides a direct measure of their respective volume percentage.

A more versatile linear traverse instrument was developed by Brown and Pierson (1950) which was capable of examining larger concrete specimens. They recorded only the cumulative length traversed across air-void profiles and the total length traversed across aggregate and paste combined. They also used a separate counter to record the total number of void profiles intercepted. From this information, they were able to calculate the Powers spacing factor and the volume percent of air.

The general linear traverse procedure detailed by Brown and Pierson has subsequently served as the basis for standardizing the linear traverse procedure as a means of characterizing entrained air in hardened concrete. Suggested improvements have included tabulating the individual chord lengths for use in obtaining size distributions. The development of automatic recording devices makes the collection of individual chord lengths less tedious and more practical for regular use.

Larson et al. (1967) developed a mechanized linear traverse device in which the individual chord lengths as well as the cumulative percent of each constituent was recorded. They were thus able to estimate the volume percent of aggregate, paste, and air in addition to obtaining a distribution of chord lengths. A computer-based recording system was presented by Roberts and Scheiner (1981). The operator depressed a button while an air-void was being traversed and a magnetic transducer then sensed the distance traversed. The individual chord lengths along with the total traverse length were recorded for future processing.

Point Count.– The point-counting method of measuring air in hardened concrete was introduced by Mather (1950). She described modifications to the Chayes point-counting stage to accommodate larger specimens. In using this procedure, tabulating counters are incremented depending upon which constituent falls beneath the microscope cross hairs at predetermined regular intervals along the traverse. The total air content is the only air-void parameter directly obtained by this method. If the average chord length and Powers spacing factor are to be determined, it is necessary to also record the total length of traverse and the total number of void profiles intercepted by the traverse.

Automated Techniques.– All of the aforementioned linear traverse and point-counting techniques require the equipment operator to actively observe the specimen through a microscope while it is being traversed. Subjective decisions must be made continually with regard to defining the void edges. Also, when the traverse line is tangent to a void profile, a decision must be made as to whether to include it in the count. Automatic void recognition would relieve the operator of these subjective decisions and would presumably increase the accuracy and consistency of measurements.

Browne and Cady (1970) attempted to develop an automated void recognition linear traverse device. The central component of their system was a photomultiplier tube which was used to sense when a void was being traversed. Contrast between air voids and paste was provided by staining the polished concrete surface red with a felt-tip marker and then filling in the voids with hydrated lime. An opaque projector was used to cast a magnified image of the prepared surface onto the photomultiplier tube. Because the voids were lighter in color, they reflected more light onto the photomul-

tiplier tube resulting in higher voltage output. Based on voltage output, the system automatically recorded which constituent (void or other) was being sensed every 0.00001 inch (0.254 μm) of traverse. Comparing results from their automated system with those obtained manually indicated that their system was unreliable when measuring chord lengths of less than 0.0039 in. (100 μm). Because most air-void chord lengths are shorter than this, the device proved of little practical use.

Image Analysis.– Computer-based image analysis systems are capable of analyzing images from widely diverse image sources – from satellites to electron microscopes. A very common imaging source is a television camera used to view a sample through a microscope. The magnified image is digitized into a two-dimensional array of individual picture elements or pixels. The actual dimensions represented by each pixel is a function of both the pixel density of the particular system and the magnification of the image. Each pixel location and signal intensity (gray level) is stored in a host computer. Gray level ranges are then identified, or "thresheld", to represent features of interest for analysis. Numerous types of analysis can then be performed on the thresheld image by the computer. The simplest such analysis consists of scanning individual lines of pixels and identifying connected groups of thresheld pixels. These connected pixels represent chord lengths. More sophisticated analyses may include area, perimeter, maximum and/or minimum diameter measurements. The type of analysis performed depends on the particular image analysis system used and the software available.

There are numerous common problems associated with the use of all image analysis systems. First of all, it is necessary to obtain sufficient contrast between the features of interest and other constituents in the specimen. This is vital so that

the features of interest can be accurately identified by a distinct gray level range. It is also important to develop a standard (Joyce Loebl 1981, Darwin et al. 1990) to use in adjusting the contrast and brightness levels of the incoming image signal. This is necessary for consistent representation of gray levels, which ensures repeatability of measurements and intersample consistency. Another common concern is feature edge detection. Because each pixel represents a discrete area on the sample, those pixels representing feature edges will also generally represent some area outside the feature boundary. The gray level of these edge pixels will be an average of the sample area each represents. This value will therefore vary depending upon what percentage of each pixel falls within the feature of interest. The particular gray level limits used to define the features of interest will then determine whether or not these edge pixels are assigned to the thresheld feature. The measured size of the features will, thus, vary depending on the actual threshold limits used. Because the pixel density is usually fixed, the total number of pixels representing a particular feature will vary depending on the image magnification. As the magnification is decreased, the number of pixels required to represent each feature will also decrease, but the percentage of each feature represented by edge pixels increases. The measured size of features therefore becomes more sensitive to the threshold limits used as the magnification decreases.

A potentially significant source of systematic error, when using image analysis techniques, is the frame edge effect. Because each frame represents a finite field of view, some features will inevitably be truncated by the frame edges. The measured size of these truncated features will be smaller than their true size. The effect of measuring only the visible portion of these truncated features is twofold. First,

feature size distributions developed from this data will be skewed to the smaller sizes. Second, numerical density determinations (number of features per unit area) will overestimate the true density value. The magnitude of the frame edge effect is dependent on the frame size relative to the measured features. For a given feature size, more features will be truncated at higher magnifications. The three general categories of methods that have been developed for handling frame edge effects are the edge inclusion method, associated point method, and statistical corrections.

The edge inclusion method (Gundersen 1977) by itself is used only for counting feature densities. Features that are included in the count are only those that are entirely within the field of view or which intersect one or both of a particular pair of predetermined adjacent edges. Features that intersect one of the other edges are excluded from analysis. A variation of this method extends the exclusion edges beyond the frame corners.

The associated point method (Jensen and Sundberg 1986) assigns a unique reference point, such as the center of gravity, to represent each feature. A feature is counted and/or measured only if its associated point falls within the field of view. Because some analyzed features will extend beyond the field of view, information must be available from outside the viewing field if these features are to be measured. To accommodate this, an internal subframe, or guard ring, within the field of view can be defined as the area in which the associated point must fall for a feature to be analyzed (Russ 1986). To insure accurate measurement, the guard area must be sized so that the largest expected feature will still remain completely inside the field of view when its associated point is within the guard area.

Statistical correction methods use geometric probability arguments to correct

the feature measurements for the distortions due to edge effects. Bockstiegel (1972) and Exner (1972) presented iterative methods to correct measured numerical densities (features per unit length) of linear intercepts. Attiogbe and Darwin (1986) developed a statistical procedure to correct size distributions of randomly oriented linear features, with which they successfully applied to the measurement of submicroscopic cracks in cement paste using a scanning electron microscope.

Hougardy and Stienen (1978) developed a correction procedure that combines the statistical approach with a type of associated point method. They used geometric probability relationships to develop a procedure to estimate the true size distribution from the measurement of only those features which lie entirely within the field of view. They present separate methods for linear and areal measurements. Measuring only those features which do not intersect the frame edges is, in effect, like using a variable size guard ring. The size of the effective guard ring is different for each feature size. A significant limitation of this method is that the image analysis equipment must be able to determine if a feature touches an edge.

Chatterji and Gudmundsson (1977) first adapted digital image analysis technology to measuring air voids. To obtain adequate feature contrast, they blackened the polished concrete surface with a stamping pad and then filled the voids with a mixture of Vaseline paste and zinc oxide. Gypsum powder was subsequently spread over the surface, adhering to the ZnO paste in the voids. They worked at a magnification of 48x yielding a 1 mm^2 field of view for each image. They reported similar, but lower, values for total air content and Powers spacing factor to those obtained from a traditional linear traverse.

Houde and Meilleur (1983) explored the use of image analysis to measured air-

void chord lengths. Some of their results are contrary to those of other users of image analysis techniques to measure entrained-air. Their reported values of specific surface, based on the mean chord length, were usually smaller than obtained from traditional linear traverse analyses. This resulted in typically larger calculated values of the Powers spacing factor.

Roberts and Scali (1984) explored some of the issues affecting the results of image analysis of air voids. They noted the sensitivity of results to sample preparation procedures. The impact of frame edge effects was also acknowledged but no effort was made to adjust the results accordingly. They chose to work at a lower magnification (31x) to reduce the extent of frame edge effects.

In studying the effect of superplasticizers on the air-void system, MacInnis and Racic (1986) used an image analysis system to characterize the air-void system. No effort was reported to account for the frame edge effects or to compare their results with other methods.

1.5 Object and Scope

The use of computer-based image analysis techniques to automatically identify and measure air voids in hardened concrete specimens has been previously demonstrated. All of the previous users of image analysis have used only chord length measurements to characterize the air-void system. Also, the resulting data was not corrected for distortions due to frame edge effects.

The objective of this study is to demonstrate the use of image analysis techniques to measure void profile areas as a means of characterizing the air-void system in hardened concrete. In addition, procedures are developed for correcting image analysis results for biases resulting from frame edge effects. The goal is to

provide a more consistent and accurate description of the true air volume fraction and void size distribution than is obtained with current methods. This is a necessary step in the development of a truly definitive measure of the effectiveness of entrained air in minimizing damage due to freeze-thaw action.

Concrete specimens containing three different air-entraining agents are analyzed. In addition, non-air-entrained samples are examined. An image analysis system is used to measure both linear intercepts and profile areas, from which size distributions are developed based on chord lengths and area equivalent diameters, respectively. Using the concepts of geometric probability, procedures are developed to correct these size distributions for frame edge effects. By use of standard stereological procedures, the corrected planar size distributions obtained from areal traverses are used to estimate the corresponding three-dimensional void distributions.

Void profile perimeters are also measured for use in calculating a shape factor. The shape factor is used to compare the void shapes obtained with the different admixtures.

The results obtained from chord lengths are compared to those obtained from profile areas. Traditional measures of frost protection: total air content, average specific surface, and Powers spacing factor are calculated for each. These values are compared to the corresponding values obtained from a modified point count analysis and to the freeze-thaw performance of companion samples.

CHAPTER 2

EXPERIMENTAL STUDY

The experimental study was designed to demonstrate the use of image analysis to measure air voids in hardened concrete. The image analysis results are compared to the results of a traditional microscopic examination (ASTM C 457-82a). Additionally, the air-void size distributions produced by different air-entraining admixtures are studied.

Air-entrained concrete samples were prepared by Solvay Construction Materials, Inc. for use in this study. Specimens for microscopic examination were cut from the test samples, and petrographically examined by Professional Services Industries, Inc. prior to delivery to the University of Kansas. The specimens were then further prepared and analyzed using image analysis equipment at magnifications of both 12x and 30x. The image analysis of the air-void profiles included the measurement of both linear intercepts and areas.

2.1 Test Specimens

Materials.–The cement was Medusa brand Type I with the following composition: 53.9 percent tricalcium silicate, 18.9 percent dicalcium silicate, 10.1 percent tetracalcium aluminoferrite, and 9.3 percent tricalcium aluminate.

The fine aggregate was obtained from Jefferson Sand, Streetsboro, Ohio. It had a fineness modulus of 2.72 and a specific gravity of 2.68. All of the sand passed through a No. 4 sieve.

Crushed limestone from Cedarville, Ohio was used as the coarse aggregate. The aggregate was screened and then re-combined by taking equal proportions of material

passing the 1 in., $^3/_4$ in., $^1/_2$ in., and $^3/_8$ in. sieves and retained on the next smaller sieve. No material passed the No. 4 sieve. The specific gravity was 2.78, and the unit weight was 106 lb/ft^3.

Concrete Samples.–The concrete samples for this study were prepared by Solvay Construction Materials. In addition to two non-air-entrained samples, two replications each were prepared using three different air-entraining admixtures. The admixtures used were Catexol A.E. 260 (cocamide diethanolamine, or cocamide DEA) manufactured by Solvay Construction Materials, Vinsol Resin manufactured by Hercules Chemical, and Micro Air (multicomponent) manufactured by Master Builders, Inc. The initial cocamide DEA samples were cast, one each, using the highest and lowest water-cement ratios (w/c) of the other air-entrained samples, 0.55 and 0.53, respectively. Since cocamide DEA has water-reducing properties, the slumps of these samples were significantly higher than those obtained with the other air-entraining agents. A second pair of cocamide DEA samples were then cast with the water content adjusted to yield the same slump as the mixtures containing the other air-entraining agents. Samples of each mixture were cast to measure compressive strength and freeze-thaw resistance, as well as air-void characteristics. Concrete batching information and compressive strength data for all samples is given in Appendix A. A summary of the individual mix data including: air-entraining agent, w/c, properties of plastic concrete (air content, slump, and unit weight), as well as the 28 day compressive strength, is listed in Table 2.1. As expected, the non-air-entrained samples had a higher average compressive strength, 6270 psi, than the air-entrained samples. The average compressive strength for the air-entrained sample pairs was 5320 psi for Vinsol Resin, 5050 psi for multi-component, 5570

psi for cocamide DEA batched by w/c, and 6050 psi for cocamide DEA batched by slump. The lower strength cocamide DEA samples had the highest slumps, 6 3/4 in. and 5 3/4 in., of all the samples.

Longitudinal and transverse sections, $^3/_4$ in. thick, were cut from 3 x 6 in. cylinders for microscopic examination. The transverse sections were located at the top and middle of the cylinders. The sections were polished and microscopically examined using the modified point count method (ASTM C 457-82a) by Professional Service Industries, Inc. A report of their observations and results is provided in Appendix B. Because the results of the transverse sections do not show a trend in air content as a function of position, and are not large enough to satisfy ASTM C 457-82a minimum survey area requirements, they will not be considered further. A summary of the results from the point count analysis for the longitudinal sections is given in Table 2.2. The average Powers spacing factor for the various air-entraining agents are: 0.0045 in. for both the vinsol resin and the multicomponent air-entraining agent, and 0.008 in. for the cocamide DEA. The non-air-entrained samples had an average spacing factor of 0.015 in.

Scaling tests (ASTM C 672-84) were performed on one sample for each of the ten mixes to assess freeze-thaw performance. The scaling test results are summarized in Table 2.3. These results include both the standard ASTM C 672 criteria and the percentage of the surface area that was scaled. The vinsol resin and multicomponent samples performed similarly, with one sample each experiencing moderate scaling and one experiencing moderate to severe scaling after 25 cycles. The cocamide DEA samples, in general, performed better, with three samples experiencing only slight scaling and one sample with moderate to severe scaling after 25

cycles. The cocamide DEA sample with the moderate to severe scaling also had the highest slump, 6 3/4 in., of any of the samples (Table 2.1). The scaling may have been due to a higher surface w/c produced by increased bleed water accompanying the higher slump. As expected, the non-air-entrained samples performed poorly, showing severe scaling after only 15 cycles. For the air-entrained samples, the scaling test results do not correlate directly with the Powers spacing factor.

2.2 Surface Preparation

In the microscopic examination of materials, sample preparation is an important step in achieving accurate and consistent results. Because of the lack of continuous subjective decision making on the part of an operator during image analysis, this initial preparation phase becomes even more important. It has been observed in this and other studies (Roberts and Scali 1984) that image analysis results for air content can vary considerably with the quality of the sample surface preparation.

In traditional microscopic examinations of air-entrained concrete, shading from oblique lighting is used to help the operator distinguish between air voids and cement paste. With image analysis, features are identified by computer, based on gray-scale contrast. The naturally occurring contrast between air voids and the surrounding cement paste and aggregate is not adequate for consistent and accurate delineation of the voids by image analysis equipment. Thus, it is necessary to provide contrast enhancement as part of the surface preparation procedure. The method of final surface preparation and contrast enhancement used in this study is described next. With the exception of the polishing procedure, the method is similar to that described by Roberts and Scali (1984).

The specimens provided by Solvay Construction Materials were previously prepared for microscopic examination by Professional Service Industries, Inc. It was found that the degree of surface flatness and polishing, which was satisfactory for a visual microscopic examination, was inadequate for image analysis. Additional polishing was performed using an automatic oscillating lap table using 600 grit (15 micron) silicon carbide and water slurry. Ten ounces of lead were attached to the specimen backs with modeling clay to provide a uniform pressure on the lap surface. The specimens were left on the oscillating lap until the surface was flat and adequately polished, as evidenced by a uniform texture across the entire surface, typically taking about four hours. At this point, a 5 to 1 mixture (by volume) of acetone and fingernail hardener was brushed onto the specimen surface to stabilize the cement paste to obtain sharply defined void edges during the final lapping process. The specimens were then returned to the oscillating table for 1 hour of additional polishing. The final polishing was by hand using 1000 grit (8 micron) silicon carbide and water slurry on a glass plate. Specimens were placed in an ultrasonic water bath for one minute, between the different polishing stages and upon completion of polishing, to remove any polishing residue and silicon carbide grit from the surface and from within the voids. After examination of the specimen under a light microscope, to ensure a satisfactory degree of surface polish and void edge definition, the fingernail hardener was removed by soaking the specimen surface in acetone for one minute.

After complete air drying, the specimens were ready for contrast enhancement. Sharp contrast was achieved by painting the polished surface black and then filling in the voids with white gypsum powder. A water soluble black indian ink (Winsor and

Newton No. 110185) was applied to the specimen using a hard rubber roller (Hunt Speedball No. 49P). It is important to use a very low viscosity ink to avoid ink build-up, which could reduce the measured size of voids or completely fill in smaller voids. The specimens were placed in an oven at 60°C for 10 minutes to speed the drying of the ink. To obtain a uniform coating, a second application of ink was required on some specimens.

After the ink was dry and the samples cooled to room temperature, gypsum powder was spread over the polished surface to fill in the air voids. The gypsum powder used was U.S. Gypsum 4S80 with a 4 μm mean particle size and a 80 μm maximum size. The face of a thin plastic ruler was used to work the powder into the voids. After all of the voids were filled, the edge of the ruler was then used to scrape the excess powder from the surface. Final surface cleaning was performed by drawing a single-edged razor blade across the entire surface at an acute angle. The last step in the sample preparation process was inking over any surface voids in the aggregate, which would otherwise be measured as air voids. This was done with a black fine point felt-tipped pen. Performing this step while viewing the specimen under a light microscope at a magnification of 20x permitted accurate and complete inking of the aggregate voids.

2.3 Image Analysis

Image analysis can be broadly described as a computer-based process of extracting quantitative information by analyzing images. Automatic image analysis involves three general steps: image formation, feature recognition, and feature measurement.

Image formation.–There is an almost limitless range of image sources, from

satellites to electron microscopes. The present study used a video camera, mounted on an adjustable column camera stand, to create an optical image which was subsequently digitized into a grid of picture elements or pixels. The camera was a Dage MTI 68-series using a Newvicon imaging tube with a rated resolution of greater than 850 TV lines. The camera sweeps a standard 525-line RS-330 format at 30 frames per second. Image magnification was achieved by using a conventional 28 mm f/2.8 macro camera lens in a reversed position so that the rear lens element faces the specimen. Because of the short focal length resulting from magnifications greater than life-size, using a conventional lens in a reversed position improves the image quality and provides added magnification (Lefkowitz 1979). The focusing mechanism was rendered inoperable with the lens mounted in a reversed position. Image focusing was thus achieved by moving the entire camera along the stand column. A reduction gear box provided fine control of the camera motion. Additional magnification was achieved by using an extension tube between the camera and lens. Separate extension tubes were constructed of polyvinyl chloride pipe with lengths calibrated for actual magnifications of 30.06x and 11.96x. These magnifications are hereafter referred to as 30x and 12x, respectively.

A common problem with video microscopy is the occurrence of a bright zone or hot spot in the center of the image. This can be caused by multiple reflections at the lens or from reflections off the interior surface of the lens barrel and/or extension tube. Hot spots were controlled by using a lens that was treated with a special antireflection coating and by painting the interior surface of the extension tube flat black. The strategic placement of apertures within the lens arrangement, as shown in Fig. 2.1, also helped eliminate hot spots (Inoué 1986).

A frame grabber was used to convert the analog video signal into a digital format. The pixel density was 512 horizontally by 480 vertically. The pixels had a tonal range of 256 gray levels, from 0 (black) to 255 (white). In addition to being stored in the computer, the image was also displayed on a high resolution television monitor for viewing.

Feature recognition.–The process of feature identification is typically based on gray level. It is thus important for the features of interest to be represented by a range of gray levels that is distinct from the background. This initial problem of obtaining adequate gray-scale contrast is common to almost all image analysis endeavors. The previously described contrast enhancement of the air-entrained concrete specimens provided this separation of gray levels.

To identify features, a range of gray levels is selected which represents only the features of interest. The image is then partitioned or segmented into regions according to the preselected gray levels. This process of segmentation is often referred to as image thresholding. Each pixel in the image can now be easily identified as being part of either feature or background. The thresheld features can be pseudo-colored for display on a television monitor to permit easy visual identification.

Determining which threshold settings to use in identifying the features of interest is an important process. Even when the samples to be analyzed have adequate contrast between the features and background, the distinction between them is not always clear cut. On a digital image, those pixels located at the feature boundaries will usually represent some of both feature and background. Therefore, the gray level of these boundary pixels will be of intermediate brightness, between that of the

background and that of the features, depending on how much of each is represented. The boundary between features and background will, therefore, have an apparent finite thickness. These boundary pixels may or may not be considered as part of the associated feature, depending on the threshold values selected to define features of interest. A common threshold setting technique (Joyce Loebl 1981) is to examine a histogram of the image gray levels and then select the gray level value of the low point between the peaks which represent the background and features of interest. A typical histogram from an air-entrained concrete image is shown in Fig. 2.2. A gray level value of 80 was found to consistently represent the low point between background and air voids. The threshold range thus selected for air voids in this study was all gray levels from 80 to 255.

To insure measurement consistency and repeatability, it is necessary to use a standard procedure for adjusting the video equipment. A standard specimen was developed for this purpose. Because the video camera had both adjustable contrast and brightness levels, a two phase standard was necessary. The standard was constructed by heat casting two different phenolic resin powders, on opposite sides of a $^1/_2$ inch by 1 inch circular specimen. The specimen was cast in a Buehler Simplimet II metallographic mounting press at 4200 psi and 280° F. The resins used were PSI Testing Systems, Inc. No. PSI-201-5 Green and Buehler No. 20-3200 AB Red. The standard specimen surface was polished with 1000 grit silicon carbide paper and then successively with 6 μm, 3 μm, and 1 μm diamond paste.

To establish the correct threshold levels for the standard specimen, the specimen lighting and video controls were first adjusted to yield a satisfactory image of a typical air-entrained concrete specimen. The appropriate air-void threshold

level was established from a gray level histogram as previously described. This image was alternately observed with and without the pseudo-colored threshold file, to ensure that the air voids were accurately defined. The two phase interface of the standard specimen was next imaged under the same lighting and video settings. The range of gray levels for each phase of the specimen was measured, and standard calibration ranges were established and stored in the computer as a threshold file. The ranges used were 11 to 15 and 32 to 36 for the red and green regions, respectively. Immediately prior to the analysis of each of the air-entrained concrete specimens, the standard specimen was imaged and the contrast and brightness controls adjusted so that both phases of the standard were correctly represented by the calibration threshold levels.

Feature measurement.– Once all of the features of interest have been correctly identified by thresholding, it is a relatively straightforward process to measure them. Two common methods of feature measurement are lineal analysis and areal analysis.

Lineal analysis is probably the simplest form of analysis possible, consisting of traversing a line of pixels and determining the lengths of the adjacent thresheld pixel groups. These contiguous groups of pixels represent linear intercepts or chord lengths. The decision as to how many pixel lines per frame to scan is an important consideration. In order for each void profile to only be intercepted in proportion to its diameter, and for the resulting chord lengths to be independent of each other, the spacing between the lines scanned should be greater than the largest expected feature. As an alternative, the spacing of scanned lines should be very close, which will result in each profile yielding a number of chords in proportion to its diameter. A

line spacing between these two extremes in unacceptable (Weibel 1979). In this study, both extremes were used by performing two separate analyses, scanning 1 line and 480 lines per frame, respectively.

An areal analysis consists of sequentially examining all of the lines of pixels in a frame. Groups of thresheld pixels or chords are identified on each line as in the lineal analysis. Chords which overlap chords of the same threshold range on the previous line are considered to belong to the same feature. After all lines in the frame have been scanned, each group of adjacent thresheld pixels is then identified and counted as a feature.

Feature measurement was accomplished using a LeMont OASYS image analysis system. In this study, physical measurements for the areal analysis features included area, perimeter, length, and width. Calculated properties included perimeter squared to area ratio and area equivalent diameter.

2.4 Image Analysis Data

One 3 x 6 in. longitudinal specimen from each of the ten concrete mixes was analyzed. Separate lineal and areal analyses were performed on each specimen. The lineal analysis included sampling at both 1 line and 480 lines per frame. All measurements were performed at magnifications of both 12x and 30x.

The polished concrete specimens were individually mounted on an x-y stage positioned beneath the video camera. Modeling clay was used to attach and level the specimens on the stage.

Lighting was provided by a pair of adjustable desk lamps, each with a 100 watt incandescent bulb. The lamps were positioned 9 in. horizontally on opposite sides of the stage (in line with the video camera) and 8 in. above the face of the specimen.

The analysis was performed with non-overlapping frames, systematically arranged in passes across the short direction of the specimen. An individual frame had a dimension of 7528.0 μm by 5662.1 μm at a magnification of 12x (11.96x actual), and 2995.2 μm by 2252.8 μm at 30x (30.06x actual). At a magnification of 12x, the individual frames within a pass were located at a 6350 μm center to center spacing and the passes were spaced at 7620 μm. This spacing typically allowed for 10 frames per pass and 17 passes per specimen. At a magnification of 30x, the individual frames were spaced at 2540 μm and the passes spaced at 3040 μm. This spacing typically permitted 25 frames per pass and 43 passes per specimen.

The lineal and areal image analysis results of this study are presented in Appendix C and Appendix D, respectively. The lineal data is classified by chord length and includes the number of chords as well as the number per unit length. Class widths used are 29.41 μm and 29.25 μm for magnifications of 12x and 30x, respectively. The areal data is classified by area equivalent diameter and includes the number of features as well as the number per unit area in classes of 25 μm width. A summary of the image analysis air content results for the ten specimens studied is given in Table 2.4. Also included are the air content determinations from the pressure meter (plastic) and modified point count (manual) methods. It should be noted that, in all cases, the image analyses resulted in lower values of air content than obtained by the modified point count method. On the average, image analysis values were lower by 1.15 percent air. One possible explanation for the consistently higher manual results may be that they were obtained at a higher magnification. The modified point count analyses were performed at a magnification of 50x, while the image analyses

were performed at magnifications of 12x and 30x. For the manual methods, it has been shown (Sommer 1981) that higher magnifications will often result in higher measured air contents. However, based on the two magnifications used in this study, image analysis results for air content do not appear to be a function of magnification.

Gutmann (1988a, 1988b) felt that the shape of the entrained air voids may influence the resulting compressive strength of the concrete mix. In particular, he observed that cocamide DEA produced air voids which were more spherical in shape than those produced by either vinsol resin or multicomponent admixtures. The "form factor" (Russ 1986) can be used to describe the shape of the air void profiles measured in the areal analysis. It is a dimensionless parameter defined as

$$\text{Form Factor} = 4\pi\left(A/P^2\right) \qquad (2.1)$$

in which A and P are the feature area and perimeter, respectively.

The form factor will be equal to 1.0 for a perfect circle and will decrease in value as the perimeter of the measured feature becomes more irregular.

The average form factor for each of the 80 size classes is calculated using the area and perimeter measurements obtained from each feature in the areal analysis. The average form factor in each class for each sample is given in Tables 2.5 and 2.6 for image magnifications of 12x and 30x, respectively. The mean form factor for each sample is given in Table 2.7 for both magnifications. Also given for each sample is the diameter weighted mean form factor calculated from the features in classes 1 through 18. This includes at least 97% of the total measured features in each sample. The diameter weighted means are calculated by weighting the mean form

factor for each of the 18 classes by the midpoint diameter of that class. The sample mean form factors are influenced more by the features in the smaller size classes, where the largest number of the features are concentrated. The diameter weighted mean form factors are influenced more by the features in the larger size classes, irrespective of their actual number.

The mean form factor for the cocamide DEA samples, at a magnification of 12x, are in all cases larger than the mean values for the other samples. The average of the sample mean form factors for the different air-entraining agents are 0.742 for cocamide DEA, 0.730 for vinsol resin, and 0.726 for the multi-component air-entraining agent. At a magnification of 30x the individual results are mixed, with the average of the sample means being 0.694 for cocamide DEA, 0.718 for vinsol resin, and 0.722 for the multi-component.

The diameter weighted mean form factors for the cocamide DEA samples are higher, at both magnifications, than those of the other air-entraining agents. The average of the diameter weighted mean form factors obtained at a magnification of 12x are 0.726 for cocamide DEA, 0.608 for vinsol resin, and 0.622 for the multi-component. The average of the diameter weighted mean form factors obtained at a magnification of 30x are 0.687 for cocamide DEA, 0.633 for vinsol resin, and 0.611 for the multi-component.

The diameter weighted mean form factors for all air-entrained samples are lower than the corresponding mean form factors. The reason for this decrease can be seen in Fig. 2.3 where the mean form factors for the different air-entraining agents, obtained at a magnification of 12x, are plotted by class, up to class 18. The mean form factor plots for the air-entrained sample groups show three distinct phases.

The first phase is an initial decrease in the mean form factor from class 1 to class 2. The second phase is an increasing mean form factor with increasing class size. This increasing phase is then followed by a decrease in the mean form factor with increasing class size. The cocamide DEA samples exhibit a longer increasing phase followed by a less pronounced decreasing phase than the other air-entrained samples. This results in the cocamide DEA sample group having a larger mean form factor in all size classes greater than class 5. The decreasing phase in mean form factor with increasing feature diameter could be attributed to the coalescing of air voids into groups and adjacent to large aggregate particles. Another contributing factor could be due to edge effects, the intersection of features by the imaging frames, with the larger features having a higher probability of being intersected. The non-air-entrained samples display an initial decreasing phase in mean form factor followed by a general increasing trend with increasing class size. The absence of a subsequent decreasing phase could be a result of a lack of air-void coalescing.

From Table 2.7 it can be seen that, in most cases, the average form factors obtained at a magnification of 30x are lower than those obtained at a magnification of 12x. This reduction of form factor with increasing magnification can also be seen in Fig. 2.4 where the average form factors are plotted by class for mix 8 at magnifications of 12x and 30x up to size class 18. This reduction in form factor results from two different phenomenon, the frame edge effect and the digital nature of the feature measurements. The intersection of features by the edges of the viewing frames will decrease the calculated form factor for those features. This will have a greater effect on the average form factor at the higher magnification where the probability of features being intersected is greater. In addition, because the measurements are

made from a digital image, the measured perimeters used in the calculation of the form factors are obtained by measuring the center to center distances of the boundary pixels. The measured perimeter of a given feature will be larger at a higher magnification, because of the finer representation of the feature boundary by smaller pixels. A larger measured perimeter will result in a smaller form factor.

Overall, these observations support Gutmann's (1988a, 1988b) observation that cocamide DEA produces more spherical air voids than do vinsol resin or multicomponent admixtures. It is likely, however, that the higher strength obtained by concrete containing cocamide DEA is due to the water reducing capabilities of the admixture, rather than the air-void shape.

Statistical Analysis.–As in all experimental studies, the question of how much data to obtain is an issue that must be addressed. A primary concern in the image analysis of air voids is how many frames need to be analyzed to estimate the true air content of a particular mixture. In a random sampling of n frames, the mean value of the individual frame air contents would be referred to as the sample mean. If the sampling process were repeated a large number of times, the distribution of the resulting sample means would approximate a normal distribution, as predicted by the central limit theorem. The average value of these sample means would be expected to equal the true air content of the specimen. The standard deviation of the sample means is called the standard error of the mean, and is a measure of the average difference between the individual sample means and the true specimen air-content.

The standard error of the mean, $\sigma_{\bar{x}}$, for a particular sample size can be estimated (Zuwaylif 1974) by

$$\sigma_{\bar{x}} = \frac{\sigma}{\sqrt{n}} \qquad (2.2)$$

in which n is the number of sampling units (frames, lines, etc.) in the sample, and σ is the population standard deviation of individual sampling units. Because it is not possible to know beforehand what the population standard deviation will be, σ is replaced with the sample standard deviation, S, obtained from a preliminary sampling.

Because the distribution of sample means is normal, 68 percent of the sample mean values would be expected to fall within $\pm$ 1.0 $\sigma_{\bar{x}}$ of the true specimen air content. Likewise, 95 percent of the sample means will fall within $\pm$ 1.96 $\sigma_{\bar{x}}$ of the true value. Stated another way, it can be expected with a 68 % confidence level that a particular air content estimate is within $\pm$ 1.0 $\sigma_{\bar{x}}$ of the true air content and with a 95 % confidence level that the estimate is within $\pm$ 1.96 $\sigma_{\bar{x}}$ of the true air content.

Thus, it can be seen that there are two aspects to stating the desired accuracy of a particular estimate. First, it is necessary to specify an acceptable error (Zuwaylif 1974) between the estimated and the true air content. Second, it is necessary to select the desired degree of confidence that the difference between the estimated and true air content is less than the acceptable error. The relationship between the acceptable error and the degree of confidence can be expressed in terms of the standard error of the mean as

$$\varepsilon = Z\sigma_{\bar{x}} \qquad (2.3)$$

in which ε is the acceptable error, and Z represents the degree of confidence desired (1.0 for 68 percent confidence and 1.96 for 95 percent confidence).

Combining Eqs. 2.2 and 2.3 and rearranging the terms provides an expression for the number of frames required to obtain an estimate of the air content that is within the acceptable error of the true air content with a specified degree of confidence.

$$n = \left(\frac{SZ}{\varepsilon}\right)^2 \qquad (2.4)$$

The amount of data required for a manual linear traverse is currently specified (ASTM C 457-82a) in terms of an acceptable error in the air content equal to 0.5 percent of the concrete volume, at a confidence level of 68 percent. Thus, 68 percent the time, the estimate so obtained can be expected to be within 0.5 percent air of the true air content. Conversely, 32 percent of the time, the estimated values will be more than 0.5 percent air away from the true air content.

In this study, the acceptable error in the air content is also 0.5 percent of the concrete volume, and the required number of frames to achieve this, with confidence levels of both 68 % and 95 %, is determined.

The required number of frames calculated using Eq. 2.4 for the areal analyses and the 480 lines/frame lineal analyses is given in Tables 2.8 and 2.9, respectively. Also given is the corresponding specimen survey area. It can be seen that, while the number of frames required to achieve a given level of confidence is smaller at the lower magnification, the corresponding survey area is always larger. For example, in the areal analysis of mix 10, to estimate the specimen air content within 0.5 of

the true value with a confidence level of 68 %, 74 frames should be analyzed at a magnification of 12x. This corresponds to surveying 4.83 $in.^2$ of the sample surface. At a magnification of 30x, 235 frames or a survey area of 2.47 $in.^2$ need to be analyzed to achieve the same accuracy. It should also be noted that at a magnification of 12x, the required survey area for a 95 percent confidence level cannot always be obtained with a 3 x 6 in. specimen.

It can be seen from Eq. 2.4, that for a given acceptable error and confidence level, the number of required frames is a function of the square of the standard deviation of the individual frame air content, S. Test results show that S increases with increasing sample air content. Thus the number of required frames will be higher for those specimens with higher air content. The required survey areas, representing the average of the areal and 480 L/F lineal analyses, for a 68 percent confidence level, are plotted against air content in Fig. 2.5. It can be seen that, in general, as the air content of the sample increases so does the required survey area. The best fit for the data indicates a required survey area of 2.2 $in.^2$ (13.9 cm^2) for 2 percent air and 8.3 $in.^2$ (53.6 cm^2) for 8 percent air when working at a magnification of 12x, and 1.1 $in.^2$ (6.8 cm^2) for 2 percent air and 4.1 $in.^2$ (26.3 cm^2) for 8 percent air at a magnification of 30x. This trend is similar to that noted by Houde and Meilleur (1983) based on image analysis results obtained at a magnification of 24x. They recommended survey areas of 3.1 $in.^2$ (20 cm^2) and 4.2 $in.^2$ (27 cm^2) for air contents below and above 4 percent, respectively.

The number of required frames, and the corresponding length of specimen traverse, for the 1 line/frame lineal analyses is given in Table 2.10. In all cases, the traverse length corresponding to the required number of frames for a 68 percent

confidence level is less than the 95 in. (241 cm) specified in ASTM C 457-82a for these specimens. Because significantly less information is obtained when sampling at only 1 line/frame, as compared to 480 lines/frame, the scatter of the measured frame air contents is greater at 1 line/frame. This is evidenced by higher standard deviations. For example, the standard deviation in the frame air content for mix 10 at a magnification of 30x is 10.92 percent when sampling at 1 line/frame compared to 7.62 percent when sampling at 480 lines/frame. As a result, the required number of frames to estimate the specimen air content with the same level of confidence, is greater when sampling at 1 line/frame than at 480 lines/frame. For example, for mix 10 at a magnification of 30x, the number of frames required to estimate the air content within a range of $\pm$ 0.5 percent of the true air content with a 68 percent confidence level is 477 frames when sampling at 1 line/frame but only 232 frames when sampling at 480 lines/frame. The traverse length corresponding to the required number of frames for 68 percent confidence is plotted against measured air content in Fig. 2.6. The same general trend seen in Fig. 2.5, of increasing standard deviation and required traverse length with increasing air content, is noted.

It is apparent that the required survey area for an image analysis is influenced by both the magnification used and the specimen air content. Based on the limited range of magnifications and number of specimens analyzed in this study, it does not seem reasonable to recommend particular survey areas. Instead, the process of determining when enough data has been obtained can be a dynamic one. The standard deviation of the individual frame air contents can be continuously calculated as frames are analyzed and the required number of frames, and hence the survey area, can be determined using Eq. 2.4. The data gathering process should continue until the actual number of frames analyzed exceeds the required number.

CHAPTER 3

EDGE EFFECT CORRECTIONS AND AREA TO VOLUME TRANSFORMATION

3.1 Introduction

A traditional lineal analysis of air-entrained concrete consists of a series of traverses across the length of the specimen. In a manual analysis, the operator can choose where to start and stop a traverse; thus, the end points of a traverse will generally not fall on a feature. In an automatic image analysis, on the other hand, the specimen is analyzed using a large number of relatively small, equal-sized measuring fields, the boundaries of which are positioned on the specimen without regard to the features being measured. As such, a significant number of features can be truncated by the frame boundaries. The measured or apparent size of features that are truncated by the frame edges will be smaller than their true size. As a result, the measured feature size distributions will be skewed toward the smaller sized features, and the average feature size will be underestimated. In addition, because features with their centers outside the field of view will often be partially imaged, the number of features per unit area will be overestimated. These resulting measurement distortions due to the truncation of features by the frame edges are referred to as the frame edge effect. As the magnification increases, the size of the individual frames decreases relative to the features being measured, and hence, the magnitude of the frame edge effect increases. Area percent measurements are not affected by the frame edge effect because individual feature size is not a factor in this determination.

In this chapter, methods based on geometric probability are developed to

correct for the distortions caused by the frame edge effect in data acquired using image analysis. Separate methods are presented for both lineal and areal analyses. The methods developed are applicable for a rectangular field of view, or frame, of length L and height H.

In an attempt to measure features of interest in a solid, it is common practice to intersect that solid with a plane surface and then measure the profiles of the features on the plane surface. Information obtained from the measurement of profiles on a plane surface do not by themselves provide a direct correlation with the volume distribution. This is because larger features are more likely to be intersected by a random plane than are smaller features. Larger features will, therefore, contribute to a higher percentage of the profiles on a plane section. Also, it is not possible to know a priori what size profile will result from a random intersection with a particular size feature. Any attempt to determine the volume distribution of features based on information obtained from a plane section must consider these points.

When spherical features are intercepted by a plane, the resulting profiles on the plane surface will be circular in shape. Because of this predictable behavior, numerous efforts have been directed toward developing relationships between measured circular profiles on a plane surface and the corresponding volume distribution of spheres. In this study, use is made of one such established mathematical relationship (Cruz-Orive 1983) to predict the volume distribution of air voids from the measured distribution of profiles obtained from an areal image analysis.

3.2 Correction of Edge Effects for Lineal Features

In a lineal analysis, each field of view is scanned one or more times resulting in a corresponding number of individual test lines of length L. Features of interest that are intercepted by a test line will yield a linear intercept, or chord, of length l. The center of the chord is used as a reference point, and intercepts of length $l \pm dl/2$ are grouped together in a single size class. Chords resulting from features which lie only partially within the field of view are truncated by the frame edge, as shown in Fig. 3.1.

The edge correction method developed for linear intercepts follows the concepts developed by Attiogbe and Darwin (1986) for randomly oriented distributions of lineal features. The method is simplified to account for the fact that in a lineal image analysis all of the intercepts are aligned in the direction of the scan. The resulting method is applicable for all chords with lengths less than or equal to the frame length, L.

The general method of this procedure is to first develop a relationship to express the expected distribution of apparent chord lengths per unit length in terms of a true distribution which would be obtained if a single test line of infinite length were used. The inverse of this relationship is then used to express the true distribution in terms of a measured distribution obtained using test lines of finite length L.

If f(l) is the true probability density or relative frequency distribution of the chord lengths, then $f(l_i)dl$ is the probability that a chord has a length of $l_i \pm dl/2$, in which dl is an infinitesimally small length interval. The range of values of l is $0 < l \leq l_{max}$, where l_{max} is some value less than the frame length, L, such that

$$\int_0^{l_{max}} f(l_i)dl = 1 \qquad (3.1)$$

If N_L is the true number of all chords per unit length, then

$$N_L(i) = N_L f(l_i)\,dl \qquad (3.2)$$

is the true number of chords per unit length with length $l_i \pm dl/2$.

Measured chords with apparent lengths of $l_i \pm dl/2$ can be grouped together in a class. The number of chords in the class is the sum of two components, n_1 and n_2. n_1 is the number of chords with length, $l_i \pm dl/2$, in the field of view that have not been truncated by a frame edge, and n_2 is the number of chords that have been truncated and have a resulting visible length of $l_i \pm dl/2$.

A chord of length l_i will be visible, in whole or part, if its center is located within the field of view or not more than $l_i/2$ outside the field of view as shown in Fig. 3.2. The total number of measured chords resulting from chords with a true length of l_i is the product of the true number of l_i chords per unit length and the distance along which an l_i chord center can be located and be at least partially visible in the field of view. This is given as

$$n(i) = N_L(i)(L + l_i) \qquad (3.3a)$$

$$n(i) = N_L f(l_i)\,dl(L + l_i) \qquad (3.3b)$$

A chord of length l_i, visible in the field of view, will not be intersected by an edge if its center is not located closer than $l_i/2$ to an edge. This condition is shown in Fig. 3.3. The probability that a visible chord of length l_i will not be intersected by an edge is given by the ratio of the length within the field of view along which the center of an l_i chord can be located and not be truncated to the total length which an l_i chord can be located and be at least partially visible within the field of view.

$$P(l_{ia}|\, l_i) = \frac{(L-l_i)}{(L+l_i)} \tag{3.4}$$

The estimated or expected number of visible chords of length l_i not intersected by a frame edge is then the product of the total number of visible l_i chords and the probability that a visible l_i chord will not be truncated.

$$n_1 = n(i)P(l_{ia}|\, l_i) \tag{3.5a}$$

$$n_1 = N_L f(l_i)\, dl\, (L-l_i) \tag{3.5b}$$

in which $P(l_{ia}|\, l_i)$ is the probability that a chord of length l_i produces an apparent length, l_{ia}, of l_i.

To determine the number of chords that have been truncated by a frame edge which then result in a measured or visible length of $l_i \pm dl/2$, it is necessary to look at chords of length l_j, which are larger than or equal to length l_i. A chord of length l_j will be visible, in whole or part, if its center is located within the viewing field or not more than $l_j/2$ outside of the viewing field. The total number of visible chords of length l_j is

$$n(j) = N_L(j)(L+l_j) \tag{3.6a}$$

$$n(j) = N_L f(l_j)\, dl\, (L+l_j) \tag{3.6b}$$

A visible chord of length l_j will be intersected by an edge if its center is located within a distance of $l_j/2$ on either side of a frame edge. This range is shown in Fig. 3.4. The probability that a visible l_j chord is truncated by a frame edge, $P(\uparrow|l_j)$, is given by the ratio of the total length along which the center of an l_j chord can be located causing the chord to be truncated by a frame edge to the total length along which the center of an l_j chord can be located causing the chord to be at least partially visible in the field of view.

$$P(\uparrow|l_j) = \frac{2l_j}{(L+l_j)} \tag{3.7}$$

A truncated chord of length l_j can contribute to any one of l_j/dl classes. Contributions to each of the classes are equally likely to occur. Therefore, the probability of a truncated chord of length l_j, yielding a chord of apparent length $l_i \pm dl/2$ is dl/l_j.

Thus, the expected number of visible chords of length l_j that are truncated by a frame edge and which then result in an apparent chord length of $l_i \pm dl/2$ is

$$n_{2j} = n(j)\, P(\uparrow|l_j)\, dl/l_j \tag{3.8a}$$

$$n_{2j} = N_L f(l_j)\, dl\, (2dl) \tag{3.8b}$$

The expected total number of chords of apparent length l_i resulting from truncated chords is obtained by integrating Eq. 3.8b over all possible lengths, $l_j \geq l_i$.

$$n_2 = 2\left(\int_{l_i}^{l_{max}} N_L f(l_j)\, dl\right) dl \qquad (3.9)$$

The total number of chords of apparent length $l_i \pm dl/2$ in the field of view, n(i)*, can be obtained by summing n_1 and n_2.

$$n(i)^* = n_1 + n_2 = N_L f(l_i) dl\,(L - l_i) + 2\left(\int_{l_i}^{l_{max}} N_L f(l_j)\, dl\right) dl \qquad (3.10)$$

The number of chords of apparent length $l_i \pm dl/2$ per unit length is obtained by dividing both sides of Eq. 3.10 by the frame length, L.

$$N_L(i)^* = \frac{n(i)^*}{L} = N_L f(l_i)\, dl\left(\frac{L - l_i}{L}\right) + \frac{2}{L}\left(\int_{l_i}^{l_{max}} N_L f(l_j)\, dl\right) dl \qquad (3.11)$$

If finite width class sizes are used and f(l) is approximated as a uniform distribution within each class, Eq. 3.11 can be integrated over class i to obtain the number of chords per unit length with apparent length within class i.

$$N_L(i)^* = \left(\frac{L - l_i}{L}\right)\int_{i-\Delta i/2}^{i+\Delta i/2} N_L f(l)\, dl + \frac{2}{L}\int_{i-\Delta i/2}^{i+\Delta i/2}\left[\int_{l_i}^{l_{max}} N_L f(l)\, dl\right] dl \qquad (3.12a)$$

$$N_L(i)^* = \left(\frac{L - l_i}{L}\right) N_L(i) + \frac{2}{L}\left(\frac{1}{2} N_L(i) + \sum_{j=i+1}^{s} N_L(j)\right)\Delta l_i \qquad (3.12b)$$

$$N_L(i)^* = \left(\frac{L - l_i + \Delta l_i}{L}\right) N_L(i) + \frac{2}{L} \sum_{j=i+1}^{s} \Delta l_i N_L(j) \qquad (3.12c)$$

in which Δl_i is the width of class i and s is the maximum size class. It becomes obvious upon study of Eq. 3.12c that an alternative derivation is possible. In that determination, the contribution of each class j, j = i to s, to the apparent number of features in class i, n(i)* in Eq. 3.10, is equal to the product of the density $N_L(j)$ and the length of the line segment in which the center of the chord can lie and produce an apparent length $l_i \pm \Delta l_i/2$.

This relationship between apparent and actual numbers of chords per unit length can be expressed in the matrix form as

$$\{N_L(i)^*\} = [K_{ij}]\{N_L(j)\} \qquad (3.13)$$

in which the dimensionless coefficients, K_{ij}, form an upper triangular matrix and are given as

$$K_{ij} = \begin{cases} \dfrac{L - l_i + \Delta l_i}{L} & (i=1, \ldots, s;\ j=i) \\ \dfrac{2\Delta l_i}{L} & (i=1, \ldots, s-1;\ j=i+1, \ldots, s) \\ 0 & (i=2, \ldots, s;\ j=1, \ldots, i-1) \end{cases}$$

It should be noted that for a constant class size and test line, the off diagonal terms of $[K_{ij}]$ are constant. From this relationship, an estimate of the actual number of chords per unit length is thus

$$\{N_L(i)\} = [\alpha_{ij}]\{N_L(j)^*\} \qquad (3.14)$$

in which $[\alpha_{ij}]$ is obtained by inverting $[K_{ij}]$.

3.3 Correction of Edge Effects for Areal Features

In an areal analysis, the field of view consists of discrete frames of length L and height H. The individual areas of the features of interest within each field of view are measured. For those features which are intersected by a frame edge, only that portion that is visible within the field of view is measured, as shown in Fig. 3.5. The measured or apparent areas can be represented by an equivalent circular feature that is described in terms of an area equivalent diameter (AED), y_{ia}.

$$y_{ia} = \text{AED} = \sqrt{4A/\pi} \qquad (3.15)$$

in which A is the measured feature area. Measured features with an AED of $y_i \pm dy/2$ are grouped together in a class.

In this section, a method for correcting the measured size distributions to account for the frame edge effect is developed in a manner similar to that for lineal features. The development of the correction method assumes that the true data consists entirely of circular features. The center of each circular feature is used as

a reference point.

The general method is to first develop a relationship expressing the expected distribution of measured features per unit area in terms of the true distribution, which would be obtained if the viewing frame were of infinite area. The inverse of this relationship is then used to express the true distribution in terms of the measured distribution.

If f(y) is the true probability density or relative frequency distribution of diameters of circular features, then $f(y_i)dy$ is the probability that a feature has a diameter of $y_i \pm dy/2$. The range of values of y is from 0 to y_{max}, where y_{max} is some value less than the shortest frame dimension, such that

$$\int_0^{y_{max}} f(y_i)dy = 1 \qquad (3.16)$$

If N_A is the true number of all features per unit area, then

$$N_A(i) = N_A f(y_i)\, dy \qquad (3.17)$$

is the true number of features per unit area with diameter $y_i \pm dy/2$.

The number of measured features with an AED of $y_i \pm dy/2$ is the sum of two components, n_1 and n_2. n_1 is the number of features with an AED of y_i in the field of view that have not been truncated by a frame edge and n_2 is the number of features that have been truncated by one or more frame edges and have a resulting visible AED of $y_i \pm dy/2$.

A circular feature of diameter y_i will be visible, in whole or part, if its center is located within the field of view or not more than $y_i/2$ outside of the field of view, as shown in Fig. 3.6. The total number of visible features of diameter y_i is equal to the product of the number of features per unit area with diameter y_i and the total area in which such features could be located and be at least partially visible within the field of view.

$$n(i) = N_A(i)\left[(L+y_i)(H+y_i)-y_i^2(1-\pi/4)\right] \qquad (3.18a)$$

$$n(i) = N_A f(y_i)\,dy\left[(L+y_i)(H+y_i)-y_i^2(1-\pi/4)\right] \qquad (3.18b)$$

A visible feature of diameter y_i will not be intersected by a frame edge if its center is located within the frame at a distance of more than $y_i/2$ from any edge, as shown in Fig. 3.7. The probability that a visible feature of diameter y_i will not be intersected by an edge is given by the ratio of the area in which a feature of diameter y_i can be located and not be truncated to the total area in which such a feature could be located and be at least partially visible in the viewing field.

$$P(y_{ia}|y_i) = \frac{(L-y_i)(H-y_i)}{(L+y_i)(H+y_i)-y_i^2(1-\pi/4)} \qquad (3.19)$$

The number of visible circular features with diameter y_i not intersected by a frame edge, is equal to the product of the number of visible features with diameter y_i and the probability that such a feature will not be intersected by a frame edge.

$$n_1 = n(i)P(y_{ia}|y_i) \tag{3.20a}$$

$$n_1 = N_A f(y_i)dy[(L-y_i)(H-y_i)] \tag{3.20b}$$

To determine the number of features that have been truncated by the edge of the viewing field and which then result in a measured AED of $y_i \pm dy/2$, it is necessary to look at features with diameters y_j larger than or equal to y_i. A feature of diameter y_j will be visible, in whole or part, if its center is located within the field of view or at a distance of not more than $y_j/2$ outside of the field of view. The total number of visible features with diameter y_j is equal to the product of total number of features per unit area with diameter y_j and the area in which such a feature can be located and be at least partially visible in the field of view.

$$n(j) = N_A(j)\left[(L+y_i)(H+y_i)-y_j^2(1-\pi/4)\right] \tag{3.21a}$$

$$n(j) = N_A f(y_j)dy\left[(L+y_i)(H+y_i)-y_j^2(1-\pi/4)\right] \tag{3.21b}$$

There is a region around the image frame in which the center of a feature of diameter y_j can be located and result in an AED in the frame of size $y_i \pm dy/2$. Such a region is shown in Fig. 3.8. The area of this region is designated A_{ij}. A procedure for calculating the areas A_{ij} is presented in Appendix E.

The probability that a visible feature of diameter y_j is truncated by a frame

edge and results in a measured AED of $y_i \pm dy/2$ is equal to ratio of the area A_{ij} to the total area in which the center of a y_j feature can be located and be at least partially visible in the field of view.

$$P(AED_i \mid y_j) = \frac{A_{ij}}{\left[(L+y_j)(H+y_j) - y_j^2(1-\pi/4)\right]} \tag{3.22}$$

The number of features of apparent size $y_i \pm dy/2$ resulting from truncated features of size y_j is equal to the product of the number of visible features of size y_j and the probability that such a feature will be truncated and result in a measured AED of $y_i \pm dy/2$.

$$n_{2j} = n(j)\, P(AED_i \mid y_j) \tag{3.23a}$$

$$n_{2j} = N_A f(y_j)\, dy\, A_{ij} \tag{3.23b}$$

The expected total number of features with an apparent AED of $y_i \pm dy/2$, resulting from truncated features, is obtained by integrating Eq. 3.23b over all possible feature diameters $y_j \geq y_i$.

$$n_2 = \int_{y_i}^{y_{max}} A_{ij} N_A f(y_j)\, dy \tag{3.24}$$

The total number of features with an apparent AED of $y_i \pm dy/2$, n(i)*, can be

obtained by summing n_1 and n_2.

$$n(i)^* = n_1 + n_2 = N_A f(y_i)\, dy\left[(L-y_i)(H-y_i)\right] + \int_{y_i}^{y_{max}} A_{ij} N_A f(y_j)\, dy \qquad (3.25)$$

The number of features with an apparent AED of $y_i \pm dy/2$ per unit area is obtained by dividing both sides of Eq. 3.25 by the frame area, LH.

$$N_A(i)^* = \frac{n(i)^*}{LH} = N_A f(y_i)\, dy\left[\frac{(L-y_i)(H-y_i)}{LH}\right] + \frac{1}{LH}\int_{y_i}^{y_{max}} A_{ij} N_A f(y_j)\, dy \qquad (3.26)$$

If discrete class sizes are used and it is assumed that the features are uniformly distributed within each class, then (using Eq. 3.17) Eq. 3.26 reduces to

$$N_A(i)^* = \frac{1}{LH}\left[(L-y_i)(H-y_i)\right] N_A(i) + \frac{1}{LH}\sum_{j=i}^{s} A_{ij} N_A(j) \qquad (3.27)$$

As observed following Eq. 3.12, an alternative derivation exists for Eq. 3.27. In this case, the contribution of each class j, j = i to s, to the apparent number of features in class i, n(i)* in Eq. 3.25, is equal to the product of the density $N_A(j)$ and the area in which the center of the feature can lie and produce an AED of $y_i \pm \Delta y_i/2$.

Eq. 3.27 can be expressed in matrix form as

$$\{N_A(i)^*\} = [M_{ij}]\ \{N_A(j)\} \qquad (3.28)$$

in which

$$M_{ij} = \begin{cases} \dfrac{(L-y_i)(H-y_i) + A_{ii}}{LH} & (i=1, \ldots, s;\ j=i) \\ \dfrac{A_{ij}}{LH} & (i=2, \ldots, s;\ j=i+1, \ldots, s) \\ 0 & (i=2, \ldots, s;\ j=1, \ldots, i-1) \end{cases}$$

in which A_{ii} and A_{ij} are the areas of the regions around the image frame in which the center of a feature of diameter y_i and y_j, respectively, can be located and result in a measured AED of size $y_i \pm dy/2$ (see appendix E).

From this relationship, an estimate of the number of circular features per unit area is thus

$$\{N_A(i)\} = [N_{ij}]\ \{N_A(j)^*\} \qquad (3.29)$$

in which $[N_{ij}]$ is obtained by inverting $[M_{ij}]$.

3.4 Area to Volume Conversion

It is common in microscopic investigations to use information obtained from the examination of a plane surface to estimate the corresponding structure in the volume. The general mathematical approach used to extrapolate information obtained from a plane surface to three-dimensional space is known as stereology. It can be

shown (Hilliard 1968) that the volume percent of a particular constituent can be estimated directly from measurements made on a plane surface. The estimation of three-dimensional size distributions, on the other hand, is not as direct.

In this study, it is assumed that the features of interest are randomly distributed spheres of varying sizes. The resulting profiles, obtained on a random section, are therefore circular. It is not possible, a priori, to determine the size of an intersected sphere that is responsible for a particular circular profile. This is because a sphere of a given size, when randomly intersected, will contribute profiles to all size classes smaller than or equal to the sphere diameter. Therefore, a particular size circular profile could be generated by the intersection of any size sphere of diameter greater than or equal to the profile diameter.

The measurement of linear intercepts on a plane surface is a convenient and fast method of characterizing the features of interest, and provides a reasonable way to estimate area percentages. There have been methods developed to use measured size distributions of linear intercepts to estimate the corresponding volume distribution of spheres (Lord and Willis 1951, Spector 1950). While it is possible to use linear intercepts to estimate volume size distributions, it is believed that methods based on profile diameters or areas provide better results (Cruz-Orive 1983).

There have been numerous methods developed for estimating sphere size distributions from measured distributions of profile diameters. A review of these methods is given by Cruz-Orive (1983). The methods can be classified into two general groups, parametric and distribution-free. Parametric methods require an initial assumption to be made as to the form of the sphere size distribution. The

problem then becomes one of determining the parameters which characterize the chosen distribution. Distribution-free methods require no assumptions about the distribution. The goal of the distribution-free approach is to develop a relationship expressing the expected profile distribution function f(y) in terms of a known sphere size distribution function g(x). This can be accomplished by means of geometric probability arguments. In the case of a plane surface, the result is an Abel integral equation (Cruz-Orive 1983) which can be inverted to express the sphere distribution in terms of a measured profile distribution. Closed-form solutions of the resulting Abel equation can easily become unwieldy. Numerical methods have been developed (Wicksell 1925, Saltykov 1949, Cruz-Orive 1977) to replace the integrals with summations over discrete classes, resulting in an upper triangular matrix of coefficients relating an expected profile distribution to a known sphere distribution. This matrix of coefficients can be inverted to provide a more useful relationship expressing the unknown sphere size distribution in terms of an empirical profile distribution. The development and comparison of these methods is given by Weibel (1980).

The numerical method adopted in this study is a simplification of one presented by Cruz-Orive (1983). The method, as originally presented, included provisions for handling overprojection and missing profiles. The method is significantly simplified by not considering these two phenomena. Overprojection occurs when the sampling section is a thin section of finite thickness, causing the projection of some features to appear larger than their true dimension on the plane surface. This is not a consideration when the sampling section used constitutes a true plane. Missing profiles refers to the undercounting of the smaller sized features due

to finite resolution limits of the imaging equipment and imperfect sample preparation. Ignoring the effect of the missing smaller profiles will only affect the estimated number of spheres of sizes equal to or smaller than the diameter of the resolution limits.

The method of obtaining the initial expressions which relate the expected distribution of profiles with a known distribution of spheres per unit area is to look first at the probability of a particular sphere size, x, being intersected by a random plane. This probability is then expanded to include a range of sphere sizes contained in a given size class, i. Next, given that a sphere of size x is intersected, the probability of that intersection resulting in a profile of particular size y is obtained. This probability is expanded to include the range of expected sizes, y, included in a given profile size class j. The probability of obtaining a size class j profile from a particular size, x, sphere is then extended to consider a range of sphere sizes contained in the given sphere size class, i. Using both the probability of a sphere in class i being intersected by a random plane and the probability that if a size class i sphere is intersected that a size class j profile will result, an expression is obtained for the number of size class j profiles expected from the intersections of size class i spheres. Summing over all possible sphere size classes, a relationship is then obtained expressing the profile distribution in terms of a known sphere distribution.

If g(x) is the relative frequency or probability density of spheres, then g(x)dx is the probability that a sphere has a diameter of $x \pm dx/2$, in which dx is an infinitesimally small diameter increment. Spheres can range in diameter from 0 to some maximum diameter, x_m, such that

$$\int_0^{x_m} g(x)dx = 1 \qquad (3.30)$$

The probability that a sphere of size x ± dx/2 located within the sample volume, V, will be intercepted by a random plane with an area A inside the sample volume is equal to the ratio of the volume of an x by A prism to the total sample volume.

$$P(\uparrow|x) = \frac{xA}{V} \qquad (3.31)$$

The probability of a sphere in the finite size class i being intercepted by the random plane of area A is obtained by integrating, over the range of class i, the product of the probability of a sphere of size x being intersected and the probability density of spheres in class i.

$$P(\uparrow|i) = \int_i P(\uparrow|x)g(x|i)\,dx \qquad (3.32)$$

in which g(x|i) is the probability density of spheres in class i. g(x|i) is equal to the probability that a sphere within class i is of diameter x, divided by the sum of all such probabilities over the class i.

$$g(x|i) = \frac{g(x)}{\int_i g(x)dx} \qquad (3.33)$$

If g(x) is assumed to be uniform over each class i, then Eq. 3.33 reduces to

$$g(x|i) = \frac{1}{\int_i dx} = \frac{1}{\Delta_i} \tag{3.34}$$

in which Δ_i is the width of class i.

Substituting Eqs. 3.31 and 3.34 into Eq. 3.32 yields

$$P(\uparrow|i) = \frac{A}{\Delta_i V}\int_i x\, dx \tag{3.35}$$

The total number of spheres in size class i is equal to the product of the number of spheres of size i per unit volume, $N_V(i)$, and the total sample volume.

$$n(i) = N_V(i)V \tag{3.36}$$

The expected number of spheres in class i that are intercepted by the random section and therefore result in profiles on the plane surface is equal to the product of the number of spheres of size class i and the probability that a class i sphere will be intercepted.

$$n(\uparrow|i) = N_V(i)VP(\uparrow|i) \tag{3.37a}$$

$$n(\uparrow|i) = \frac{N_V(i)A}{\Delta_i} \int_i x\,dx \qquad (3.37b)$$

To determine the expected distribution of profiles on a plane surface resulting from intersected spheres, it is helpful to look first at the profile distribution obtained from the random intersection of a single sphere size, x.

The intersection of a sphere with a random plane will result in a circular profile of size y that is dependent on the position of intersecting plane with respect to the center of the sphere. This position is designated as z in Fig. 3.9. Expressing the resulting profile diameter in terms of the sphere diameter and intersection position gives

$$y = 2\sqrt{x^2/4 - z^2} \qquad (3.38)$$

The probability that a profile of diameter $y \pm dy/2$ will result from a random intersection of sphere of diameter x, $f(y|x)dy$, is equal to the ratio of the range of intersection positions 2dz, that will result in a profile diameter of $y \pm dy/2$, to the total range of all possible intersection positions, which is the sphere diameter, x.

$$f(y|x)dy = \frac{2dz}{x} \qquad (3.39)$$

Eq. 3.38 can be rearranged to express the intersection position z as, $z = \left(\sqrt{x^2 - y^2}\right)/2$.

Differentiating z with respect to the profile diameter y yields

$$dz = \frac{-y}{2\sqrt{x^2-y^2}}\,dy \qquad (3.40)$$

Changing the sign of Eq. 3.40 to give only positive probabilities, an expression for the probability density of circular profiles resulting from a random intersection of a sphere of size x, $f(y|x)$, can be obtained by substituting Eq. 3.40 into Eq. 3.39.

$$f(y|x)\,dy = \frac{y}{x\sqrt{x^2-y^2}}\,dy \qquad (3.41)$$

The probability of obtaining a profile in finite size class j from the intersection of a sphere of size x can be obtained by integrating Eq. 3.41 over the range of class j

$$P(j|x) = \int_j \frac{y}{x\sqrt{x^2-y^2}}\,dy \qquad (3.42)$$

It is next desirable to obtain the probability of obtaining a profile in size class j resulting from the intersection of a sphere in size class i. This is achieved by integrating, over the range of sphere sizes in class i, the product of the probability of obtaining a profile in size class j due to a sphere of diameter x and the probability density of truncated spheres in class i, $g(x|i\uparrow)$.

$$P(j|i) = \int_i P(j|x)\ g(x|i\uparrow)dx \tag{3.43}$$

$g(x|i\uparrow)$ is obtained by dividing the probability that a sphere of size x will be intercepted by the sum of all such probabilities over class i. Using Eq. 3.31, this becomes

$$g(x|i\uparrow) = \frac{P(\uparrow|x)\ g(x)}{\int_i P(\uparrow|x)\ g(x)dx} = \frac{\left(\frac{A}{V}\right) x g(x)}{\left(\frac{A}{V}\right)\int_i x g(x)dx} \tag{3.44}$$

As before, if it is assumed that g(x) is uniform over each class, Eq. 3.44 reduces to

$$g(x|i\uparrow) = \frac{x}{\int_i x\ dx} \tag{3.45}$$

Substituting Eqs. 3.42 and 3.45 into Eq. 3.43 gives

$$P(j|i) = \left[\int_i \left[\int_j \frac{y}{\sqrt{x^2 - y^2}} dy\right] dx\right] \left(\int_i x\ dx\right)^{-1} \tag{3.46}$$

The expected number of profiles of size class j resulting from spheres of size class i is equal to the product of the number of intersected size class i spheres, Eq. 3.37b, and the probability that an intersected class i sphere will generate a size class j profile, Eq. 3.46.

$$n(j|i) = n(\uparrow|i)\, P(j|i) \tag{3.47a}$$

$$n(j|i) = \frac{N_V(i)A}{\Delta_i} \int_i \left[\int_j \frac{y}{\sqrt{x^2 - y^2}}\, dy \right] dx \tag{3.47b}$$

The number of class j profiles per unit area resulting from class i spheres is obtained by dividing both sides of Eq. 3.47b by the area of the intersecting plane, A.

$$N_A(j|i) = \frac{N_V(i)}{\Delta_i} \int_i \left[\int_j \frac{y}{\sqrt{x^2 - y^2}}\, dy \right] dx \tag{3.48}$$

The number of profiles of size class j per unit area resulting from all spheres is obtained by summing over all sphere sizes greater than or equal to j.

$$N_A(j) = \sum_{i=j}^{s} N_A(j|i) \tag{3.49a}$$

$$N_A(j) = \sum_{i=j}^{s} \left[\frac{1}{\Delta_i} \int_i \left[\int_j \frac{y}{\sqrt{x^2-y^2}}\, dy \right] dx \right] N_V(i) \qquad (3.49b)$$

in which s is the largest size class.

Equation 3.49b can be expressed in matrix form as

$$\{N_A(j)\} = \frac{1}{\Delta_i}[C_{ij}]\{N_V(i)\} \qquad (3.50)$$

in which the C_{ij} coefficients form an upper triangular matrix. The coefficients are in units of length squared and are given as

$$C_{ij} = \int_i \left[\int_j \frac{y}{\sqrt{x^2-y^2}}\, dy \right] dx \qquad (3.51)$$

Integrating Eq. 3.51 yields

$$C_{ij} = \frac{1}{2}\begin{cases} \left[U(i)\sqrt{U(i)^2 - L(i)^2} - L(i)^2 \ln\left(\left(U(i) + \sqrt{U(i)^2 - L(i)^2}\right) / L(i)\right)\right] & (i=1,\ldots,s;\ j=i) \\ \left[U(j)\sqrt{U(j)^2 - L(i)^2} - L(i)^2 \ln\left(\left(U(j) + \sqrt{U(j)^2 - L(i)^2}\right) / L(i)\right)\right] & \\ - \left[U(j)\sqrt{U(j)^2 - U(i)^2} - U(i)^2 \ln\left(\left(U(j) + \sqrt{U(j)^2 - U(i)^2}\right) / U(i)\right)\right] & \\ + \left[L(j)\sqrt{L(j)^2 - U(i)^2} - U(i)^2 \ln\left(\left(L(j) + \sqrt{L(j)^2 - U(i)^2}\right) / U(i)\right)\right] & (i=1,\ldots,s;\ j=i+1,\ldots,s) \\ - \left[L(j)\sqrt{L(j)^2 - L(i)^2} - L(i)^2 \ln\left(\left(L(j) + \sqrt{L(j)^2 - L(i)^2}\right) / L(i)\right)\right] & \\ 0 & \text{(otherwise)} \end{cases}$$

in which U and L are the upper and lower class limits, respectively.

The more useful relationship, expressing the unknown sphere distribution in terms of the measured profile distribution is given as

$$\{N_V(i)\} = \Delta_i [D_{ij}] \{N_A(j)\} \qquad (3.52)$$

in which $[D_{ij}]$ is obtained by inverting $[C_{ij}]$.

If a constant class size, $\Delta_i = \Delta$, is used the relationship given in Eq. 3.50 can be expressed (Blodner 1984) as

$$\{N_A(j)\} = \Delta [B_{ij}] \{N_V(i)\} \qquad (3.53)$$

in which the dimensionless coefficients B_{ij} are given as

$$B_{ij} = \frac{1}{2}\begin{cases} 1 & (i = 1;\ j = 1) \\ i\sqrt{i^2-(i-1)^2} - (i-1)^2\left[\ln\left(i+\sqrt{i^2-(i-1)^2}\right)-\ln(i-1)\right] & (i = 2,\ldots,s;\ j = i) \\ j\left(\sqrt{j^2-(i-1)^2}-\sqrt{j^2-i^2}\right) & \\ -(j-1)\left(\sqrt{(j-1)^2-(i-1)^2}-\sqrt{(j-1)^2-i^2}\right) & \\ +\,i^2\left[\ln\left(j+\sqrt{j^2-i^2}\right)-\ln\left((j-1)+\sqrt{(j-1)^2-i^2}\right)\right] & (i = 1,\ldots,\ s;\ j=i+1,\ldots,\ s) \\ -(i-1)^2\left[\ln\left(j+\sqrt{j^2-(i-1)^2}\right)-\ln\left((j-1)+\sqrt{(j-1)^2-(i-1)^2}\right)\right] & \\ 0 & (i = 2,\ldots,\ s;\ j=1,\ldots,\ i-1) \end{cases}$$

The relationship of the sphere distributions in terms of the profile distribution is then given as

$$\{N_V(i)\} = \frac{1}{\Delta}[J_{ij}]\{N_A(j)\} \qquad (3.54)$$

in which $[J_{ij}]$ is obtained by inverting $[B_{ij}]$.

3.5 Examples

The methods described in Sections 3.2 and 3.3 for the correction of frame edge effects are demonstrated in this section for both lineal and areal image analysis

data. The methods described in Section 3.4 for the conversion of an areal distribution to a volume distribution are also demonstrated.

The examples include the use of experimental results as well as synthetic data. The experimental data was obtained at an actual magnification of 30.06x. For the image analysis equipment used in this study, the corresponding frame dimensions were L = 2995.2 μm and H = 2252.8 μm. These same frame dimensions were used in the edge effect correction of the synthetic data. Features are separated into individual classes based on chord length for lineal data and area equivalent diameter (AED) for areal data. For analysis purposes, all features within a class are assumed to have a size equal to the class midpoint. In an image analysis, each feature is measured in terms of the number of thresheld pixels (Section 2.3). In a lineal analysis, this is equivalent to discrete units of pixel length. It is therefore important, for accurate data classification, that the individual class widths be in increments of pixel length. In an areal analysis, features measured in terms of numbers of pixels is equivalent to discrete units of pixel area. Because areal features are classified in terms of AED (Eq. 3.15), the individual class limits are related to the square root of the number of pixels. As such, the class limits, in an areal analysis, will not be in exact units of pixel area.

Features measured in an image analysis of air-entrained concrete can range in size from a single pixel to an entire image frame. An actual distribution of measured features is typically a continuous function over this range. Representing this continuous function as a histogram of discrete size classes results in some distortions. Using a small class width can help minimize these distortions but requires the use of a large number of classes. Examples are presented in which the size of the

individual classes and the number of classes used to represent a given distribution are varied.

While the potential range of feature sizes is large, most of the measured features from a typical air-entrained concrete specimen, at a magnification of 30x, are of the smaller sizes. If a small class size is used, the larger size classes will often contain only a small number of features or no features at all. The small number of features in the larger classes can be ignored by truncating the distribution at an arbitrary chord length. This allows for a small class size to be used while, at the same time, minimizing the number of classes. Examples are presented in which the distribution of chord lengths is truncated at progressively smaller chord lengths. This is accomplished by holding the class size constant while the number of classes used to represent a given distribution is reduced.

Lineal Edge Correction.– The edge correction procedure for lineal data is developed in Section 3.2 by first obtaining the relationship between a distribution of known chord lengths, $\{N_L(i)\}$, and the expected distribution of measured chord lengths, $\{N_L(j)^*\}$, in the image analysis of a plane surface. The measured chord length distribution will be affected by edge effects. The coefficients relating $N_L(j)^*$ to $N_L(i)$ are expressed in matrix form as $[K_{ij}]$ in Eq. 3.13. An example $[K_{ij}]$ coefficient matrix is given in Table 3.1 for data which is split into 20 classes. For this particular example, a constant class width of 29.25 μm (five pixels) is used. As noted in Section 3.2, the off diagonal K_{ij} coefficient terms are constant for a given class width and magnification. Table 3.2 shows the calculated distribution of measured chords for a true chord distribution consisting entirely of one chord per cm in size class 20. It can be seen that the chords in class 20 contribute measured

chords to all size classes of 20 or less. The calculated number of measured chords in class 20 represents those chords in class 20 which either are not intersected by a frame edge or, if intersected, have a measured length within the size limits of class 20. The calculated number of measured chords assigned to classes smaller than 20 represent those chords in class 20 which have been intersected by a frame edge and have a resulting measured length within the size limits of the class to which they are assigned. The summation of the expected number of measured chords per unit length in all classes is equal to 1.76, which means that, unless the edge effects are accounted for, the actual chord density will be overestimated by 76%.

The coefficients relating a true distribution of chord lengths, $\{N_L(i)\}$, corresponding to a measured chord length distribution, $\{N_L(j)^*\}$, are expressed in matrix form as $[\alpha_{ij}]$ in Eq. 3.14. The α_{ij} coefficients are obtained by inverting the K_{ij} coefficients. An example $[\alpha_{ij}]$ coefficient matrix for data split into 20 classes, of 29.25 μm width, obtained by inverting $[K_{ij}]$ in Table 3.1 is given in Table 3.3. A hypothetical measured distribution consisting of 10 chords per cm in each of 20 classes is used to demonstrate the use of Eq. 3.14 to determine the corresponding true chord distribution. The hypothetical distribution, along with the calculated true distribution, is shown in Table 3.4. It can be seen that, compared to the measured distribution, the calculated true distribution has a reduced number of chords per unit length in the smaller size classes and an increased number of chords in the larger size classes. Also, the calculated total number of chords per unit length is reduced to 180 from the measured value of 200, while the average chord length is increased to 324 μm from 293 μm. This is consistent with the observation made during the development of the edge correction procedure, i.e. that larger chords are

more likely than smaller chords to be intersected by the frame edges and thus more likely to produce measured chord lengths which are smaller than the true lengths. This results in a measured distribution that underrepresents the larger chords and overrepresents the smaller chords.

The lineal image analysis data for mix 8 (Chapter 2) is used to demonstrate the edge effect correction method for an air entrained concrete sample. The data has been classified into 80 classes, each with a size range of 29.25 μm. Chord lengths up to 2340 μm are considered in this classification, which includes 99.9% of the chords measured on this particular specimen. The 0.1% of measured chords which are larger than 2340 μm are ignored. The measured data and the results after correction for edge effects are presented in Table 3.5 in terms of both the number of chords and the number of chords per unit length. The general trend observed in the previous example, decreased numbers of features in the smaller classes and increased numbers in the larger classes after correction for edge effects, is seen. The total density of chords decreases from 3.25 chords per cm in the measured distribution to 3.07 chords per cm in the true distribution, while the average chord length increases from 159.5 μm to 168.4 μm

The effect of changing the class size can be investigated by varying the number of classes used to represent a distribution while keeping the total range of chord lengths constant. The results of analyzing the mix 8 data using class sizes of 58.5 μm, 117.0 μm, and 234.0 μm, representing 40, 20, and 10 classes, respectively, are presented in Tables 3.6, 3.7, and 3.8. The coefficient matrix $[K_{ij}]$ and its inverse, $[\alpha_{ij}]$, for the example using 20 classes of size 117.0 μm are given in Tables 3.9 and 3.10. A summary of the results obtained for the different class size

analyses is given in Table 3.11.

The air content and average chord length steadily increase with increasing class size. As the class size is increased from 29.25 μm to 2340.0 μm, the air content from the measured distribution increases from 5.18% to 6.19% and the average chord length increases from 159.5 μm to 190.8 μm. These increases result from the assumption that the distribution is uniform within each class. Since the number of features in an air-void distribution decreases with size, increasing the class width in this case results in a systematic overestimation of feature size. The reverse would be true if the distribution were skewed toward the larger sizes. These distortions in the measured distribution are similarly reflected in the calculated true distributions. It is interesting to note that the Powers spacing factor, calculated from the true distributions, is little affected by the increase in class width, only increasing from 159 μm to 160 μm as the class size is increased from 29.25 μm to 234.0 μm. This lack of change occurs because, for this sample, the paste to air content ratio (P/A) is less than 4.33 in all cases, which results in the use of Eq. 1.1 to calculate the spacing factor. Substituting $\alpha = 4/\bar{l}$ into Eq. 1.1 gives $\bar{L} = (P/4)(\bar{l}/A)$. The term (P/4) is constant for a particular specimen, so the spacing factor is a function of the ratio $(\bar{l}/A)$, which remains almost constant as the class size is increased. If P/A exceeded 4.33, Eq. 1.2 would be used to calculate the spacing factor, and the resulting value would show a greater increase with increasing class size.

The consequences of ignoring the relatively small number of features in the larger size classes is investigated by keeping the class size constant while decreasing the number of classes. The results of the edge effect correction method using the

smallest 40, 20, and 10 classes of the 80 class (class size = 29.25 μm) data are presented in Tables 3.12, 3.13, and 3.14, respectively. The percentage of the measured chords included in the different analyses is 99.3% for 40 classes, 97.0% for 20 classes, and 85.0% for 10 classes. A summary of the results for analyses of the truncated distributions is presented in Table 3.15.

Reducing the number of classes from 80 to 40 has a relatively modest impact on the results. The air content decreases from 5.18% to 4.84%, a 7% reduction, and the average chord length decreases from 168.4 μm to 158.0 μm, a 6% reduction. At the same time, the Powers spacing factor remains unchanged at 159 μm. Further reducing the number of classes to 20 causes the air content and average chord length to drop to 4.26% and 141.7 μm, respectively, but the Powers spacing factor changes only from 159 μm to 158 μm, less than a 1% reduction. Considering only the 10 smallest classes has a significant impact on the results. The air content drops to 2.72%, while the average chord length and spacing factor decrease to 102.0 μm and 139 μm, respectively.

It is common practice, in a manual linear traverse of air-entrained concrete, for chords longer than 1000 μm to be ignored (equivalent to retaining the smallest 35 classes in the current example). The rationale most often given for doing so is that air voids with diameters greater than 1000 μm are considered to be entrapped air rather than entrained air voids. While the contribution of entrapped air to the total air content is significant, the contribution to frost durability is considered negligible. Truncating the distribution at this arbitrarily defined break point, between entrapped and entrained air, does not entirely remove the contribution of entrapped air voids to the analysis. This is because these larger voids contribute

measured features to all size classes smaller than or equal to the diameter of the void. Because the measured numbers of these larger voids is typically very small in an air-entrained sample, the inclusion of these chords in the smaller classes is not significant. The practice of truncating the distribution at 1000 μm can have a significant effect on the measured air content but only a minor impact on the value of the Powers spacing factor, the most commonly used measure of frost durability.

Areal Edge Correction.– The edge correction procedure for areal data is developed in Section 3.3. A relationship is obtained between a known distribution of circular profiles, $\{N_A(i)\}$, and an expected measured distribution of area equivalent diameters, $\{N_A(j)^*\}$. The coefficients relating an expected measured distribution to a known true distribution are expressed in matrix form as $[M_{ij}]$ in Eq. 3.28. An example $[M_{ij}]$ coefficient matrix is given in Table 3.16 for data which is split into 20 classes, each 25 μm in width. Table 3.17 shows the calculated AED size distribution for an areal analysis of a true distribution consisting entirely of one circular profile per cm^2 in size class 20. Circular profiles in size class 20 contribute to measured features in all size classes of 20 or less. The calculated number of features in size class 20 represents those circular profiles in class 20 that either are not intersected by a frame edge or, if intersected, have a measured AED within the limits of class 20. The calculated number of measured features assigned to classes smaller than 20 represent those features in class 20 which have been intersected and have a resulting AED within the size limits of the class to which they are assigned. The summation of the expected number of measured features per unit area in all classes is 1.41, which is 41% greater than the true value of 1.0. Also, the mean feature diameter of the measured features is 387.3 μm compared to 487.5

μm (midpoint of class 20).

The coefficient matrix $[M_{ij}]$ can be inverted to obtain the coefficients N_{ij} for use in Eq. 3.29 to estimate a true size distribution of circular features corresponding to a measured distribution. The N_{ij} coefficients obtained from inverting $[M_{ij}]$ in Table 3.16 are given in Table 3.18.

A hypothetical distribution of measured AEDs consisting of 10 features per cm^2 in each of 20 classes is used to demonstrate the use of Eq. 3.29 to calculate the corresponding true feature distribution. This hypothetical distribution along with the calculated true distribution of circular features is shown in Table 3.19. As expected, after correction for edge effects, the feature density decreases in the smaller size classes while increasing in the larger size classes. Also, the total numerical density of features decreases from 200.0 per cm^2 in the measured distribution to 162.3 per cm^2 in the calculated true distribution. These changes result in the average diameter increasing from 250.0 μm to 283.4 μm, a 13.4% increase.

The areal image analysis data for mix 8 is used to demonstrate the areal edge effect correction method for an air-entrained concrete sample. The data has been classified into 80 classes, each 25 μm in width. Measured features with an AED up to 2000 μm are considered in such a classification, which includes all but one feature measured on this particular specimen (that feature would be in class 104, if the classes went that far). The measured data, along with the results after correction for edge effects, are presented in Table 3.20, both in terms of the number of features and the number of features per unit area.

In the smaller size classes, the feature density is reduced after edge

correction, while in the middle and larger classes, the effect of edge correction is not as clear. Some classes increase while others decrease, and some classes even have negative values. The reason for this apparently erratic behavior is due to the fact that the number of features in the middle to larger size classes is quite small compared to the number in the smaller size classes. Some of the larger size classes contain no measured features. The surface area surveyed on this particular sample is thus not large enough to provide a statistically valid sampling of features in individual classes with an AED greater than about 600 μm. For the sample surface area surveyed, the number of features in many classes would be more correctly represented by non-integer values. It is obvious that a negative number of features cannot truly exist. The mathematical correctness of the procedure is evident, however, since the air content obtained from the calculated true size distribution, including negative values, is equal to that obtained from the measured distribution, to three significant figures. The minor difference in the air contents for the two distributions is due to assumption that the distributions are uniform within each class. As demonstrated next, as the number of classes is reduced and the class size increased, the differences in air contents for the measured and true distributions also increases.

The effect of changing the class width is investigated by varying the number of classes used to represent a distribution, while keeping the total range of feature sizes constant (0 to 2000 μm). The results of analyzing the mix 8 data using class sizes of 50 μm, 100 μm, and 200 μm, representing 40, 20, and 10 classes, are given in Tables 3.21, 3.22, and 3.23, respectively. A summary of the results for the different class size analyses is given in Table 3.24.

Because it is assumed that the distribution is uniform within each class, increasing the class width increases the difference between the idealized distribution and the actual distribution. These differences can be seen by the changes in the value of the air content obtained from the measured data. The air content increases from 5.30% for 80 classes 25 μm in width to 6.95% for 10 classes 200 μm in width. Increasing the class width also causes a difference in the value of air content calculated before and after correction for edge effects. With 80 classes, the air content obtained from the measured data and the edge effect corrected data are essentially the same, 5.30% and 5.29%, respectively, whereas with 10 classes 200 μm wide, the air content changes from 6.95% to 6.64% with correction for edge effects. The average profile diameter obtained from the measured data also becomes larger with increasing class width, changing from 84.7 μm to 129.6 μm as the class size increases from 25 μm to 200 μm. This dramatic increase occurs because the smallest classes contain the largest numbers of features. With all of the features in a class treated as if they have a diameter equal to the class midpoint, increasing the class width increases the assumed size of these features in the smallest classes. The Powers spacing factor, calculated from the corrected distributions, decreases with increasing class size, from 182 μm, using a class width of 25 μm, to 121 μm, using a class width of 200 μm. The magnitude of the increases in the various parameters with increasing class width is similar to that observed in the lineal analysis of the same specimen. Because of these distortions in the distribution caused by increasing class width, it is desireable to use a small class size.

As with the lineal analysis, the number of features in the larger size classes is typically small in an areal analysis of air-entrained concrete at a magnification of

30x. The consequences of ignoring this small number of larger features is investigated by truncating the measured distribution at progressively smaller feature sizes. This is accomplished by keeping the class size constant while disregarding an increasing number of the larger size classes. The results of the edge effect correction using the smallest 40, 20, and 10 classes, of the original 80 classes of 25 μm are presented in Tables 3.25, 3.26 and 3.27, respectively. The percentage of the total number of measured features considered in the different analyses is 99.9% for 40 classes, 98.9% for 20 classes, and 92.6% for 10 classes. A summary of the results from analyses of the truncated distributions is presented in Table 3.28.

Because the class size (25 μm) is small for these analyses, the air content obtained from the calculated true distributions is essentially equal to that obtained from the measured distributions, in all cases. The air content significantly decreases as more features are ignored, decreasing from 5.30% for 80 classes to 1.75% for 10 classes. This drop in air content results because the larger features, while few in number, represent a major portion of the total air content. The calculated number of circular features per unit area and the average feature diameter, after correction of edge effects, are plotted against the number of classes in Figs. 3.10 and 3.11, respectively, and are seen to be affected less than the total air content by the truncation of the distribution. The total feature density using 40 classes, 317.85 per cm^2 is almost identical to that obtained using 80 classes, 317.89 per cm^2, while the average feature diameter decreases only 1% using 40 instead of 80 classes, from 84.5 μm to 85.3 μm. The Powers spacing factor is the same, 182 μm, using either 80 or 40 classes, but decreases as more classes are ignored, down to 176 μm and 158 μm, using 20 and 10 classes, respectively. As

such, with the exception of the air content, these parameters are reasonably calculated considering only the first 40 classes of data (0 - 1000 μm range).

Area to Volume Conversion.–The conversion of a distribution of circular profiles to a volume distribution of spheres is presented in Section 3.4 by first obtaining a relationship between a known size distribution of spheres within a volume, $\{N_V(i)\}$, and the distribution of circular profiles, $\{N_A(j)\}$, expected on a random plane intersecting that volume. The inverse of this relationship is then used to predict the volume distribution of spheres corresponding to a measured distribution of circular profiles. To use this procedure, measured circular profile data from the image analysis of a plane surface must first be corrected for edge effects, as described in Section 3.3.

The coefficients relating a known distribution of spheres to an expected distribution of circular profiles is expressed in matrix form as $[B_{ij}]$ in Eq. 3.53. An example $[B_{ij}]$ coefficient matrix is given in Table 3.29 for 10 classes of data. These coefficients are dimensionless and are not dependent on the class size or the magnification used to obtain the measured data. The only requirement is that the class width be the same for all classes.

The procedure for predicting the expected distribution of circular profiles, $\{N_A(j)\}$, resulting from a plane intersecting a given volume distribution of spheres, $\{N_V(i)\}$, is demonstrated by using a dispersion of spheres of a single size. A classification system consisting of 10 classes, each 0.2 μm in width is used. The hypothetical sphere distribution contains 1000 spheres per mm^3 in class 10. Using the B_{ij} coefficients of Table 3.29 in Eq. 3.53, the size distribution of circular profiles expected on an intersecting random plane surface is given in Table 3.30 and

plotted in Figure 3.12. Spheres of class 10 size are seen to contribute circular profiles in decreasing amounts to all size classes of 10 or less.

The coefficient matrix $[B_{ij}]$ can be inverted to obtain the coefficients J_{ij} for use in Eq. 3.54 to predict a distribution of spheres, $\{N_V(j)\}$, corresponding to a distribution of circular profiles, $\{N_A(i)\}$ obtained from a plane surface. The J_{ij} coefficients obtained from inverting $[B_{ij}]$ in Table 3.29 are given in Table 3.31. A synthetic example developed by Cruz-Orive (Weibel 1980, pg. 203) is used to demonstrate the use of the area-to-volume conversion method. Table 3.32 shows the generated synthetic distribution of circular profiles, along with the true distribution of spheres, each divided into 10 classes of 0.2 μm width. The volume distribution of spheres corresponding to this distribution of profiles, calculated using the J_{ij} coefficients of Table 3.31 in Eq. 3.54, is also shown. The calculated distribution of spheres is very close to the true sphere distribution. The calculated total sphere density of 99.23 x 10^6 per mm^3 is nearly identical to the true value of 99.05 x 10^6, and the calculated average sphere diameter is the same as the true value, 1.05 μm. The calculation tends to underestimate the true value of sphere density in the lower and upper classes, while slightly overestimating the true value in the middle classes. The calculated volume percentage of spheres, 7.58%, is only slightly less than the true value of 7.67%.

Profile data obtained from the areal image analysis of mix 8 is used to demonstrate the calculation of the corresponding volume distribution of air voids. The distribution of measured profiles, corrected for edge effects, and the calculated distribution of spherical air voids are both shown in Table 3.33 for 80 classes of 25 μm.

In this example, the total calculated number of spheres per unit volume, 102348, is 3 orders of magnitude greater than the total number of profiles per unit area, 318. The air content obtained from the sphere distribution, 5.26%, is slightly less than that obtained from the profile distribution, 5.29%. The calculated numerical density of spheres, N_V, in the middle to upper size classes is seen to appear erratic and in some cases even negative. Blodner et. al (1986) noted similar behavior in a comparative study of non-parametric stereological methods using simulated distributions. They noted that negative N_V values are generally balanced by adjacent classes which tend to overestimate the true value. These 'waves' are the result of the deterministic nature of the relationship between spheres and profiles. An actual volume distribution of spherical voids intersected by a random plane would yield non-integer theoretical densities for circular profiles. Thus, measured circular profile data with small numbers or no features in some classes cannot accurately represent the true values. The distortions in the N_A distribution created by similar effects in the edge effect correction procedure are amplified by the subsequent estimation of the volume distribution. In a typical air-void analysis, the majority of features are in the smaller size classes and the calculation of the total number of features per unit volume and the average size parameters are not sensitive to the presence of these 'waves' in the distribution.

The effect of varying the class size is investigated for mix 8 by changing the number of classes while keeping the range of feature sizes constant (0 - 2000 μm). The results of the area-to-volume conversion for mix 8 using class sizes of 25 μm, 50 μm, 100 μm, and 200 μm, representing 80, 40, 20, and 10 classes, are given in Tables 3.33, 3.34, 3.35, and 3.36, respectively. A summary of the results of the

different class size analyses is given in Table 3.37.

The calculated total number of voids per unit volume decreases and the average void diameter increases as the class size increases. This shift in the void size distribution in the direction of the larger sizes, combined with a decrease in numerical density, causes the air content calculated from the volume distribution to remain almost constant up to a class width of 100 μm. The Powers spacing factor (Eqs. 1.1 and 1.2) calculated using a paste content of 19.5% decreases only slightly, from 181 μm to 180 μm, as the class size changes from 25 μm to 50 μm. A more significant decrease in Powers spacing factor occurs as the class size increases above 50 μm, dropping to 168 μm and 152 μm for class widths of 100 μm and 200 μm, respectively.

It is useful to compare the results in Table 3.37 with those for the areal analysis edge correction in Table 3.24. The comparison shows that conversion to a volume distribution gives final values of air content and spacing factor that are less sensitive to class size than obtained with the areal analysis. For example, the area-to-volume conversion yields a nearly constant air content up to a class size of 100 μm, changing only from 5.26% to 5.25%, and an increase to only 5.69% for a class size of 200 μm. In comparison, the areal analysis yields an increase from 5.29% at 25 μm to 5.55% at 100 μm and 6.65% at 200 μm. Changes in the Powers spacing factor obtained from the volume distribution are relatively small compared to those from the areal analysis, which produces values of 182 μm, 175 μm, 156 μm, and 121 μm for the four class sizes. Since both sets of results are based on the same data, these results strongly suggest that a volume analysis is always preferable to an areal analysis for accuracy, since it produces results that are much less sensitive to

class size.

In this example, the Philleo factor (Eq. 1.3), which is inversely proportional to the cube root of the numerical density of spheres, increases in value as the class size increases. The Philleo factor increases from 99 μm for a class width of 25 μm to 108 μm for a class width 50 μm. The Philleo factor further increases to 127 μm and 153 μm with class widths of 100 μm and 200 μm, respectively. For this particular example the air content and Powers spacing factor are accurately calculated with a class size up to 50 μm.

The consequences of ignoring the small number of features in the larger size classes is investigated by truncating the distribution at progressively smaller feature sizes. This is accomplished by keeping the class size constant at 25 μm while disregarding an increasing number of the larger size classes. The results of the area to volume conversion for the smallest 40, 20, and 10 classes, of 25 μm width, are presented in Tables 3.38, 3.39, and 3.40, respectively. A summary of the results from the truncated analyses is provided in Table 3.41.

Because most of the features are located in the smaller size classes, progressively truncating the larger classes has little effect on the calculated volume density of features, which is calculated at 102348 per cm^3 using 80 classes and 102395 per cm^3 using 10 classes. The average sphere diameter decreases from 31.1 μm to 30.9 μm as the number of classes decreases from 80 to 20, and to 29.3 μm for 10 classes. The Powers spacing factor decreases only slightly, from 181 μm for 80 classes to 178 μm for 20 classes, but decreases to 160 μm for 10 classes. The Philleo factor increases from 99 μm for 80 classes to only 105 μm for 20 classes, but increases to 120 μm for 10 classes. The results obtained here closely match

those obtained using the areal analysis (Table 3.28), indicating that the two methods of analysis have a similar sensitivity to truncating the larger size classes.

For air-entrained concrete samples, where most of the features are in the smaller size classes, ignoring the small numbers of features in the larger size classes has a significant impact on the volume percent calculations, but only a minor impact on the Powers spacing factor and the Philleo factor. The practice of ignoring measured features greater than 1000 μm (class 40) seems reasonable if the objective of the analysis is to calculate these traditional void spacing factors. This point is further illustrated in Table 3.42 for the ten samples analyzed in this study. The table gives the Powers and Philleo factors for the samples imaged at 12x and 30x and analyzed using the smallest 85 and 40 25 μm classes. The non-air-entrained mixes, 1 and 2, are greatly affected by truncating the larger size classes, producing decreases in the Powers factor of 8.6 to 16.8 percent (note, the fact that the Powers spacing factor decreases, rather than increases, is an anomaly and is discussed in Chapter 1). The other mixes show changes ranging from -5.5% to +2.1%, with changes of less than 2% in most cases. The Philleo factor increases by 4.2% and 4.5% at 12x and by 2.6% and 5.5% at 30x for samples 1 and 2, respectively. The other mixes show increases ranging from 0.9 to 3.3 percent, with most of the increases at 2.0 percent or less.

CHAPTER 4

DATA EVALUATION

4.1 Introduction

In this chapter, the results of the lineal and areal image analyses of the specimens described in Chapter 2 are summarized. Both the lineal and areal experimental data are corrected for edge effects using the procedures developed in Sections 3.2 and 3.3, respectively. The corrected areal data is then used to obtain a size distribution of spherical air-voids using the procedures developed in Section 3.4.

The Powers spacing factor is calculated, for each sample, from the chord, profile, and sphere distributions. The Philleo factor is also calculated from the sphere distributions. These void spacing parameters, along with the Powers spacing factor obtained from the manual modified point count, are compared to each other and with the results of the surface scaling tests.

The differences between the air-void size distributions for the various air-entraining admixtures are studied by comparing the cumulative percent of total air content as a function of feature size.

4.2 Data Analysis

Lineal Analysis.–The measured chord data for each sample obtained from the 480 line/frame lineal analysis is classified into 85 classes of constant size. Because of the digital nature of the data collection, each chord length is measured in terms of discrete increments of pixel length. It is therefore important for accurate size classification that the individual class widths be in increments of the actual

pixel length. The class sizes used in this study are 29.41 μm for the 12x magnification (11.96x actual) and 29.25 μm for the 30x magnification (30.06x actual). The number of chords in each class is divided by the total length of the test line (number of frames x 480 x frame width) in order to obtain the numerical chord density in number of chords per unit length of test line (chords/cm). The measured lineal data is corrected for edge effects using the procedures described in Section 3.2. The measured lineal data along with the edge effect corrected data is given in Appendix C for all ten specimens at both magnifications.

A summary of the lineal analysis results is given in Table 4.1. For each sample, the total number of chords per cm of test line in all classes is given as measured and after correction for edge effects. Also given is the percentage change. At a magnification of 12x, the overestimation of total chord density due to edge effects varies from a low of 1.4% for mix 6 to a high of 3.3% for mix 2, with the average for all samples being 2.3%. At a magnification of 30x, the overestimation varies from a low of 3.2% for mix 5 to a high of 6.7% for mix 2, with the average for all samples being 5.0%. The total chord densities for each specimen, before and after correction for edge effects, are plotted in Figs. 4.1 and 4.2 for magnifications of 12x and 30x, respectively. General agreement in the numerical values between the two magnifications is seen, along with larger changes at the higher magnification between values after correction for edge effects. For the most part, the densities are somewhat higher for the higher magnification, presumably because of the larger number of small features that can be observed at 30x compared to 12x. The cumulative effect of the frame edge effect can be seen in a typical plot of the cumulative chord density, as measured and after correction for edge effects, versus

chord length in Fig. 4.3.

Areal Analysis.–The areal data is measured in terms of discrete units of pixel area, but is classified by area equivalent diameter (Eq. 3.15). Because the class size is related to the square root of the number of pixels, the class limits will not be in exact units of pixel area. A class width of 25 μm was found (Sec. 3.5) to yield satisfactory results and is used to classify the measured areal data in this study. The number of features in each size class is divided by the total survey area of the sample (frame area x number of frames) to obtain the numerical density of features expressed as the number of features per unit area (features/cm^2). The measured areal analysis data is corrected for edge effects using the procedures developed in Section 3.3. The measured areal data along with the corrected results are given in Appendix D for each sample at both magnifications.

A summary of the areal analysis results is given in Table 4.2. For each sample, the total number of profiles per cm^2 in all classes is given as measured and after correction for edge effects, along with the percentage change. At a magnification of 12x, the overestimation due to edge effects of the total feature density varies from a low of 2.4% for mix 6 to a high of 4.4% for mix 10, with an average of 3.3%. At a magnification of 30x, the overestimation varies from a low of 3.3% for mix 10 to a high of 7.9% for mix 7, with an average of 5.9%. Total specimen feature densities before and after correction are plotted in Figs. 4.4 and 4.5 for magnifications of 12x and 30x, respectively. While there is general agreement between the two magnifications in terms of the relative differences between samples, the values at a magnification of 30x are, for all samples, significantly greater than those obtained at a magnification of 12x. This is due mainly to the differences in the

number of profiles measured in the smallest size class. At a magnification of 12x, many of the smallest size features are not measured due to low end resolution limits of the imaging equipment. The cumulative effect of the frame edge effect can be seen in a typical plot of the cumulative profile density, as measured and after correction for edge effects, versus feature diameter in Fig. 4.6. The smaller size classes can be seen to contain a large percentage of the total features.

Two-Dimensional to Three-Dimensional Conversion.–The results of the conversion of the corrected areal image analysis data to a distribution of spherical air voids is given, along with the areal data, in Appendix D for each sample at both magnifications. While the range of sizes of the air voids is large, most of the air voids are in the smaller size classes. For the samples used in this study, over 99% of all air voids are in the first 15 size classes, representing air voids up to 375 μm in diameter. The calculated numerical density of spherical air voids (voids/cm^3) for the first 15 classes of all samples is given in Tables 4.3 and 4.4 for magnifications of 12x and 30x, respectively. Also given for each sample is the total density in voids/cm^3 for air voids in all 85 classes. At a magnification of 30x, the average total void density for the different air-entraining admixtures is 110,144 voids/cm^3 for the vinsol resin, 113,444 voids/cm^3 for the multicomponent, and 76,451 voids/cm^3 for the cocamide DEA samples. These values compare to values of 61,788, 74,484, and 28,095, respectively, obtained at a magnification of 12x, and values of 18,182 and 44,744 for the non-air-entrained samples at 12x and 30x respectively. The highest total void density measured at 30x (mix 4) is equivalent to 97 billion air voids per cubic yard of concrete.

The differences between the calculated void densities at the two magnifications

are primarily the result of significantly fewer voids at 12x in the first class, which represents voids from 0 to 25 μm in diameter. This difference can be seen in Fig. 4.7, where the volume density of voids for the first 15 classes at both magnifications is plotted against class for mix 6.

4.3 Air-void Parameters

Average Feature Measures.–The average feature size is a convenient method to characterize the measured air-void system. The average feature sizes for the ten samples used in this study are presented in Table 4.5 for magnifications of both 12x and 30x. The average chord length is obtained from the corrected results of the 480 line/frame lineal image analysis. The average circular profile diameter is obtained from the corrected results of areal image analysis. The average air-void diameter is obtained from the results of the stereological conversion of the corrected profile data to a volume distribution of spherical air-voids.

It is interesting to note that for every sample, the average chord length is larger than the average profile diameter, which in turn is larger than the average air void diameter. This relationship may at first appear to be contradictory. When sampling a system of circular profiles on a plane surface with a random test line, it would seem reasonable to anticipate the average linear intercept to be smaller in size than the average profile diameter. This would be the case if the profiles being sampled all had the same diameter. However, with a dispersion of different profile sizes, the larger profiles have a higher probability of being intercepted by the random test line. It is therefore reasonable, for such a dispersion, that the average linear intercept length will be larger than the average diameter of the entire system of profiles. In a lineal analysis where a large number of closely spaced test lines is

used, as in the 480 lines/frame lineal analysis, the same result is possible. In such a systematic sampling scheme, all features are expected to be sampled but, the number of times each feature will be intercepted will be in proportion to its diameter. Thus again, the larger diameter profiles have a greater influence on the calculation of the average intercept length than the smaller diameter profiles.

Similar reasoning can be used to understand the relationship between the average profile diameter and the corresponding average sphere diameter. A random test plane intercepting a volume containing a system of spherical voids (or solids) will result in a deterministic system of circular profiles. If the spheres are all of the same diameter, the average diameter of the resulting profiles will be smaller than that of the spheres. However, if the system of spheres represents a range of different sizes, then the larger spheres have a greater probability of being intercepted by a random test plane. The larger spheres therefore contribute to the number of profiles on the test plane in greater proportion than their numbers.

The average chord length, profile diameter, and sphere diameter are always significantly larger at a magnification of 12x than at 30x. This is because of the lower resolution limit at the lower magnification, which causes many features in the smallest class to go undetected. For each sample, the proportion of the total features (from the chord, profile, and sphere distributions) verses feature size is plotted for each sample in Figs. 4.8 to 4.17 for magnification 12x, and in Figs. 4.18 to 4.27 for magnification 30x. The lack of features in the smallest class is clearly evident in the 12x plots. Also evident is a progressive shift to the smaller feature sizes in the distributions going from the lineal to areal to volume data. This is consistent with the observation that the average chord length is larger than the average profile

diameter, which in turn, is larger than the average air-void diameter.

Frost durability Measures.–The Powers spacing factor is currently the most widely used parameter for measuring the frost durability of air-entrained concrete. The Powers spacing factors for the ten mixes used in this study are calculated using the results of the different microscopic examinations. From Eqs. 1.1 and 1.2 it can be seen that the total air-void specific surface is used to characterize the air-void system in calculating the Powers spacing factor. The modified point count (ASTM C 457-82a) and the lineal image analysis methods use the mean chord length in estimating the total specific surface, while the areal image analysis uses both the first and second moments of the profile AED distribution. The specific surface from the calculated volume distributions is obtained directly by dividing the total area of the spherical voids by their total volume. The Powers spacing factors from the four different analyses and the Philleo factors, for a 90% protected paste, calculated from the volume distributions, are given in Table 4.6.

The Powers spacing factors for each sample obtained from the manual analysis and the magnification 30x lineal and areal image analyses are plotted in Fig. 4.28. While general agreement between the various methods is apparent, the lineal image analysis consistently yields lower values for spacing factor than does the areal image analysis. Because the Powers spacing factor is inversely proportional to the total specific surface, the lineal analysis yields a higher estimate of the air-void specific surface than the areal analysis. The reason for the consistently higher estimate of specific surface by the lineal analysis is not completely clear, but may be due to the assumption that the features being measured result from a random intersection of a volume distribution of spherical voids. If such a volume distribu-

tion were intersected by a plane, the resulting profiles on the plane surface would be perfectly circular. It is generally agreed (Cruz-Orive 1983) that profile diameters provide a better measure of circular features than do random lines intersecting the features. Also, while spheres and circles make for convenient mathematical models, the actual air voids and their resulting profiles on a plane surface clearly do not fit these idealizations. This topic is worthy of additional study.

The Powers spacing factor and Philleo factor for each sample obtained from the areal image analysis are compared in Figs. 4.29 and 4.30 for magnifications of 12x and 30x, respectively. There appears to be a close relationship between the two factors. Therefore, it is not clear that one of the factors would have any advantage over the other as a relative indicator of frost durability, at least for these test mixes.

Scaling Results.–The results of the surface scaling tests (Table 2.3) are plotted against the Powers spacing factors obtained from the manual analysis and the magnification 30x lineal and areal image analyses in Figs. 4.31, 4.32, and 4.33, respectively. In all cases, a general trend of increased surface scaling with increasing spacing factor is apparent, except for the cocamide-DEA samples from mixes 8, 9, and 10. These three samples, while having a relatively large spacing factor, exhibited very little surface scaling.

The surface scaling results are plotted against the Philleo factor obtained from the magnification 30x areal analyses in Fig. 4.34. The same trend observed with the spacing factor is apparent here. This is consistent with the close relationship between the Powers spacing factor and the Philleo factor noted above.

The total air content from the magnification 30x areal analysis is plotted

against the surface scaling results in Fig. 4.35. There is little correlation between air content and scaling performance, except for the two non-air-entrained mixes.

The total air-void density in voids/cm^3 for each sample, obtained from the 30x areal analyses, is plotted against the percent surface scaled in Fig. 4.36. The results exhibit a strong trend of increased scaling with decreased total air void density, except for the three cocamide-DEA samples which provided the lowest scaling in spite of the fact that they did not have the highest air-void densities. The higher durabilities of the cocamide DEA mixes is likely due to the greater water reducing properties of this admixture compared to the other air entraining agents, as described in Section 2.1.

The surface scaling results of mix 7 did not follow the same patterns displayed by the other cocamide DEA samples. As pointed out in Section 2.1, this is probably due to the higher bleed water accompanying the high slump, 6 3/4 in., of this sample.

4.5 Comparison of Admixtures

Roberts and Scheiner (1981) and MacInnis (1986) noted a similarity in the size distributions of measured chords in different concrete mixtures for particular air-entraining admixtures. Such a similarity implies that an admixture produces a consistent distribution of air void sizes, regardless of the total quantity of entrained air. Such a consistency could provide a basis for comparing the air void systems produced by different air entraining admixtures.

The magnification 30x data is used to study the differences between the air-void systems produced by the different air entraining admixtures used in this study. For the purposes of this comparison, the feature distributions are truncated at a size

of 1000 μm. In all cases, the features up to a size of 1000 μm represent at least 97% of the total number of features. The small numbers in the classes representing features larger than 1000 μm typically do not represent a statistically valid sample. Because of the highly random nature of the occurrence of these larger features, their inclusion tends to mask the similarities in the distributions that are readily apparent when the distributions are truncated. The cumulative percent of total air (where 100% of total air represents the air content calculated considering only features up to 1000 μm in size) versus feature size is plotted in Figs. 4.37 to 4.40, Figs. 4.41 to 4.44, and Figs. 4.45 to 4.48, for chord, profiles, and air-void distributions, respectively. The calculated void distributions show the 'waves' at the upper end of the curves discussed in Section 3.5.

Fig. 4.45 shows the cumulative percent of total air content plotted against void diameter for mixes 1 and 2. Because these samples were non-air-entrained, the air voids represent only entrapped air. The samples produce almost identical void size distributions. The contribution to total air content is seen to be almost linear with respect to void diameter. This would indicate that the larger voids, while obviously fewer in number, make a similar contribution to the total air content as do the smaller voids.

A plot of the cumulative percent air versus void size for the vinsol resin samples, mixes 3 and 4, is given in Fig. 4.46. While there are differences between the curves for these two samples, their shapes are very similar. A significantly larger percentage of the total air content is provided by the smaller voids than observed for the non-air-entrained samples.

A plot of the cumulative percent air verses void size for the multi-component

air-entrained samples, mixes 5 and 6, is given in Fig. 4.47. The two samples are seen to have very similar void size distributions, which are, also, similar in shape to the vinsol resin curves.

The cumulative percent air versus void size curves for the cocamide-DEA samples, mixes 7 through 10, are given in Fig. 4.48. These four samples represent w/c's of 0.35, 0.36, and 0.38, air contents ranging from 4.9% to 7.7%, and concrete slumps ranging from 3 1/4 in. to 6 3/4 in. Even with these significant differences, the void size distributions for these samples are nearly identical.

The average values of the cumulative percent of total air for features up to 1000 μm, for the samples representing the different air-entraining agents and non-air-entrained concrete, are plotted versus feature size in Figs. 4.49, 4.50, and 4.51 for chord, profile, and air-void distributions, respectively. As might be expected, the chord, profile and void distribution curves for each air entraining agent are similar in shape.

As seen in Fig. 4.51, of the four sample groups, the multicomponent admixture produces, on the average, a void distribution that contains the largest percentage of the total air content in the smallest feature sizes. On the average, about 50% of the total air in the multi-component samples is represented by voids with diameters smaller than 190 μm. The vinsol resin void distributions are similar to those produced by the multicomponent agent, but with a slightly smaller percentage of the total air content in the smaller void sizes. On the average, the vinsol resin samples contain about 50% of total air content in voids with diameters smaller than 210 μm. The air void distribution produced by cocamide DEA has a noticeably smaller percentage of its total air contained in the smaller size voids. The cocamide

DEA samples typically have the higher proportion of total features in the smallest size class, but also typically have a higher proportion of total features in the size classes greater than 125 μm, when compared to concrete made with the other air-entraining agents. Because the air content of a spherical void is a function of the cube of the diameter, the cocamide DEA distributions typically contain a smaller percentage of their total air in the smaller size voids, than do the other admixtures. For the cocamide DEA samples, 50% of the total air is represented by voids with diameters smaller than 360 μm. The non-air-entrained distributions show a nearly linear relationship between cumulative percent of total air and void diameter. For the non-air-entrained samples, about 50% of the sample air content, for voids below 1000 μm in size, is represented by profiles with diameters less than 500 μm.

CHAPTER 5

SUMMARY AND CONCLUSIONS

5.1 Summary

The major purpose of this study is to demonstrate the use of image analysis techniques to characterize the air-void system in hardened concrete. The experimental part of the study used a computer based image analysis system to measure individual air-void profiles on polished concrete sections. Two different measuring techniques were explored, the measurement of linear intercepts and the measurement of profile areas. Because of the finite size of the individual measuring frames many of the measured features were truncated by the edges of the viewing frames. The measured size of these truncated features is smaller than their true size, resulting in distortions in the feature size distributions. The analytical part of this study includes the development of correction techniques to eliminate the distortions in the measured data due to frame edge effects. Correction methods, based on geometric probability, are developed for both the lineal and areal distributions. The corrected areal data is also used to obtain size distributions of spherical air-voids using established stereological techniques.

Ten concrete samples were analyzed in the experimental part of the study. The samples represent air-entrained concrete made with three different air-entraining admixtures as well as non-air-entrained concrete. Surface preparation of the 3 x 6 in. test specimens, prior to microscopic examination, included polishing and contrast enhancement. A two phase standard specimen was developed for use in adjusting the video equipment to insure intersample consistency and repeatability of

measurements.

Both lineal and areal image analysis of the air-voids were made at magnifications of 12x and 30x. In addition to the total air content, feature size distributions were obtained from both types of analysis. The areal analysis also included the measurement of individual void profile perimeters for use in comparing void shapes.

Correction methods, based on geometric probability, are developed to remove the distortions in the measured data due to frame edge effects. Separate methods are developed for lineal and areal measurements. The areal analysis correction procedure is based on the assumption that the shape of the features is circular. The measured feature areas are, thus, converted to an area equivalent circular diameter. Using discrete class sizes, both correction methods are expressed in a matrix format. A matrix of coefficients is first developed, expressing an expected distribution of measured features in terms of a known distribution of features unaffected by frame edge effects. The inverse of this relationship is then used to express the true feature distribution in terms of the measured feature distribution obtained from an image analysis. The corrected areal feature distributions are used to obtain volume distributions of spherical air voids using standard stereological procedures.

Air-void parameters from the edge effect corrected image analysis results are compared to results from a modified point count, and to freeze-thaw results obtained from surface scaling tests of companion samples. The differences in the air-void systems created by the various air-entraining admixtures are studied by comparing various characteristics including; profile shape, average feature size, numerical density of features, and the cumulative percent of total air content versus feature size.

5.2 Conclusions

The findings of this report support the following conclusions.

1. Image analysis techniques offer a viable alternative to the traditional lineal traverse and modified point count methods (ASTM C 457-82a) for the characterization of the air-void system in hardened concrete.

2. Lineal and areal image analysis techniques provide similar determinations of total air content. The air contents obtained using image analysis were on the average lower by 1.15% air than the values obtained from a modified point count of the same samples.

3. Lineal image analysis, consistently provides a higher estimate of the total specific surface, and thus, a lower Powers spacing factor than does the areal analysis.

4. Image analysis results are sensitive to the quality of the sample surface preparation. The specimen surface needs to be polished to a higher degree of flatness than required in a traditional microscopic examination. Also, because of the lack of operator subjectivity in determining the location of void edges, the paste edges at the interface of voids, must be sharply defined.

5. Contrast enhancement of the polished concrete specimen surface is necessary to provide an adequate grey level separation between cement paste and the air voids.

6. A conventional flat field of view, macro lens, mounted in a reversed position, in conjunction with extension tubes and internal apertures, can be successfully used to provide distortion free video images in the magnification range of 10x to 50x.

7. A two phase standard specimen, for use in adjusting the video equipment and lighting, prior to an image analysis, is an absolute necessity for consistent and

repeatable measurements.

8. Frame edge effects skew the image analysis feature size measurements toward the smaller features, and also result in an overestimation of the total feature density. The frame edge effect correction methods, developed in this study, remove these distortions from the measured distributions. For the ten samples analyzed in this study, application of the correction method for lineal features resulted in a decrease in total chord density by an average of 2.3% and 5.0% for magnifications of 12x and 30x, respectively. Application of the correction procedure for areal features resulted in a decrease in profile density by an average of 3.3% and 5.9% for magnifications 12x and 30x, respectively.

9. For air-void distributions, the average measured chord length will be larger than the average circular profile diameter, which in turn will be larger than the average spherical void diameter. This is a result of the higher probability of larger size voids being intercepted by a random linear and planar intercept, respectively.

10. With the instrumentation used in this study, at a magnification 12x, resolution limits prevent the accurate measurement of features in the smallest size class.

11. When classifying features by size, a small class width should be used. For lineal features, the class width should be an exact increment of pixel length. A similar requirement does not seem necessary in an areal analysis. For lineal features, a class width of 29.41 μm for 12x data and 29.25 μm for 30x data was found to be satisfactory. For areal features, a class width of 25 μm was found to be satisfactory.

12. Chords with lengths greater than 1000 μm, or profile areas with an AED greater than 1000 μm are not measured often enough to provide a statistically valid

sample. The truncation of the measured feature distributions at 1000 μm can have a significant impact on the total air content calculation, but typically has a minimal impact on the calculated values of the Powers spacing factor and the Philleo factor.

13. The required number of frames which must be analyzed to obtain an estimate of the sample air content, within an acceptable range of the true value and with a specified degree of confidence, is a function of both the image magnification and the air content. The required number of image frames for a individual sample can be obtained during an analysis by continuously calculating the standard deviation of the individual frame air contents using Eq. 2.4. Frames should be analyzed until the actual number of frames exceeds the calculated required number.

14. At a magnification of 12x, a 3 x 6 in. test specimen may not be large enough to obtain an estimate of the sample air content within 0.5% air of the true value, with a confidence level of 0.95.

15. In a lineal analysis, a larger number of image frames must be analyzed when sampling at 1 line per frame than at 480 lines per frame, to obtain a sample air content estimate within a given acceptable error of the true value, with the same level of confidence.

16. The Powers spacing factor and the Philleo factor, while based on different void parameters, provide a similar relative frost durability measure.

17. Cocamide DEA has significant water reducing properties, which is believed to be the major reason that the cocamide DEA samples achieve higher 28 day compressive strengths than the vinsol resin and multicomponent admixture samples.

18. Cocamide DEA produces an air-void system in which the individual voids are typically more spherical, but fewer in number and of smaller average size, than

those produced by either vinsol resin or multicomponent admixtures. The cocamide DEA samples, in spite of having a larger Powers spacing factor, performed better in surface scaling tests than the other air-entrained samples.

19. The three air-entraining admixtures analyzed in this study, as well as the non-air-entrained samples, produced characteristic air-void systems. For features up to 1000 μm, in size, the non-air entrained samples obtain, on the average, 50% of their total air from voids smaller than 500 μm. The air entrained samples obtain, on the average, 50% of their total air from voids smaller than 210 μm, 190 μm, and 360 μm, for the vinsol resin, multicomponent, and cocamide DEA admixtures, respectively.

5.3 Future Work

1. Image analysis techniques have been shown to be an viable alternative to the currently used manual methods, but to become accepted several items still need to be addressed.

Sample preparation procedures include both surface polishing and contrast enhancement. Use of a vibrating lap for polishing will ensure a flat surface, which is difficult to obtain with a hand held specimen on a rotary lap. One significant shortcoming of the currently used contrast enhancement techniques is that the paste phase is indistinguishable from the aggregate, which prevents the measurement of paste content. Alternative contrast enhancement techniques, which provide for a grey level distinction between aggregate and paste, should be explored.

Consistency of measurements, both between different laboratories and between different equipment operators, needs to be demonstrated. An essential element in establishing this consistency is the use of a universal standard for

equipment setup. In addition to providing two distinct grey levels for adjusting video gain and contrast, a standard specimen could also provide for sizing of calibrated features to assist in the establishment of a correct threshold level.

As part of establishing which image analysis technique (lineal or areal analysis) is more appropriate, further investigation should be made of the observation made in this study, that a lineal analysis consistently provides a higher estimate of the total specific surface than does an areal analysis. This occurs in spite of the fact that both methods provide a similar estimate of total air content.

2. Development of an analytical procedure to convert lineal measurements into a volume distribution of spherical air voids is justified. The same logical sequence followed in section 3.4 could be used as a basis. In addition to being used with lineal image analysis results, such a procedure could also be used with current lineal traverse techniques when individual chord lengths are recorded.

REFERENCES

ACI Committee 201 (1977). "Guide to Durable Concrete (ACI 201.2 R-77)," *1990 ACI Manual of Concrete Practice,* 37 pp.

Amsler, D. E., Eucker, A. J., Chamberlin, W. P. (1973). "Techniques for Measuring Air-Void Characteristics of Concrete," Research Report 11, *Engineering Research and Development Bureau*, New York State Dept. of Transportation, Albany, 35 pp.

ASTM. (1978). "Standard Test Method for Air Content of Freshly Mixed Concrete by the Volumetric Method," (ASTM C 173-78) *1980 Annual Book for ASTM Standards*, Vol. 04.02, American Society for Testing and Materials, Philadelphia, PA, pp. 61-62.

ASTM. (1982). "Standard Practice for Microscopical Determination of Air-Void Content and Parameters of the Air-Void System in Hardened Concrete," (ASTM C 457-82a) *1980 Annual Book for ASTM Standards*, Vol. 04.02, American Society for Testing and Materials, Philadelphia, PA, pp. 134-141.

ASTM. (1984). "Standard Test Method for Scaling Resistance of Concrete Surfaces Exposed to Deicing Chemicals," (ASTM C 672-84) *1980 Annual Book for ASTM Standards*, Vol. 04.02, American Society for Testing and Materials, Philadelphia, PA, pp. 333-334.

ASTM. (1988). "Standard Definitions of Terms Relating to Concrete and Concrete Aggregates," (ASTM C 125-88), *1990 Annual Book for ASTM Standards,* Vol. 04.02, American Society for Testing and Materials, Philadelphia, PA, pp. 61-62.

ASTM (1989). "Standard Test Method for Air Content of Freshly Mixed Concrete by the Pressure Method," (ASTM C 231-89a), *1990 Annual Book for ASTM Standards,* Vol. 04.02, American Society for Testing and Materials, Philadelphia, PA, pp. 227-237.

Attiogbe, E. K. and Darwin, D. (1986). "Correction of Window Size Distortion of Crack Distributions on Plane Sections," *Jour. of Microscopy*, Vol. 144, Pt. 1, Oct., pp. 71-82.

Backstrom, J. E., Burrows, R. W., and Wolkodoff, V. E. (1954) Discussion of a paper by Powers, T. C., "Void Spacing as a Basis for Producing Air-Entrained Concrete," ACI Journal, *Proceedings* Vol. 25, No. 9, May, pp. 760.1-760.13.

Blodner, R., Muhlig, P., and Nagel, W., (1984). "The Comparison by Simulation of Solutions of Wicksell's Corpuscle Problem," *Jour. of Microscopy*, Vol. 135, Pt. 1, July, pp. 61-74.

Bockstiegel, G. (1972). "A New Formula Permitting Straightforward Correction of Edge Errors in Size Distribution Measurements with Linear Scanning Instruments," *Practical Metallography*, Vol. 9, No. 6, June, pp. 329-341.

Brown, L. S. and Pierson, C. U. (1950). "Linear Traverse Technique for Measurement of Air in Hardened Concrete," ACI Journal, *Proceedings* Vol. 22, No. 2, Oct., pp.1025-1039.

Browne, F. P., and Cady, P. D. (1970). "An Automated Linear Traverse Device," *Materials Research and Standards*, MTRSA, Vol. 10, No. 8, August, pp. 12-16.

Chatterji, S. and Gudmundsson, H. (1977). "Characterization of Entrained Air Bubble Systems in Concrete by Means of an Image Analysing Microscope," *Cement and Concrete Research*, Vol. 7, No. 4, Aug., pp. 423-428.

Chayes, F. (1955) "A Simple Point Counter Based on the Leitz Mechanical Stage," *American Mineralogist*, Vol. 40, No. 2, Feb., pp. 126-127.

Chayes, F. (1956) *Petrographic Model Analysis*, John Wiley & Sons, Inc., New York,, 113 pp.

Cruz-Orive, L. M., (1983). "Distribution-Free Estimation of Sphere Size Distributions Form Slab Showing Overprojection and Truncation, with a Review of Previous Methods," *Jour. of Microscopy*, Vol. 131, Pt. 3, Sept., pp. 265-290.

Darwin, D., Hong, Z., Dewey, G. R., Martin, J. L. (1990). "Microfracture of Cement-Based Materials in Compression," *Micromechanics of Failure of Quasi-Brittle Materials*, S. P. Shah, S. E. Swartz, and M. L. Wang, Eds., Elsevier Applied Science Publishers, Ltds., London and New York, pp. 62-71.

Delesse, A. (1848). "Procédé méchanique pour déterminer la composition des roches," *Ann. Mines*, Vol. 13, No. 4, pp. 379-388.

Exner, H. E. (1972) "Methods for Edge Error Correction in Lineal Analysis," *Practical Metallography*, Vol. 9, No. 7, July, pp. 383-392.

Glagolev, A. A. (1933). "On the Geometrical Methods of Quantitative Mineralogic Analysis of Rocks," *Trans. Inst. Econ. Min.*, Moscow, Vol. 59, p. 1.

Gundersen, H. J. G. (1977). "Notes on the Estimation of the Numerical Density of Arbitrary Profiles: The Edge Effect," *Jour. of Microscopy*, Vol. 111, Pt. 2, Nov. , pp. 219-223.

Gutmann, P. F. (1988a). "Bubble Characteristics As They Pertain to Compressive Strength and Freeze-Thaw Durability," *Bonding in Cementitious Composites*, S. Mindess and S. P. Shah, Eds., Materials Research Society Symposium Proceedings, Vol. 114, pp. 271-276.

Gutmann, P. F. (1988b). "Bubble Characteristics As They Pertain to Compressive Strength and Freeze-Thaw Durability," *ACI Materials Journal*, Vol. 85, No. 5, Sept.-Oct., pp. 361- 366.

Hilliard, J. E. (1968). "Measurement of Volume in Volume," Chapter 3, *Quantitative Microscopy*, McGraw-Hill Book Company, pp 45-77.

Houde, J. and Meilleur, S. (1983). "Adaptation des procédé stéréologiques à la mesure des bulles d'air et des fissures dan le béton," *Canadian Journal of Civil Engineering*, Vol. 10, No. 3, Sept. , pp. 415-428.

Hougardy, H. P. and Stienen, H. (1978). "Edge Error Correction in Digital Image Analysis," *Quantitative Analysis of Microstructures in Materials Science, Biology and Medicine*, T. L. Chermant, Editor, Practical Metallography, Special Issue No. 8, pp. 25-35.

Jensen, E. B. and Sundberg, R. (1986) "Generalized Associated Point Methods for Sampling Planar Objects," *Jour. of Microscopy*, Vol. 144, Pt. 1, Oct., pp. 55-70.

Joyce Loebl. (1981). *Image Analysis: Principles and Practice*, published by Joyce Loebl, London, England.

Klieger, P. (1978). "Air-Entraining Admixtures," Chapter 45, *Significance of Tests and Properties of Concrete and Concrete-Making Materials*, ASTM Special Technical Publications 169B, 1978, pp. 787-803.

Larson, T. D., Cady, P. D., and Malloy, J. J. (1967). "The Protected Paste Volume Concept Using New Air-Void Measurements and Distribution Techniques," *Journal of Materials*, Vol. 2, No. 1, March , p. 202-224.

Lawton, E. C. (1939). "Durability of Concrete Pavements--Experiences in New York State," ACI Journal, *Proceedings* Vol. 35, June, pp. 561-578.

Lord, G. W., and Willis, T. F. (1951). "Calculation of Air Bubble Size Distribution from Results of a Rosiwal Traverse of Aerated Concrete," *ASTM Bulletin* 177, pp. 56-61.

MacInnis, C. and Racic, D. (1986) "The Effect of Superplasticizers on the Air-Void System in Concrete," *Cement and Concrete Research*, Vol. 16, No. 3, May, pp. 345-352.

Mather, K. (1950). Discussion of a Paper by Brown and Pierson, "Linear Traverse Technique for Measurement of Air in Hardened Concrete," ACI Journal, *Proceedings* Vol. 22, No. 2, Oct., pp.1025-1039.

Mielenz, R. C., Wolkodoff, V. E., Backstrom, J. E., and Burrows, A. E. (1958). "Origin, Evolution and Effects of the Air Void System in Concrete. Part 4–The Air Void System in Job Concrete," ACI Journal, *Proceedings* Vol. 55, Oct. , pp.507-517.

Neville, A. M. (1981). *Properties of Concrete*, Pitman Publishing Inc., 779 pp.

Ozyildirim, C. H. (1978). "Distribution of Voids in Field Concrete," Report VHTRC 78-R35, *Virginia Highway and Transportation Research Council*, Charlottesville, Va., Feb., 28 pp.

Philleo, R. E. (1983). "A Method for Analyzing Void Distribution in Air-Entrained Concrete," *Cement, Concrete, and Aggregates,* CCAGDP, Vol. 5, No. 2, Winter, pp. 128-130.

Philleo, R. E. (1987). "Frost Susceptibility of High-Strength Concrete," *Concrete Durability*, ACI Special Publication SP-100, pp. 819-842.

Powers, T. C. (1945) " A Working Hypothesis for Further Studies of Frost Resistance of Concrete," ACI Journal, *Proceedings* Vol. 16, No. 4, Feb., pp. 245-272.

Powers, T. C. and Brownyard, T. L. (1947). Studies of the Physical Properties of Hardened Portland Cement Paste, Part 8, "The Freezing of Water in Hardened Portland Cement Paste," ACI Journal, *Proceedings* Vol. 18, No. 8, April, pp. 933-969.

Powers, T. C. (1949). " The Air Requirement of Frost-Resistant Concrete," Highway Research Board, *Proceedings*, Vol. 29, pp.184-211.

Powers, T. C. (1954). "Void Spacing as a Basis for Producing Air-Entrained Concrete," ACI Journal, *Proceedings* Vol. 25, No. 9, May, pp. 741-760.

Powers, T. C. (1956). "Resistance of Concrete to Frost at Early Ages," *Proceedings*, RILEM Symposium on Winter Concreting, Danish National Institute of Building Research, Copenhagen, pp. C1–C47. Also, *Research Bulletin* No. 71, Portland Cement Association, Skokie, Illinois.

Powers, T. C. (1975). "Freezing Effects in Concrete," *Durability of Concrete*, ACI Special Publication SP-47-1, pp. 1-12.

Rexford, E. P. (1947). Discussion of a paper by Verbeck, G. J., "The Camera Lucida Method for Measuring Air Voids in Hardened Concrete," ACI Journal, *Proceedings* Vol. 18, No. 9, May, pp. 1025-1039.

Roberts, L. R. and Scali, M. J. (1984). "Factors Affecting Image Analysis for Measurement of Air Content in Hardened Concrete," *Proceedings*, Sixth International Conference on Cement Microscopy, Albuquerque, N.M., pp. 402-419.

Roberts, L. R., and Scheiner, P. (1981) "Microprocessor Based Linear Traverse Apparatus for Air-Void Distribution Analysis," *Proceedings*, Third International Conference on Cement Microscopy, Houston, Texas, pp. 211-226.

Rosiwal, A. (1898). "Über geometrische Gesteinsanalysen, usw.", *Verhandl. der k.-k. geologischen Reichanstalt*, Vol. 5-6, p. 143.

Russ, J. C. (1986). *Practical Stereology,* Plenum Press, New York, 185 pp.

Thomson, E. (1930). "Quantitative Microscopic Analysis," *Journal of Geology*, Vol. 38, No. 3, April–May, pp. 193-222.

Underwood, E. E. (1970). *Quantitative Stereology*, Addison-Wesley Publishing Co., Inc., Reading, MA, 274 pp.

Verbeck, J. (1947). "The Camera Lucida Method for Measuring Air Voids in Hardened Concrete", ACI Journal, *Proceedings* Vol. 18, No. 9, May, pp. 1025-1039.

Verbeck, G. (1978). "Pore Structure," Chapter 18 in ASTM Special Technical Publication 169B, *Significance of Tests and Properties of Concrete and Concrete-Making Materials*, pp. 262-274.

Walker, H. M. (1980). "Formula for Calculating Spacing Factor for Entrained Air Voids," *Cement Concrete and Aggregates*, CCAGDP, Vol. 2, No. 2, Winter, pp. 63-63.

Walker, H. M. (1984). "Correlation of Hardened Concrete Air-Void Parameters Obtained by Linear Traverse with Freeze-Thaw Durability As Found by ASTM C 666," *Cement, Concrete, and Aggregates*, CCAGDP, Vol. 6, No. 1, Summer, pp. 52-55.

Warren, C. (1953). "Determination of the Properties of Air Voids in Concrete," *Highway Research Board*, Bulletin No. 70, pp. 1-10.

Weibel, E. R. (1979). *Stereological Methods,* Vol. II, Theoretical Foundations, Academic Press, London, 340 pp.

Wicksell, S. D., "The Corpuscle Problem. A Mathematical Study of a Biometric Problem," *Biometrika*, Vol. 17, pp. 84-99.

Willis, T. F (1949). Discussion of a paper by Powers "The Air Requirement of Frost-Resistant Concrete," Highway Research Board,*Proceedings*, Vol. 29, pp.184-211.

Willis, T. F. (1951). Unpublished paper showing derivation of equations for void parameters in an areal traverse. Available from the Missouri Highway and Transportion Department, Materials and Research Division, Jefferson City, MO.

Zuwaylif, F. H. (1974). *General Applied Statistics*, Addison-Wesley Publishing Co., Inc., Ready, MA, pp. 313

Table 2.1 Individual mix properties and compressive strength results

Specimen	Air-Entraining Agent	w/c	Air[1] (%)	Slump[2] (in.)	Unit Weight[3] (lb/ft^3)	Compressive Strength[4] (lb/in^2)
1	Non-Air	0.61	1.9	3 1/2	151.3	6120
2	Non-Air	0.58	2.0	3	151.5	6420
3	Vinsol Resin[5]	0.55	6.5	4	144.5	5350
4	Vinsol Resin[5]	0.53	6.5	3 3/4	144.5	5290
5	Micro Air[6]	0.53	6.0	3 3/4	146.1	5120
6	Micro Air[6]	0.53	6.3	3 3/4	145.5	4980
7	Catexol AE 260[7]	0.55	7.0	6 3/4	145.1	5380
8	Catexol AE 260[7]	0.53	6.8	5 3/4	145.1	5760
9	Catexol AE 260[7]	0.51	6.5	3 1/2	145.3	5950
10	Catexol AE 260[7]	0.51	6.5	3 1/4	145.1	6150

1. ASTM C 231
2. ASTM C 143
3. ASTM C 138
4. Tested at 28 Days
5. Manufactored by Master Builders, Inc.
6. Manufactored by Hercules Chemical
7. Manufactored by Solvay Construction Materials

Table 2.2 Modified point count test results[1]

Specimen	Air Content (%)	Paste Content (%)	Specific Surface (cm^2/cm^3)	Specific Surface (in^2/in^3)	Powers Spacing Factor (μm)	Powers Spacing Factor (in)
1	3.3	26.8	146.0	370.9	396	0.016
2	2.8	26.0	175.7	446.4	349	0.014
3	7.6	23.5	273.5	694.8	113	0.004
4	6.9	21.6	263.8	670.0	119	0.005
5	6.0	20.0	283.8	720.9	117	0.005
6	7.2	19.9	275.9	700.9	100	0.004
7	7.2	21.6	131.7	334.4	228	0.009
8	6.2	19.5	161.7	410.6	195	0.008
9	6.1	20.1	154.4	392.1	213	0.008
10	8.1	24.7	145.6	369.7	209	0.008

1. ASTM C 457-82a

Table 2.3 Scaling test results

Specimen	Visual Surface Rating* Freeze-Thaw Cycles					Surface Scaled† (%)
	5	10	15	20	25	
1	2	3	5	-	-	100
2	2	4	5	-	-	100
3	1	1-2	2-3	3	3-4	55.63
4	0	1	2	3	3	37.61
5	0	0	1-2	3	3	36.34
6	0	0-1	1-2	3	3-4	41.84
7	0	1	2	3	4	70.21
8	0	0	0	0-1	1	1.99
9	0	0	0	0-1	1	1.42
10	0	0	1	1-2	2	8.37

* From ASTM C 672-84

Rating	Condition of Surface
0	No Scaling
1	Very Slight Scaling (1/8 in. depth max., no coarse aggregate visible)
2	Slight to Moderate Scaling
3	Moderate Scaling (some coarse aggregate visible)
4	Moderate to Severe Scaling
5	Severe Scaling (coarse aggregate visible over entire surface)

† After 25 Freeze-Thaw Cycles

Table 2.4 Air content results[1]

Specimen	Plastic[2]	Manual[3]	Image Analysis						Mean[4]	Range[5]
			Lineal 1 Line/Frame		Lineal 480 Lines/Frame		Areal			
			12 X	30 X	12 X	30 X	12 X	30 X		
1	1.9	3.3	2.51	2.56	2.16	2.27	2.16	2.14	2.30	0.42
2	1.9	2.8	1.81	2.15	2.25	2.33	2.21	2.23	2.16	0.52
3	6.5	7.6	5.55	5.65	5.42	5.31	5.37	5.29	5.43	0.36
4	6.5	6.9	5.60	5.86	6.15	5.87	6.35	5.96	5.97	0.75
5	6.0	6.0	4.26	4.90	4.69	4.35	4.78	4.79	4.63	0.64
6	6.3	7.2	5.43	4.82	5.10	5.23	5.65	4.90	5.19	0.83
7	7.0	7.2	6.02	5.77	6.45	6.23	6.43	6.22	6.19	0.68
8	6.8	6.2	5.54	5.27	5.49	5.28	5.30	5.38	5.38	0.27
9	6.5	6.1	5.46	4.55	4.82	4.89	4.89	4.89	4.92	0.91
10	6.5	8.1	8.12	7.78	7.63	7.67	7.51	7.57	7.71	0.61

1. Percent of concrete volume
2. ASTM C 231
3. ASTM C 457-82a, modified point count
4. Mean of all image analysis results
5. Range of all image analysis results

Table 2.5 Average form factor[1] - 12x magnification

Class[2]	Specimen									
	1	2	3	4	5	6	7	8	9	10
1	0.753	0.757	0.752	0.749	0.720	0.750	0.754	0.754	0.724	0.751
2	0.691	0.690	0.714	0.721	0.721	0.719	0.696	0.691	0.701	0.700
3	0.684	0.684	0.741	0.772	0.746	0.742	0.719	0.701	0.726	0.721
4	0.701	0.699	0.763	0.753	0.754	0.756	0.754	0.736	0.762	0.755
5	0.713	0.715	0.753	0.726	0.739	0.730	0.764	0.764	0.783	0.773
6	0.718	0.737	0.738	0.692	0.717	0.703	0.781	0.777	0.794	0.779
7	0.756	0.721	0.717	0.658	0.683	0.672	0.780	0.781	0.796	0.778
8	0.728	0.737	0.707	0.636	0.662	0.640	0.775	0.785	0.790	0.767
9	0.736	0.719	0.687	0.616	0.651	0.625	0.763	0.778	0.797	0.763
10	0.768	0.762	0.685	0.612	0.626	0.620	0.765	0.775	0.773	0.748
11	0.713	0.770	0.670	0.600	0.609	0.597	0.746	0.745	0.771	0.733
12	0.745	0.735	0.653	0.577	0.628	0.578	0.731	0.734	0.748	0.727
13	0.771	0.780	0.685	0.575	0.600	0.597	0.710	0.743	0.736	0.704
14	0.732	0.785	0.652	0.595	0.604	0.608	0.720	0.746	0.717	0.686
15	0.741	0.732	0.648	0.544	0.586	0.603	0.715	0.729	0.715	0.678
16	0.767	0.726	0.626	0.600	0.598	0.542	0.698	0.717	0.734	0.666
17	0.691	0.749	0.603	0.570	0.646	0.618	0.705	0.667	0.681	0.640
18	0.779	0.746	0.646	0.511	0.567	0.590	0.675	0.708	0.708	0.628
19	0.818	0.790	0.663	0.596	0.582	0.602	0.672	0.672	0.662	0.637
20	0.790	0.768	0.626	0.636	0.649	0.564	0.671	0.680	0.679	0.619
21	0.732	0.726	0.608	0.553	0.654	0.566	0.630	0.642	0.680	0.599
22	0.732	0.779	0.618	0.538	0.579	0.548	0.667	0.627	0.666	0.588
23	0.743	0.764	0.617	0.649	0.505	0.570	0.660	0.662	0.633	0.625
24	0.614	0.825	0.605	0.541	0.641	0.551	0.597	0.625	0.555	0.606
25	0.750	0.831	0.549	0.650	0.741	0.591	0.626	0.633	0.658	0.544
26	0.763	0.744	0.486	0.488	0.639	0.551	0.570	0.557	0.632	0.541
27	0.720	0.747	0.597	0.589	0.635	0.616	0.642	0.634	0.679	0.524
28	0.799	0.780	0.649	0.633	0.551	0.593	0.566	0.652	0.655	0.488
29	0.846	0.673	0.610	0.688	0.668	0.573	0.630	0.669	0.733	0.496
30	0.508	0.769	0.644	0.624	0.400	0.688	0.629	0.561	0.709	0.442
31	0.745	0.758	0.618	0.509	0.521	0.512	0.596	0.668	0.565	0.623
32	0.774	0.630	0.668	0.357	0.682	0.613	0.527	0.595	0.500	0.446
33	0.730	0.779	0.654	0.621	0.475	0.699	0.528	0.476	0.608	0.613
34	0.715	0.723	0.531	0.458	0.677	0.700	0.596	0.578	0.661	0.437
35	0.770	0.766	0.426	0.749	0.663	0.585	0.519	0.675	0.655	0.531
36	0.757	0.357	0.269	0.462	0.593	0.603	0.582	0.584	0.516	0.456
37	0.720	0.877	0.680	0.606	0.750	0.533	0.815	0.585	-	0.467
38	-	0.714	0.400	0.837	0.650	0.290	0.482	0.600	0.642	0.520
39	0.623	0.734	0.538	0.508	0.627	-	0.672	0.491	0.702	0.455
40	0.559	-	0.582	0.558	0.636	0.368	0.602	0.470	0.691	0.496
41	0.690	0.746	-	0.374	0.849	0.556	0.612	-	0.844	0.333
42	0.608	0.699	-	0.641	0.608	0.509	0.461	0.451	0.689	0.354
43	0.722	0.820	0.543	-	-	0.495	0.551	0.505	0.631	0.476
44	0.626	0.475	-	0.714	-	0.476	0.555	0.655	0.648	0.536
45	0.269	0.657	0.705	0.713	0.645	0.500	0.500	0.709	0.546	0.346
46	-	0.758	0.500	0.325	0.758	-	0.393	0.558	0.823	0.585
47	0.816	-	0.525	0.346	0.536	-	-	-	0.740	0.623
48	0.572	0.397	-	0.653	0.650	-	0.218	-	0.506	0.552

Table 2.5 Continued

Class[1]	Specimen									
	1	2	3	4	5	6	7	8	9	10
49	-	-	-	0.711	0.690	0.174	0.781	-	0.706	0.445
50	0.716	0.781	0.669	-	-	0.449	-	-	-	-
51	0.651	0.637	0.477	-	0.502	0.451	-	-	-	0.646
52	0.712	0.696	0.654	-	0.693	-	-	0.660	-	0.281
53	-	-	0.370	0.431	-	0.589	0.479	0.458	0.329	-
54	-	-	0.407	0.593	0.580	0.635	0.483	0.357	0.720	-
55	0.695	0.826	0.501	-	-	0.454	0.220	-	-	0.512
56	-	-	-	-	-	0.691	-	-	0.581	0.363
57	0.509	0.850	0.643	-	-	0.276	0.814	0.471	-	0.388
58	-	-	-	-	-	0.542	-	-	0.855	0.243
59	0.293	-	0.475	-	-	0.483	-	0.673	-	0.426
60	-	-	-	-	0.503	0.354	0.564	0.465	-	0.704
61	-	0.503	-	-	-	0.506	-	-	0.413	-
62	0.731	-	-	-	-	-	-	-	0.395	-
63	0.706	-	-	-	-	-	-	0.228	-	-
64	-	0.760	-	0.532	-	0.521	-	-	-	-
65	-	-	0.352	-	-	0.694	-	-	-	-
66	0.680	0.519	-	-	-	0.500	-	-	-	-
67	-	-	0.525	-	-	-	0.522	-	-	0.179
68	-	-	0.539	-	-	-	0.644	-	-	-
69	-	-	-	-	-	-	0.697	0.673	-	0.548
70	0.559	-	0.480	-	0.635	-	-	0.777	-	-
71	-	-	-	0.457	-	-	0.462	-	-	-
72	0.662	0.332	0.548	-	-	-	0.480	-	-	-
73	0.379	-	-	-	-	-	-	-	-	-
74	-	0.466	-	-	-	-	-	-	-	-
75	-	-	0.507	-	-	-	-	-	-	0.440
76	-	0.788	-	-	-	-	-	-	-	-
77	-	0.574	-	-	-	0.443	-	-	-	-
78	-	0.654	-	-	-	-	0.351	0.618	-	0.247
79	-	-	0.484	-	-	-	-	0.378	-	0.419
80	-	-	-	0.558	-	-	-	-	-	-

1. Form factor = 4π (P/A^2)
2. 25 μm class width

Table 2.6 Average form factor[1] - 30x magnification

Class[2]	Specimen									
	1	2	3	4	5	6	7	8	9	10
1	0.683	0.674	0.685	0.693	0.684	0.693	0.672	0.676	0.649	0.667
2	0.650	0.628	0.681	0.742	0.713	0.723	0.664	0.636	0.646	0.648
3	0.627	0.633	0.723	0.773	0.747	0.759	0.699	0.659	0.699	0.690
4	0.629	0.638	0.740	0.771	0.745	0.763	0.738	0.695	0.743	0.723
5	0.642	0.667	0.726	0.737	0.720	0.746	0.749	0.718	0.754	0.734
6	0.671	0.680	0.710	0.711	0.691	0.718	0.756	0.738	0.772	0.739
7	0.694	0.671	0.686	0.685	0.664	0.689	0.743	0.742	0.775	0.732
8	0.707	0.675	0.672	0.673	0.659	0.667	0.747	0.737	0.758	0.718
9	0.668	0.690	0.651	0.648	0.630	0.664	0.738	0.725	0.764	0.712
10	0.692	0.680	0.661	0.671	0.607	0.635	0.719	0.725	0.735	0.689
11	0.695	0.682	0.634	0.613	0.618	0.643	0.710	0.700	0.735	0.672
12	0.717	0.663	0.623	0.638	0.606	0.643	0.691	0.690	0.732	0.677
13	0.719	0.701	0.625	0.647	0.594	0.619	0.693	0.694	0.715	0.658
14	0.707	0.731	0.605	0.639	0.588	0.624	0.693	0.697	0.690	0.634
15	0.693	0.676	0.611	0.597	0.609	0.649	0.695	0.676	0.728	0.621
16	0.667	0.627	0.581	0.631	0.631	0.632	0.652	0.664	0.683	0.597
17	0.715	0.686	0.602	0.602	0.551	0.624	0.672	0.633	0.695	0.610
18	0.672	0.718	0.630	0.625	0.572	0.620	0.620	0.629	0.668	0.588
19	0.711	0.666	0.581	0.611	0.625	0.651	0.658	0.628	0.646	0.558
20	0.678	0.681	0.577	0.624	0.585	0.582	0.599	0.636	0.658	0.606
21	0.602	0.643	0.563	0.587	0.590	0.601	0.630	0.630	0.704	0.540
22	0.662	0.634	0.614	0.617	0.541	0.641	0.557	0.594	0.556	0.561
23	0.563	0.707	0.579	0.609	0.611	0.578	0.603	0.612	0.625	0.542
24	0.603	0.705	0.601	0.678	0.614	0.583	0.568	0.582	0.617	0.539
25	0.596	0.699	0.537	0.624	0.471	0.623	0.567	0.592	0.695	0.531
26	0.707	0.580	0.489	0.650	0.681	0.629	0.577	0.547	0.578	0.510
27	0.612	0.456	0.554	0.612	0.685	0.445	0.651	0.567	0.689	0.494
28	0.596	0.670	0.520	0.696	0.537	0.508	0.622	0.554	0.547	0.502
29	0.702	0.444	0.531	0.611	0.648	0.520	0.614	0.633	0.619	0.415
30	0.431	0.667	0.693	0.615	0.551	0.700	0.570	0.484	0.637	0.387
31	0.677	0.562	0.623	0.632	0.644	0.506	0.591	0.552	0.583	0.552
32	0.727	0.635	0.526	0.562	0.437	0.710	0.606	0.569	0.634	0.522
33	0.553	0.590	0.532	0.737	0.510	0.779	0.560	0.694	0.500	0.444
34	0.506	0.486	-	0.634	0.564	0.591	0.513	0.566	0.606	0.535
35	0.651	0.680	0.615	0.456	0.633	0.566	0.626	0.606	0.670	0.549
36	0.606	0.773	0.386	-	0.580	-	0.552	0.318	0.539	0.401
37	0.457	0.739	0.551	0.731	0.473	0.332	0.492	0.460	0.752	0.428
38	0.631	0.645	0.395	0.507	0.760	-	0.779	0.650	0.510	0.429
39	0.442	0.609	0.608	0.570	0.811	0.736	0.423	0.539	0.605	0.534
40	0.606	0.504	0.558	0.390	0.686	0.547	0.468	0.595	0.640	0.452
41	0.505	0.493	0.663	0.543	-	0.553	0.433	0.504	0.689	0.772
42	0.485	0.674	0.594	0.426	0.530	0.276	0.430	0.327	0.567	0.559
43	-	-	-	0.602	-	0.572	0.622	0.472	0.603	0.504
44	0.625	0.391	-	-	0.672	-	-	0.600	-	0.585
45	0.749	0.408	-	-	0.595	0.375	0.543	0.660	0.701	0.210
46	0.683	0.658	0.519	0.548	0.632	0.413	0.208	-	0.365	-
47	0.694	-	-	-	-	-	0.704	-	-	0.433
48	-	-	0.577	0.618	0.311	-	0.416	-	0.800	0.549

Table 2.6 Continued

Class[2]	Specimen									
	1	2	3	4	5	6	7	8	9	10
49	-	0.656	0.411	-	-	-	-	-	-	0.453
50	0.562	0.756	0.311	0.552	0.535	-	0.456	0.383	0.731	0.288
51	-	0.716	-	0.530	-	-	0.594	-	0.393	0.451
52	-	0.800	0.573	0.482	-	-	-	0.581	0.552	0.238
53	0.598	-	0.696	0.585	-	-	-	0.488	-	0.437
54	0.580	0.563	0.360	-	-	0.787	0.438	0.739	-	0.312
55	-	0.500	0.471	-	0.682	0.554	-	-	-	0.214
56	0.649	0.587	-	-	-	-	0.548	0.356	-	0.208
57	-	-	0.484	0.608	-	-	0.507	0.807	-	0.382
58	0.092	-	0.330	0.663	0.664	-	-	-	0.697	0.549
59	-	0.360	0.471	-	-	-	0.254	0.399	0.522	-
60	-	-	-	0.849	-	-	0.709	0.576	-	-
61	-	0.613	-	0.500	-	0.414	0.511	-	0.772	0.406
62	-	0.484	-	-	-	-	-	-	-	-
63	0.734	-	0.455	0.380	0.469	-	-	-	-	0.396
64	-	-	-	0.336	-	-	0.409	-	-	-
65	-	0.625	0.504	0.482	0.553	0.428	0.572	-	-	0.467
66	-	0.520	0.522	-	0.472	-	-	-	0.341	-
67	-	0.667	-	-	-	-	-	-	-	0.645
68	-	0.624	-	0.541	-	0.362	-	0.746	-	-
69	-	-	-	-	0.705	0.444	0.376	-	-	-
70	-	0.486	0.551	-	0.459	-	-	0.589	-	0.525
71	-	-	-	-	-	-	-	-	-	-
72	-	0.686	0.545	-	-	-	-	-	-	-
73	-	-	-	0.516	0.565	-	-	0.734	-	-
74	-	-	0.432	0.547	-	-	-	-	-	0.456
75	-	-	-	-	-	-	-	-	-	-
76	-	-	-	0.477	0.609	0.289	-	-	-	-
77	-	-	-	-	-	-	-	-	-	-
78	-	-	0.555	-	-	-	-	-	-	-
79	-	-	0.588	0.396	0.432	-	0.658	-	0.403	-
80	-	-	0.569	0.563	-	-	-	-	-	-

1. Form factor = 4π (A/P^2)
2. 25 µm class width

Table 2.7 Form factors

Specimen	Mean Form Factor		Diameter Weighted Mean Form Factor[1]	
	12 X	30 X	12 X	30 X
1	0.713	0.714	0.740	0.690
2	0.714	0.656	0.744	0.682
3	0.732	0.699	0.667	0.635
4	0.728	0.737	0.598	0.645
5	0.726	0.716	0.628	0.616
6	0.725	0.728	0.616	0.649
7	0.740	0.701	0.726	0.693
8	0.735	0.678	0.735	0.685
9	0.752	0.709	0.740	0.717
10	0.739	0.686	0.703	0.654

1. Calculated from size classes 1 through 18

Table 2.8 Statistical summary of image analysis areal data

12 x Magnification

Specimen	Actual Sample Size			Required Sample Size[1]			
				68% Confidence		95% Confidence	
	Frames[2]	% Air	S[4]	Frames[2]	Area (in^2)	Frames[2]	Area (in^2)
1	170	2.16	2.38	23	1.49	87	5.71
2	170	2.21	3.08	38	2.49	146	9.56
3	150	5.37	4.03	65	4.26	250	16.36
4	170	6.35	4.79	92	6.02	353	23.12
5	170	4.78	4.31	74	4.87	285	18.72
6	170	5.65	5.52	122	7.99	468	30.70
7	170	6.43	4.13	68	4.47	262	17.18
8	170	5.30	3.84	59	3.87	227	14.86
9	174	4.89	3.26	43	2.79	163	10.71
10	170	7.51	4.29	74	4.83	283	18.54

30 x Magnification

Specimen	Actual Sample Size			Required Sample Size[1]			
				68% Confidence		95% Confidence	
	Frames[3]	% Air	S[4]	Frames[3]	Area (in^2)	Frames[3]	Area (in^2)
1	1075	2.14	4.72	89	0.93	342	3.59
2	1074	2.23	5.61	126	1.32	484	5.07
3	924	5.29	7.01	197	2.06	755	7.92
4	1073	5.96	7.17	206	2.16	790	8.29
5	1072	4.79	6.47	167	1.76	643	6.75
6	1035	4.90	7.45	222	2.33	853	8.95
7	1074	6.22	7.53	227	2.38	871	9.14
8	1075	5.38	6.15	151	1.59	581	6.10
9	1075	4.89	5.63	127	1.33	487	5.11
10	1075	7.57	7.67	235	2.47	904	9.48

1. Sample size to produce a measured air content within 0.5 percent air by volume of the true air content within the specified confidence
2. Frame dimensions for 12 X magnification are 7528.0 µm x 2662.1 µm
3. Frame dimensions for 30 X magnification are 2995.2 µm x 2252.8 µm
4. Standard deviation of measured frame air contents

Table 2.9 Statistical summary of image analysis 480 lines/frame lineal data

12 x Magnification

Specimen	Actual Sample Size			Required Sample Size[1]			
				68% Confidence		95% Confidence	
	Frames[2]	% Air	S [4]	Frames[2]	Area (in^2)	Frames[2]	Area (in^2)
1	170	2.16	2.40	23	1.51	89	5.80
2	170	2.25	3.19	41	2.67	156	10.24
3	150	5.42	4.03	65	4.26	250	16.38
4	170	6.15	4.58	84	5.50	322	21.14
5	170	4.69	3.63	53	3.45	202	13.25
6	170	5.10	5.09	104	6.79	398	26.07
7	170	6.45	4.07	66	4.35	255	16.71
8	170	5.49	3.87	60	3.93	230	15.10
9	169	4.82	3.34	45	2.93	172	11.27
10	170	7.63	4.62	85	5.59	328	21.48

30 x Magnification

Specimen	Actual Sample Size			Required Sample Size[1]			
				68% Confidence		95% Confidence	
	Frames[3]	% Air	S [4]	Frames[3]	Area (in^2)	Frames[3]	Area (in^2)
1	1073	2.27	5.08	103	1.08	397	4.16
2	1050	2.33	5.83	136	1.43	522	5.48
3	925	5.31	7.12	203	2.12	778	8.16
4	650	5.87	7.80	243	2.55	935	9.80
5	925	4.35	5.78	134	1.40	513	5.38
6	1073	5.23	7.55	228	2.39	875	9.18
7	1075	6.23	7.39	219	2.29	840	8.81
8	1075	5.28	6.14	151	1.58	580	6.08
9	1075	4.89	5.56	124	1.30	475	4.99
10	1060	7.67	7.62	232	2.44	893	9.36

1. Sample size to produce a measured air content within 0.5 percent air by volume of the true air content within the specified confidence
2. Frame dimensions for 12 X magnification are 7528.0 μm x 2662.1 μm
3. Frame dimensions for 30 X magnification are 2995.2 μm x 2252.8 μm
4. Standard deviation of measured frame air contents

Table 2.10 Statistical summary of image analysis 1 line/frame lineal data

12 X Magnification

Specimen	Actual Sample Size			Required Sample Size[1]			
				68% Confidence		95% Confidence	
	Frames[2]	% Air	S [4]	Frames[2]	Length (in)	Frames[2]	Length (in)
1	170	2.51	4.70	88	26	340	100
2	170	1.81	4.79	92	27	353	104
3	150	5.55	6.49	168	50	646	191
4	170	5.60	6.77	183	54	704	208
5	170	4.26	6.09	148	44	569	168
6	170	5.43	7.10	202	60	775	229
7	170	6.02	6.13	150	44	578	171
8	170	5.54	6.33	160	47	616	182
9	170	5.46	5.93	141	42	541	160
10	170	8.12	8.66	300	89	1152	340

30 X Magnification

Specimen	Actual Sample Size			Required Sample Size[1]			
				68% Confidence		95% Confidence	
	Frames[3]	% Air	S [4]	Frames[3]	Length (in)	Frames[3]	Length (in)
1	1075	2.56	7.10	202	24	775	92
2	1075	2.15	7.38	218	26	837	99
3	925	5.65	10.47	438	52	1684	199
4	1075	5.86	9.07	329	39	1265	149
5	1075	4.90	8.74	306	36	1174	139
6	1075	4.82	9.56	366	43	1405	166
7	1050	5.77	10.21	417	49	1602	189
8	1075	5.27	8.98	322	38	1238	146
9	1075	4.55	7.93	251	30	966	114
10	1075	7.78	10.92	477	56	1832	216

1. Sample size to produce a measured air content within 0.5 percent air by volume of the true air content within the specified confidence
2. Frame length for 12 X magnification is 7528.0 µm
3. Frame length for 30 X magnification is 2995.2 µm
4. Standard deviation of measured frame air contents

Table 3.1 Matrix of coefficients K_{ij} used in the calculation of a measured distribution, $N_L(i)^*$, by Eq. 3.13.
20 classes, L = 2995.2 μm, class width = 29.25 μm

1.0049	0.0195	0.0195	0.0195	0.0196	0.0196	0.0196	0.0196	0.0196	0.0196	0.0195	0.0195	0.0195	0.0195	0.0195	0.0195	0.0195	0.0195	0.0195	0.0195
0	0.9951	0.0195	0.0195	0.0195	0.0195	0.0195	0.0195	0.0195	0.0195	0.0195	0.0195	0.0195	0.0195	0.0195	0.0195	0.0195	0.0195	0.0195	0.0195
0	0	0.9853	0.0195	0.0195	0.0195	0.0195	0.0195	0.0195	0.0195	0.0195	0.0196	0.0196	0.0196	0.0196	0.0196	0.0195	0.0195	0.0195	0.0195
0	0	0	0.9756	0.0195	0.0195	0.0195	0.0195	0.0195	0.0196	0.0196	0.0195	0.0195	0.0195	0.0195	0.0195	0.0195	0.0195	0.0196	0.0196
0	0	0	0	0.9658	0.0196	0.0195	0.0195	0.0195	0.0196	0.0196	0.0195	0.0195	0.0195	0.0195	0.0196	0.0196	0.0195	0.0195	0.0195
0	0	0	0	0	0.9560	0.0195	0.0196	0.0195	0.0195	0.0195	0.0196	0.0195	0.0195	0.0195	0.0196	0.0195	0.0195	0.0195	0.0196
0	0	0	0	0	0	0.9463	0.0195	0.0195	0.0196	0.0195	0.0195	0.0195	0.0195	0.0195	0.0195	0.0195	0.0195	0.0195	0.0196
0	0	0	0	0	0	0	0.9365	0.0195	0.0196	0.0195	0.0195	0.0195	0.0195	0.0196	0.0195	0.0195	0.0195	0.0195	0.0196
0	0	0	0	0	0	0	0	0.9268	0.0195	0.0195	0.0195	0.0195	0.0195	0.0195	0.0195	0.0196	0.0195	0.0196	0.0195
0	0	0	0	0	0	0	0	0	0.9170	0.0195	0.0195	0.0196	0.0195	0.0196	0.0195	0.0195	0.0195	0.0195	0.0195
0	0	0	0	0	0	0	0	0	0	0.9072	0.0195	0.0195	0.0196	0.0195	0.0195	0.0196	0.0195	0.0195	0.0195
0	0	0	0	0	0	0	0	0	0	0	0.8974	0.0195	0.0195	0.0196	0.0195	0.0195	0.0196	0.0195	0.0195
0	0	0	0	0	0	0	0	0	0	0	0	0.8877	0.0196	0.0195	0.0195	0.0195	0.0195	0.0196	0.0196
0	0	0	0	0	0	0	0	0	0	0	0	0	0.8780	0.0195	0.0195	0.0195	0.0196	0.0196	0.0196
0	0	0	0	0	0	0	0	0	0	0	0	0	0	0.8681	0.0195	0.0195	0.0195	0.0195	0.0195
0	0	0	0	0	0	0	0	0	0	0	0	0	0	0	0.8584	0.0195	0.0195	0.0195	0.0195
0	0	0	0	0	0	0	0	0	0	0	0	0	0	0	0	0.8486	0.0195	0.0195	0.0195
0	0	0	0	0	0	0	0	0	0	0	0	0	0	0	0	0	0.8389	0.0195	0.0195
0	0	0	0	0	0	0	0	0	0	0	0	0	0	0	0	0	0	0.8291	0.0196
0	0	0	0	0	0	0	0	0	0	0	0	0	0	0	0	0	0	0	0.8193

Table 3.2 Example showing the calculation of a measured distribution, $N_L(i)^*$, using a hypothetical true distribution, $N_L(j)$

			N_L (#/cm)	
CLASS	LIMITS (μm)		TRUE	MEASURED[1]
1	0.00	29.25	0	0.0781
2	29.25	58.50	0	0.0781
3	58.50	87.75	0	0.0781
4	87.75	117.00	0	0.0781
5	117.00	146.25	0	0.0781
6	146.25	175.50	0	0.0781
7	175.50	204.75	0	0.0781
8	204.75	234.00	0	0.0781
9	234.00	263.25	0	0.0781
10	263.25	292.50	0	0.0781
11	292.50	321.75	0	0.0781
12	321.75	351.00	0	0.0781
13	351.00	380.25	0	0.0781
14	380.25	409.50	0	0.0781
15	409.50	438.75	0	0.0781
16	438.75	468.00	0	0.0781
17	468.00	497.25	0	0.0781
18	497.25	526.50	0	0.0781
19	526.50	555.75	0	0.0781
20	555.75	585.00	1.00	0.2773
		N_L(total)	1.00	1.76

1. Calculated using Eq. 3.13 and the K_{ij} coefficients in Table 3.1

Table 3.3 Matrix of coefficients α_{ij} used in the calculation of a true distribution, $N_L(i)$, by Eq. 3.14.
20 Classes, L = 2995.2 μm, Class Width = 29.25 μm

0.9951	-0.0195	-0.0193	-0.0191	-0.0190	-0.0188	-0.0186	-0.0184	-0.0182	-0.0180	-0.0178	-0.0176	-0.0174	-0.0172	-0.0170	-0.0168	-0.0166	-0.0164	-0.0162	-0.0160
0	1.0049	-0.0199	-0.0197	-0.0195	-0.0193	-0.0191	-0.0189	-0.0187	-0.0185	-0.0183	-0.0181	-0.0179	-0.0177	-0.0175	-0.0173	-0.0171	-0.0169	-0.0167	-0.0165
0	0	1.0149	-0.0203	-0.0201	-0.0199	-0.0197	-0.0195	-0.0193	-0.0191	-0.0189	-0.0187	-0.0185	-0.0183	-0.0181	-0.0179	-0.0176	-0.0174	-0.0172	-0.0170
0	0	0	1.0250	-0.0207	-0.0205	-0.0203	-0.0201	-0.0199	-0.0197	-0.0195	-0.0192	-0.0190	-0.0188	-0.0186	-0.0184	-0.0182	-0.0180	-0.0178	-0.0176
0	0	0	0	1.0354	-0.0212	-0.0209	-0.0207	-0.0205	-0.0203	-0.0201	-0.0198	-0.0196	-0.0194	-0.0192	-0.0190	-0.0188	-0.0185	-0.0183	-0.0181
0	0	0	0	0	1.0460	-0.0216	-0.0214	-0.0211	-0.0209	-0.0207	-0.0205	-0.0202	-0.0200	-0.0198	-0.0196	-0.0193	-0.0191	-0.0189	-0.0187
0	0	0	0	0	0	1.0568	-0.0220	-0.0218	-0.0216	-0.0213	-0.0211	-0.0209	-0.0206	-0.0204	-0.0202	-0.0199	-0.0197	-0.0195	-0.0193
0	0	0	0	0	0	0	1.0678	-0.0225	-0.0223	-0.0220	-0.0218	-0.0215	-0.0213	-0.0211	-0.0208	-0.0206	-0.0203	-0.0201	-0.0199
0	0	0	0	0	0	0	0	1.0790	-0.0230	-0.0227	-0.0225	-0.0222	-0.0220	-0.0217	-0.0215	-0.0213	-0.0210	-0.0208	-0.0205
0	0	0	0	0	0	0	0	0	1.0905	-0.0235	-0.0232	-0.0230	-0.0227	-0.0225	-0.0222	-0.0219	-0.0217	-0.0214	-0.0212
0	0	0	0	0	0	0	0	0	0	1.1023	-0.0240	-0.0237	-0.0235	-0.0232	-0.0229	-0.0227	-0.0224	-0.0221	-0.0219
0	0	0	0	0	0	0	0	0	0	0	1.1143	-0.0245	-0.0242	-0.0240	-0.0237	-0.0234	-0.0232	-0.0229	-0.0226
0	0	0	0	0	0	0	0	0	0	0	0	1.1265	-0.0251	-0.0248	-0.0245	-0.0242	-0.0239	-0.0237	-0.0234
0	0	0	0	0	0	0	0	0	0	0	0	0	1.1390	-0.0256	-0.0253	-0.0250	-0.0248	-0.0245	-0.0242
0	0	0	0	0	0	0	0	0	0	0	0	0	0	1.1519	-0.0262	-0.0259	-0.0256	-0.0253	-0.0250
0	0	0	0	0	0	0	0	0	0	0	0	0	0	0	1.1650	-0.0268	-0.0265	-0.0262	-0.0259
0	0	0	0	0	0	0	0	0	0	0	0	0	0	0	0	1.1784	-0.0274	-0.0271	-0.0268
0	0	0	0	0	0	0	0	0	0	0	0	0	0	0	0	0	1.1921	-0.0281	-0.0277
0	0	0	0	0	0	0	0	0	0	0	0	0	0	0	0	0	0	1.2061	-0.0288
0	0	0	0	0	0	0	0	0	0	0	0	0	0	0	0	0	0	0	1.2205

Table 3.4 Example showing the calculation of a true distribution, $N_L(i)$, using a hypothetical measured distribution, $N_L(j)$*

			N_L (#/cm)		
CLASS	LIMITS (μm)		MEASURED	TRUE[1]	%CHANGE
1	0	29.25	10	6.57	-34.3
2	29.25	58.50	10	6.77	-32.3
3	58.50	87.75	10	6.97	-30.3
4	87.75	117.00	10	7.19	-28.1
5	117.00	146.25	10	7.41	-25.9
6	146.25	175.50	10	7.64	-23.6
7	175.50	204.75	10	7.88	-21.2
8	204.75	234.00	10	8.14	-18.6
9	234.00	263.25	10	8.40	-16.0
10	263.25	292.50	10	8.67	-13.3
11	292.50	321.75	10	8.96	-10.4
12	321.75	351.00	10	9.26	-7.4
13	351.00	380.25	10	9.57	-4.3
14	380.25	409.50	10	9.90	-1.0
15	409.50	438.75	10	10.24	2.4
16	438.75	468.00	10	10.60	6.0
17	468.00	497.25	10	10.97	9.7
18	497.25	526.50	10	11.36	13.6
19	526.50	555.75	10	11.77	17.7
20	555.75	585.00	10	12.21	22.1
	N_L (total)		200	180	
	Average Chord Length (μm)		292.5	324.0	

1. Calculated using Eq. 3.14 and the α_{ij} coefficients of Table 3.3

Table 3.5 Edge effect correction of mix 8 lineal data using 80 classes of 29.25 μm width

			MEASURED		TRUE[1]	
CLASS	LIMITS (μm)		CHORDS	N_L (#/cm)	N_L (#/cm)	CHORDS
1	0.00	29.25	117906	0.7656	0.7161	110277
2	29.25	58.50	57044	0.3704	0.3325	51203
3	58.50	87.75	48957	0.3179	0.2882	44383
4	87.75	117.00	44976	0.2921	0.2700	41580
5	117.00	146.25	38786	0.2519	0.2359	36325
6	146.25	175.50	32727	0.2125	0.2012	30992
7	175.50	204.75	27828	0.1807	0.1733	26686
8	204.75	234.00	23130	0.1502	0.1456	22415
9	234.00	263.25	18919	0.1229	0.1201	18497
10	263.25	292.50	14708	0.0955	0.0936	14409
11	292.50	321.75	12163	0.0790	0.0780	12018
12	321.75	351.00	9980	0.0648	0.0645	9932
13	351.00	380.25	8532	0.0554	0.0558	8599
14	380.25	409.50	6389	0.0415	0.0415	6396
15	409.50	438.75	5769	0.0375	0.0382	5887
16	438.75	468.00	4931	0.0320	0.0331	5093
17	468.00	497.25	4001	0.0260	0.0270	4151
18	497.25	526.50	3167	0.0206	0.0213	3282
19	526.50	555.75	2767	0.0180	0.0189	2907
20	555.75	585.00	2106	0.0137	0.0142	2187
21	585.00	614.25	1734	0.0113	0.0117	1797
22	614.25	643.50	1476	0.0096	0.0100	1534
23	643.50	672.75	1093	0.0071	0.0071	1095
24	672.75	702.00	949	0.0062	0.0062	948
25	702.00	731.25	906	0.0059	0.0060	928
26	731.25	760.50	782	0.0051	0.0052	797
27	760.50	789.75	649	0.0042	0.0042	647
28	789.75	819.00	549	0.0036	0.0035	535
29	819.00	848.25	477	0.0031	0.0030	456
30	848.25	877.50	430	0.0028	0.0026	408
31	877.50	906.75	548	0.0036	0.0039	595
32	906.75	936.00	531	0.0034	0.0039	596
33	936.00	965.25	357	0.0023	0.0024	363
34	965.25	994.50	229	0.0015	0.0012	186
35	994.50	1023.75	184	0.0012	0.0008	126
36	1023.75	1053.00	218	0.0014	0.0012	184
37	1053.00	1082.25	150	0.0010	0.0006	86
38	1082.25	1111.50	207	0.0013	0.0012	181
39	1111.50	1140.75	139	0.0009	0.0005	79
40	1140.75	1170.00	166	0.0011	0.0008	127
41	1170.00	1199.25	129	0.0008	0.0005	71
42	1199.25	1228.50	127	0.0008	0.0005	72
43	1228.50	1257.75	242	0.0016	0.0018	275
44	1257.75	1287.00	150	0.0010	0.0008	127
45	1287.00	1316.25	226	0.0015	0.0018	270
46	1316.25	1345.50	255	0.0017	0.0022	338
47	1345.50	1374.75	151	0.0010	0.0011	162

Table 3.5 continued

			MEASURED		TRUE[1]	
CLASS	LIMITS (μm)		CHORDS	N_L (#/cm)	N_L (#/cm)	CHORDS
48	1374.75	1404.00	156	0.0010	0.0012	181
49	1404.00	1433.25	125	0.0008	0.0009	131
50	1433.25	1462.50	214	0.0014	0.0020	314
51	1462.50	1491.75	165	0.0011	0.0015	234
52	1491.75	1521.00	157	0.0010	0.0015	232
53	1521.00	1550.25	119	0.0008	0.0011	166
54	1550.25	1579.50	60	0.0004	0.0003	51
55	1579.50	1608.75	90	0.0006	0.0008	119
56	1608.75	1638.00	72	0.0005	0.0006	87
57	1638.00	1667.25	81	0.0005	0.0007	113
58	1667.25	1696.50	66	0.0004	0.0006	86
59	1696.50	1725.75	86	0.0006	0.0009	140
60	1725.75	1755.00	25	0.0002	0.0000	1
61	1755.00	1784.25	31	0.0002	0.0001	16
62	1784.25	1813.50	24	0.0002	0.0000	-1
63	1813.50	1842.75	27	0.0002	0.0000	7
64	1842.75	1872.00	32	0.0002	0.0001	21
65	1872.00	1901.25	33	0.0002	0.0002	26
66	1901.25	1930.50	39	0.0003	0.0003	45
67	1930.50	1959.75	33	0.0002	0.0002	31
68	1959.75	1989.00	41	0.0003	0.0004	58
69	1989.00	2018.25	29	0.0002	0.0002	26
70	2018.25	2047.50	48	0.0003	0.0006	89
71	2047.50	2076.75	54	0.0004	0.0008	118
72	2076.75	2106.00	47	0.0003	0.0007	106
73	2106.00	2135.25	62	0.0004	0.0011	170
74	2135.25	2164.50	34	0.0002	0.0006	85
75	2164.50	2193.75	62	0.0004	0.0013	201
76	2193.75	2223.00	29	0.0002	0.0006	94
77	2223.00	2252.25	9	0.0001	0.0002	23
78	2252.25	2281.50	9	0.0001	0.0002	26
79	2281.50	2310.75	13	0.0001	0.0003	48
80	2310.75	2340.00	17	0.0001	0.0005	73
Totals			499929	3.246	3.070	473317
Average Chord Length (μm)				159.5	168.4	
Air Content (%)				5.18	5.18	
Powers Spacing Factor (μm)				150.1	158.5	

1. Calculated using Eq. 3.14

Table 3.6 Edge effect correction of mix 8 lineal data using 40 classes of 58.50 μm width

			MEASURED		TRUE[1]	
CLASS	LIMITS (μm)		CHORDS	N_L (#/cm)	N_L (#/cm)	CHORDS
1	0.00	58.50	174950	1.1360	1.0467	161199
2	58.50	117.00	93933	0.6100	0.5581	85953
3	117.00	175.50	71513	0.4644	0.4370	67294
4	175.50	234.00	50958	0.3309	0.3187	49081
5	234.00	292.50	33627	0.2184	0.2135	32886
6	292.50	351.00	22143	0.1438	0.1425	21940
7	351.00	409.50	14921	0.0969	0.0973	14984
8	409.50	468.00	10700	0.0695	0.0713	10976
9	468.00	526.50	7168	0.0465	0.0482	7429
10	526.50	585.00	4873	0.0316	0.0330	5089
11	585.00	643.50	3210	0.0208	0.0216	3329
12	643.50	702.00	2042	0.0133	0.0133	2042
13	702.00	760.50	1688	0.0110	0.0112	1724
14	760.50	819.00	1198	0.0078	0.0077	1181
15	819.00	877.50	907	0.0059	0.0056	863
16	877.50	936.00	1079	0.0070	0.0077	1191
17	936.00	994.50	586	0.0038	0.0036	548
18	994.50	1053.00	402	0.0026	0.0020	310
19	1053.00	1111.50	357	0.0023	0.0017	267
20	1111.50	1170.00	305	0.0020	0.0013	207
21	1170.00	1228.50	256	0.0017	0.0009	143
22	1228.50	1287.00	392	0.0025	0.0026	401
23	1287.00	1345.50	481	0.0031	0.0040	608
24	1345.50	1404.00	307	0.0020	0.0022	343
25	1404.00	1462.50	339	0.0022	0.0029	447
26	1462.50	1521.00	322	0.0021	0.0030	466
27	1521.00	1579.50	179	0.0012	0.0014	216
28	1579.50	1638.00	162	0.0011	0.0013	206
29	1638.00	1696.50	147	0.0010	0.0013	199
30	1696.50	1755.00	111	0.0007	0.0009	139
31	1755.00	1813.50	55	0.0004	0.0001	15
32	1813.50	1872.00	59	0.0004	0.0002	28
33	1872.00	1930.50	72	0.0005	0.0005	71
34	1930.50	1989.00	74	0.0005	0.0006	89
35	1989.00	2047.50	77	0.0005	0.0008	116
36	2047.50	2106.00	101	0.0007	0.0015	224
37	2106.00	2164.50	96	0.0006	0.0016	254
38	2164.50	2223.00	91	0.0006	0.0019	294
39	2223.00	2281.50	18	0.0001	0.0003	50
40	2281.50	2340.00	30	0.0002	0.0008	121
Totals			499929	3.246	3.071	472924
Average Chord Length (μm)				162.1	171.0	
Air Content (%)				5.26	5.25	
Powers Spacing Factor (μm)				150.2	158.8	

1. Calculated using Eq. 3.14

Table 3.7 Edge effect correction of mix 8 lineal data using 20 classes of 117.0 μm width

CLASS	LIMITS (μm)		MEASURED		TRUE[1]	
			CHORDS	N_L (#/cm)	N_L (#/cm)	CHORDS
1	0	117	268883	1.7460	1.6004	246459
2	117	234	122471	0.7953	0.7546	116209
3	234	351	55770	0.3621	0.3553	54719
4	351	468	25621	0.1664	0.1683	25921
5	468	585	12041	0.0782	0.0811	12493
6	585	702	5252	0.0341	0.0348	5356
7	702	819	2886	0.0187	0.0188	2898
8	819	936	1986	0.0129	0.0134	2059
9	936	1053	988	0.0064	0.0056	855
10	1053	1170	662	0.0043	0.0031	473
11	1170	1287	648	0.0042	0.0036	548
12	1287	1404	788	0.0051	0.0061	947
13	1404	1521	661	0.0043	0.0059	913
14	1521	1638	341	0.0022	0.0027	422
15	1638	1755	258	0.0017	0.0022	337
16	1755	1872	114	0.0007	0.0003	43
17	1872	1989	146	0.0009	0.0010	159
18	1989	2106	178	0.0012	0.0022	342
19	2106	2223	187	0.0012	0.0036	548
20	2223	2340	48	0.0003	0.0011	173
Totals			499929	3.246	3.064	471874
Average Chord Length (μm)				169.2	178.1	
Air Content (%)				5.49	5.46	
Powers Spacing Factor (μm)				150.2	159.0	

1. Calculated using Eq. 3.14

Table 3.8 Edge effect correction of mix 8 lineal data using 10 classes of 234 μm width

			MEASURED		TRUE[1]	
CLASS	LIMITS	(μm)	CHORDS	N_L (#/cm)	N_L (#/cm)	CHORDS
1	0	234	391354	2.5413	2.3398	360331
2	234	468	81391	0.5285	0.5200	80085
3	468	702	17293	0.1123	0.1149	17698
4	702	936	4872	0.0316	0.0321	4939
5	936	1170	1650	0.0107	0.0086	1320
6	1170	1404	1436	0.0093	0.0098	1514
7	1404	1638	1002	0.0065	0.0086	1322
8	1638	1872	372	0.0024	0.0024	369
9	1872	2106	324	0.0021	0.0034	519
10	2106	2340	235	0.0015	0.0045	700
Total Chords			499929	3.246	3.044	468796
Average Chord Length (μm)				190.8	198.9	
Air Content (%)				6.19	6.06	
Powers Spacing Factor(μm)				150.3	160.0	

1. Calculated using Eq. 3.14

Table 3.9 Matrix of coefficients K_{ij} used in the calculation of of a measured distribution, $N_L(i)^*$, by Eq. 3.13

20 classes, L = 2995.2 μm, class width =117.0 μm

1.0195	0.0781	0.0781	0.0781	0.0781	0.0781	0.0781	0.0781	0.0781	0.0781	0.0781	0.0781	0.0781	0.0781	0.0781	0.0781	0.0781	0.0781	0.0781	0.0781
0	0.9805	0.0781	0.0781	0.0781	0.0781	0.0781	0.0781	0.0781	0.0781	0.0781	0.0781	0.0781	0.0781	0.0781	0.0781	0.0781	0.0781	0.0781	0.0781
0	0	0.9414	0.0781	0.0781	0.0781	0.0781	0.0781	0.0781	0.0781	0.0781	0.0781	0.0781	0.0781	0.0781	0.0781	0.0781	0.0781	0.0781	0.0781
0	0	0	0.9023	0.0781	0.0781	0.0781	0.0781	0.0781	0.0781	0.0781	0.0781	0.0781	0.0781	0.0781	0.0781	0.0781	0.0781	0.0781	0.0781
0	0	0	0	0.8633	0.0781	0.0781	0.0781	0.0781	0.0781	0.0781	0.0781	0.0781	0.0781	0.0781	0.0781	0.0781	0.0781	0.0781	0.0781
0	0	0	0	0	0.8242	0.0781	0.0781	0.0781	0.0781	0.0781	0.0781	0.0781	0.0781	0.0781	0.0781	0.0781	0.0781	0.0781	0.0781
0	0	0	0	0	0	0.7852	0.0781	0.0781	0.0781	0.0781	0.0781	0.0781	0.0781	0.0781	0.0781	0.0781	0.0781	0.0781	0.0781
0	0	0	0	0	0	0	0.7461	0.0781	0.0781	0.0781	0.0781	0.0781	0.0781	0.0781	0.0781	0.0781	0.0781	0.0781	0.0781
0	0	0	0	0	0	0	0	0.7070	0.0781	0.0781	0.0781	0.0781	0.0781	0.0781	0.0781	0.0781	0.0781	0.0781	0.0781
0	0	0	0	0	0	0	0	0	0.6680	0.0781	0.0781	0.0781	0.0781	0.0781	0.0781	0.0781	0.0781	0.0781	0.0781
0	0	0	0	0	0	0	0	0	0	0.6289	0.0781	0.0781	0.0781	0.0781	0.0781	0.0781	0.0781	0.0781	0.0781
0	0	0	0	0	0	0	0	0	0	0	0.5898	0.0781	0.0781	0.0781	0.0781	0.0781	0.0781	0.0781	0.0781
0	0	0	0	0	0	0	0	0	0	0	0	0.5508	0.0781	0.0781	0.0781	0.0781	0.0781	0.0781	0.0781
0	0	0	0	0	0	0	0	0	0	0	0	0	0.5117	0.0781	0.0781	0.0781	0.0781	0.0781	0.0781
0	0	0	0	0	0	0	0	0	0	0	0	0	0	0.4727	0.0781	0.0781	0.0781	0.0781	0.0781
0	0	0	0	0	0	0	0	0	0	0	0	0	0	0	0.4336	0.0781	0.0781	0.0781	0.0781
0	0	0	0	0	0	0	0	0	0	0	0	0	0	0	0	0.3945	0.0781	0.0781	0.0781
0	0	0	0	0	0	0	0	0	0	0	0	0	0	0	0	0	0.3555	0.0781	0.0781
0	0	0	0	0	0	0	0	0	0	0	0	0	0	0	0	0	0	0.3164	0.0781
0	0	0	0	0	0	0	0	0	0	0	0	0	0	0	0	0	0	0	0.2773

Table 3.10 Matrix of coefficients α_{ij} used in the calculation of a true distribution, $N_L(i)$, by equation 3.14.
20 classes, L = 2995.2 μm, class width =117.0 μm

0.9808	-0.0782	-0.0749	-0.0717	-0.0684	-0.0652	-0.0619	-0.0587	-0.0555	-0.0522	-0.0490	-0.0457	-0.0425	-0.0392	-0.0360	-0.0328	-0.0295	-0.0263	-0.0230	-0.0198
0	1.0199	-0.0846	-0.0810	-0.0773	-0.0736	-0.0700	-0.0663	-0.0627	-0.0590	-0.0553	-0.0517	-0.0480	-0.0443	-0.0407	-0.0370	-0.0333	-0.0297	-0.0260	-0.0224
0	0	1.0622	-0.0920	-0.0878	-0.0836	-0.0795	-0.0753	-0.0712	-0.0670	-0.0628	-0.0587	-0.0545	-0.0504	-0.0462	-0.0420	-0.0379	-0.0337	-0.0295	-0.0254
0	0	0	1.1082	-0.1003	-0.0955	-0.0908	-0.0860	-0.0813	-0.0765	-0.0718	-0.0670	-0.0623	-0.0575	-0.0528	-0.0480	-0.0433	-0.0385	-0.0337	-0.0290
0	0	0	0	1.1584	-0.1098	-0.1043	-0.0989	-0.0934	-0.0879	-0.0825	-0.0770	-0.0716	-0.0661	-0.0606	-0.0552	-0.0497	-0.0442	-0.0388	-0.0333
0	0	0	0	0	1.2133	-0.1207	-0.1144	-0.1081	-0.1018	-0.0954	-0.0891	-0.0828	-0.0765	-0.0702	-0.0638	-0.0575	-0.0512	-0.0449	-0.0386
0	0	0	0	0	0	1.2736	-0.1334	-0.1260	-0.1186	-0.1113	-0.1039	-0.0965	-0.0892	-0.0818	-0.0744	-0.0671	-0.0597	-0.0523	-0.0449
0	0	0	0	0	0	0	1.3403	-0.1481	-0.1394	-0.1308	-0.1221	-0.1135	-0.1048	-0.0961	-0.0875	-0.0788	-0.0702	-0.0615	-0.0528
0	0	0	0	0	0	0	0	1.4144	-0.1654	-0.1551	-0.1449	-0.1346	-0.1243	-0.1140	-0.1038	-0.0935	-0.0832	-0.0730	-0.0627
0	0	0	0	0	0	0	0	0	1.4971	-0.1860	-0.1737	-0.1613	-0.1490	-0.1367	-0.1244	-0.1121	-0.0998	-0.0874	-0.0751
0	0	0	0	0	0	0	0	0	0	1.5901	-0.2106	-0.1957	-0.1807	-0.1658	-0.1509	-0.1359	-0.1210	-0.1060	-0.0911
0	0	0	0	0	0	0	0	0	0	0	1.6954	-0.2405	-0.2221	-0.2038	-0.1854	-0.1670	-0.1487	-0.1303	-0.1120
0	0	0	0	0	0	0	0	0	0	0	0	1.8156	-0.2772	-0.2543	-0.2314	-0.2085	-0.1856	-0.1626	-0.1397
0	0	0	0	0	0	0	0	0	0	0	0	0	1.9542	-0.3230	-0.2939	-0.2648	-0.2357	-0.2066	-0.1775
0	0	0	0	0	0	0	0	0	0	0	0	0	0	2.1157	-0.3812	-0.3435	-0.3057	-0.2680	-0.2302
0	0	0	0	0	0	0	0	0	0	0	0	0	0	0	2.3063	-0.4567	-0.4065	-0.3563	-0.3061
0	0	0	0	0	0	0	0	0	0	0	0	0	0	0	0	2.5347	-0.5571	-0.4883	-0.4195
0	0	0	0	0	0	0	0	0	0	0	0	0	0	0	0	0	2.8132	-0.6946	-0.5968
0	0	0	0	0	0	0	0	0	0	0	0	0	0	0	0	0	0	3.1605	-0.8903
0	0	0	0	0	0	0	0	0	0	0	0	0	0	0	0	0	0	0	3.6056

Table 3.11 Summary of edge effect correction of mix 8 lineal data using different class sizes

		MEASURED			TRUE[1]			
Classes (#)	Class Size (μm)	Air Content (%)	Average Chord Length (μm)	Total N_L (#/cm)	Air Content (%)	Average Chord Length (μm)	Total N_L (#/cm)	Powers Spacing Factor (μm)
80	29.25	5.18	159.5	3.246	5.18	168.4	3.070	159
40	58.50	5.26	162.1	3.246	5.25	171.0	3.071	159
20	117.0	5.49	169.2	3.246	5.46	178.1	3.064	159
10	234.0	6.19	190.8	3.246	6.06	198.9	3.044	160

1. Calculated using Eq. 3.14

Table 3.12 Edge effect correction of mix 8 lineal data truncated at 40 classes of 29.25 μm width

			MEASURED		TRUE [1]	
CLASS	LIMITS (μm)		CHORDS	N_L (#/cm)	N_L (#/cm)	CHORDS
1	0.00	29.25	117906	0.7656	0.7163	110310
2	29.25	58.50	57044	0.3704	0.3327	51237
3	58.50	87.75	48957	0.3179	0.2884	44418
4	87.75	117.00	44976	0.2921	0.2702	41615
5	117.00	146.25	38786	0.2519	0.2361	36362
6	146.25	175.50	32727	0.2125	0.2015	31030
7	175.50	204.75	27828	0.1807	0.1735	26725
8	204.75	234.00	23130	0.1502	0.1458	22455
9	234.00	263.25	18919	0.1229	0.1204	18539
10	263.25	292.50	14708	0.0955	0.0938	14452
11	292.50	321.75	12163	0.0790	0.0783	12062
12	321.75	351.00	9980	0.0648	0.0648	9978
13	351.00	380.25	8532	0.0554	0.0561	8647
14	380.25	409.50	6389	0.0415	0.0419	6445
15	409.50	438.75	5769	0.0375	0.0386	5937
16	438.75	468.00	4931	0.0320	0.0334	5146
17	468.00	497.25	4001	0.0260	0.0273	4206
18	497.25	526.50	3167	0.0206	0.0217	3338
19	526.50	555.75	2767	0.0180	0.0193	2965
20	555.75	585.00	2106	0.0137	0.0146	2247
21	585.00	614.25	1734	0.0113	0.0121	1860
22	614.25	643.50	1476	0.0096	0.0104	1599
23	643.50	672.75	1093	0.0071	0.0075	1163
24	672.75	702.00	949	0.0062	0.0066	1018
25	702.00	731.25	906	0.0059	0.0065	1001
26	731.25	760.50	782	0.0051	0.0057	873
27	760.50	789.75	649	0.0042	0.0047	726
28	789.75	819.00	549	0.0036	0.0040	617
29	819.00	848.25	477	0.0031	0.0035	541
30	848.25	877.50	430	0.0028	0.0032	497
31	877.50	906.75	548	0.0036	0.0045	688
32	906.75	936.00	531	0.0034	0.0045	693
33	936.00	965.25	357	0.0023	0.0030	464
34	965.25	994.50	229	0.0015	0.0019	292
35	994.50	1023.75	184	0.0012	0.0015	236
36	1023.75	1053.00	218	0.0014	0.0019	300
37	1053.00	1082.25	150	0.0010	0.0013	206
38	1082.25	1111.50	207	0.0013	0.0020	307
39	1111.50	1140.75	139	0.0009	0.0014	211
40	1140.75	1170.00	166	0.0011	0.0017	266
Totals			496560	3.224	3.063	471671
Average Chord Length (μm)				150.2	158.0	
Air Content (%)				4.84	4.84	
Powers Spacing Factor (μm)				151.3	159.1	

1. Calculated using Eq. 3.14

Table 3.13 Edge effect correction of mix 8 lineal data truncated at 20 classes of 29.25 μm width

			MEASURED		TRUE[1]	
CLASS	LIMITS (μm)		CHORDS	N_L (#/cm)	N_L (#/cm)	CHORDS
1	0.00	29.25	117906	0.7656	0.7174	110484
2	29.25	58.50	57044	0.3704	0.3339	51416
3	58.50	87.75	48957	0.3179	0.2896	44603
4	87.75	117.00	44976	0.2921	0.2715	41806
5	117.00	146.25	38786	0.2519	0.2374	36558
6	146.25	175.50	32727	0.2125	0.2028	31232
7	175.50	204.75	27828	0.1807	0.1749	26934
8	204.75	234.00	23130	0.1502	0.1472	22671
9	234.00	263.25	18919	0.1229	0.1218	18761
10	263.25	292.50	14708	0.0955	0.0953	14682
11	292.50	321.75	12163	0.0790	0.0799	12299
12	321.75	351.00	9980	0.0648	0.0664	10223
13	351.00	380.25	8532	0.0554	0.0578	8900
14	380.25	409.50	6389	0.0415	0.0436	6707
15	409.50	438.75	5769	0.0375	0.0403	6208
16	438.75	468.00	4931	0.0320	0.0352	5426
17	468.00	497.25	4001	0.0260	0.0292	4496
18	497.25	526.50	3167	0.0206	0.0236	3639
19	526.50	555.75	2767	0.0180	0.0213	3277
20	555.75	585.00	2106	0.0137	0.0167	2570
Totals			484786	3.148	3.006	462894
Average Chord Length (μm)				135.3	141.7	
Air Content (%)				4.26	4.26	
Powers Spacing Factor (μm)				150.5	157.6	

1. Calculated using Eq. 3.14

Table 3.14 Edge effect correction of mix 8 lineal data truncated at 10 classes of 29.25 μm width

			MEASURED		TRUE[1]	
CLASS	LIMITS (μm)		CHORDS	N_L (#/cm)	N_L (#/cm)	CHORDS
1	0.00	29.25	117906	0.7656	0.7241	111512
2	29.25	58.50	57044	0.3704	0.3408	52476
3	58.50	87.75	48957	0.3179	0.2967	45695
4	87.75	117.00	44976	0.2921	0.2788	42931
5	117.00	146.25	38786	0.2519	0.2449	37719
6	146.25	175.50	32727	0.2125	0.2106	32429
7	175.50	204.75	27828	0.1807	0.1829	28168
8	204.75	234.00	23130	0.1502	0.1555	23945
9	234.00	263.25	18919	0.1229	0.1304	20076
10	263.25	292.50	14708	0.0955	0.1042	16039
Totals			424981	2.760	2.669	410989
Average Chord Length (μm)				98.7	102.0	
Air Content (%)				2.72	2.72	
Powers Spacing Factor (μm)				134.7	139.2	

1. Claculated using Eq. 3.14

Table 3.15 Summary of edge effect correction of mix 8 lineal data truncated at different classes of 29.25 μm

		MEASURED			TRUE[1]			
Classes (#)	Class Size (μm)	Air Content (%)	Average Chord Length (μm)	Total N_L (#/cm)	Air Content (%)	Average Chord Length (μm)	Total N_L (#/cm)	Powers Spacing Factor (μm)
80	29.25	5.18	159.5	3.246	5.18	168.4	3.070	159
40	29.25	4.84	150.2	3.224	4.84	158.0	3.063	159
20	29.25	4.26	135.3	3.148	4.26	141.7	3.006	158
10	29.25	2.72	98.7	2.760	2.72	102.0	2.669	139

1. Calculated using Eq. 3. 14

Table 3.16 Matrix of coefficients M_{ij} used in the calculation of a measured distribution, $N_A(i)^*$, by Eq. 3.28.

20 classes, L = 2995.2 μm, H = 2252.8 μm, class width = 25 μm

1.0097	0.0268	0.0216	0.0193	0.0179	0.0169	0.0163	0.0158	0.0154	0.0151	0.0148	0.0147	0.0145	0.0144	0.0144	0.0143	0.0143	0.0143	0.0143	0.0143
0	1.0025	0.0383	0.0312	0.0280	0.0260	0.0246	0.0236	0.0229	0.0223	0.0218	0.0214	0.0210	0.0208	0.0206	0.0204	0.0202	0.0201	0.0200	0.0200
0	0	0.9891	0.0441	0.0360	0.0324	0.0301	0.0286	0.0274	0.0265	0.0258	0.0252	0.0248	0.0244	0.0241	0.0238	0.0236	0.0234	0.0232	0.0231
0	0	0	0.9743	0.0483	0.0394	0.0354	0.0330	0.0313	0.0301	0.0291	0.0283	0.0277	0.0272	0.0268	0.0264	0.0261	0.0259	0.0257	0.0255
0	0	0	0	0.9588	0.0516	0.0421	0.0378	0.0352	0.0335	0.0321	0.0311	0.0303	0.0297	0.0291	0.0287	0.0283	0.0280	0.0277	0.0275
0	0	0	0	0	0.9428	0.0543	0.0442	0.0398	0.0371	0.0352	0.0338	0.0328	0.0319	0.0312	0.0307	0.0302	0.0298	0.0295	0.0292
0	0	0	0	0	0	0.9267	0.0565	0.0460	0.0414	0.0386	0.0367	0.0352	0.0341	0.0333	0.0326	0.0320	0.0315	0.0311	0.0307
0	0	0	0	0	0	0	0.9104	0.0585	0.0476	0.0428	0.0399	0.0379	0.0364	0.0353	0.0344	0.0337	0.0331	0.0326	0.0322
0	0	0	0	0	0	0	0	0.8941	0.0602	0.0489	0.0440	0.0410	0.0390	0.0375	0.0363	0.0354	0.0347	0.0341	0.0336
0	0	0	0	0	0	0	0	0	0.8777	0.0617	0.0501	0.0450	0.0420	0.0399	0.0384	0.0372	0.0363	0.0356	0.0349
0	0	0	0	0	0	0	0	0	0	0.8613	0.0630	0.0511	0.0460	0.0429	0.0408	0.0392	0.0380	0.0371	0.0363
0	0	0	0	0	0	0	0	0	0	0	0.8450	0.0642	0.0520	0.0468	0.0436	0.0415	0.0399	0.0387	0.0378
0	0	0	0	0	0	0	0	0	0	0	0	0.8288	0.0652	0.0529	0.0475	0.0443	0.0421	0.0405	0.0393
0	0	0	0	0	0	0	0	0	0	0	0	0	0.8126	0.0661	0.0536	0.0481	0.0449	0.0427	0.0411
0	0	0	0	0	0	0	0	0	0	0	0	0	0	0.7965	0.0669	0.0542	0.0487	0.0454	0.0432
0	0	0	0	0	0	0	0	0	0	0	0	0	0	0	0.7805	0.0676	0.0548	0.0492	0.0459
0	0	0	0	0	0	0	0	0	0	0	0	0	0	0	0	0.7646	0.0683	0.0553	0.0496
0	0	0	0	0	0	0	0	0	0	0	0	0	0	0	0	0	0.7488	0.0688	0.0557
0	0	0	0	0	0	0	0	0	0	0	0	0	0	0	0	0	0	0.7331	0.0693
0	0	0	0	0	0	0	0	0	0	0	0	0	0	0	0	0	0	0	0.7176

Table 3.17 Example showing the calculation of a measured distribution, $N_A(i)^*$, using a hypothetical true distribution, $N_A(j)$

			N_A (#/cm^2)	
CLASS	LIMITS (μm)		TRUE	MEASURED[1]
1	0	25	0	0.0143
2	25	50	0	0.0200
3	50	75	0	0.0231
4	75	100	0	0.0255
5	100	125	0	0.0275
6	125	150	0	0.0292
7	150	175	0	0.0307
8	175	200	0	0.0322
9	200	225	0	0.0336
10	225	250	0	0.0349
11	250	275	0	0.0363
12	275	300	0	0.0378
13	300	325	0	0.0393
14	325	350	0	0.0411
15	350	375	0	0.0432
16	375	400	0	0.0459
17	400	425	0	0.0496
18	425	450	0	0.0557
19	450	475	0	0.0693
20	475	500	1.00	0.7176
	N_A (total)		1.00	1.41
	Average Profile Diameter (μm)		487.5	387.3

1. Calculated using Eq. 3.28 and the M_{ij} coefficients of Table 3.16

Table 3.18 Matrix of coefficients N_{ij} used in the calculation of of a true distriubution, $N_A(i)$, by Eq. 3.29.
20 classes, L = 2995.2 μm, H = 2252.8 μm, class width = 25 μm

0.9904	-0.0265	-0.0206	-0.0178	-0.0160	-0.0147	-0.0137	-0.0129	-0.0123	-0.0117	-0.0112	-0.0108	-0.0104	-0.0100	-0.0097	-0.0095	-0.0092	-0.0090	-0.0088	-0.0086
0	0.9975	-0.0386	-0.0302	-0.0261	-0.0235	-0.0215	-0.0200	-0.0188	-0.0177	-0.0168	-0.0160	-0.0153	-0.0146	-0.0141	-0.0135	-0.0130	-0.0126	-0.0122	-0.0118
0	0	1.0110	-0.0458	-0.0357	-0.0308	-0.0277	-0.0253	-0.0235	-0.0220	-0.0207	-0.0196	-0.0187	-0.0178	-0.0170	-0.0163	-0.0157	-0.0151	-0.0145	-0.0140
0	0	0	1.0264	-0.0517	-0.0401	-0.0346	-0.0310	-0.0283	-0.0262	-0.0245	-0.0231	-0.0218	-0.0207	-0.0197	-0.0188	-0.0180	-0.0173	-0.0166	-0.0160
0	0	0	0	1.0430	-0.0571	-0.0440	-0.0378	-0.0338	-0.0309	-0.0286	-0.0267	-0.0251	-0.0237	-0.0225	-0.0214	-0.0204	-0.0195	-0.0187	-0.0179
0	0	0	0	0	1.0606	-0.0621	-0.0477	-0.0409	-0.0365	-0.0333	-0.0307	-0.0287	-0.0269	-0.0254	-0.0241	-0.0229	-0.0218	-0.0208	-0.0199
0	0	0	0	0	0	1.0791	-0.0670	-0.0512	-0.0438	-0.0390	-0.0355	-0.0328	-0.0305	-0.0286	-0.0270	-0.0255	-0.0242	-0.0231	-0.0220
0	0	0	0	0	0	0	1.0984	-0.0718	-0.0546	-0.0466	-0.0414	-0.0376	-0.0347	-0.0323	-0.0302	-0.0285	-0.0269	-0.0255	-0.0243
0	0	0	0	0	0	0	0	1.1185	-0.0767	-0.0581	-0.0494	-0.0438	-0.0397	-0.0366	-0.0340	-0.0318	-0.0299	-0.0282	-0.0268
0	0	0	0	0	0	0	0	0	1.1394	-0.0816	-0.0615	-0.0521	-0.0462	-0.0418	-0.0384	-0.0357	-0.0333	-0.0313	-0.0296
0	0	0	0	0	0	0	0	0	0	1.1610	-0.0865	-0.0649	-0.0549	-0.0485	-0.0439	-0.0403	-0.0373	-0.0349	-0.0327
0	0	0	0	0	0	0	0	0	0	0	1.1834	-0.0916	-0.0685	-0.0577	-0.0509	-0.0460	-0.0421	-0.0390	-0.0364
0	0	0	0	0	0	0	0	0	0	0	0	1.2066	-0.0968	-0.0720	-0.0606	-0.0533	-0.0481	-0.0440	-0.0407
0	0	0	0	0	0	0	0	0	0	0	0	0	1.2306	-0.1021	-0.0757	-0.0635	-0.0558	-0.0502	-0.0459
0	0	0	0	0	0	0	0	0	0	0	0	0	0	1.2555	-0.1076	-0.0795	-0.0665	-0.0583	-0.0524
0	0	0	0	0	0	0	0	0	0	0	0	0	0	0	1.2812	-0.1133	-0.0834	-0.0696	-0.0609
0	0	0	0	0	0	0	0	0	0	0	0	0	0	0	0	1.3079	-0.1193	-0.0874	-0.0727
0	0	0	0	0	0	0	0	0	0	0	0	0	0	0	0	0	1.3355	-0.1254	-0.0916
0	0	0	0	0	0	0	0	0	0	0	0	0	0	0	0	0	0	1.3640	-0.1317
0	0	0	0	0	0	0	0	0	0	0	0	0	0	0	0	0	0	0	1.3936

Table 3.19 Example showing the calculation of a true distribution, $N_A(i)$, using a hypothetical measured distribution, $N_A(j)$*

CLASS	LIMITS (μm)		N_A (#/cm^2) MEASURED	N_A (#/cm^2) TRUE[1]
1	0	25	10	7.470
2	25	50	10	6.611
3	50	75	10	6.307
4	75	100	10	6.178
5	100	125	10	6.149
6	125	150	10	6.192
7	150	175	10	6.291
8	175	200	10	6.440
9	200	225	10	6.636
10	225	250	10	6.879
11	250	275	10	7.169
12	275	300	10	7.511
13	300	325	10	7.910
14	325	350	10	8.373
15	350	375	10	8.911
16	375	400	10	9.540
17	400	425	10	10.285
18	425	450	10	11.185
19	450	475	10	12.323
20	475	500	10	13.936
	N_A (total)		200	162.30
	Average Profile Diameter (μm)		250.0	283.4

1. Calculated using Eq. 3.29 and the N_{ij} coefficients of Table 3.18

Table 3.20 Edge effect correction of mix 8 areal data using 80 classes of 25 μm width

			MEASURED		TRUE	
CLASS	LIMITS (μm)		FEATURES	N_A (#/cm^2)	N_A (#/cm^2)	FEATURES
1	0	25	8379	118.26	112.90	7999
2	25	50	5105	72.05	68.01	4818
3	50	75	2386	33.68	30.57	2166
4	75	100	1681	23.73	21.27	1507
5	100	125	1294	18.26	16.35	1159
6	125	150	1051	14.83	13.43	951
7	150	175	797	11.25	10.14	719
8	175	200	626	8.84	7.96	564
9	200	225	578	8.16	7.70	545
10	225	250	389	5.49	5.01	355
11	250	275	363	5.12	4.94	350
12	275	300	236	3.33	3.06	217
13	300	325	194	2.74	2.53	179
14	325	350	159	2.24	2.07	147
15	350	375	148	2.09	2.03	144
16	375	400	119	1.68	1.64	116
17	400	425	95	1.34	1.31	93
18	425	450	97	1.37	1.48	105
19	450	475	60	0.85	0.85	60
20	475	500	45	0.64	0.62	44
21	500	525	36	0.51	0.47	34
22	525	550	41	0.58	0.64	45
23	550	575	22	0.31	0.27	19
24	575	600	22	0.31	0.29	20
25	600	625	30	0.42	0.52	37
26	625	650	18	0.25	0.28	20
27	650	675	16	0.23	0.26	19
28	675	700	15	0.21	0.27	19
29	700	725	7	0.10	0.09	7
30	725	750	4	0.06	0.02	1
31	750	775	11	0.16	0.22	16
32	775	800	5	0.07	0.08	6
33	800	825	2	0.03	0.00	0
34	825	850	4	0.06	0.06	5
35	850	875	1	0.01	-0.02	-2
36	875	900	3	0.04	0.03	2
37	900	925	4	0.06	0.07	5
38	925	950	2	0.03	0.02	1
39	950	975	3	0.04	0.05	4
40	975	1000	2	0.03	0.02	2
41	1000	1025	3	0.04	0.07	5
42	1025	1050	1	0.01	0.00	0
43	1050	1075	2	0.03	0.04	3
44	1075	1100	2	0.03	0.05	3
45	1100	1125	2	0.03	0.06	4
46	1125	1150	0	0.00	-0.01	-1
47	1150	1175	0	0.00	-0.02	-1

Table 3.20 Continued

			MEASURED		TRUE[1]	
CLASS	LIMITS (μm)		FEATURES	N_A (#/cm^2)	N_A (#/cm^2)	FEATURES
48	1175	1200	0	0.00	-0.02	-1
49	1200	1225	0	0.00	-0.03	-2
50	1225	1250	1	0.01	0.02	1
51	1250	1275	0	0.00	-0.03	-2
52	1275	1300	1	0.01	0.02	1
53	1300	1325	1	0.01	0.02	1
54	1325	1350	1	0.01	0.03	2
55	1350	1375	0	0.00	-0.03	-2
56	1375	1400	1	0.01	0.03	2
57	1400	1425	1	0.01	0.04	3
58	1425	1450	0	0.00	-0.03	-2
59	1450	1475	1	0.01	0.04	3
60	1475	1500	1	0.01	0.06	4
61	1500	1525	0	0.00	-0.01	-1
62	1525	1550	0	0.00	-0.01	-1
63	1550	1575	0	0.00	-0.01	-1
64	1575	1600	0	0.00	-0.02	-1
65	1600	1625	0	0.00	-0.03	-2
66	1625	1650	0	0.00	-0.04	-3
67	1650	1675	0	0.00	-0.06	-4
68	1675	1700	1	0.01	0.05	3
69	1700	1725	0	0.00	-0.09	-6
70	1725	1750	2	0.03	0.18	13
71	1750	1775	0	0.00	-0.04	-3
72	1775	1800	0	0.00	-0.09	-7
73	1800	1825	2	0.03	0.25	17
74	1825	1850	0	0.00	0.00	0
75	1850	1875	0	0.00	0.00	0
76	1875	1900	0	0.00	0.00	0
77	1900	1925	0	0.00	0.00	0
78	1925	1950	0	0.00	0.00	0
79	1950	1975	0	0.00	0.00	0
80	1975	2000	0	0.00	0.00	0
Totals			24073	339.77	317.89	22523
Average Feature Diameter (μm)				84.7	85.3	
Air Content (%)				5.30	5.29	
Powers Spacing Factor (μm)				169	182	

1. Calculated using Eq. 3.29

Table 3.21 Edge effect correction of mix 8 areal data using 40 classes of 50 μm width

			MEASURED		TRUE[1]	
CLASS	LIMITS (μm)		FEATURES	N_A (#/cm^2)	N_A (#/cm^2)	FEATURES
1	0	50	13484	190.32	180.61	12796
2	50	100	4067	57.40	51.74	3666
3	100	150	2345	33.10	29.75	2108
4	150	200	1423	20.08	18.09	1282
5	200	250	967	13.65	12.66	897
6	250	300	599	8.45	7.95	563
7	300	350	353	4.98	4.59	325
8	350	400	267	3.77	3.66	259
9	400	450	192	2.71	2.79	198
10	450	500	105	1.48	1.46	103
11	500	550	77	1.09	1.12	79
12	550	600	44	0.62	0.56	40
13	600	650	48	0.68	0.79	56
14	650	700	31	0.44	0.54	38
15	700	750	11	0.16	0.11	8
16	750	800	16	0.23	0.29	21
17	800	850	6	0.08	0.07	5
18	850	900	4	0.06	0.02	1
19	900	950	6	0.08	0.09	6
20	950	1000	5	0.07	0.08	6
21	1000	1050	4	0.06	0.07	5
22	1050	1100	4	0.06	0.09	7
23	1100	1150	2	0.03	0.04	3
24	1150	1200	0	0.00	-0.04	-3
25	1200	1250	1	0.01	-0.01	0
26	1250	1300	1	0.01	-0.01	-1
27	1300	1350	2	0.03	0.05	3
28	1350	1400	1	0.01	0.00	0
29	1400	1450	1	0.01	0.00	0
30	1450	1500	2	0.03	0.09	7
31	1500	1550	0	0.00	-0.02	-2
32	1550	1600	0	0.00	-0.04	-3
33	1600	1650	0	0.00	-0.07	-5
34	1650	1700	1	0.01	-0.02	-1
35	1700	1750	2	0.03	0.13	10
36	1750	1800	0	0.00	-0.11	-8
37	1800	1850	2	0.03	0.21	15
38	1850	1900	0	0.00	0.00	0
39	1900	1950	0	0.00	0.00	0
40	1950	2000	0	0.00	0.00	0
TOTALS			24073	339.77	317.31	22481
Average Feature Diameter (μm)				87.2	87.9	
Air Content (%)				5.34	5.32	
Powers Spacing Factor (μm)				165	175	

1. Calculated using Eq.3.29

Table 3.22 Edge effect correction of mix 8 areal data using 20 classes of 100 μm width

			MEASURED		TRUE[1]	
CLASS	LIMITS (μm)		FEATURES	N_A (#/cm^2)	N_A (#/cm^2)	FEATURES
1	0	100	17551	247.72	230.18	16308
2	100	200	3768	53.18	47.56	3370
3	200	300	1566	22.1	20.44	1448
4	300	400	620	8.75	8.23	583
5	400	500	297	4.19	4.19	297
6	500	600	121	1.71	1.66	118
7	600	700	79	1.12	1.3	92
8	700	800	27	0.38	0.42	30
9	800	900	10	0.14	0.08	6
10	900	1000	11	0.16	0.17	12
11	1000	1100	8	0.11	0.16	12
12	1100	1200	2	0.03	-0.01	0
13	1200	1300	2	0.03	-0.02	-1
14	1300	1400	3	0.04	0.04	3
15	1400	1500	3	0.04	0.11	7
16	1500	1600	0	0	-0.07	-5
17	1600	1700	1	0.01	-0.05	-3
18	1700	1800	2	0.03	0.02	2
19	1800	1900	2	0.03	0.17	12
20	1900	2000	0	0	0	0
TOTALS			24073	339.77	314.58	22291
Average Feature Diameter (μm)				98.6	99.6	
Air Content (%)				5.62	5.55	
Powers Spacing Factor (μm)				146	156	

1. Calculated using Eq. 3.29

Table 3.23 Edge effect correction of mix 8 areal data using 10 classes of 200 μm width

			MEASURED		TRUE[1]	
CLASS	LIMITS (μm)		FEATURES	N_A (#/cm^2)	N_A (#/cm^2)	FEATURES
1	0	200	21319	300.9	271.5	19236
2	200	400	2186	30.85	28.03	1986
3	400	600	418	5.9	5.69	403
4	600	800	106	1.5	1.63	115
5	800	1000	21	0.3	0.27	19
6	1000	1200	10	0.14	0.13	9
7	1200	1400	5	0.07	0.05	4
8	1400	1600	3	0.04	0	0
9	1600	1800	3	0.04	0.03	2
10	1800	2000	2	0.03	0.13	9
TOTALS			24073	339.77	307.46	21783
Average Feature Diameter (μm)				129.6	131.0	
Air Content (%)				6.95	6.65	
Powers Spacing Factor (μm)				111	121	

1. Calculated using Eq.3.29

Table 3.24 Summary of edge effect correction of mix 8 areal data using different class sizes

		MEASURED			TRUE[1]			
Classes (#)	Class Size (μm)	Air Content (%)	Average Profile Diameter (μm)	Total N_A (#/cm^2)	Air Content (%)	Average Profile Diameter (μm)	Total N_A (#/cm^2)	Powers Spacing Factor (μm)
80	25	5.30	84.7	339.77	5.29	85.3	317.89	182
40	50	5.34	87.2	339.77	5.32	87.9	317.31	175
20	100	5.62	98.6	339.77	5.55	99.6	314.58	156
10	200	6.95	129.6	339.77	6.65	131.0	307.46	121

1. Calculated using Eq. 2.29

Table 3.25 Edge effect correction of mix 8 areal data truncated at 40 classes of 25 μm width

			MEASURED		TRUE[1]	
CLASS	LIMITS (μm)		FEATURES	N_A (#/cm^2)	N_A (#/cm^2)	FEATURES
1	0	25	8379	118.26	112.91	7999
2	25	50	5105	72.05	68.01	4818
3	50	75	2386	33.68	30.57	2166
4	75	100	1681	23.73	21.28	1507
5	100	125	1294	18.26	16.36	1159
6	125	150	1051	14.83	13.43	951
7	150	175	797	11.25	10.15	719
8	175	200	626	8.84	7.96	564
9	200	225	578	8.16	7.7	546
10	225	250	389	5.49	5.02	355
11	250	275	363	5.12	4.94	350
12	275	300	236	3.33	3.06	217
13	300	325	194	2.74	2.53	179
14	325	350	159	2.24	2.07	147
15	350	375	148	2.09	2.03	144
16	375	400	119	1.68	1.65	117
17	400	425	95	1.34	1.31	93
18	425	450	97	1.37	1.48	105
19	450	475	60	0.85	0.86	61
20	475	500	45	0.64	0.62	44
21	500	525	36	0.51	0.48	34
22	525	550	41	0.58	0.64	46
23	550	575	22	0.31	0.27	19
24	575	600	22	0.31	0.29	21
25	600	625	30	0.42	0.52	37
26	625	650	18	0.25	0.29	20
27	650	675	16	0.23	0.27	19
28	675	700	15	0.21	0.28	20
29	700	725	7	0.1	0.1	7
30	725	750	4	0.06	0.03	2
31	750	775	11	0.16	0.23	17
32	775	800	5	0.07	0.09	7
33	800	825	2	0.03	0.01	1
34	825	850	4	0.06	0.08	6
35	850	875	1	0.01	-0.01	-1
36	875	900	3	0.04	0.05	4
37	900	925	4	0.06	0.1	7
38	925	950	2	0.03	0.04	3
39	950	975	3	0.04	0.08	6
40	975	1000	2	0.03	0.06	5
Totals			24050	339.45	317.85	22521
Average Feature Diameter (μm)				83.5	84.5	
Air Content (%)				4.83	4.83	
Powers Spacing Factor (μm)				172	182	

1. Calculated using Eq. 3.29

Table 3.26 Edge effect correction of mix 8 areal data truncated at 20 classes of 25 μm width

			MEASURED		TRUE[1]	
CLASS	LIMITS (μm)		FEATURES	N_A (#/cm^2)	N_A (#/cm^2)	FEATURES
1	0	25	8379	118.26	112.93	8001
2	25	50	5105	72.05	68.04	4821
3	50	75	2386	33.68	30.61	2169
4	75	100	1681	23.73	21.32	1511
5	100	125	1294	18.26	16.41	1162
6	125	150	1051	14.83	13.48	955
7	150	175	797	11.25	10.21	723
8	175	200	626	8.84	8.03	569
9	200	225	578	8.16	7.77	551
10	225	250	389	5.49	5.1	361
11	250	275	363	5.12	5.03	356
12	275	300	236	3.33	3.16	224
13	300	325	194	2.74	2.63	187
14	325	350	159	2.24	2.19	155
15	350	375	148	2.09	2.16	153
16	375	400	119	1.68	1.79	127
17	400	425	95	1.34	1.47	104
18	425	450	97	1.37	1.66	118
19	450	475	60	0.85	1.07	76
20	475	500	45	0.64	0.89	63
TOTALS			23802	335.95	315.96	22386
Average Feature Diameter (μm)				77.9	79.1	
Air Content (%)				3.72	3.71	
Powers Spacing Factor (μm)				168	176	

1. Calculated using Eq. 3.29

Table 3.27 Edge effect correction of mix 8 areal data truncated at 10 classes of 25 μm width

CLASS	LIMITS (μm)		MEASURED		TRUE[1]	
			FEATURES	N_A (#/cm^2)	N_A (#/cm^2)	FEATURES
1	0	25	8379	118.26	113.15	8017
2	25	50	5105	72.05	68.36	4843
3	50	75	2386	33.68	31	2197
4	75	100	1681	23.73	21.78	1543
5	100	125	1294	18.26	16.93	1199
6	125	150	1051	14.83	14.08	998
7	150	175	797	11.25	10.89	772
8	175	200	626	8.84	8.82	625
9	200	225	578	8.16	8.7	617
10	225	250	389	5.49	6.26	443
TOTALS			22286	314.55	299.97	21254
Average Feature Diameter (μm)				60.3	61.4	
Air Content (%)				1.75	1.75	
Powers Spacing Factor (μm)				154	158	

1. Calculated using Eq. 3.29

Table 3.28 Summary of edge effect correction of mix 8 areal data truncated at different classes of 25 μm

		MEASURED			TRUE[1]			
Classes (#)	Class Size (μm)	Air Content (%)	Average Profile Diameter (μm)	Total N_A (#/cm^2)	Air Content (%)	Average Profile Diameter (μm)	Total N_A (#/cm^2)	Powers Spacing Factor (μm)
80	25	5.30	84.7	339.77	5.29	85.3	317.89	182
40	25	4.83	83.5	339.45	4.83	84.5	317.85	182
20	25	3.72	77.9	335.95	3.71	79.1	315.96	176
10	25	1.75	60.3	314.55	1.75	61.4	299.97	158

1. Calculated using Eq. 3.29

Table 3.29 Matrix of coefficients B_{ij} used in the calculation of an areal distribution, $N_A(i)$, from a volume distribution, $N_V(j)$, using Eq. 3.53

0.50000	0.42643	0.21230	0.14702	0.11302	0.09194	0.07754	0.06707	0.05910	0.05283
0	1.07357	0.85844	0.48795	0.35843	0.28584	0.23851	0.20496	0.17984	0.16029
0	0	1.42926	1.15267	0.68467	0.51632	0.41964	0.35527	0.30882	0.27351
0	0	0	1.71236	1.38906	0.84371	0.64585	0.53104	0.45382	0.39757
0	0	0	0	1.95482	1.59185	0.98007	0.75752	0.62777	0.54004
0	0	0	0	0	2.17035	1.77210	1.10102	0.85678	0.71408
0	0	0	0	0	0	2.36631	1.93590	1.21069	0.94684
0	0	0	0	0	0	0	2.54723	2.08704	1.31168
0	0	0	0	0	0	0	0	2.71612	2.22805
0	0	0	0	0	0	0	0	0	2.87511

Table 3.30 Example showing the calculation of an areal distribution, $N_A(i)$, using a hypothetical volume distribution, $N_V(j)$

CLASS	LIMITS (μm)		Hypothetical N_V (#/cm^3)	Calculated[1] N_A (#/cm^2)
1	0.0	0.2	0.0	0.132
2	0.2	0.4	0.0	0.401
3	0.4	0.6	0.0	0.684
4	0.6	0.8	0.0	0.994
5	0.8	1.0	0.0	1.350
6	1.0	1.2	0.0	1.785
7	1.2	1.4	0.0	2.367
8	1.4	1.6	0.0	3.279
9	1.6	1.8	0.0	5.570
10	1.8	2.0	1000.0	7.188
Totals			1000.0	23.75
Average Feature Diameter (μm)			1.90	1.49

1. Calculated using Eq. 3.53 and the B_{ij} coefficients of Table 3.29

Table 3.31 Matrix of coefficients J_{ij} used in the calculation of a volume distribution, $N_V(i)$, from an areal distribution, $N_A(j)$, using Eq. 3.54

2.00000	-0.79441	0.18005	-0.06655	0.01426	-0.00752	0.00049	-0.00134	-0.00038	-0.00045
0	0.93147	-0.55946	0.11117	-0.05384	0.00669	-0.00773	-0.00110	-0.00202	-0.00102
0	0	0.69967	-0.47098	0.08962	-0.04909	0.00411	-0.00796	-0.00181	-0.00240
0	0	0	0.58399	-0.41497	0.07734	-0.04544	0.00276	-0.00793	-0.00217
0	0	0	0	0.51156	-0.37520	0.06911	-0.04248	0.00195	-0.00779
0	0	0	0	0	0.46076	-0.34505	0.06308	-0.04001	0.00142
0	0	0	0	0	0	0.42260	-0.32118	0.05842	-0.03792
0	0	0	0	0	0	0	0.39258	-0.30166	0.05466
0	0	0	0	0	0	0	0	0.36817	-0.28531
0	0	0	0	0	0	0	0	0	0.34781

Table 3.32 Example showing the calculation of a volume distribution, $N_V(i)$, from a synthetic distribution, $N_A(j)$

CLASS	LIMITS (μm)		N_A (#/cm^2)[1]	N_V (#/cm^3)	
				Calculated[2]	True[1]
1	0.0	0.2	2200	278900	341000
2	0.2	0.4	7000	1413535	1703000
3	0.4	0.6	12800	5536889	5827000
4	0.6	0.8	18800	13830369	13647000
5	0.8	1.0	22067	22481156	21893000
6	1.0	1.2	19800	24831722	24063000
7	1.2	1.4	12933	18073304	18122000
8	1.4	1.6	6067	9102831	9349000
9	1.6	1.8	1933	2987755	3303000
10	1.8	2.0	400	695625	799000
Totals			104000	99232080	99047000
Average Feature Diameter (μm)			0.90	1.05	1.05

1. From a synthetic example by Cruz-Orive (Weibel 1980, pg 203)
2. Calculated using Eq. 3.54 and the J_{ij} coefficients in Table 3.31

Table 3.33 Area-to-volume conversion of mix 8 areal data using 80 classes of 25 μm width

CLASS	LIMITS (μm)		N_A (#/cm^2)	N_V(#/cm^3)[1]
1	0	25	112.90	70396.81
2	25	50	68.01	19079.19
3	50	75	30.57	4844.77
4	75	100	21.27	2454.61
5	100	125	16.35	1453.19
6	125	150	13.43	1129.04
7	150	175	10.14	779.30
8	175	200	7.96	345.09
9	200	225	7.70	609.01
10	225	250	5.01	176.78
11	250	275	4.94	347.50
12	275	300	3.06	139.33
13	300	325	2.53	116.25
14	325	350	2.07	60.90
15	350	375	2.03	81.86
16	375	400	1.64	75.68
17	400	425	1.31	16.47
18	425	450	1.48	82.97
19	450	475	0.85	33.94
20	475	500	0.62	26.75
21	500	525	0.47	-4.34
22	525	550	0.64	36.68
23	550	575	0.27	6.29
24	575	600	0.29	-10.78
25	600	625	0.52	25.34
26	625	650	0.28	7.55
27	650	675	0.26	4.03
28	675	700	0.27	14.13
29	700	725	0.09	7.98
30	725	750	0.02	-11.95
31	750	775	0.22	11.31
32	775	800	0.08	6.71
33	800	825	0.00	-4.53
34	825	850	0.06	5.75
35	850	875	-0.02	-3.32
36	875	900	0.03	-2.32
37	900	925	0.07	4.64
38	925	950	0.02	-2.37
39	950	975	0.05	2.90
40	975	1000	0.02	-2.50
41	1000	1025	0.07	4.66
42	1025	1050	0.00	-2.11
43	1050	1075	0.04	0.75
44	1075	1100	0.05	-0.15
45	1100	1125	0.06	4.67
46	1125	1150	-0.01	-0.04
47	1150	1175	-0.02	-0.46

Table 3.33 Continued

CLASS	LIMITS (μm)		N_A (#/cm^2)	N_V(#/cm^3)[1]
48	1175	1200	-0.02	0.42
49	1200	1225	-0.03	-3.16
50	1225	1250	0.02	2.83
51	1250	1275	-0.03	-2.80
52	1275	1300	0.02	0.35
53	1300	1325	0.02	-0.59
54	1325	1350	0.03	3.10
55	1350	1375	-0.03	-2.65
56	1375	1400	0.03	-0.67
57	1400	1425	0.04	3.50
58	1425	1450	-0.03	-2.91
59	1450	1475	0.04	-0.40
60	1475	1500	0.06	3.55
61	1500	1525	-0.01	-0.01
62	1525	1550	-0.01	0.01
63	1550	1575	-0.01	-0.09
64	1575	1600	-0.02	0.14
65	1600	1625	-0.03	-0.77
66	1625	1650	-0.04	1.47
67	1650	1675	-0.06	-6.81
68	1675	1700	0.05	7.43
69	1700	1725	-0.09	-11.95
70	1725	1750	0.18	8.98
71	1750	1775	-0.04	3.55
72	1775	1800	-0.09	-14.81
73	1800	1825	0.25	12.27
74	1825	1850	0.00	0.00
75	1850	1875	0.00	0.00
76	1875	1900	0.00	0.00
77	1900	1925	0.00	0.00
78	1925	1950	0.00	0.00
79	1950	1975	0.00	0.00
80	1975	2000	0.00	0.00
Totals			317.89	102347.87
Average Feature Diameter (μm)			85.32	31.06
Air Content (%)			5.29	5.26
Total Specific Surface			205.9	203.5
Powers Spacing Factor (μm)			180	182
Philleo Factor (μm)			--	99

1. Calculated using Eq. 3.54

Table 3.34 Area-to-volume conversion of mix 8 areal data using 40 classes of 50 μm width

CLASS	LIMITS (μm)		N_A (#/cm^2)	N_V(#/cm^3)[1]
1	0	50	180.61	64875.49
2	50	100	51.74	6576.73
3	100	150	29.75	2603.33
4	150	200	18.09	1138.72
5	200	250	12.66	729.19
6	250	300	7.95	437.27
7	300	350	4.59	172.74
8	350	400	3.66	125.14
9	400	450	2.79	128.86
10	450	500	1.46	40.48
11	500	550	1.12	48.17
12	550	600	0.56	0.32
13	600	650	0.79	20.89
14	650	700	0.54	27.86
15	700	750	0.11	-6.5
16	750	800	0.29	12.53
17	800	850	0.07	2.98
18	850	900	0.02	-2.61
19	900	950	0.09	1.27
20	950	1000	0.08	1.71
21	1000	1050	0.07	0.02
22	1050	1100	0.09	2.38
23	1100	1150	0.04	3.33
24	1150	1200	-0.04	-1.91
25	1200	1250	-0.01	0.36
26	1250	1300	-0.01	-2.08
27	1300	1350	0.05	1.47
28	1350	1400	0	0.77
29	1400	1450	0	-3.1
30	1450	1500	0.09	4.36
31	1500	1550	-0.02	-0.06
32	1550	1600	-0.04	0.05
33	1600	1650	-0.07	-1.02
34	1650	1700	-0.02	-6.15
35	1700	1750	0.13	9.23
36	1750	1800	-0.11	-9.99
37	1800	1850	0.21	7.34
38	1850	1900	0	0
39	1900	1950	0	0
40	1950	2000	0	0
Totals			317.3	76939.6
Average Feature Diameter (μm)			87.9	41.2
Air Content (%)			5.32	5.23
Total Specific Surface (cm^2/cm^3)			210.1	205.1
Powers Spacing Factor (μm)			175	182
Philleo Factor (μm)			--	109

1. Calculated using Eq. 3.54

Table 3.35 Area-to-volume conversion of mix 8 areal data using 20 classes of 100 μm width

CLASS	LIMITS (μm)		N_A (#/cm^2)	N_V(#/cm^3)[1]
1	0	100	230.18	42575.45
2	100	200	47.56	3355.63
3	200	300	20.44	072.10
4	300	400	8.23	313.67
5	400	500	4.19	159.01
6	500	600	1.66	33.82
7	600	700	1.30	41.20
8	700	800	0.42	14.35
9	800	900	0.08	-0.95
10	900	1000	0.17	1.32
11	1000	1100	0.16	5.42
12	1100	1200	-0.01	0.00
13	1200	1300	-0.02	-0.77
14	1300	1400	0.04	-1.60
15	1400	1500	0.11	4.19
16	1500	1600	-0.07	-1.10
17	1600	1700	-0.05	-1.13
18	1700	1800	0.02	-2.84
19	1800	1900	0.17	4.14
20	1900	2000	0.00	0.00
Totals			339.8	47571.9
Average Feature Diameter (μm)			99.6	66.1
Air Content (%)			5.55	5.25
Total Specific Surface (cm^2/cm^3)			225.9	219.1
Powers Spacing Factor (μm)			156	170
Philleo Factor (μm)			--	127

1. Calculated using Eq. 3.54

Table 3.36 Area-to-volume conversion of mix 8 areal data using 10 classes of 200 μm width

CLASS	LIMITS (μm)		N_A (#/cm^2)	N_V(#/cm^3)[1]
1	0	200	271.50	26082.56
2	200	400	28.03	1154.48
3	400	600	5.69	161.62
4	600	800	1.63	42.31
5	800	1000	0.27	4.64
6	1000	1200	0.13	2.06
7	1200	1400	0.05	1.02
8	1400	1600	0.00	-0.19
9	1600	1800	0.03	-1.25
10	1800	2000	0.13	2.20
Totals			307.5	27449.5
Average Feature Diameter (μm)			131.0	112.0
Air Content (%)			6.64	5.69
Total Specific Surface (cm^2/cm^3)			283.4	241.8
Powers Spacing Factor (μm)			121	142
Philleo Factor (μm)			--	151

1. Calculated using Eq. 3.54

Table 3.37 Summary of area-to-volume conversion of mix 8 areal data using different size classes

		Area Distribution			Volume Distribution[1]				
Classes (#)	Class Size (μm)	Air Content (%)	Average Profile Diameter (μm)	Total N_A (#/cm^2)	Air Content (%)	Average Sphere Diameter (μm)	Total N_V (#/cm^3)	Powers Spacing Factor (μm)	Philleo Factor (μm)
80	25	5.29	85.3	317.9	5.26	31.1	102348	181	99
40	50	5.32	87.9	317.3	5.23	41.2	76940	180	108
20	100	5.55	99.6	314.6	5.25	66.1	47572	168	127
10	200	6.65	131.0	307.5	5.69	112.0	27449	152	153

1. Calculated using Eq. 3.54

Table 3.38 Area-to-volume conversion of mix 8 areal data truncated at 40 classes of 25 μm width

CLASS	LIMITS (μm)		N_A (#/cm^2)	N_V (#/cm^3)[1]
1	0	25	112.91	70397.81
2	25	50	68.01	19079.48
3	50	75	30.57	4844.93
4	75	100	21.28	2454.72
5	100	125	16.36	1453.28
6	125	150	13.43	1129.11
7	150	175	10.15	779.36
8	175	200	7.96	345.14
9	200	225	7.70	609.05
10	225	250	5.02	176.81
11	250	275	4.94	347.53
12	275	300	3.06	139.35
13	300	325	2.53	116.27
14	325	350	2.07	60.92
15	350	375	2.03	81.88
16	375	400	1.65	75.70
17	400	425	1.31	16.48
18	425	450	1.48	82.99
19	450	475	0.86	33.96
20	475	500	0.62	26.76
21	500	525	0.48	-4.33
22	525	550	0.64	36.70
23	550	575	0.27	6.31
24	575	600	0.29	-10.76
25	600	625	0.52	25.37
26	625	650	0.29	7.58
27	650	675	0.27	4.06
28	675	700	0.28	14.16
29	700	725	0.10	8.03
30	725	750	0.03	-11.89
31	750	775	0.23	11.38
32	775	800	0.09	6.80
33	800	825	0.01	-4.42
34	825	850	0.08	5.89
35	850	875	-0.01	-3.16
36	875	900	0.05	-2.01
37	900	925	0.10	4.81
38	925	950	0.04	-1.31
39	950	975	0.08	2.17
40	975	1000	0.06	4.38
Totals			317.9	102351.3
Average Feature Diameter (μm)			84.5	31.1
Air Content (%)			4.83	4.80
Total Specific Surface (cm^2/cm^3)			222.5	220.8
Powers Spacing Factor (μm)			182	184
Philleo Factor (μm)			--	100

1. Calculated using Eq. 3.54

Table 3.39 Area-to-volume conversion of mix 8 areal data truncated at 20 classes of 25 μm width

CLASS	LIMITS (μm)		N_A (#/cm^2)	N_V (#/cm^3)[1]
1	0	25	112.93	70410.04
2	25	50	68.04	19084.17
3	50	75	30.61	4848.08
4	75	100	21.32	2457.20
5	100	125	16.41	1455.40
6	125	150	13.48	1131.05
7	150	175	10.21	781.21
8	175	200	8.03	346.97
9	200	225	7.77	610.93
10	225	250	5.10	178.79
11	250	275	5.03	349.67
12	275	300	3.16	141.73
13	300	325	2.63	118.95
14	325	350	2.19	64.10
15	350	375	2.16	85.50
16	375	400	1.79	80.78
17	400	425	1.47	21.32
18	425	450	1.66	95.09
19	450	475	1.07	35.79
20	475	500	0.89	85.48
Totals			316.0	102382.2
Average Feature Diameter (μm)			79.1	30.9
Air Content (%)			3.71	3.68
Total Specific Surface (cm^2/cm^3)			269.6	267.6
Powers Spacing Factor (μm)			176	178
Philleo Factor (μm)			--	105

1. Calculated using Eq.3.54

Table 3.40 Area-to-volume conversion of mix 8 areal data truncated at 10 classes of 25 μm width

CLASS	LIMITS (μm)		N_A (#/cm^2)	N_V (#/cm^3)[1]
1	0	25	113.15	70500.91
2	25	50	68.36	19127.11
3	50	75	31.00	4882.22
4	75	100	21.78	2491.11
5	100	125	16.93	1489.17
6	125	150	14.08	1178.85
7	150	175	10.89	816.24
8	175	200	8.82	471.45
9	200	225	8.70	567.87
10	225	250	6.26	870.31
Totals			300.0	102395.3
Average Feature Diameter (μm)			61.4	29.3
Air Content (%)			1.75	1.72
Total Specific Surface (cm^2/cm^3)			421.6	419.4
Powers Spacing Factor (μm)			158	160
Philleo Factor (μm)			--	119

1. Calculated using Eq. 3.54

Table 3.41 Summary of area-to-volume analyses of mix 8 areal data using distributions truncated at different classes of 25 μm width

		Area Distribution			Volume Distribution[1]				
Classes (#)	Class Size (μm)	Air Content (%)	Average Profile Diameter (μm)	Total N_A (#/cm^2)	Air Content (%)	Average Sphere Diameter (μm)	Total N_V (#/cm^3)	Powers Spacing Factor (μm)	Philleo Factor (μm)
80	25	5.29	85.3	317.9	5.26	31.1	102348	181	99
40	25	4.83	84.5	317.9	4.80	31.1	102351	184	100
20	25	3.71	79.1	316.0	3.68	30.9	102382	178	105
10	25	1.75	61.4	300.0	1.72	29.3	102395	160	120

1. Calculated using Eq. 3.54

Table 3.42 Comparison of spacing factors from volume distributions[1] calculated using the largest 85 and 40 classes[2] of measured areal data

MAGNIFICATION 12x

Sample	Powers spacing factor			Philleo factor		
	85 classes	40 classes	Change (%)	85 classes	40 classes	Change (%)
1	451	393	-12.9	212	221	4.2
2	474	405	-14.6	224	234	4.5
3	182	171	-6.0	133	136	2.3
4	119	120	0.8	110	111	0.9
5	140	135	-3.6	114	116	1.8
6	125	127	1.6	110	113	2.7
7	192	196	2.1	142	146	2.8
8	207	211	1.9	146	150	2.7
9	224	220	-1.8	167	170	1.8
10	195	198	1.5	157	160	1.9

MAGNIFICATION 30x

Sample	Powers spacing factor			Philleo factor		
	85 classes	40 classes	Change (%)	85 classes	40 classes	Change (%)
1	383	350	-8.6	156	160	2.6
2	465	387	-16.8	164	173	5.5
3	177	164	-7.3	106	109	2.8
4	113	113	0.0	92	95	3.3
5	127	120	-5.5	98	100	2.0
6	130	124	-4.6	100	101	1.0
7	186	189	1.6	115	118	2.6
8	182	184	1.1	99	100	1.0
9	217	213	-1.8	121	123	1.7
10	177	179	1.1	105	107	1.9

1. Calculated using Eq. 3.54
2. Class size = 25 μm

Table 4.1 Lineal analysis total chord density

Specimen	Total Chord Density (#/cm)					
	Magnification 12x			Magnification 30x		
	N_L*[1]	N_L[2]	% Change[3]	N_L*[1]	N_L[2]	% Change[3]
1	0.922	0.893	-3.1	1.547	1.473	-4.8
2	0.870	0.841	-3.3	1.147	1.070	-6.7
3	3.487	3.412	-2.2	3.933	3.760	-4.4
4	5.242	5.158	-1.6	5.243	5.033	-4.0
5	3.940	3.877	-1.6	4.291	4.153	-3.2
6	4.109	4.050	-1.4	4.132	3.965	-4.0
7	3.268	3.189	-2.4	3.380	3.181	-5.9
8	2.821	2.752	-2.4	3.247	3.074	-5.3
9	2.452	2.391	-2.5	2.873	2.711	-5.6
10	3.753	3.657	-2.6	4.341	4.084	-5.9
Averages			-2.3			-5.0

1. Total number of chords per unit length as measured
2. Total number of chords per unit length after correction for edge effects
3. Percentage change due to correction for edge effects

Table 4.2 Areal analysis total profile density

Specimen	Total Profile Density (#/cm^2)					
	Magnification 12x			Magnification 30x		
	N_A*[1]	N_A[2]	% Change[3]	N_A*[1]	N_A[2]	% Change[3]
1	98	95	-2.7	151	144	-5.0
2	87	85	-2.5	125	119	-5.2
3	338	328	-3.0	430	404	-6.0
4	552	537	-2.7	708	670	-5.4
5	443	432	-2.5	603	571	-5.2
6	497	485	-2.4	565	536	-5.1
7	236	227	-3.8	305	281	-7.9
8	201	194	-3.5	340	318	-6.5
9	171	164	-4.1	241	222	-7.8
10	229	219	-4.4	336	325	-3.3
Averages			-3.3			-5.9

1. Total number of profiles per unit length as measured
2. Total number of profiles per unit length after correction for edge effects
3. Percentage change due to correction for edge effects

Table 4.3 Total number of air voids per unit volume - magnification 12x

CLASS	LIMITS (μm)		TOTAL AIR-VOID DENSITY (#/cm^3)									
			Specimen									
			1	2	3	4	5	6	7	8	9	10
1	0	25	3593	3048	5674	1447	16669	8455	7951	10154	7249	3062
2	25	50	10487	9028	18466	30906	25313	28989	11781	11122	6117	8079
3	50	75	2745	2519	9117	17467	13168	14676	3841	3357	2513	3493
4	75	100	1251	1351	6519	12392	8630	10288	3211	2279	1813	2803
5	100	125	432	375	3211	5218	4368	5593	1510	1165	1239	1736
6	125	150	261	271	1826	3548	2669	3083	1500	1091	921	1250
7	150	175	167	144	1155	1515	1370	1437	709	652	741	963
8	175	200	116	69	713	1107	721	693	662	454	487	706
9	200	225	30	16	364	606	509	530	545	415	418	522
10	225	250	61	57	393	355	239	290	262	167	269	408
11	250	275	20	12	202	244	150	215	344	349	306	314
12	275	300	19	61	119	132	131	141	135	139	140	244
13	300	325	26	-11	123	102	61	56	190	118	143	187
14	325	350	20	30	74	90	73	76	88	94	102	118
15	350	375	9	6	37	19	35	43	56	52	82	141
1 - 85	0	2125	19327	17036	48211	75365	74242	74725	33138	31942	22838	24462

Table 4.4 Total number of air voids per unit volume - magnification 30x

CLASS	LIMITS (μm)		TOTAL AIR-VOID DENSITY (#/cm^3)									
			Specimen									
			1	2	3	4	5	6	7	8	9	10
1	0	25	32181	26011	46097	34386	35145	40058	34617	70397	39543	50390
2	25	50	9258	8338	20691	39432	39158	29976	14656	19079	8657	13848
3	50	75	4416	3586	10961	25681	19779	19304	4868	4845	3504	4690
4	75	100	1644	1332	7069	14044	10843	10940	3234	2455	1951	3699
5	100	125	673	551	3413	6309	5137	5425	1935	1453	1427	2105
6	125	150	292	220	2027	3056	2785	2117	1347	1129	1076	1381
7	150	175	182	114	1013	1555	1241	1295	786	779	773	987
8	175	200	69	68	677	846	713	677	694	345	320	861
9	200	225	60	16	487	596	432	336	528	609	525	444
10	225	250	56	62	314	194	211	276	256	177	260	433
11	250	275	46	20	165	267	158	138	356	348	283	361
12	275	300	12	23	184	118	93	102	165	139	82	312
13	300	325	14	29	68	105	110	38	154	116	143	180
14	325	350	27	27	61	23	11	72	115	61	149	114
15	350	375	25	-3	54	43	39	27	41	82	27	137
1 - 85	0	2125	49030	40457	93473	126815	115973	110914	64080	102348	59014	80363

Table 4.5 Average chord, profile, and air-void sizes for magnifications of 12x and 30x

SPECIMEN	AVERAGE FEATURE SIZE (μm)					
	Magnification 12x			Magnification 30x		
	Chord Length	Profile Diameter	Sphere Diameter	Chord Length	Profile Diameter	Sphere Diameter
1	242	85	49	150	66	29
2	255	84	50	217	67	29
3	147	95	68	138	81	43
4	122	85	71	124	72	53
5	122	81	58	100	70	49
6	109	83	65	126	71	48
7	188	124	69	188	104	44
8	188	122	61	169	85	31
9	192	137	72	179	105	38
10	197	145	90	189	108	41

Table 4.6 Air-void spacing parameters

SPECIMEN		POWERS SPACING FACTOR (μm)						PHILLEO FACTOR (μm)	
	Manual[1]	Lineal Distribution[2]		Areal Distribution[3]		Volume Distribution[4]		Areal Analysis	
		12x	30x	12x	30x	12x	30x	12x	30x
1	396	422	259	448	378	450	382	212	156
2	349	441	362	471	458	473	464	223	164
3	113	165	153	182	176	182	176	132	106
4	119	105	107	119	111	118	111	109	92
5	117	144	114	140	126	140	125	114	97
6	100	120	126	124	129	124	129	110	99
7	228	169	170	191	185	191	185	142	115
8	195	177	158	206	180	206	181	146	99
9	213	209	185	224	215	223	216	167	121
10	209	169	151	194	175	194	176	157	105

1. Modified point count analysis
2. Lineal image analysis
3. Areal image analysis
4. Volume distribution from areal analysis

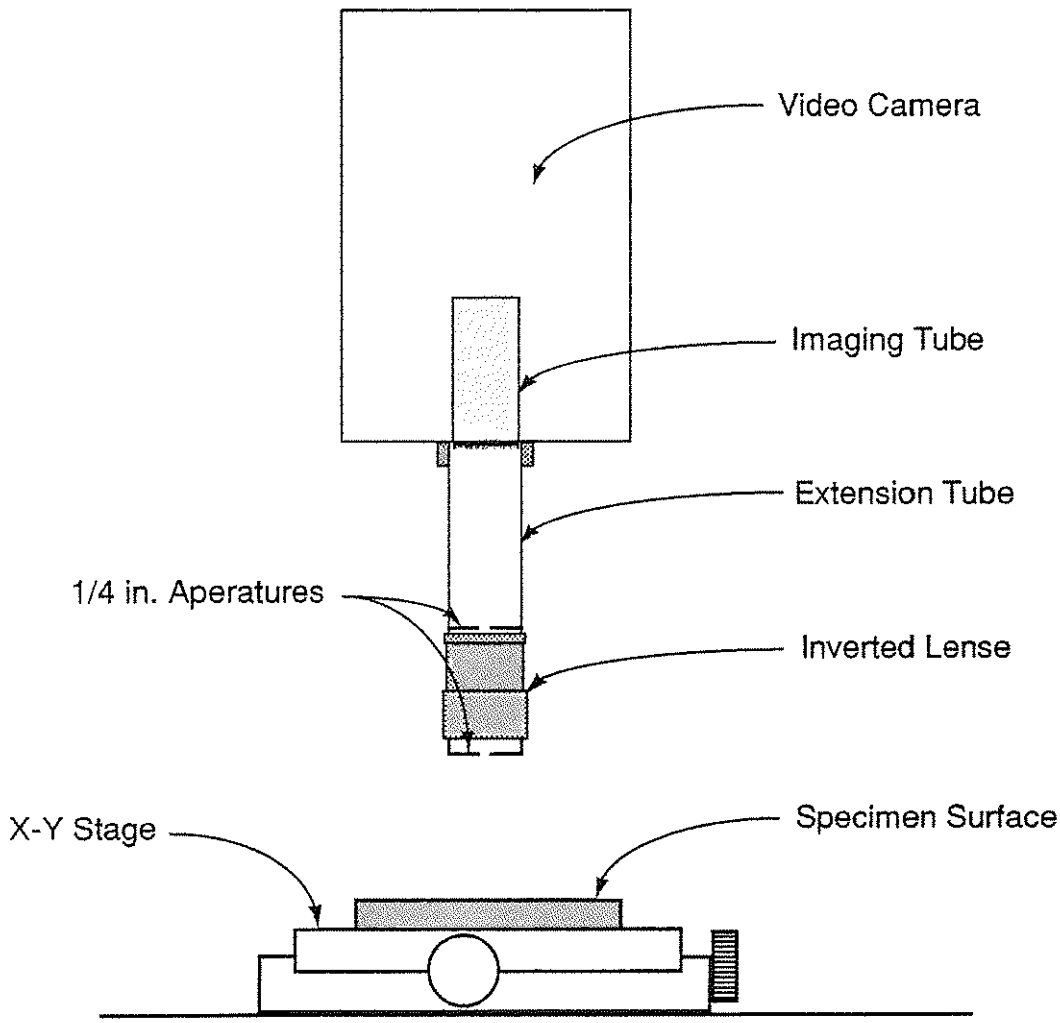

Fig. 2.1 Video camera and lens arrangement

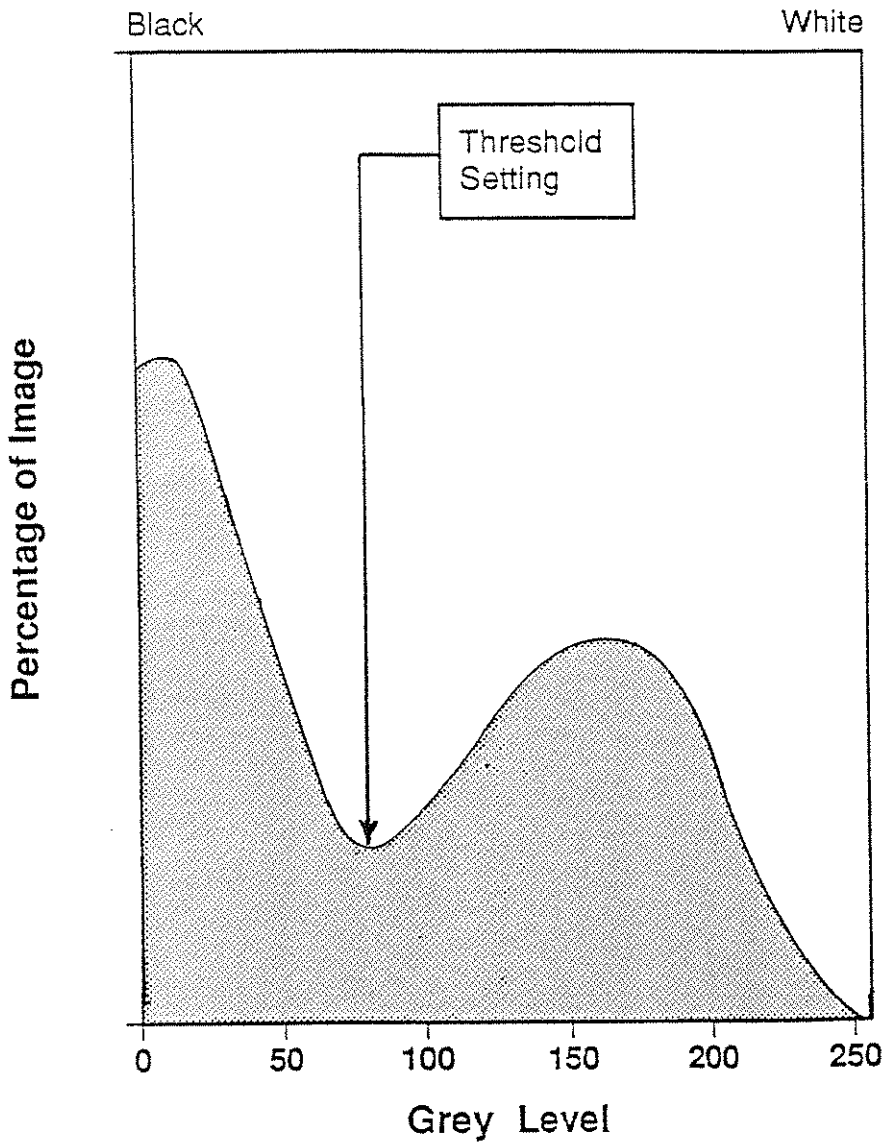

Figure 2.2 Typical grey level histogram of an air-entrained concrete image showing the threshold value distinguishing air voids from background

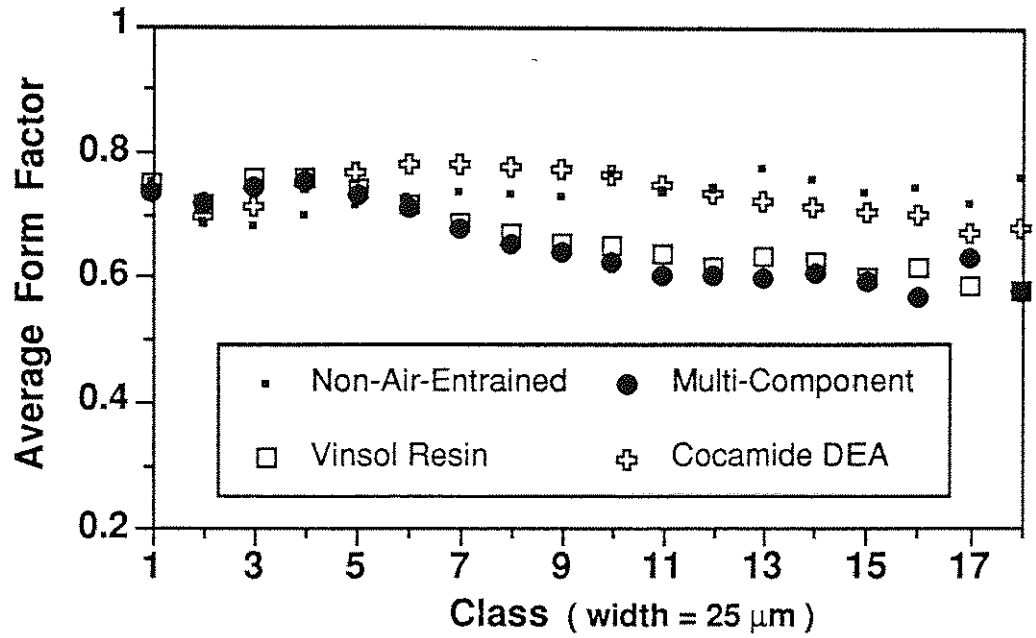

Figure 2.3 Average form factor versus class for the different admixture and non-air-entrained sample groups

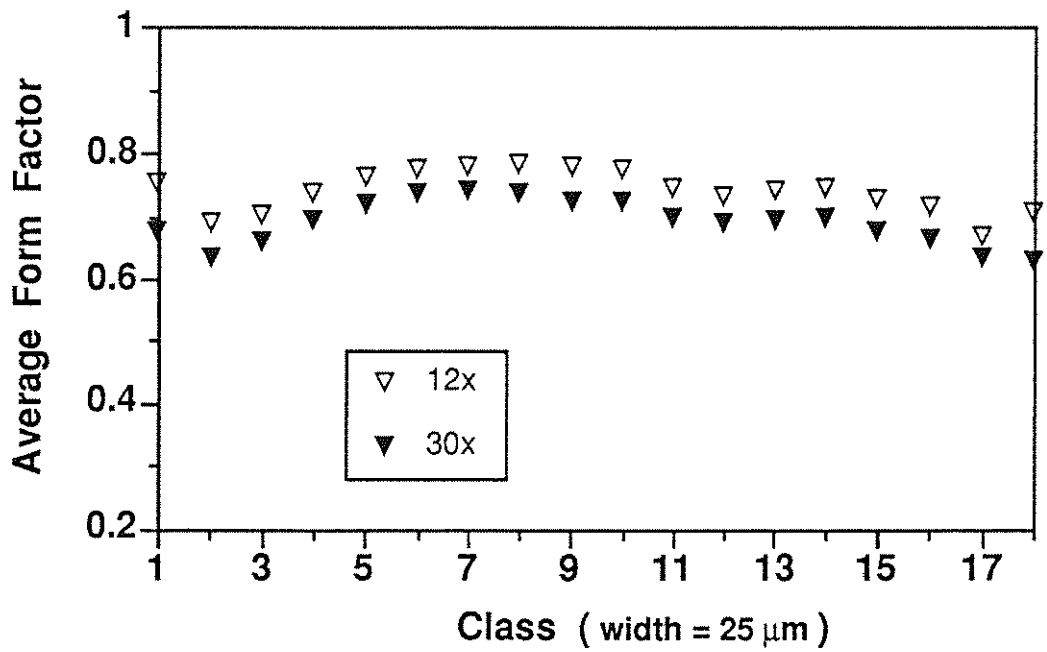

Figure 2.4 Mix 8 average form factor versus class for magnifications of 12x and 30x

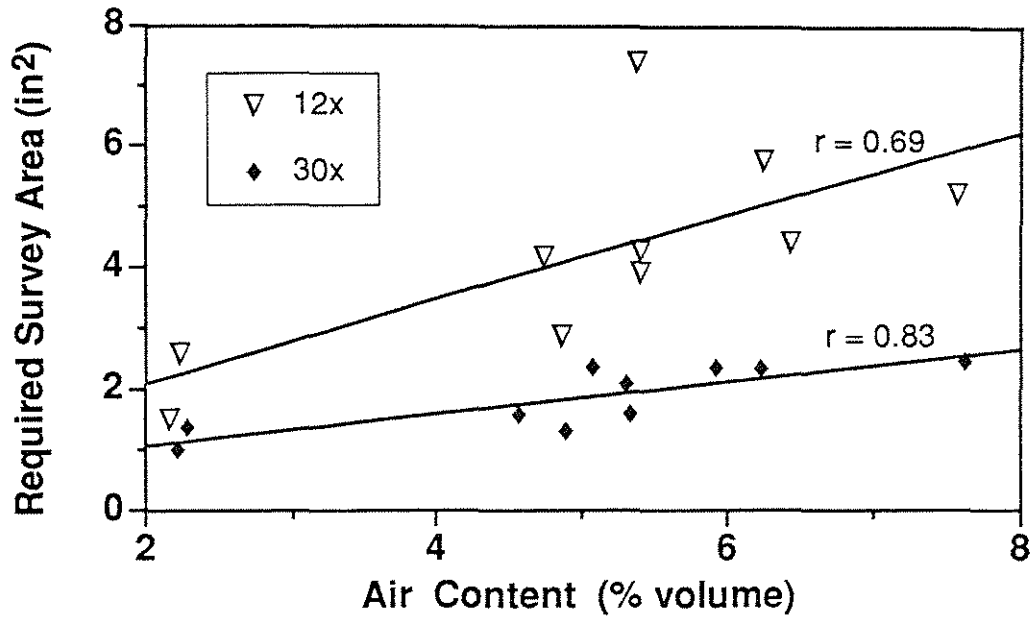

Figure 2.5 Required survey area (68% confidence) versus air content.
Plotted required survey areas are an average of the values in Tables 2.8 and 2.9.
r = correlation coefficient

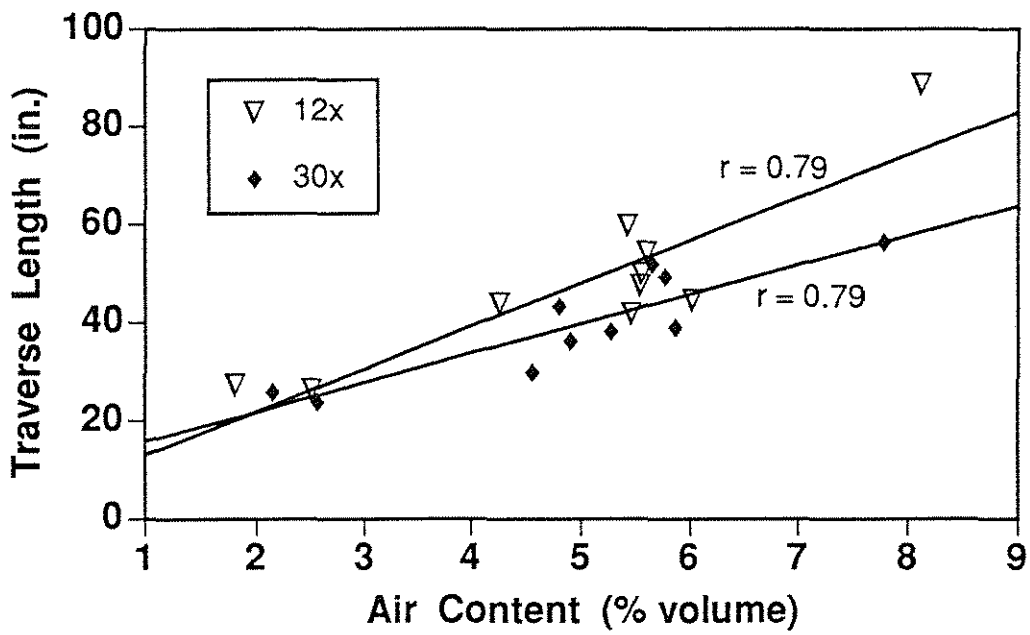

Figure 2.6 Required traverse length (68% confidence) versus air content.
r = correlation coefficient

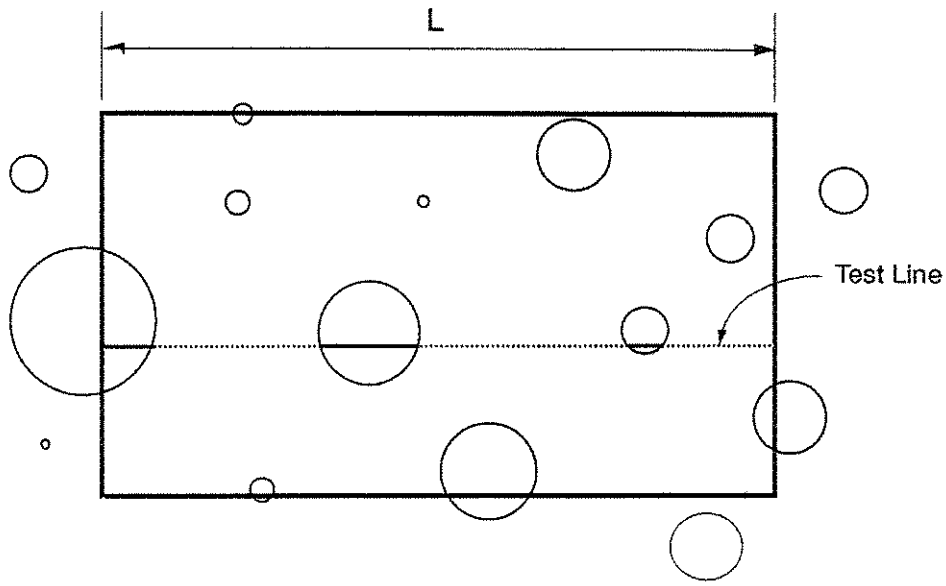

Figure 3.1 Field of view showing a feature intersected by a frame edge

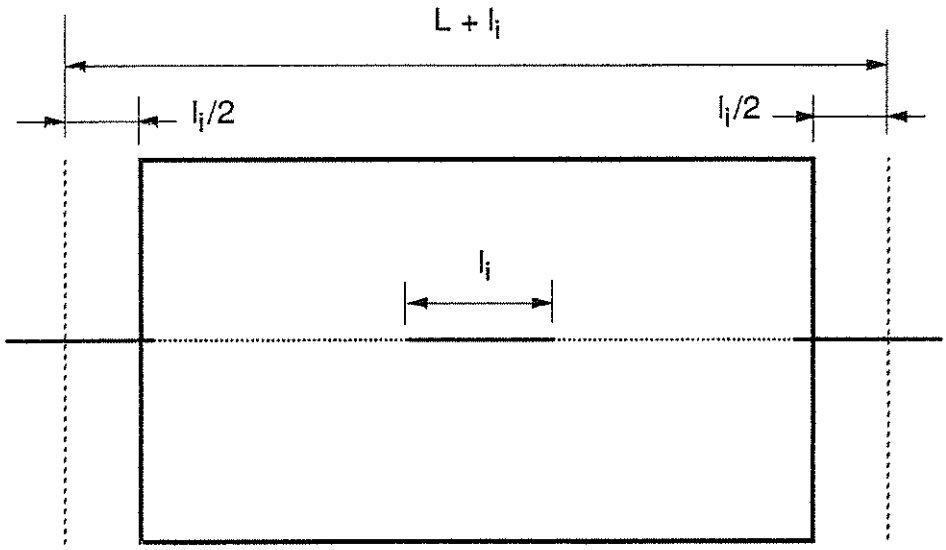

Figure 3.2 Range in which the center of lineal features, of length l_i, can be located and be at least partially visable in the field of view

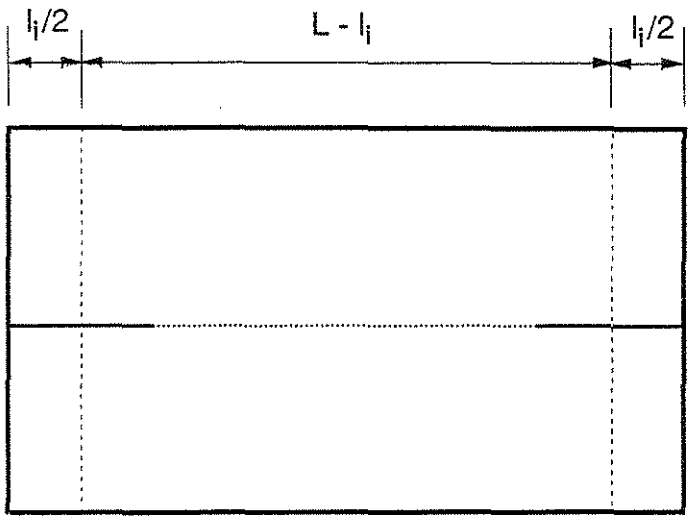

Figure 3.3 Range in which the center of lineal features, of length l_i, can be located and not be intersected by a frame edge

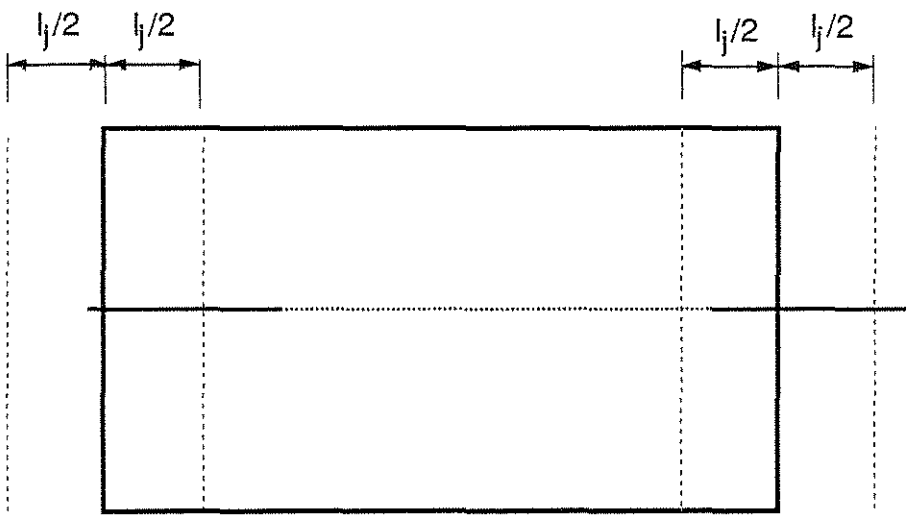

Figure 3.4 Range in which the center of lineal features, of length l_j, can be located and be intersected by a frame edge

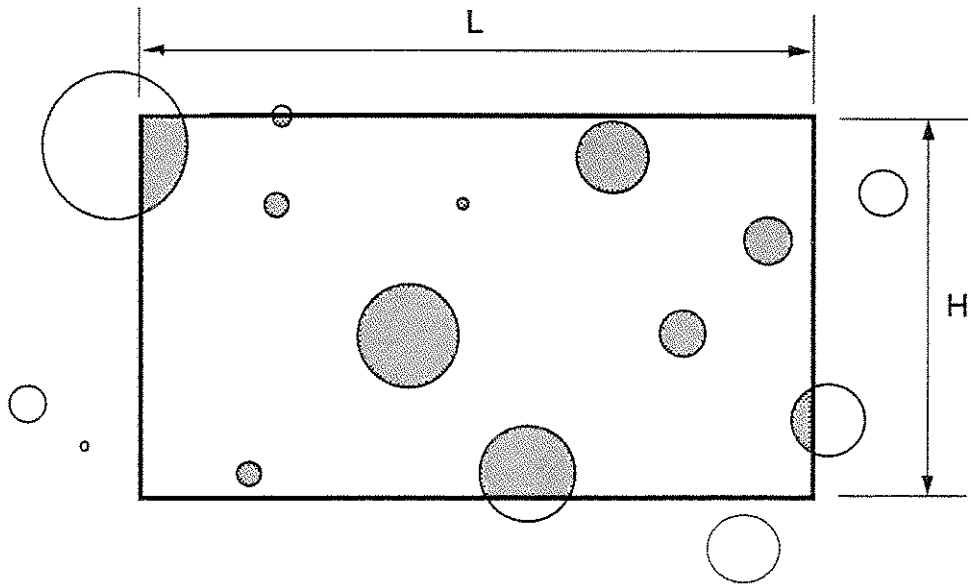

Figure 3.5 Field of view showing the intersection of areal features by the frame edges

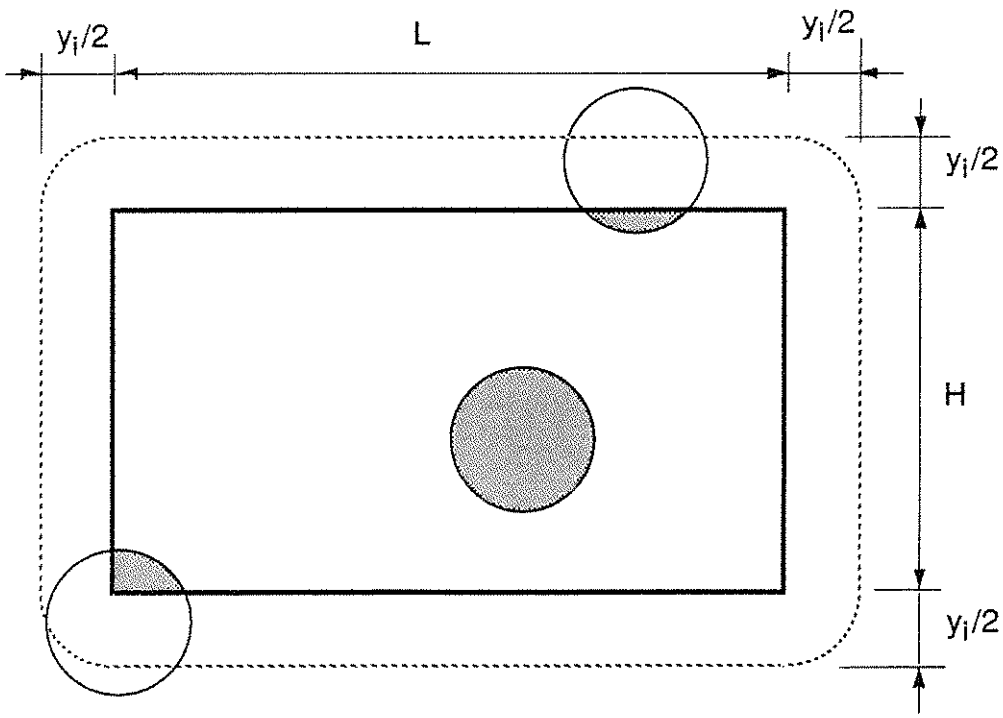

Figure 3.6 Range in which the center of circular features, of diameter y_i, can be located and be at least partially visable in the field of view

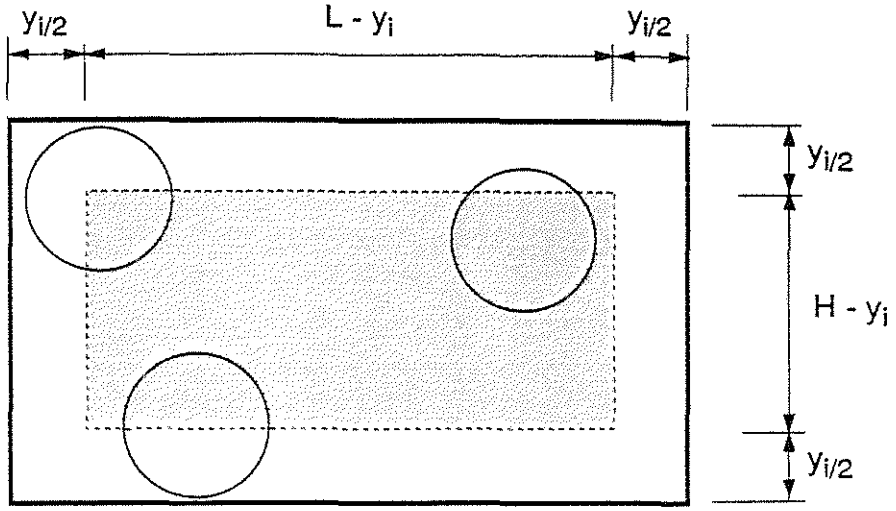

Figure 3.7 Range in which the center of diameter y_i circular features can be located and not be intersected by a frame edge

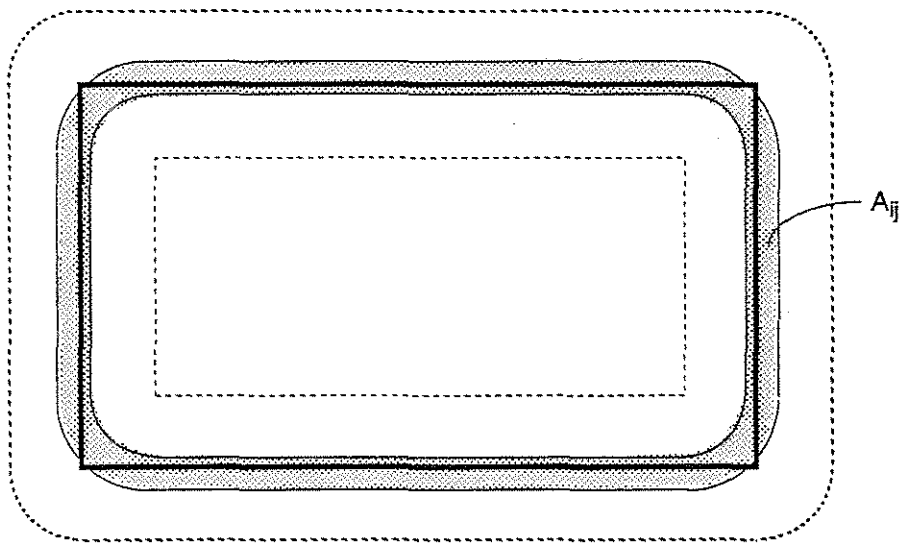

Figure 3.8 Area A_{ij} around the field of view in which the center of diameter y_j circular features can be located and have a measured area with an AED within the size limits of class i

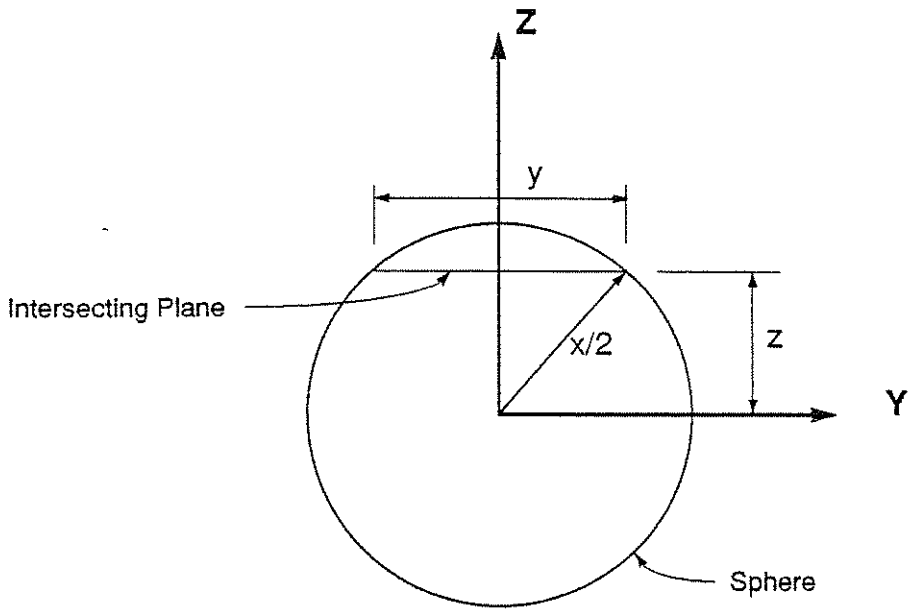

Figure 3.9 Diameter x sphere being intersected by a plane surface at a distance z from its center, resulting in a diameter y profile

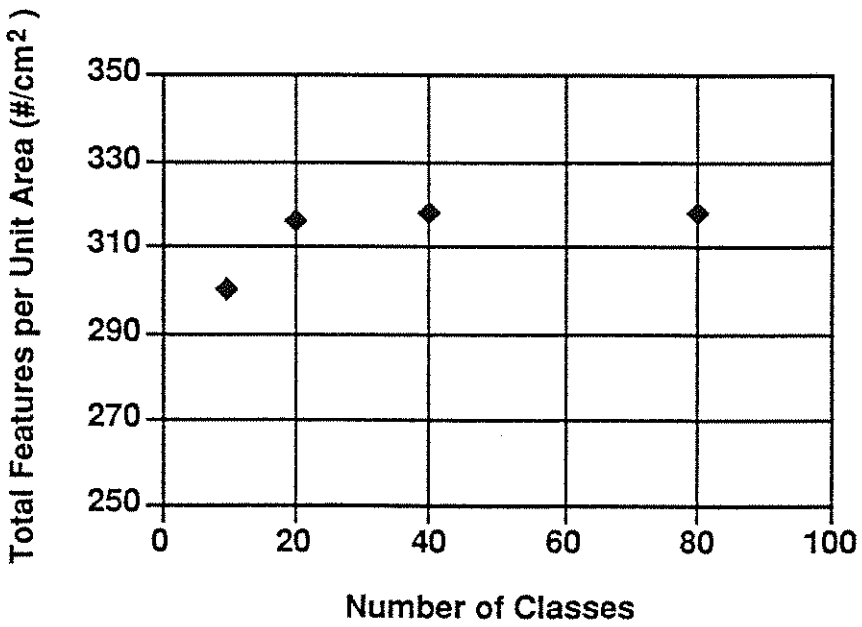

Figure 3.10 Total number of features versus the number of classes of 25 µm width for mix 8 areal data

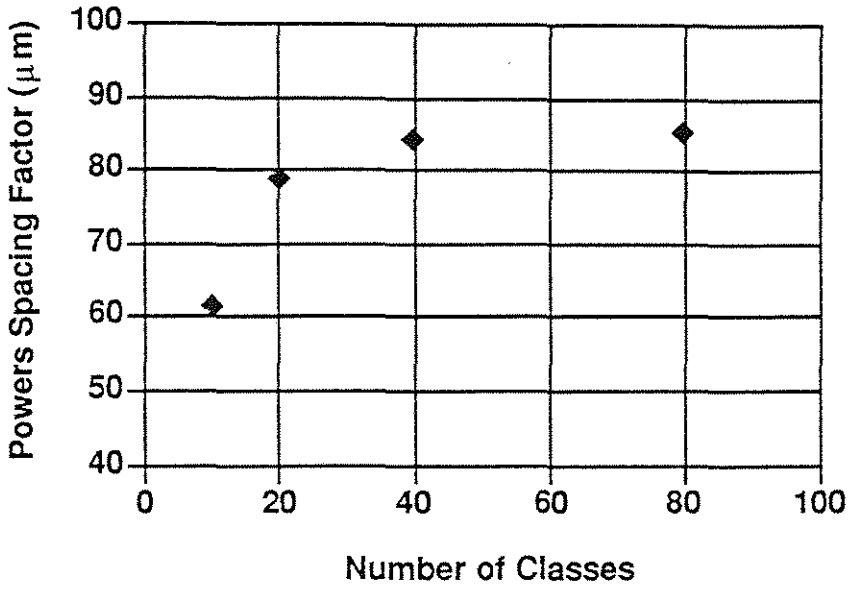

Figure 3.11 Powers spacing factor versus number of classes of 25 μm width for mix 8 areal data

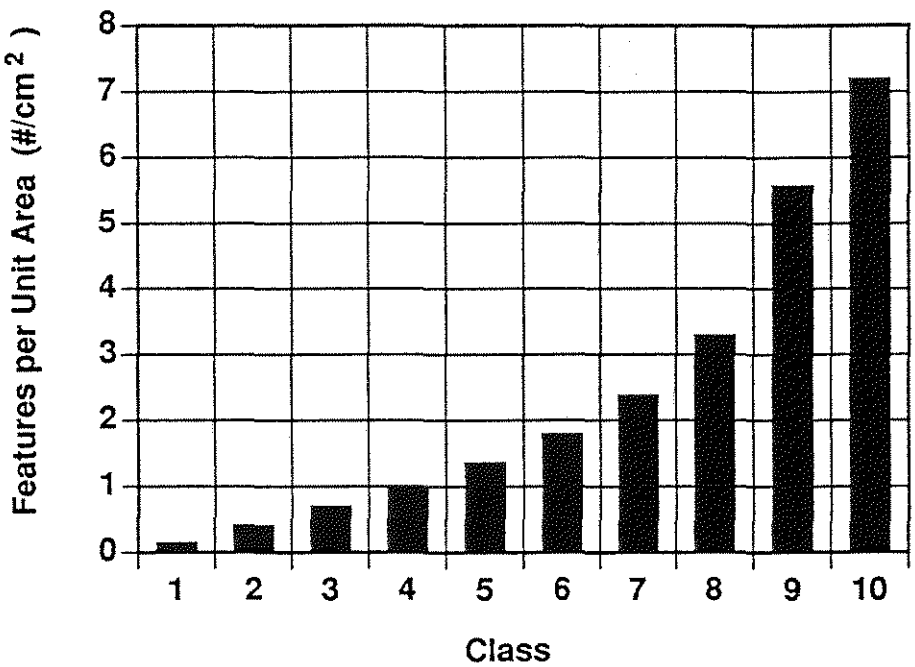

Figure 3.12 Number of features per unit area versus class resulting from intersecting a volume containing 1000 spheres per unit volume in class 10

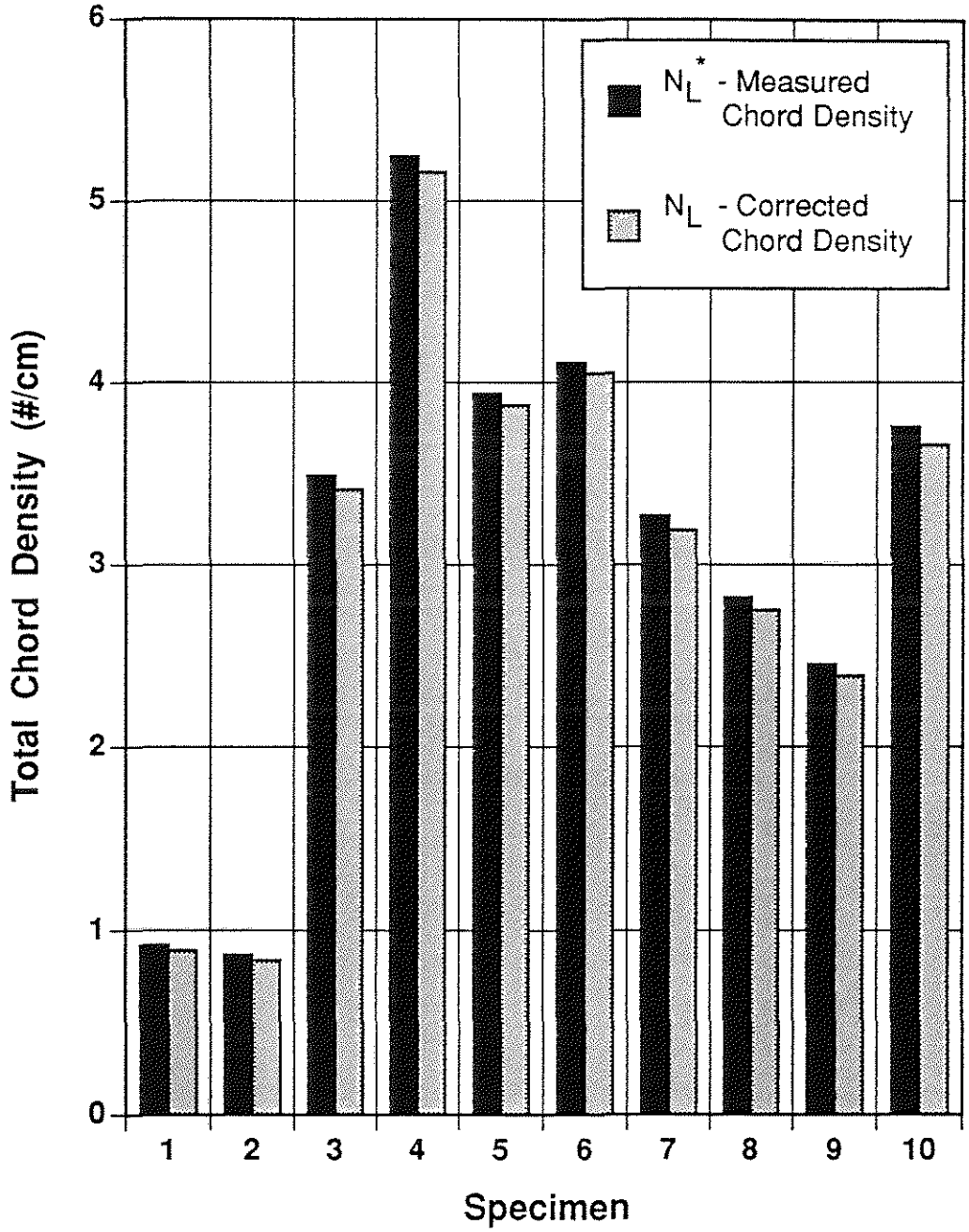

Figure 4.1 Lineal analysis total chord density - magnification 12x

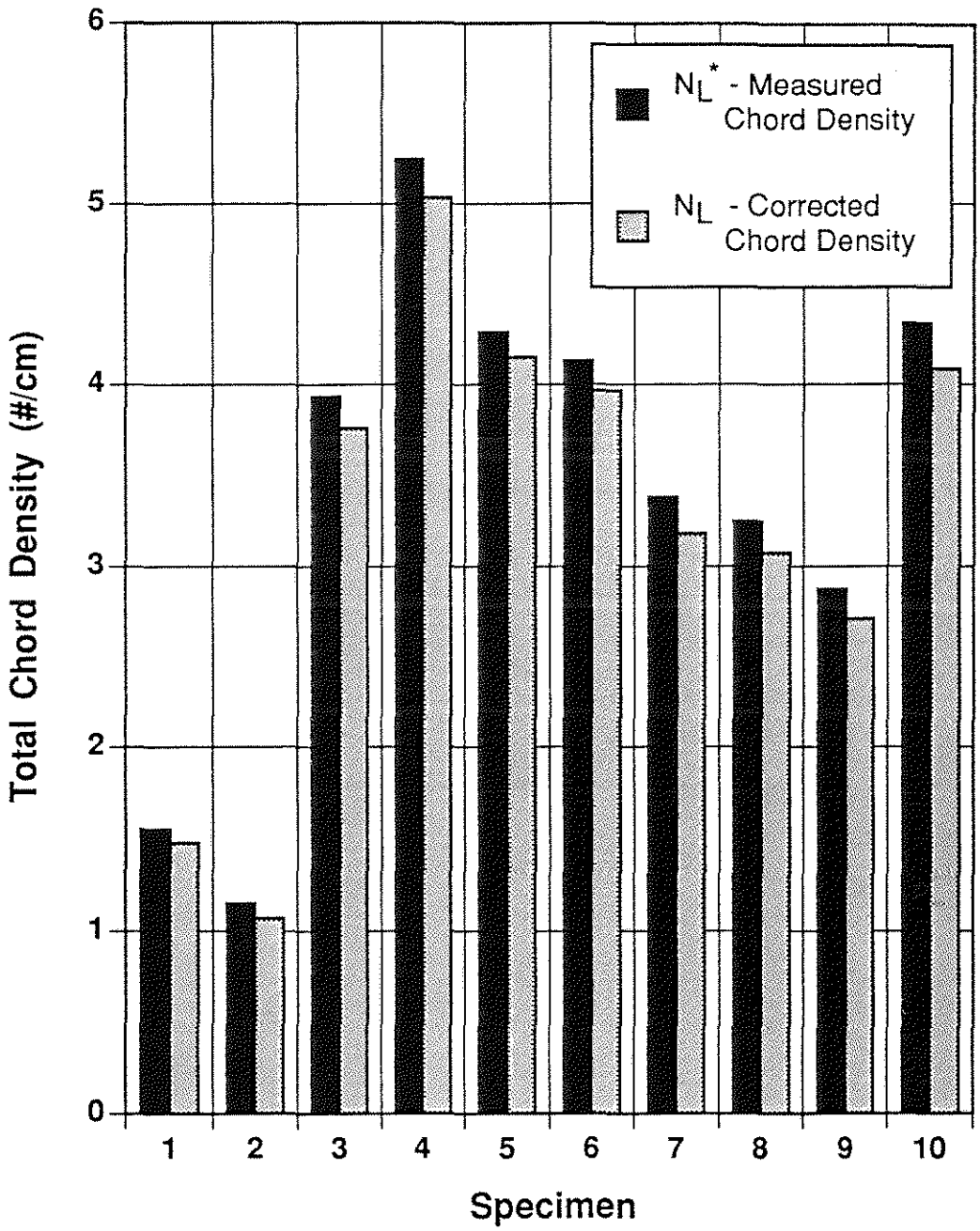

Figure 4.2 Lineal analysis total chord density - magnification 30x

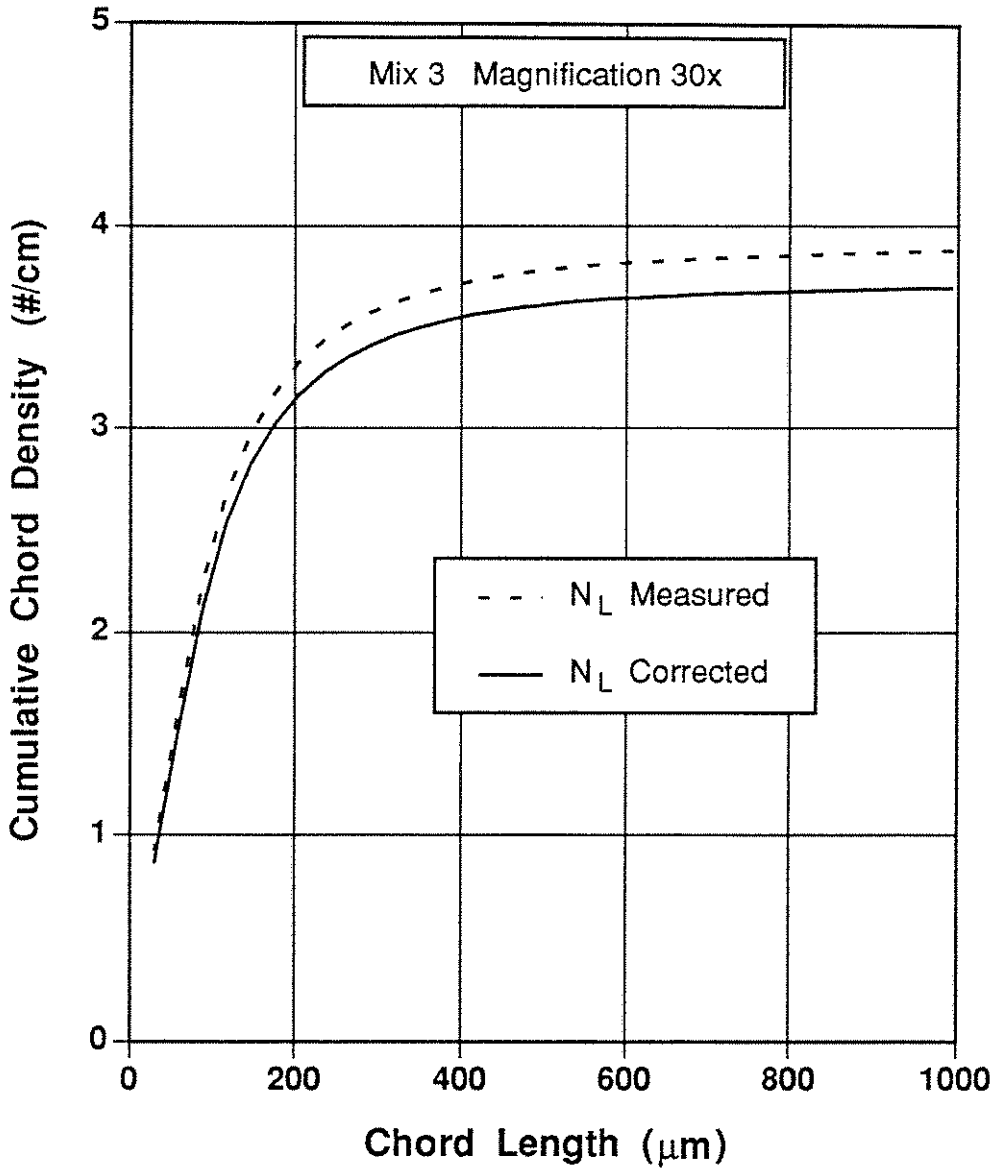

Figure 4.3 Cumulative chord density versus chord length

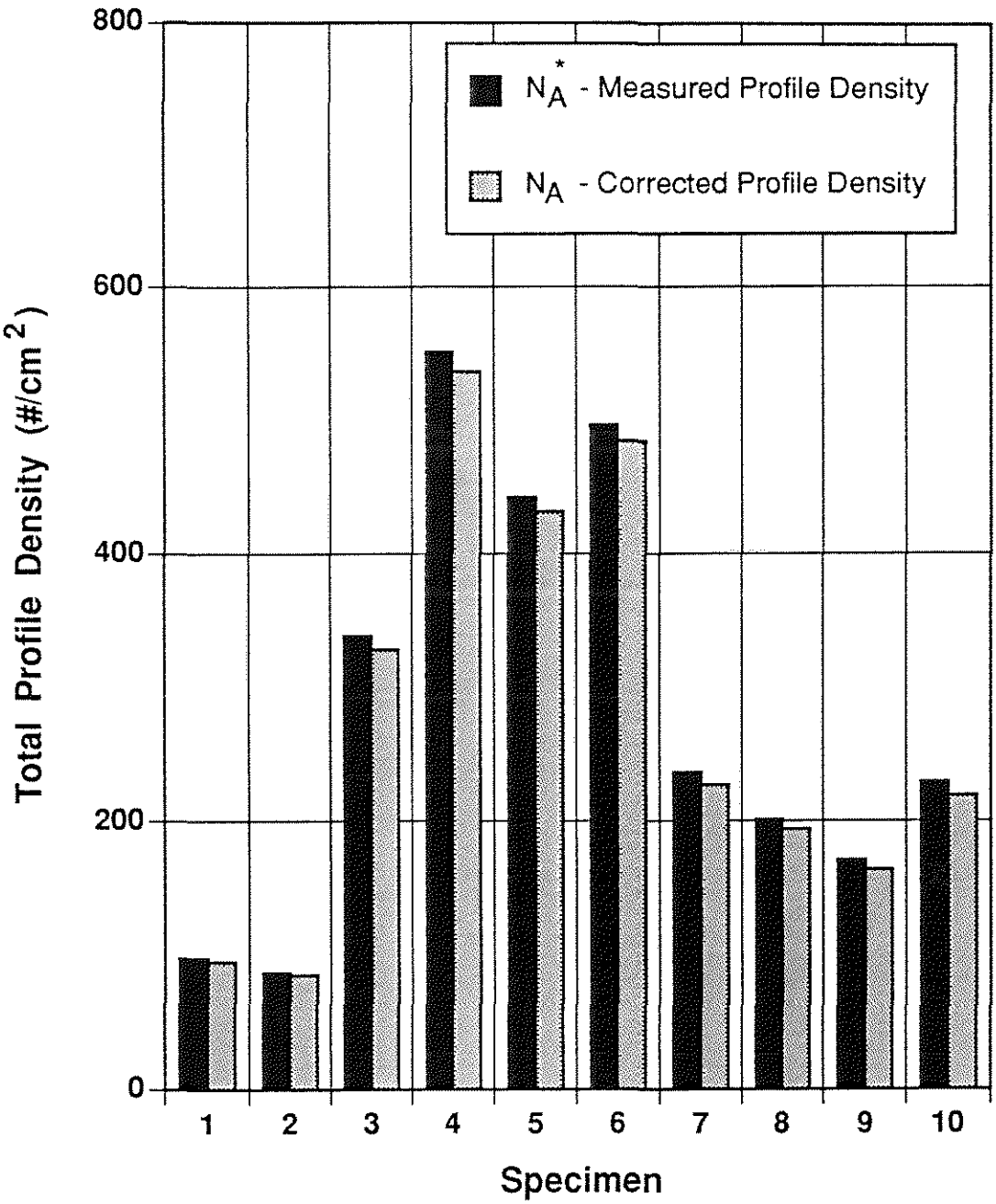

Figure 4.4 Areal analysis total profile density - magnification 12x

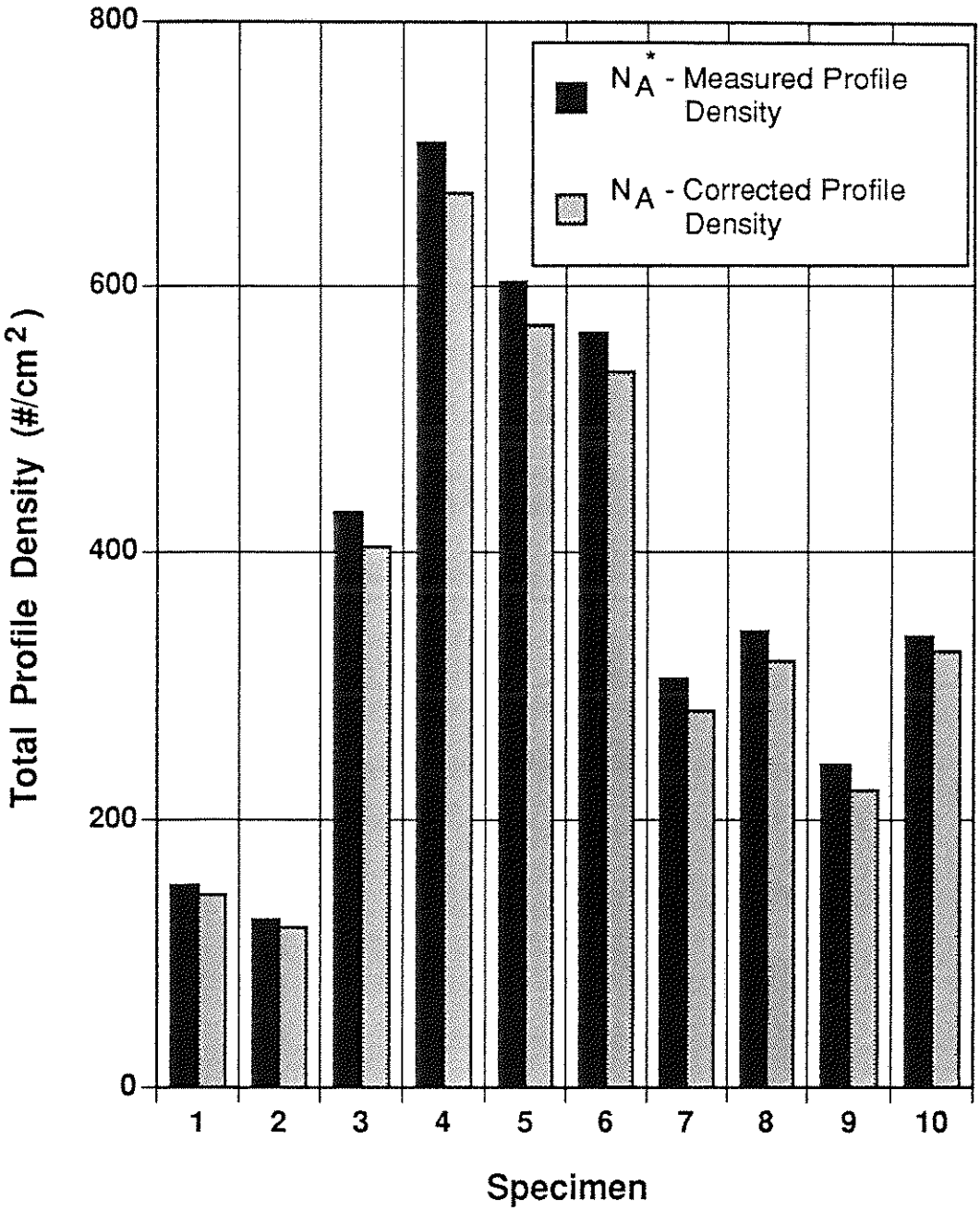

Figure 4.5 Areal analysis total profile density - magnification 30x

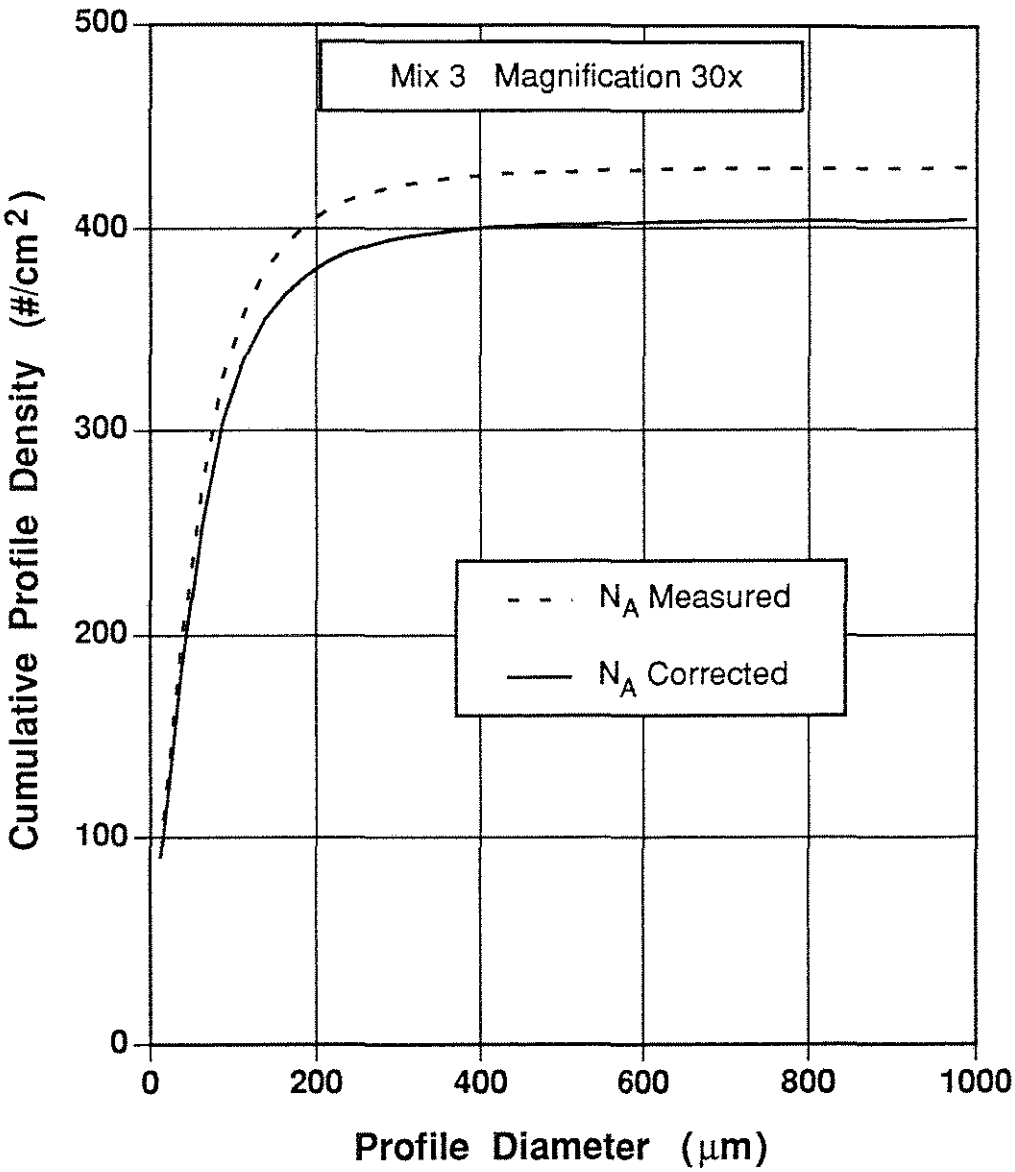

Figure 4.6 Cumulative profile density versus profile diameter

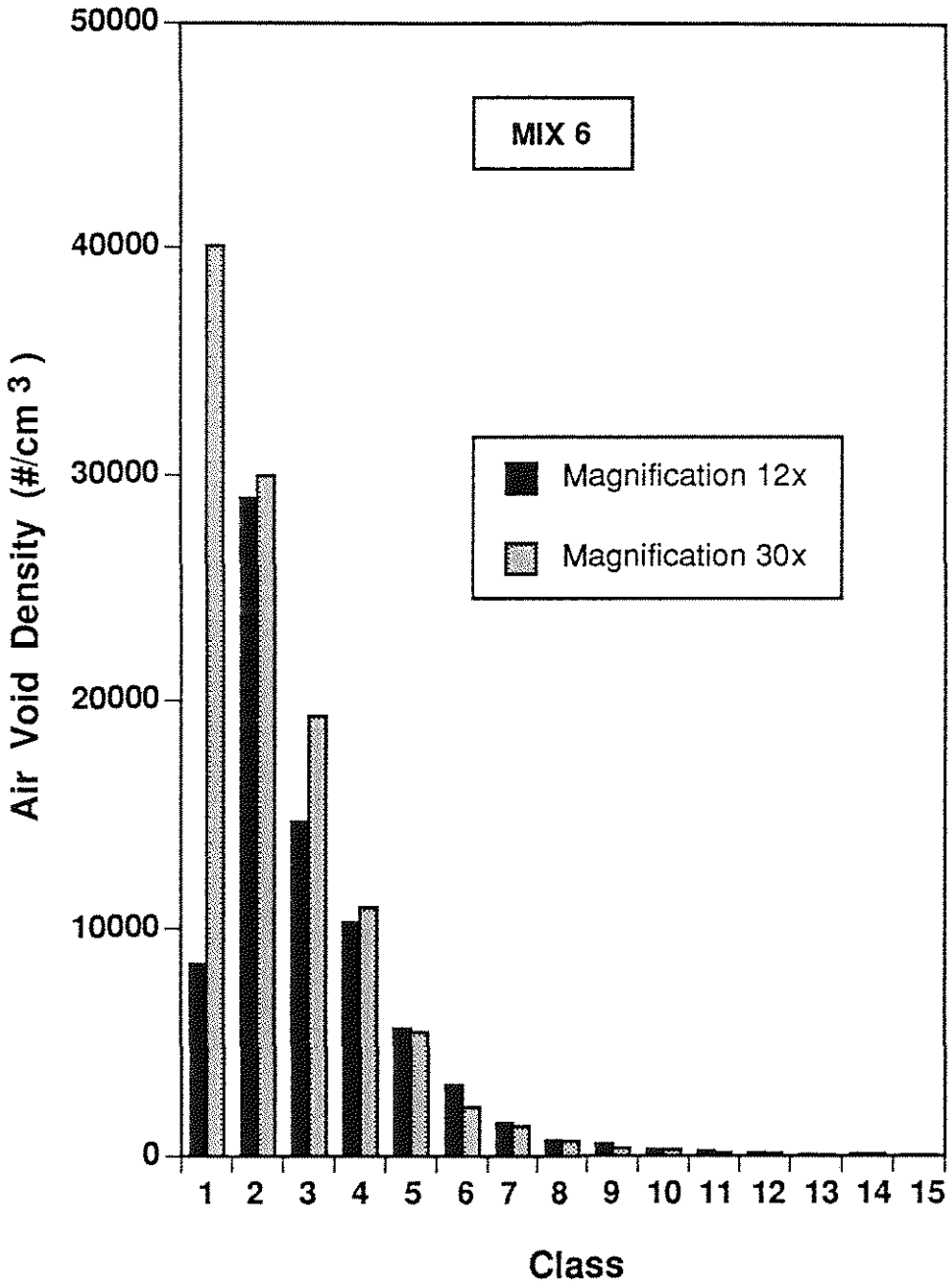

Figure 4.7 Mix 6 air-void distribution at magnifications of 12x and 30x

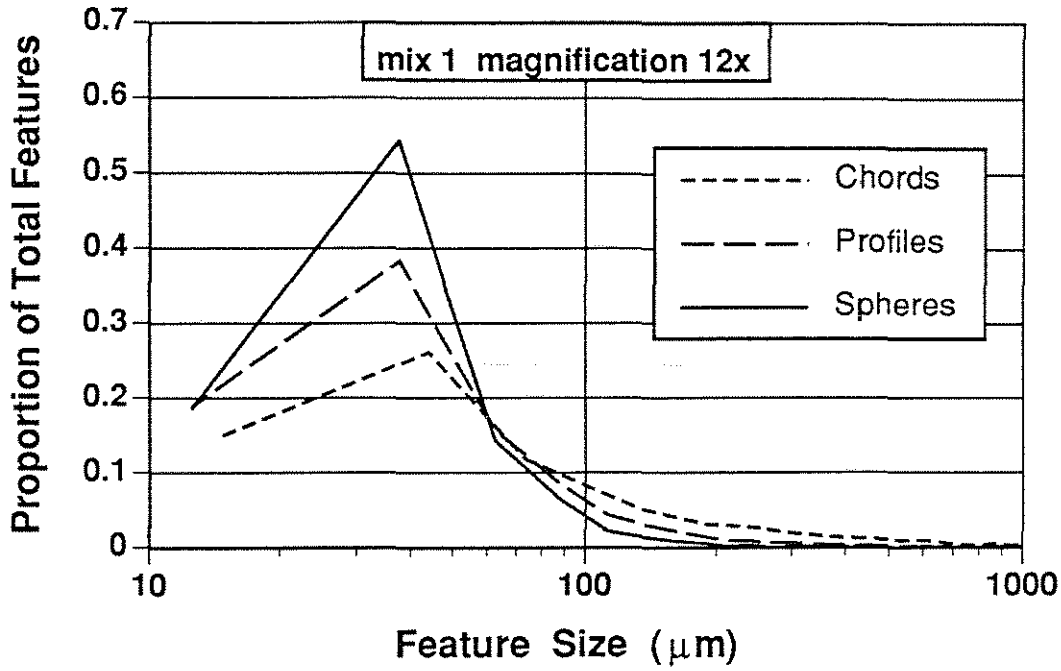

Figure 4.8 Proportion of total features versus feature size for chord, profile, and sphere distributions for mix 1 at magnification 12x.

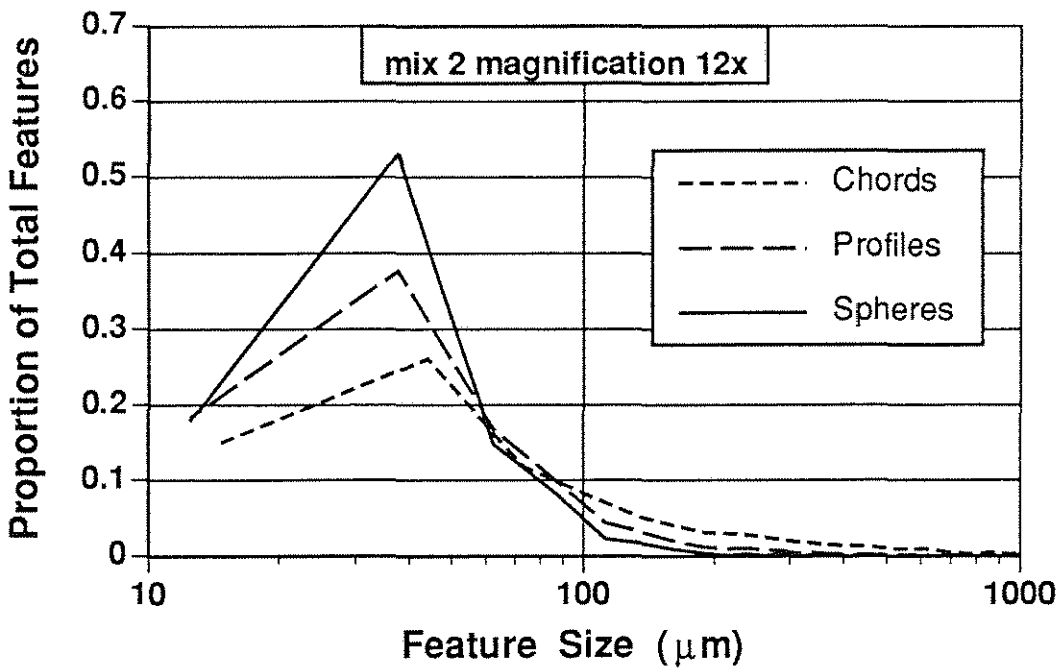

Figure 4.9 Proportion of total features versus feature size for chord, profile, and sphere distributions for mix 2 at magnification 12x.

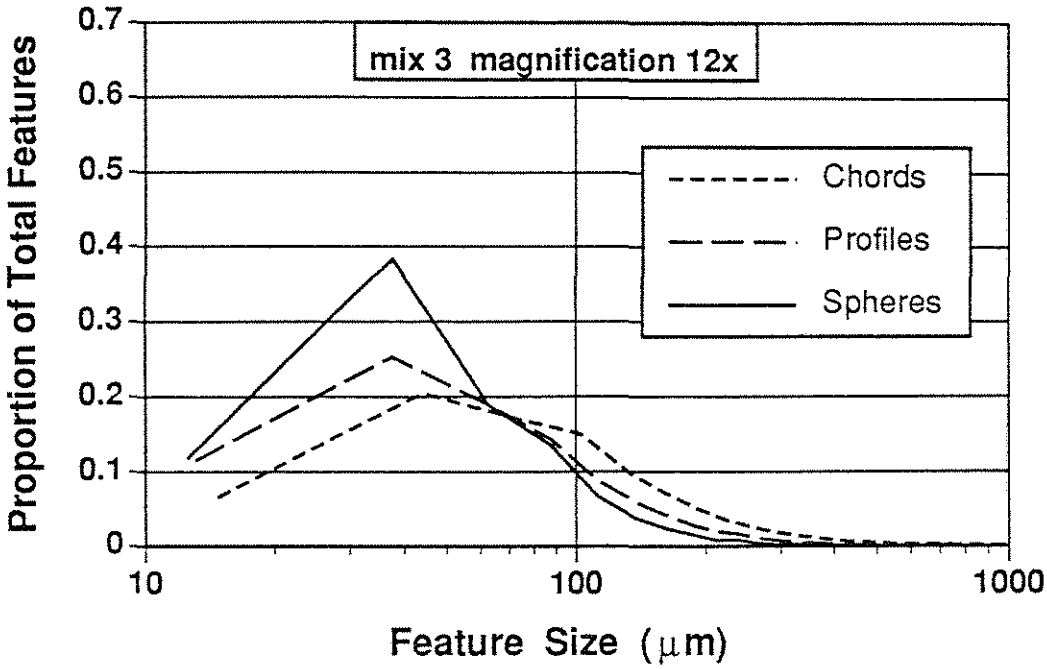

Figure 4.10 Proportion of total features versus feature size for chord, profile, and sphere distributions for mix 3 at magnification 12x.

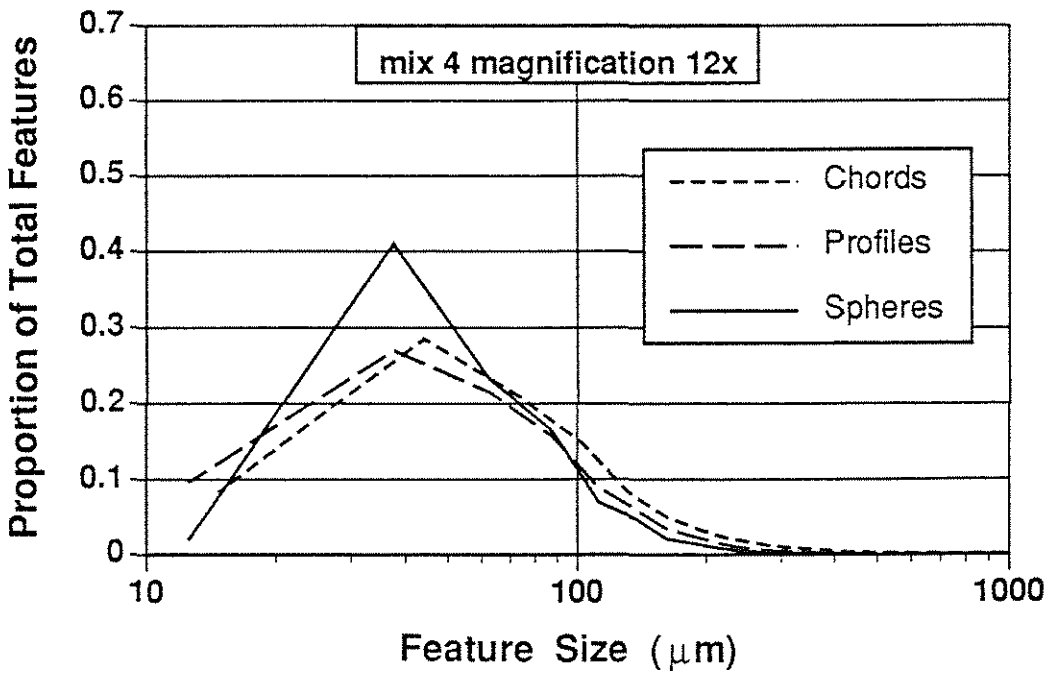

Figure 4.11 Proportion of total features versus feature size for chord, profile, and sphere distributions for mix 4 at magnification 12x.

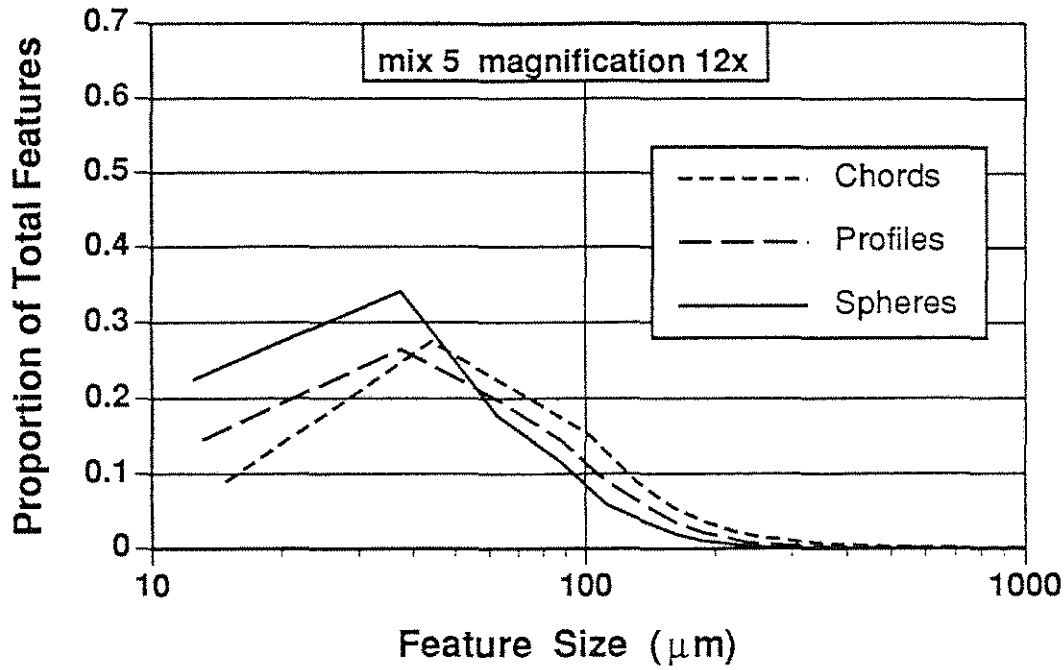

Figure 4.12 Proportion of total features versus feature size for chord, profile, and sphere distributions for mix 5 at magnification 12x.

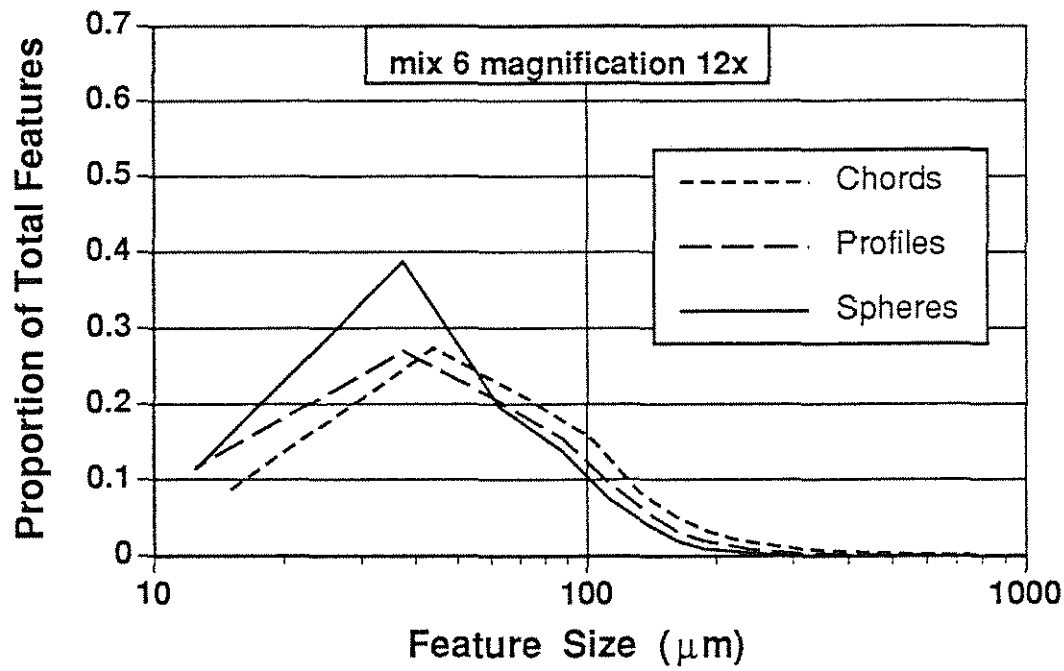

Figure 4.13 Proportion of total features versus feature size for chord, profile, and sphere distributions for mix 6 at magnification 12x.

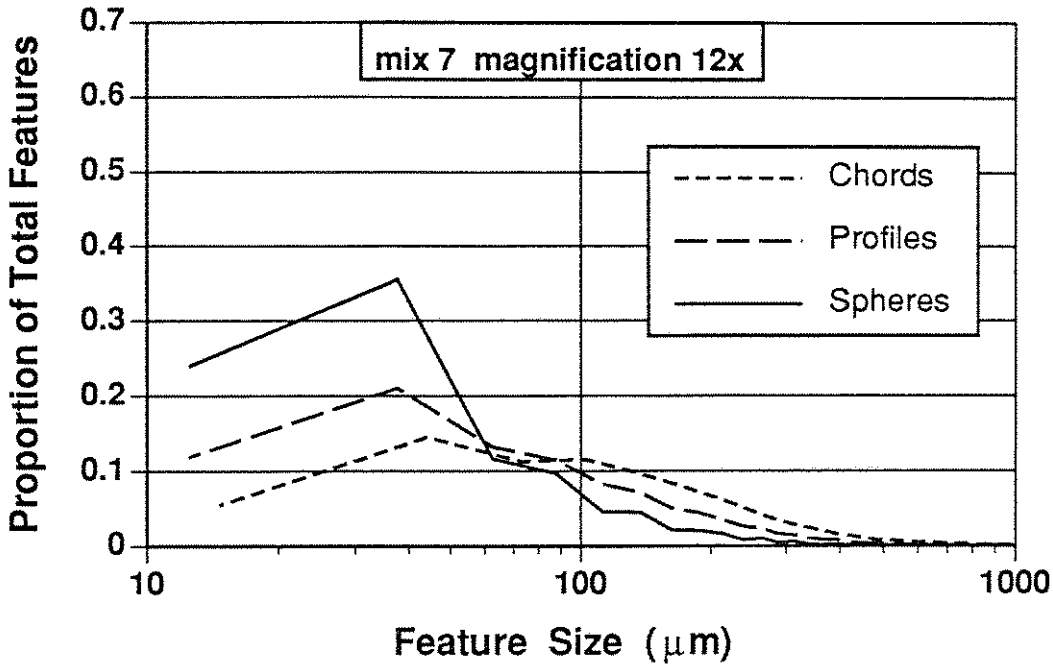

Figure 4.14 Proportion of total features versus feature size for chord, profile, and sphere distributions for mix 7 at magnification 12x.

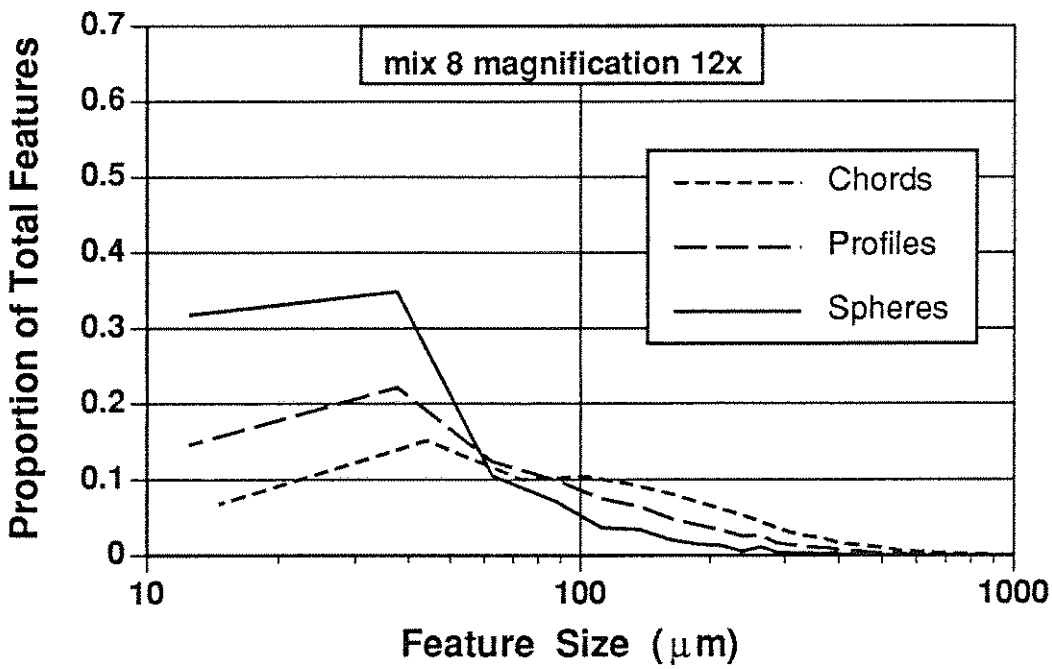

Figure 4.15 Proportion of total features versus feature size for chord, profile, and sphere distributions for mix 8 at magnification 12x.

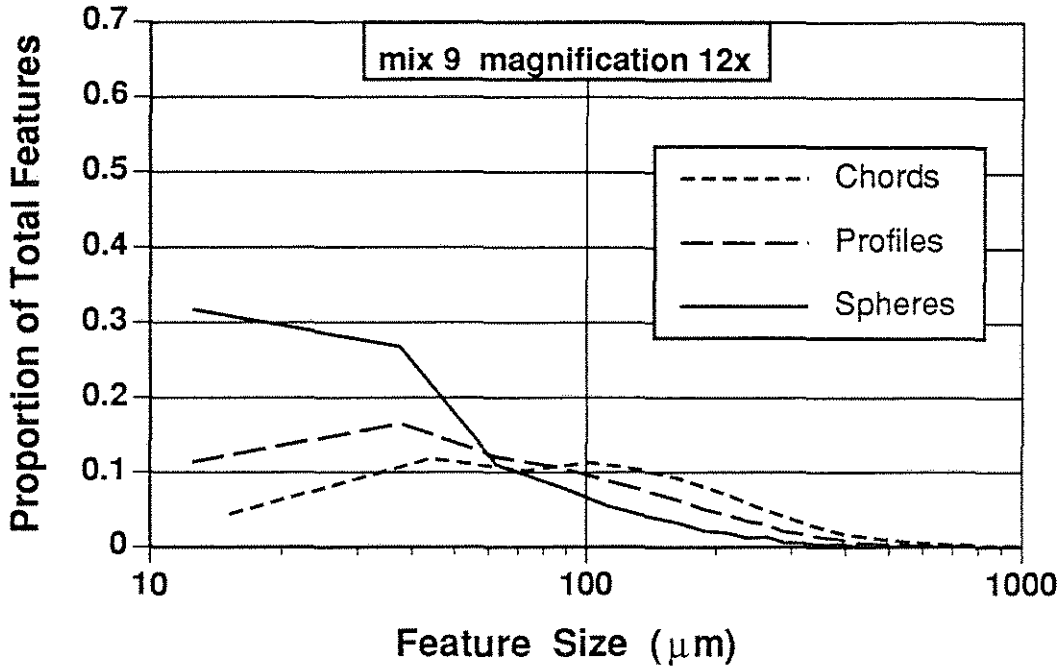

Figure 4.16 Proportion of total features versus feature size for chord, profile, and sphere distributions for mix 9 at magnification 12x.

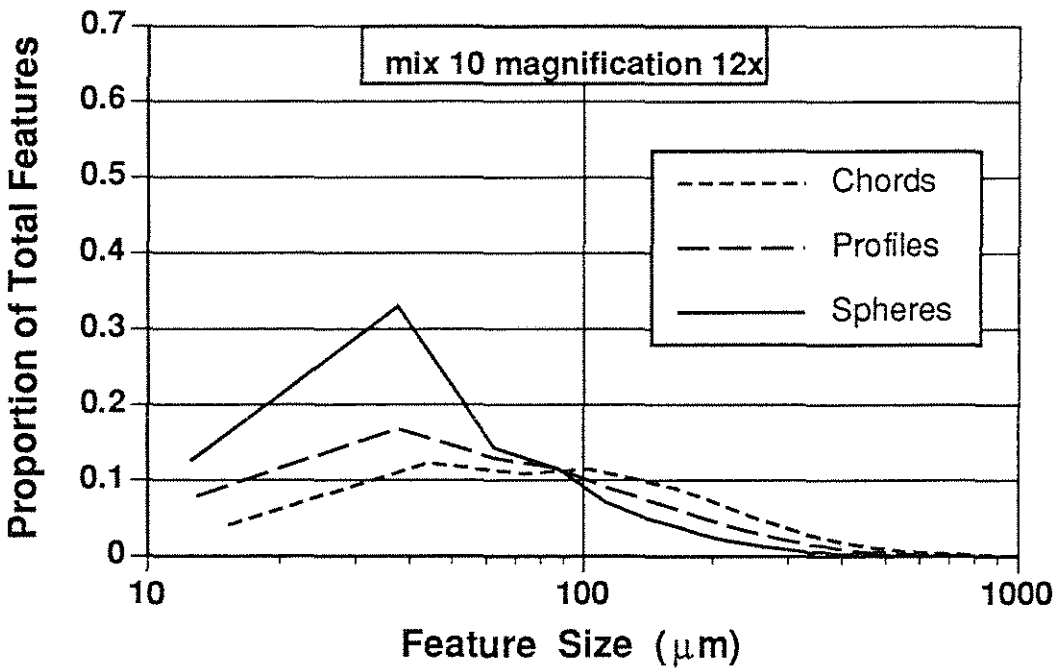

Figure 4.17 Proportion of total features versus feature size for chord, profile, and sphere distributions for mix 10 at magnification 12x.

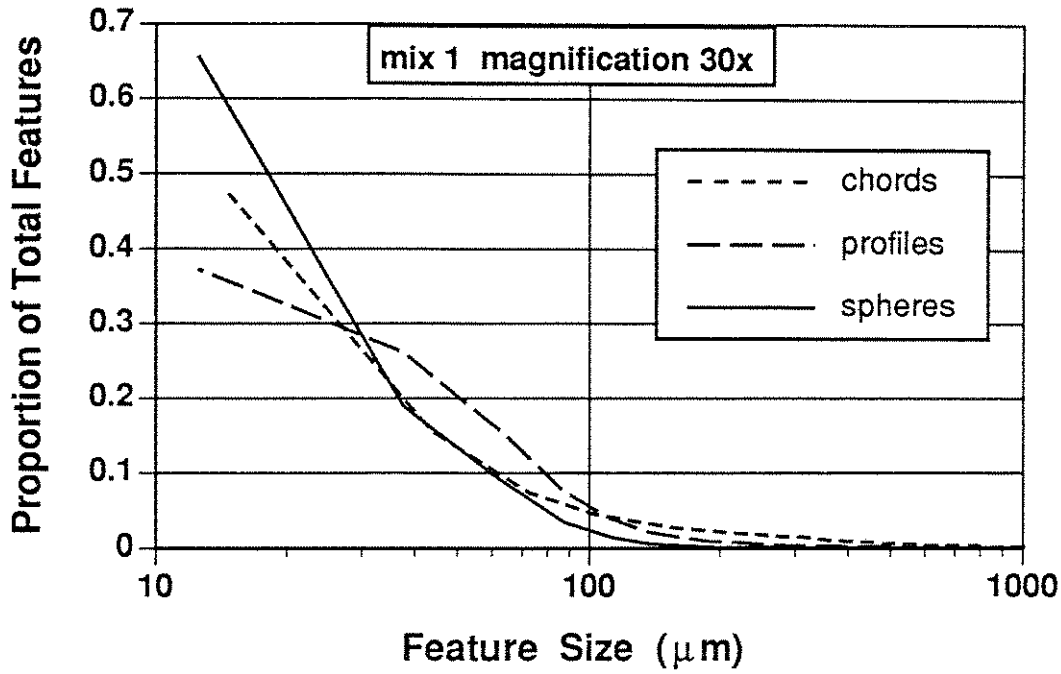

Figure 4.18 Proportion of total features versus feature size for chord, profile, and sphere distributions for mix 1 at magnification 30x.

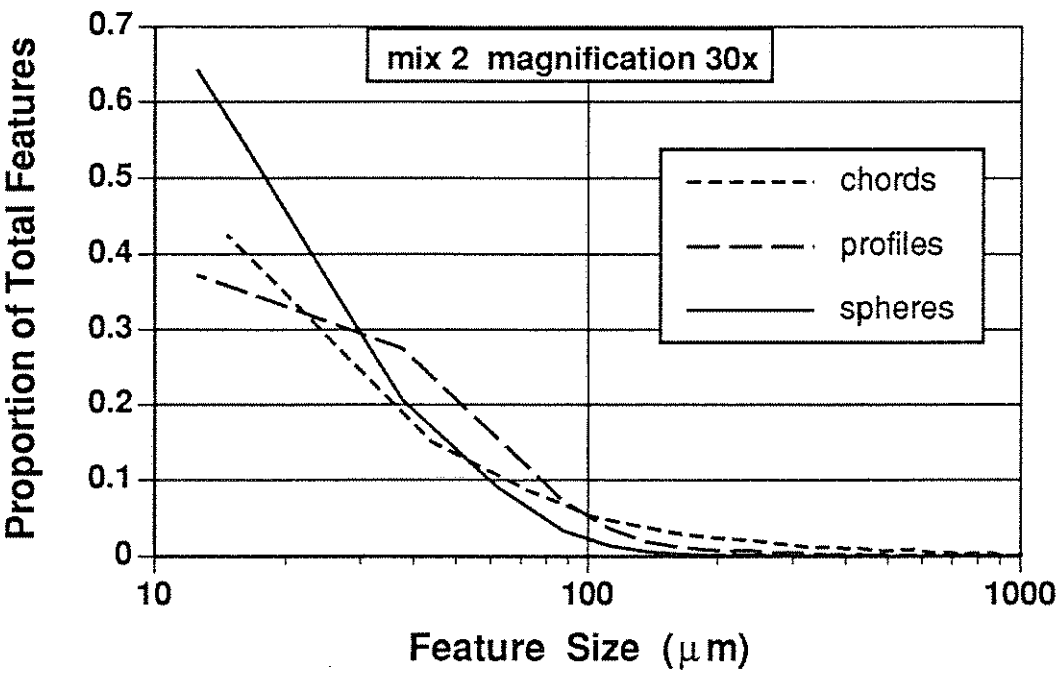

Figure 4.19 Proportion of total features versus feature size for chord, profile, and sphere distributions for mix 2 at magnification 30x.

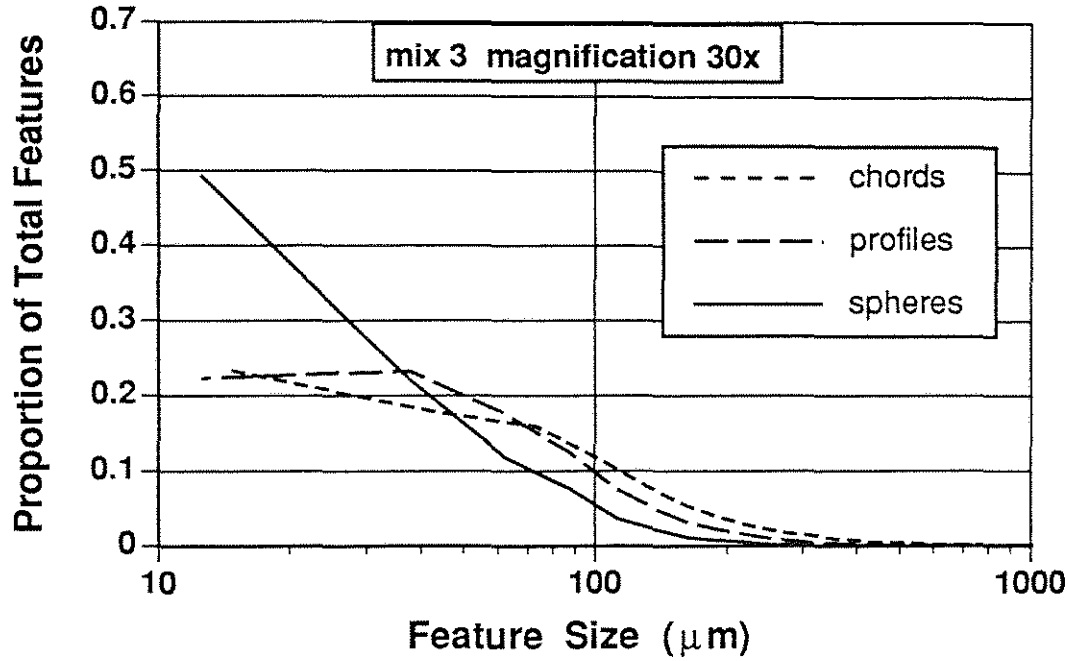

Figure 4.20 Proportion of total features versus feature size for chord, profile, and sphere distributions for mix 3 at magnification 30x.

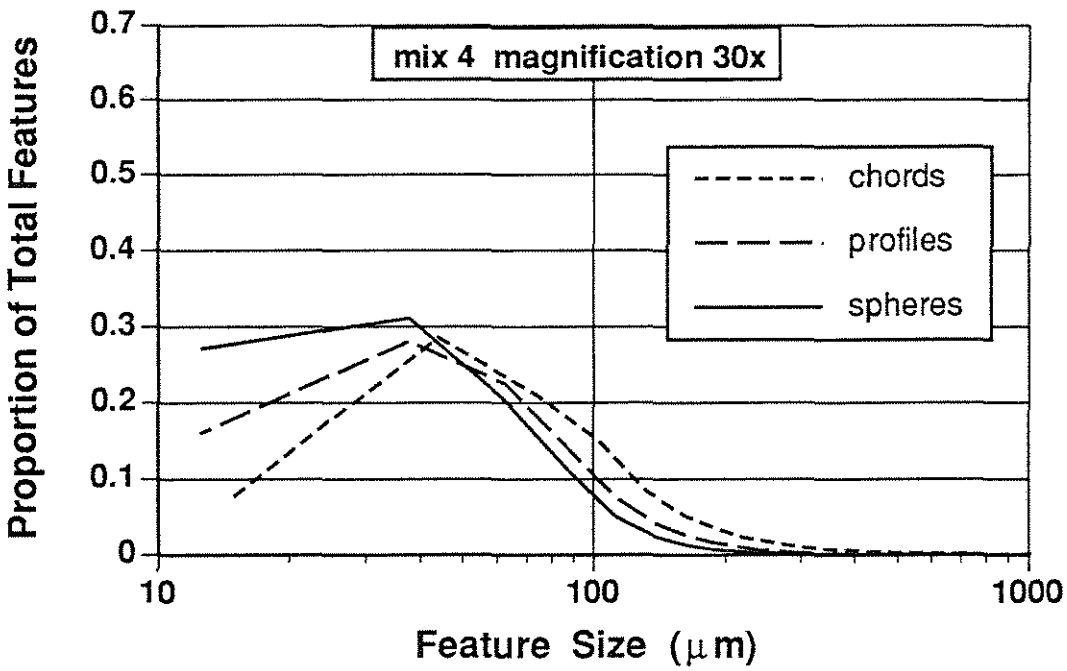

Figure 4.21 Proportion of total features versus feature size for chord, profile, and sphere distributions for mix 4 at magnification 30x.

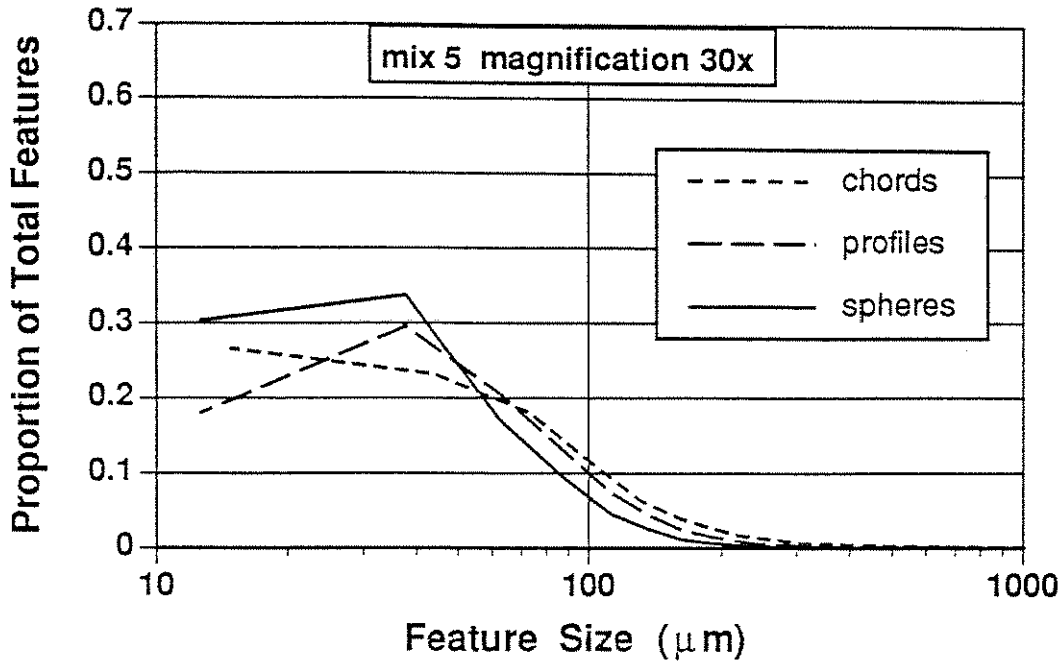

Figure 4.22 Proportion of total features versus feature size for chord, profile, and sphere distributions for mix 5 at magnification 30x.

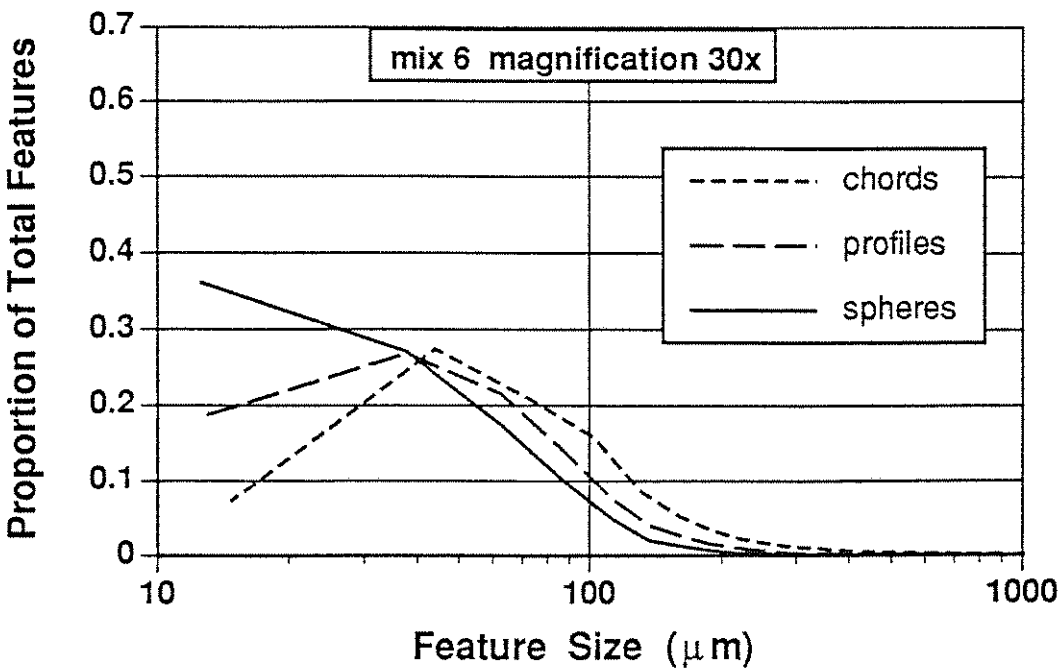

Figure 4.23 Proportion of total features versus feature size for chord, profile, and sphere distributions for mix 6 at magnification 30x.

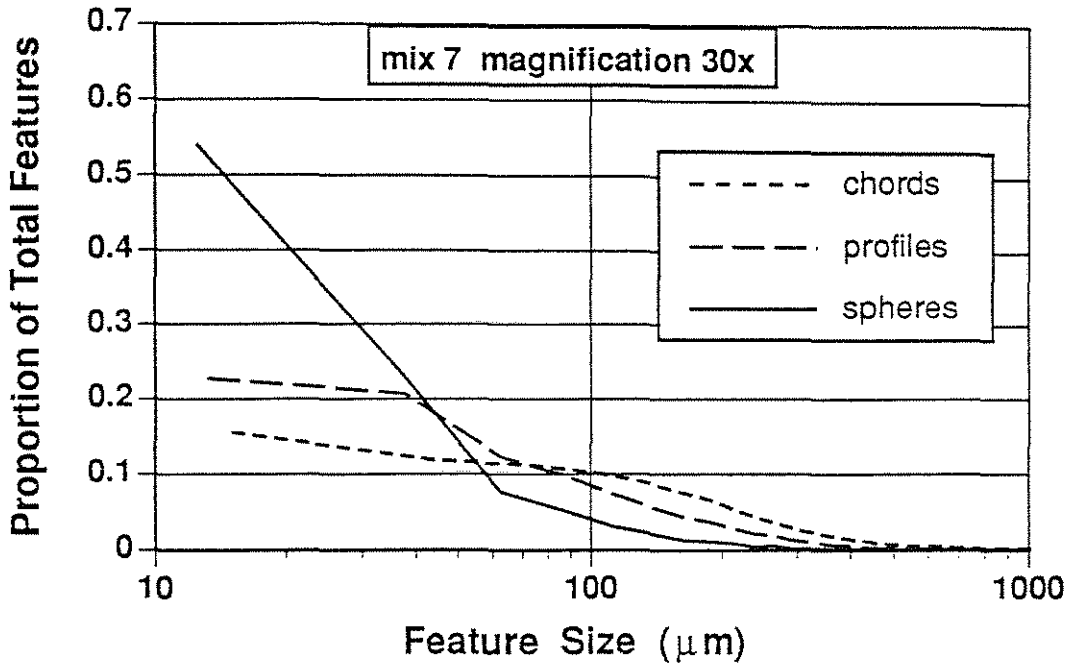

Figure 4.24 Proportion of total features versus feature size for chord, profile, and sphere distributions for mix 7 at magnification 30x.

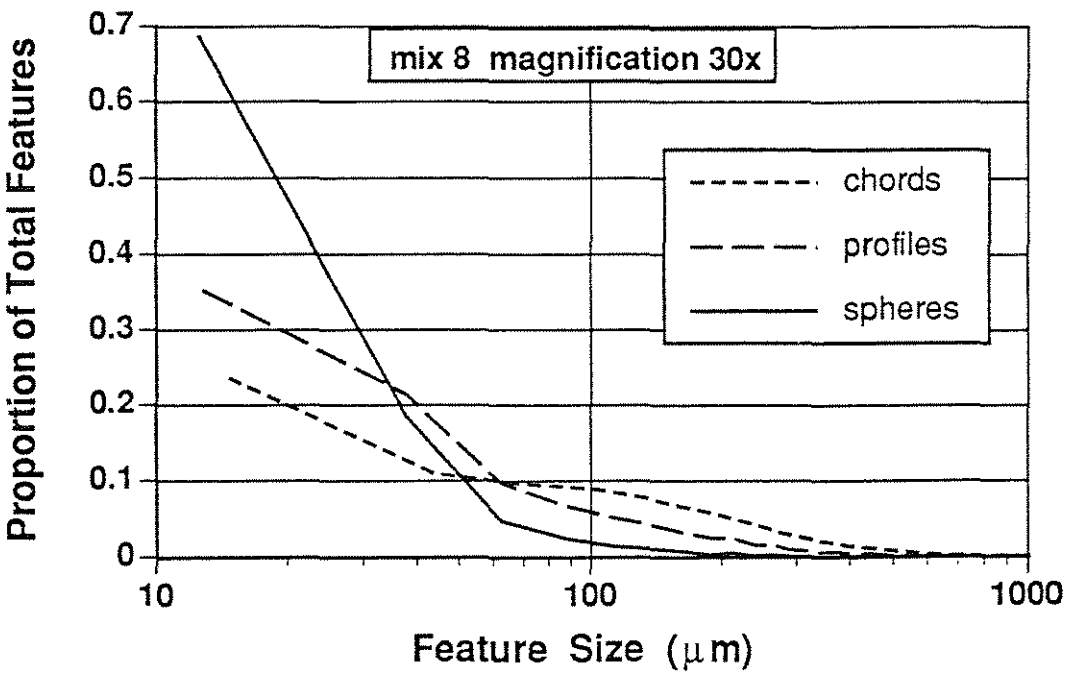

Figure 4.25 Proportion of total features versus feature size for chord, profile, and sphere distributions for mix 8 at magnification 30x.

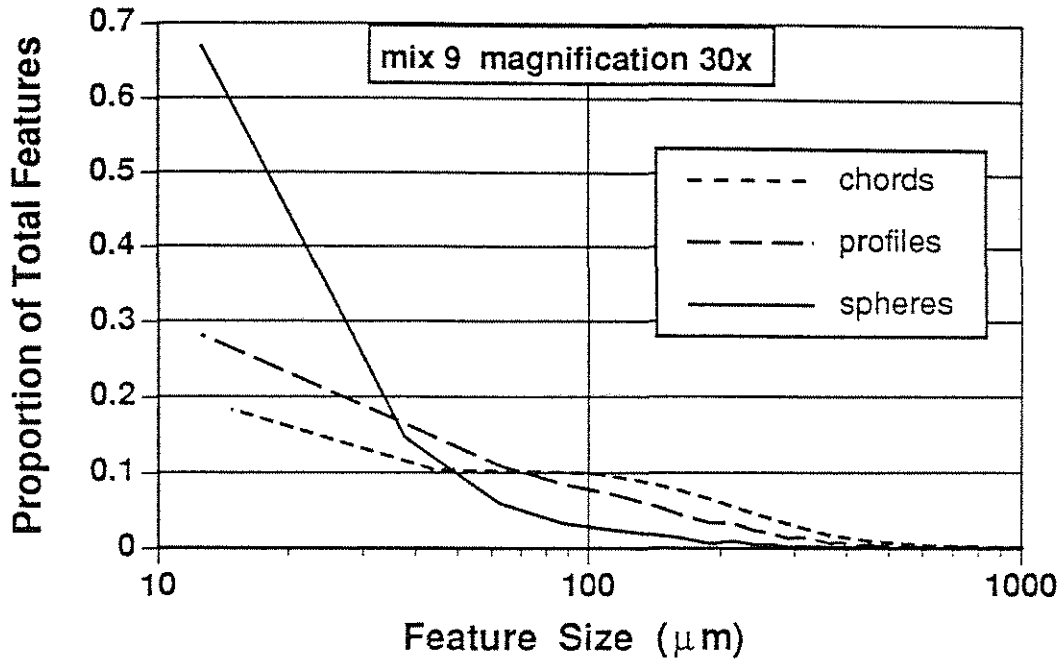

Figure 4.26 Proportion of total features versus feature size for chord, profile, and sphere distributions for mix 9 at magnification 30x.

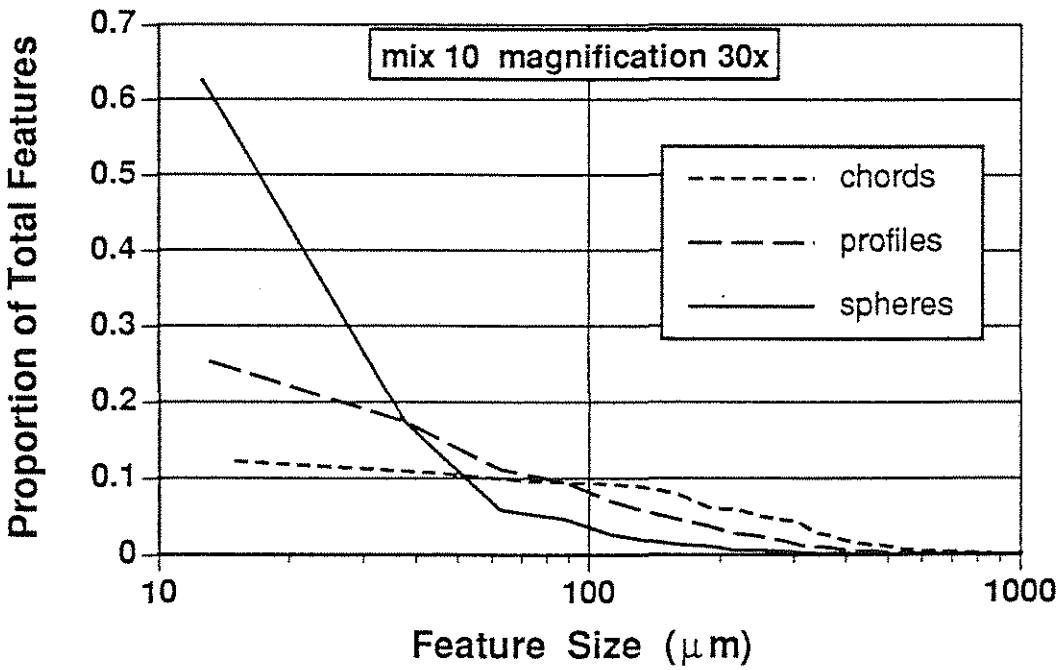

Figure 4.27 Proportion of total features versus feature size for chord, profile, and sphere distributions for mix 10 at magnification 30x.

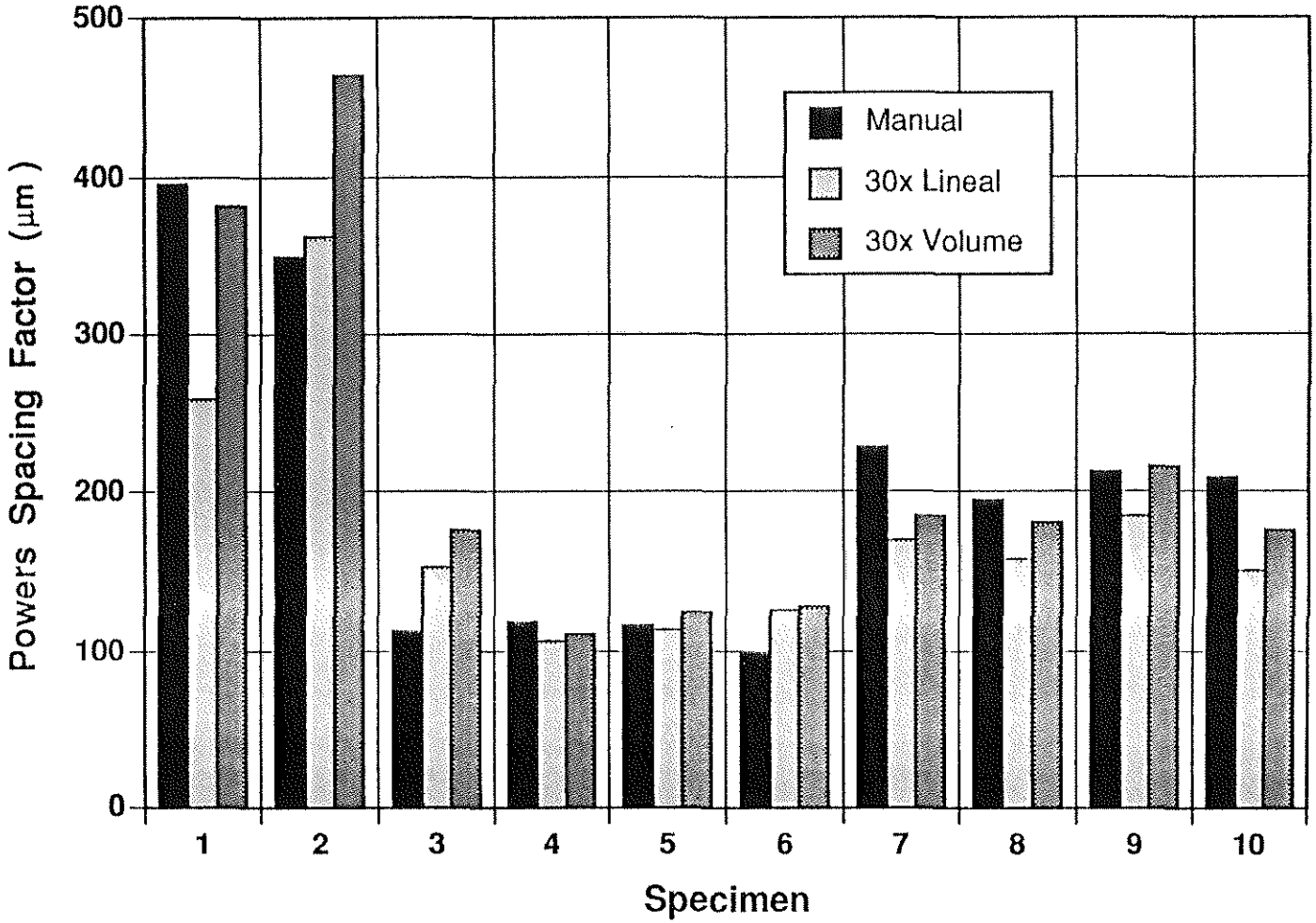

Figure 4.28 Powers spacing factor calculated from the manual analysis and the 30x lineal and volume distributions

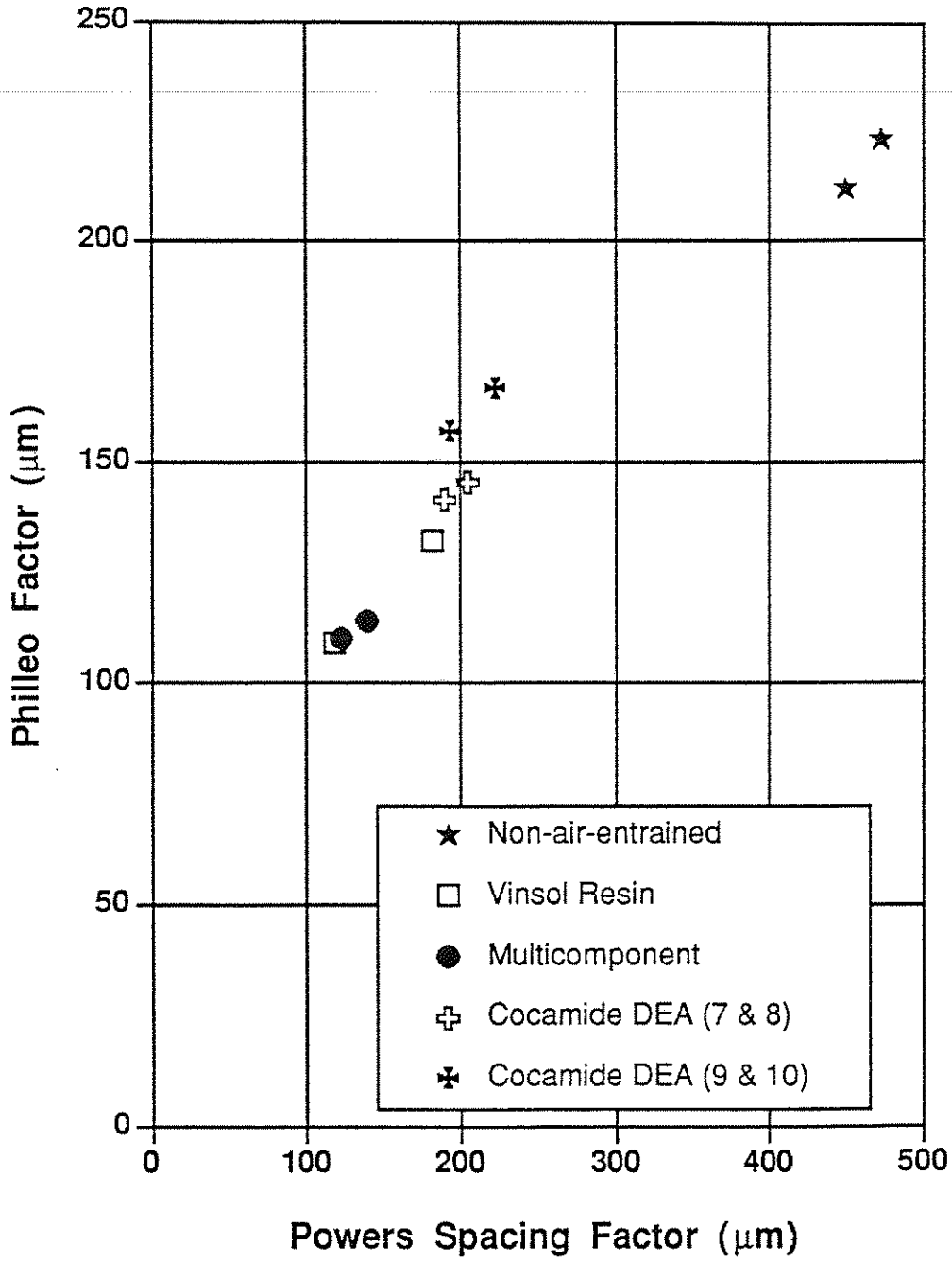

Figure 4.29 Philleo factor versus Powers spacing factor at magnification 12x

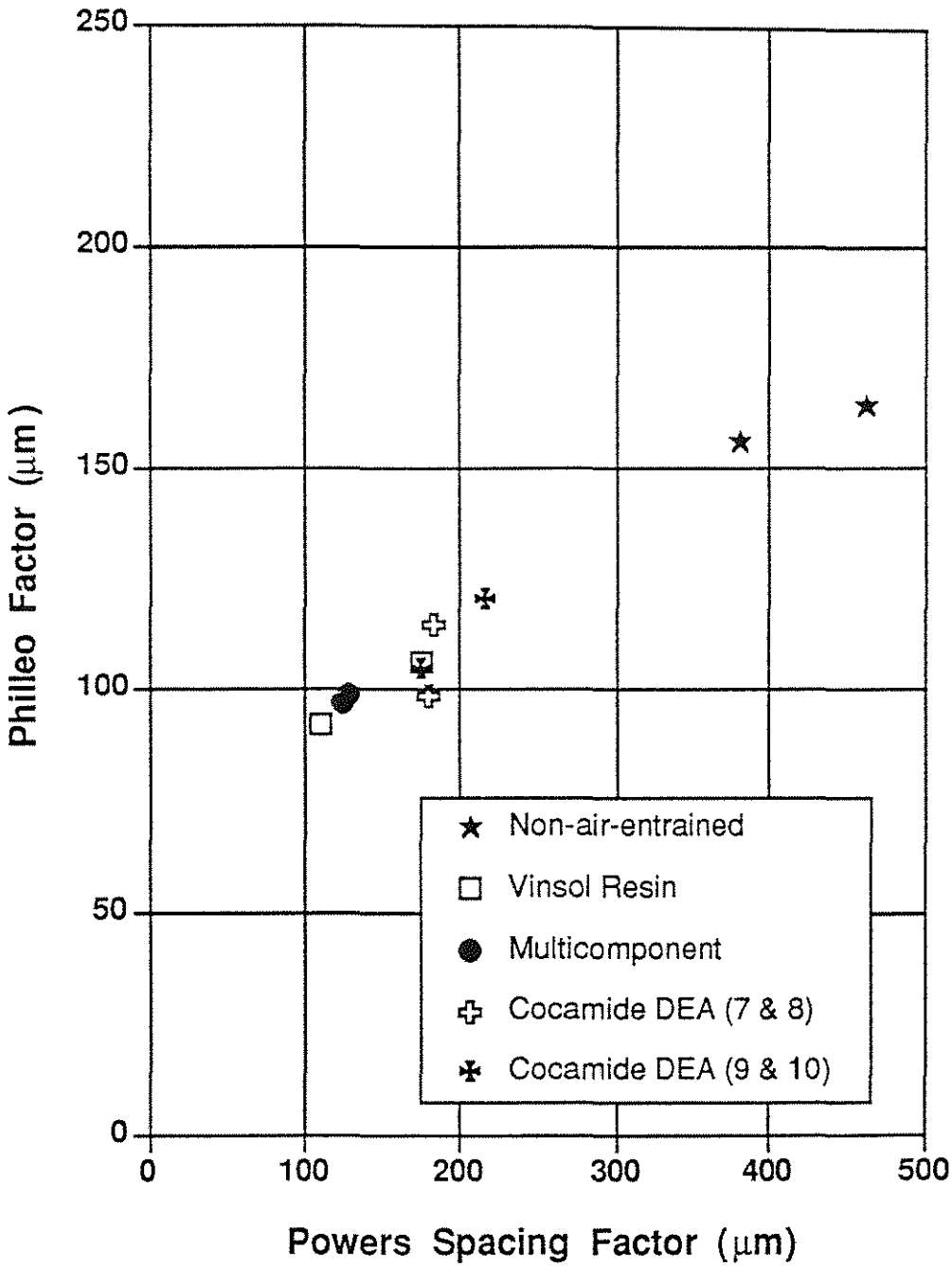

Figure 4.30 Phillleo factor versus Powers spacing factor at magnification 30x

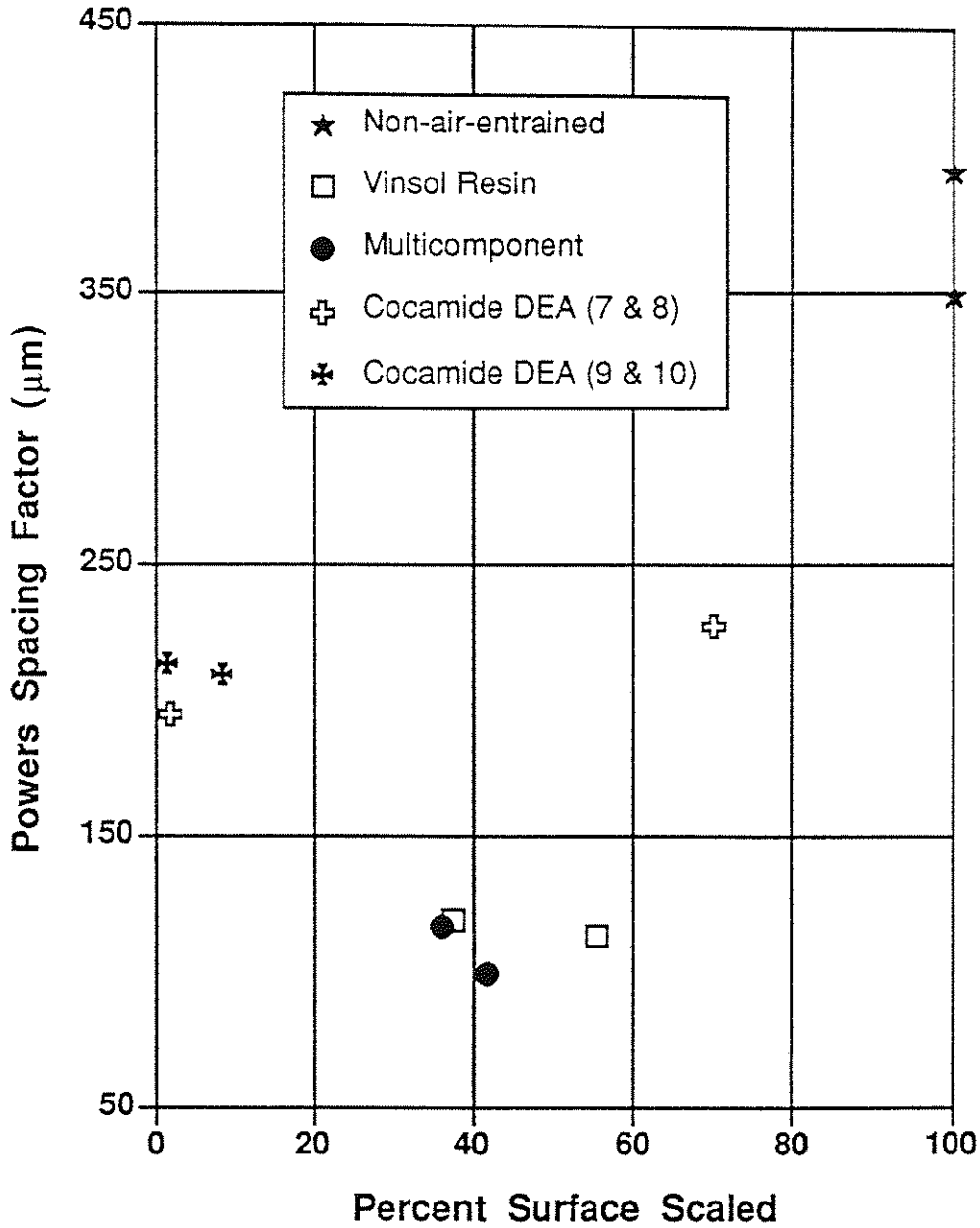

Figure 4.31 Manual analysis Powers spacing factor versus surface scaling

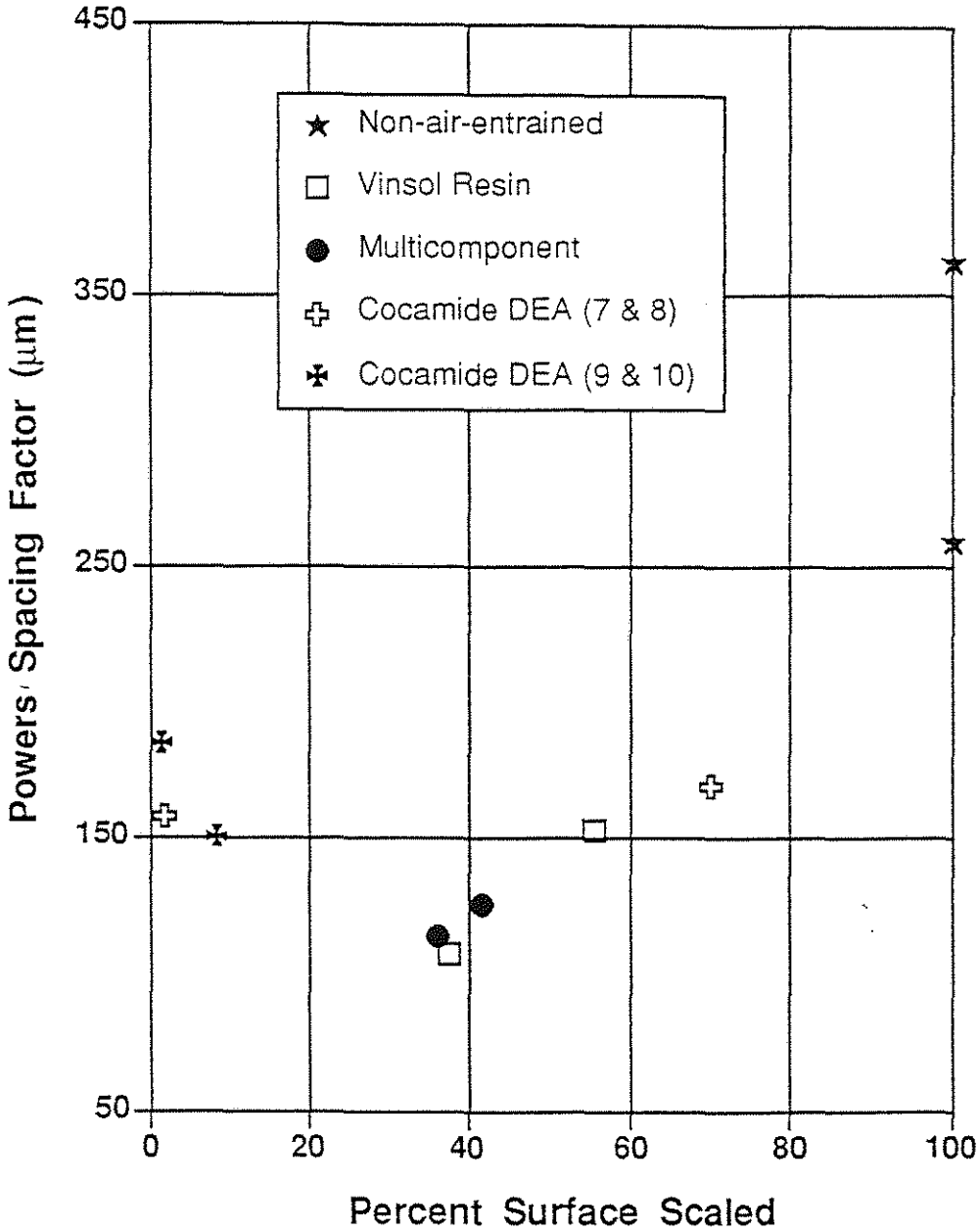

Figure 4.32 Lineal analysis Powers spacing factor versus surface scaling

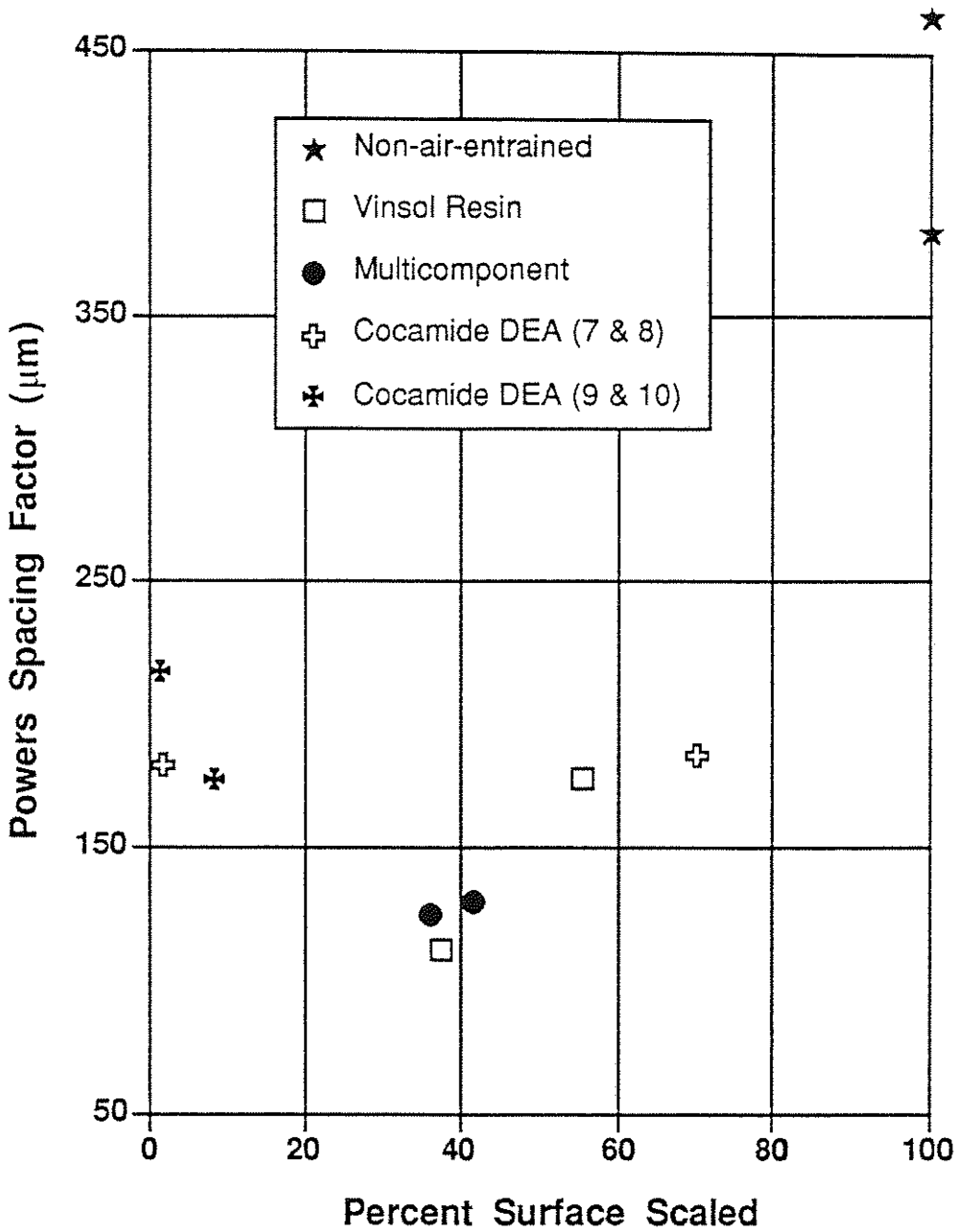

Figure 4.33 Areal analysis Powers spacing factor versus surface scaling

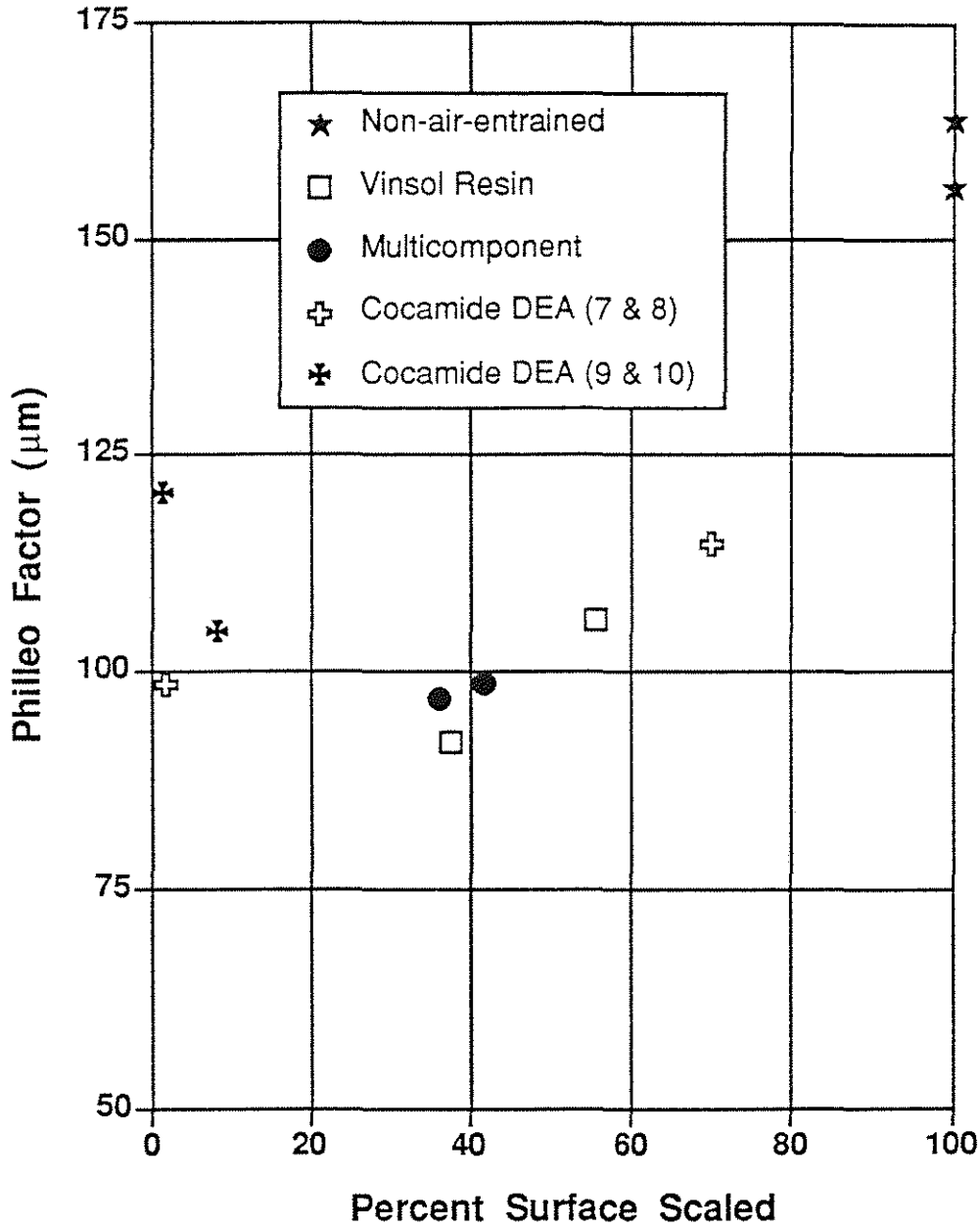

Figure 4.34 Phillleo factor versus surface scaling

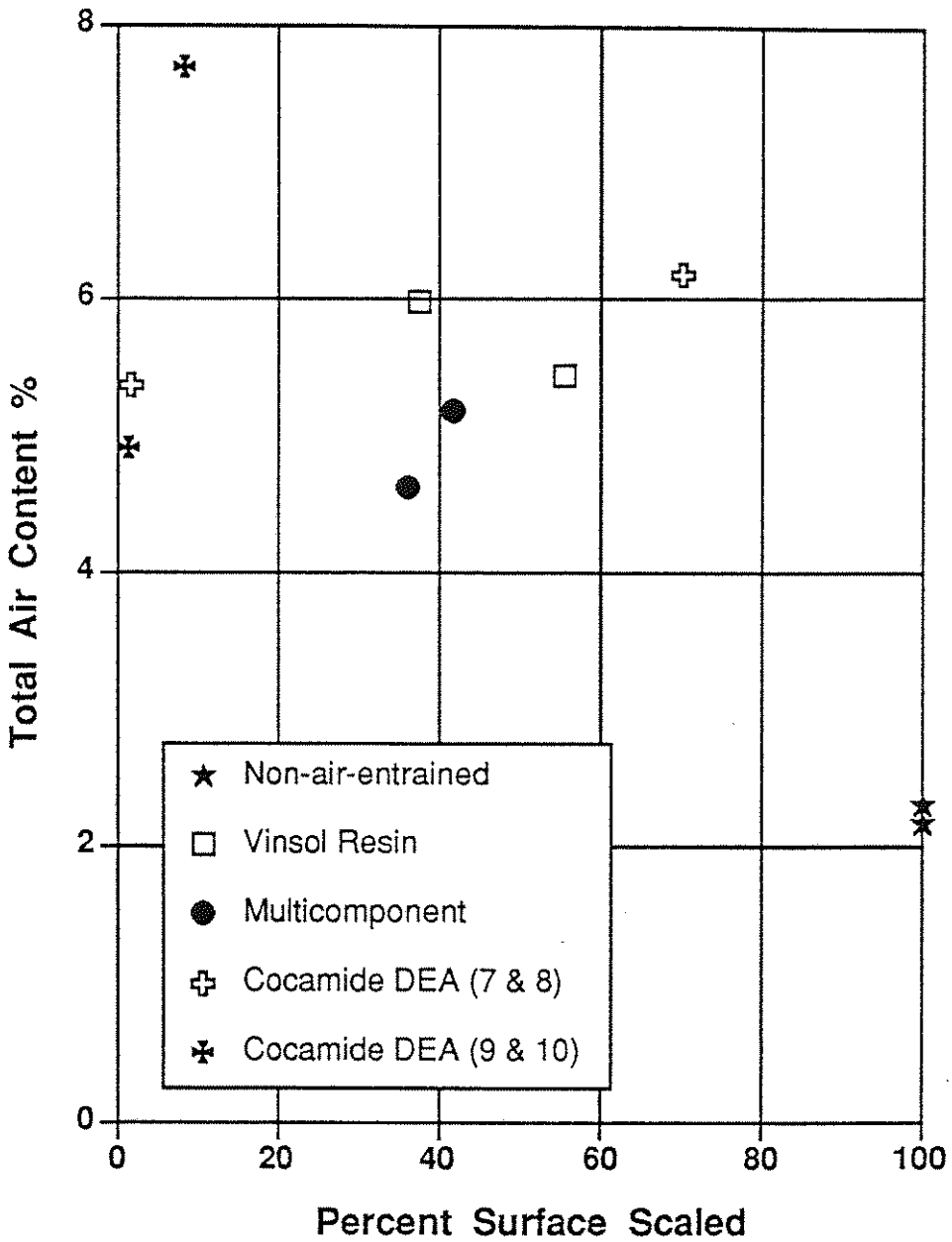

Figure 4.35 Air content versus surface scaling

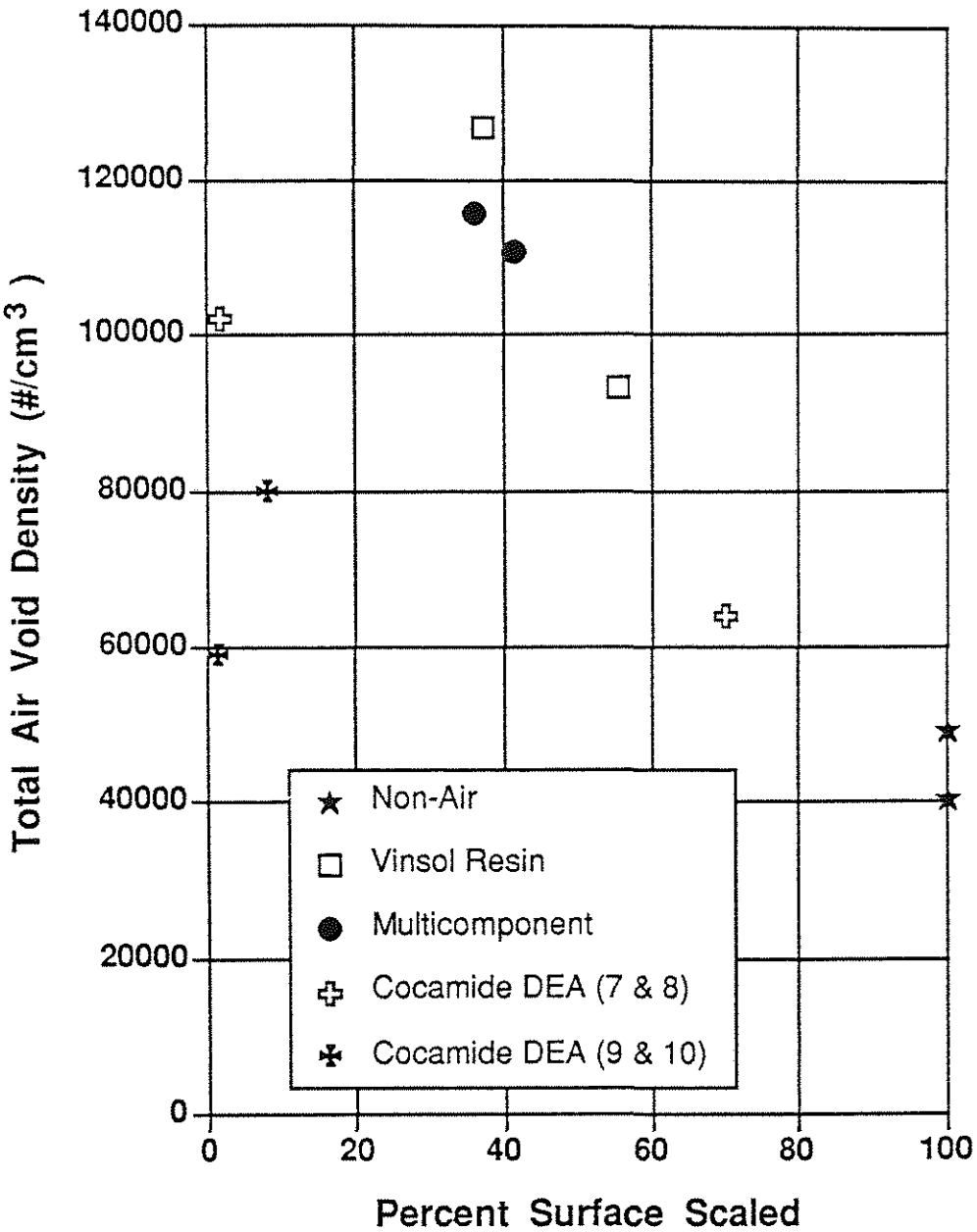

Figure 4.36 Total air-void density versus surface scaling

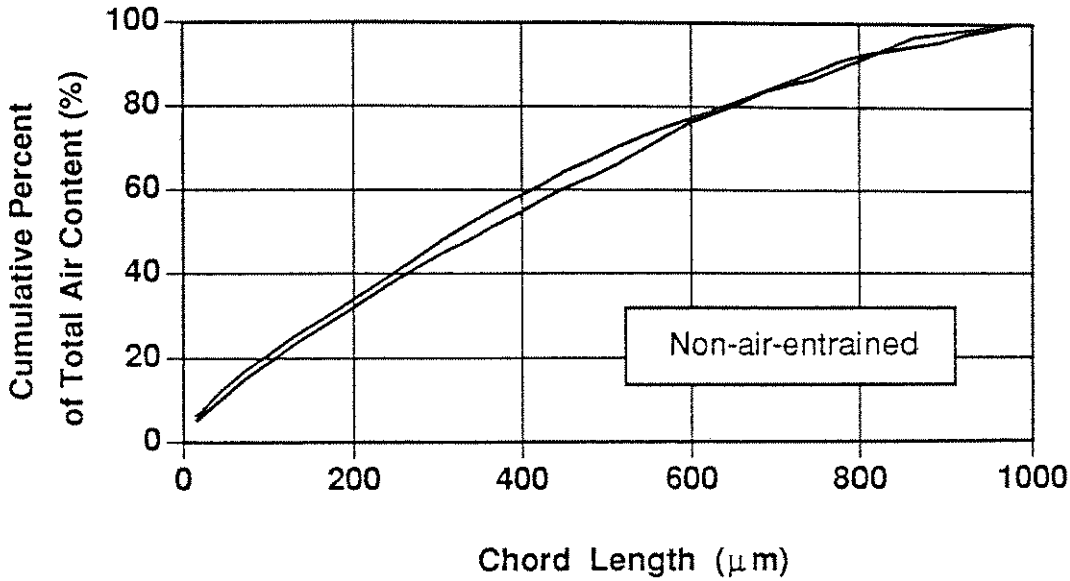

Figure 4.37 Cumulative percent of total air content versus chord length for the non-air-entrained samples

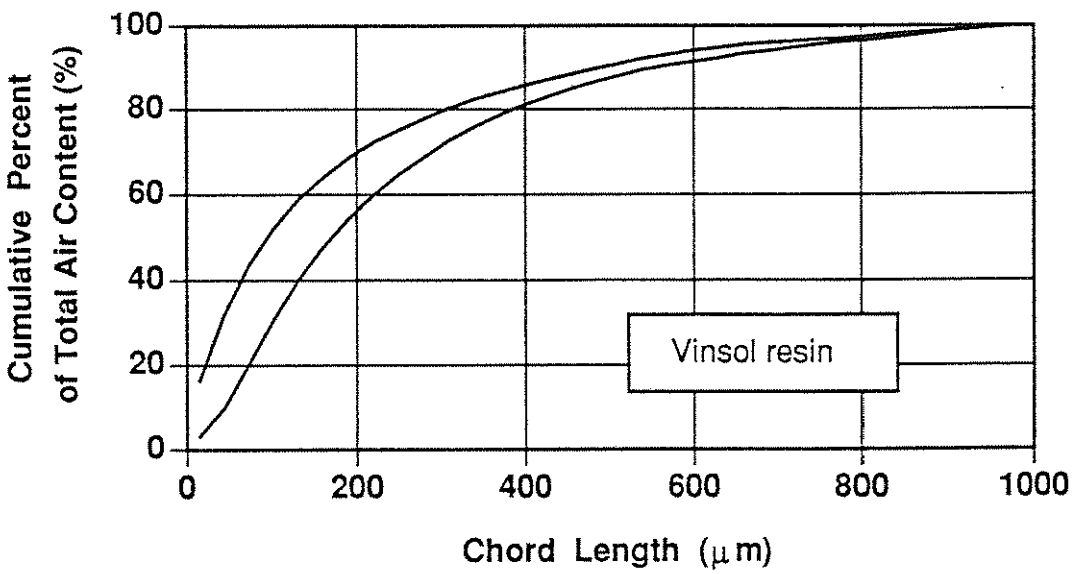

Figure 4.38 Cumulative percent of total air content versus chord length for the vinsol resin samples

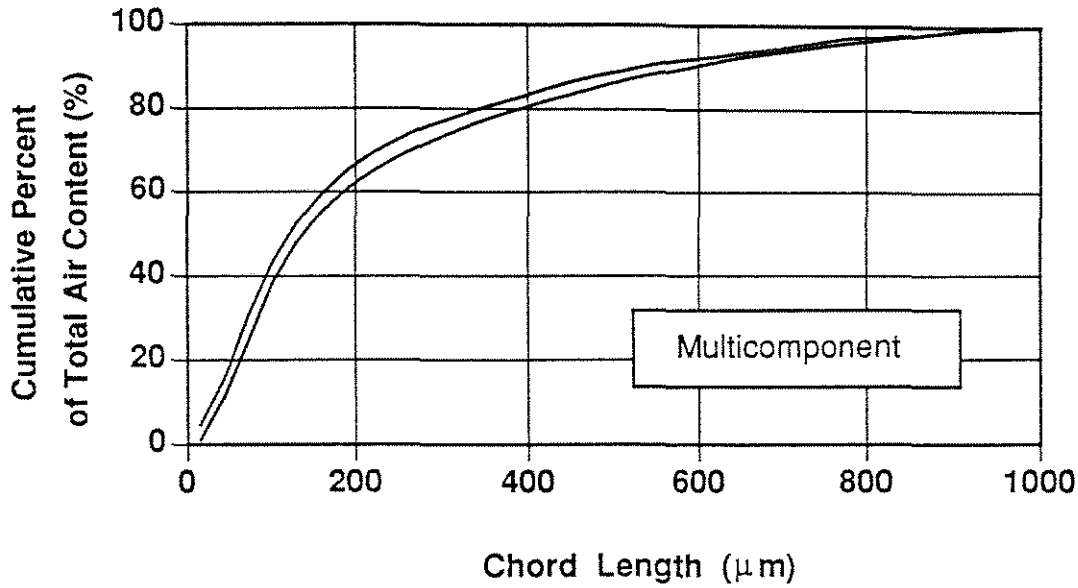

Figure 4.39 Cumulative percent of total air content versus chord length for the multicomponent samples

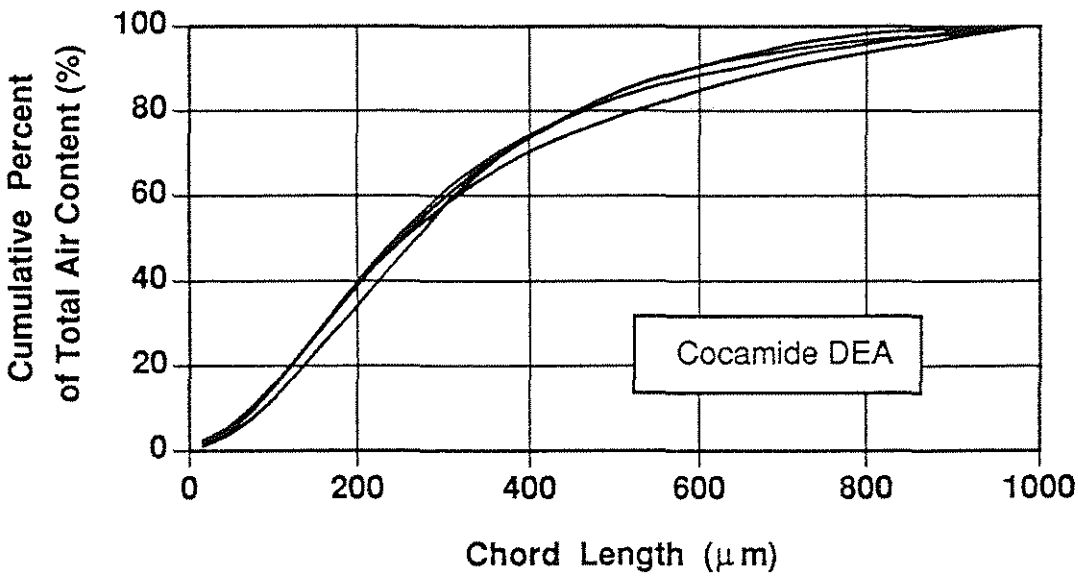

Figure 4.40 Cumulative percent of total air content versus chord length for the cocamide DEA samples

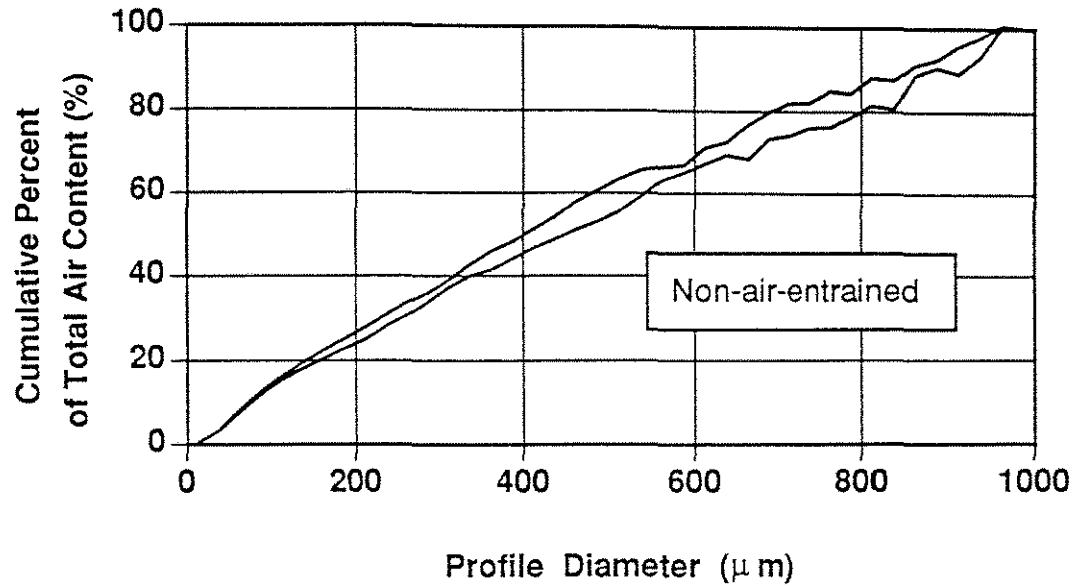

Figure 4.41 Cumulative percent of total air content versus profile diameter for the non-air-entrained samples

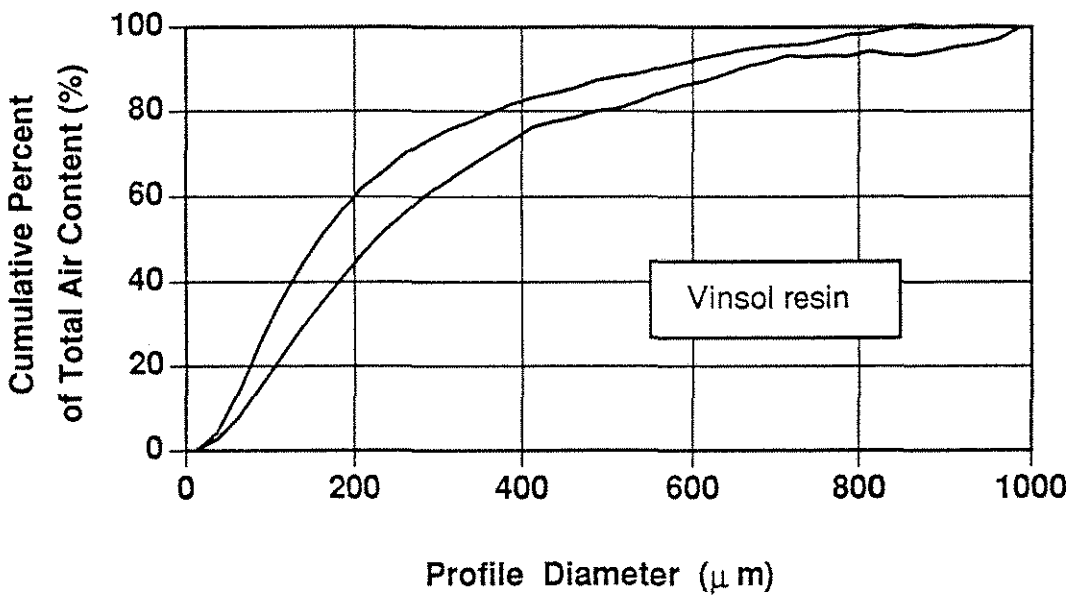

Figure 4.42 Cumulative percent of total air content versus profile diameter for the vinsol resin samples

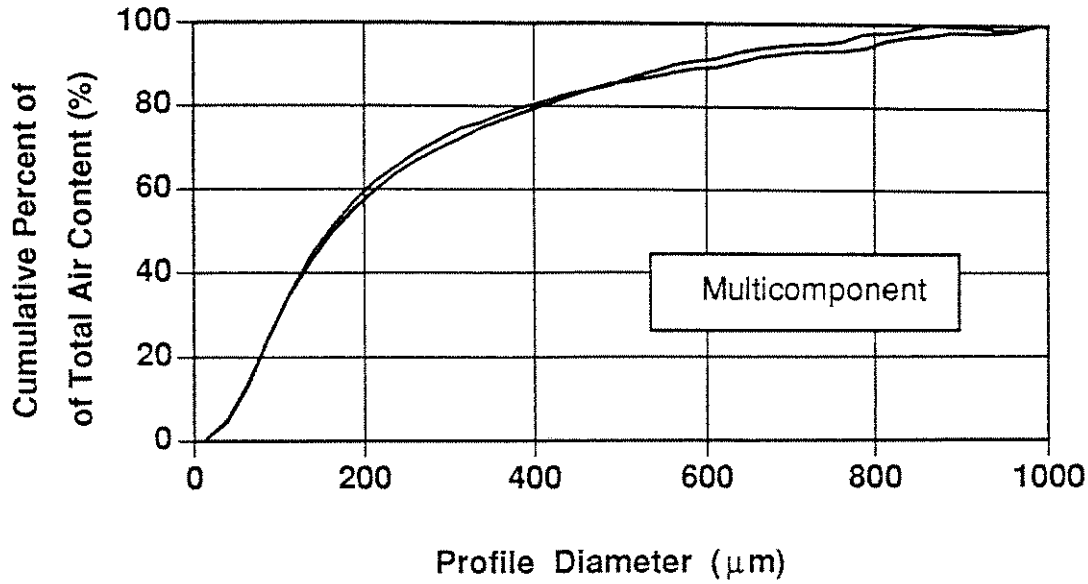

Figure 4.43 Cumulative percent of total air content versus profile diameter for the multicomponent samples

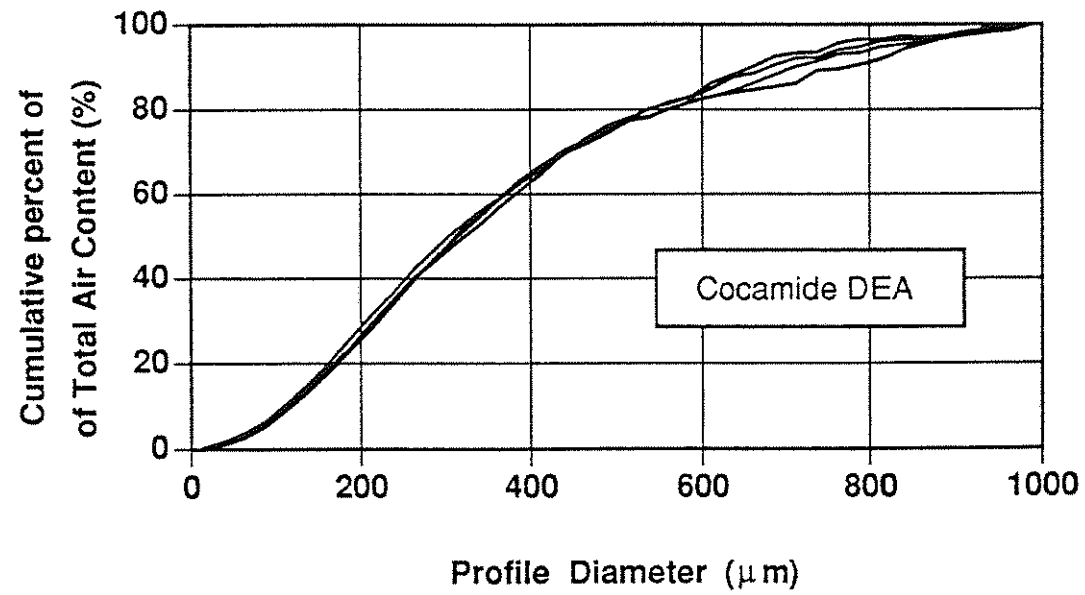

Figure 4.44 Cumulative percent of total air content versus profile diameter for the cocamide DEA samples

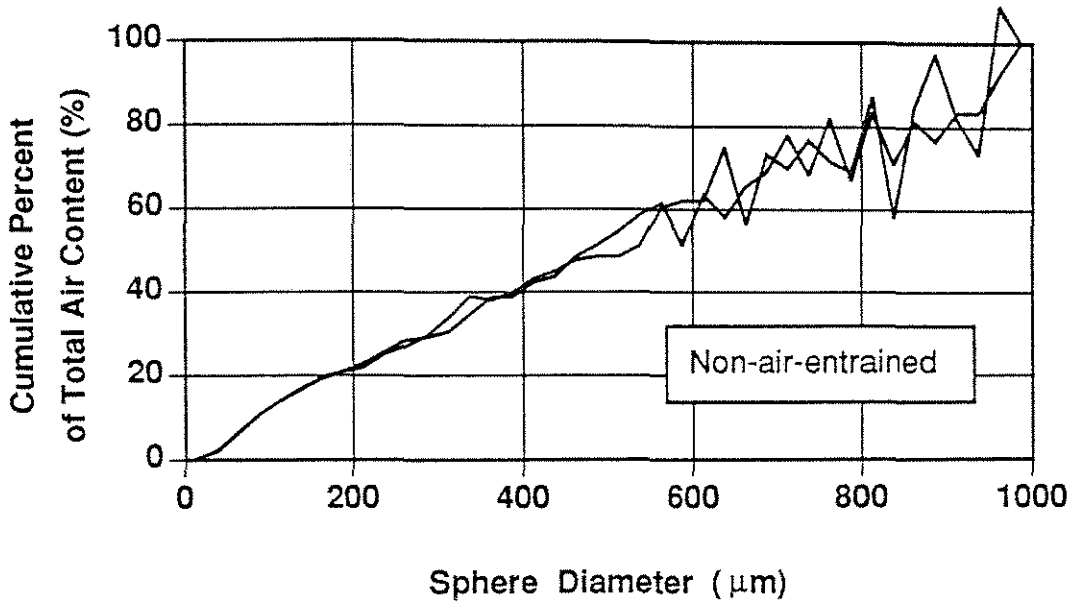

Figure 4.45 Cumulative percent of total air content versus air-void diameter for the non-air-entrained samples

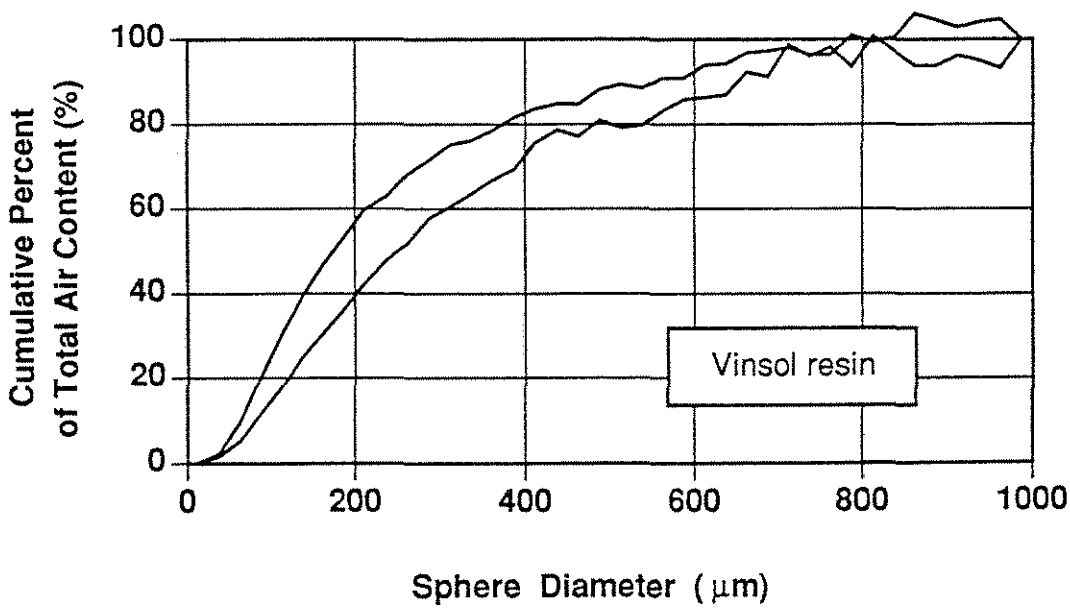

Figure 4.46 Cumulative percent of total air content versus air-void diameter for the vinsol resin samples

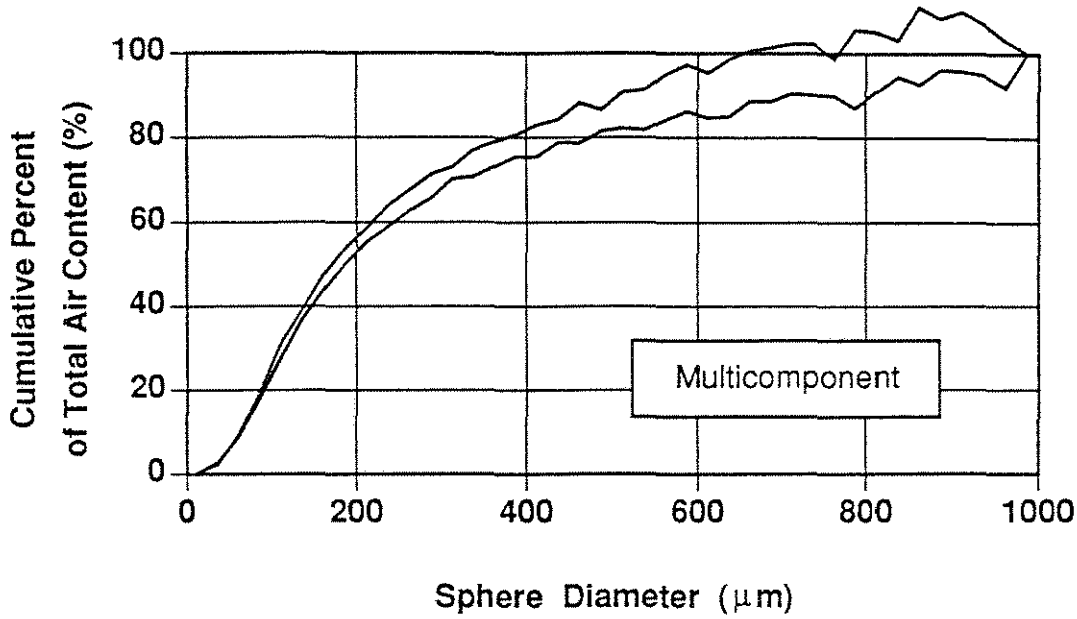

Figure 4.47 Cumulative percent of total air content versus air-void diameter for the multicomponent samples

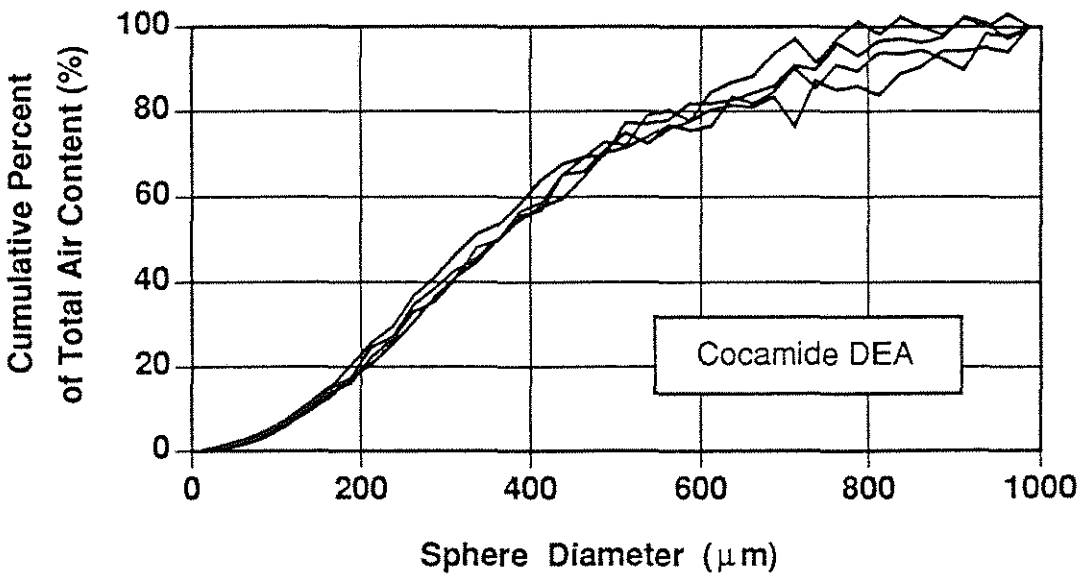

Figure 4.48 Cumulative percent of total air content versus air-void diameter for the cocamide DEA samples

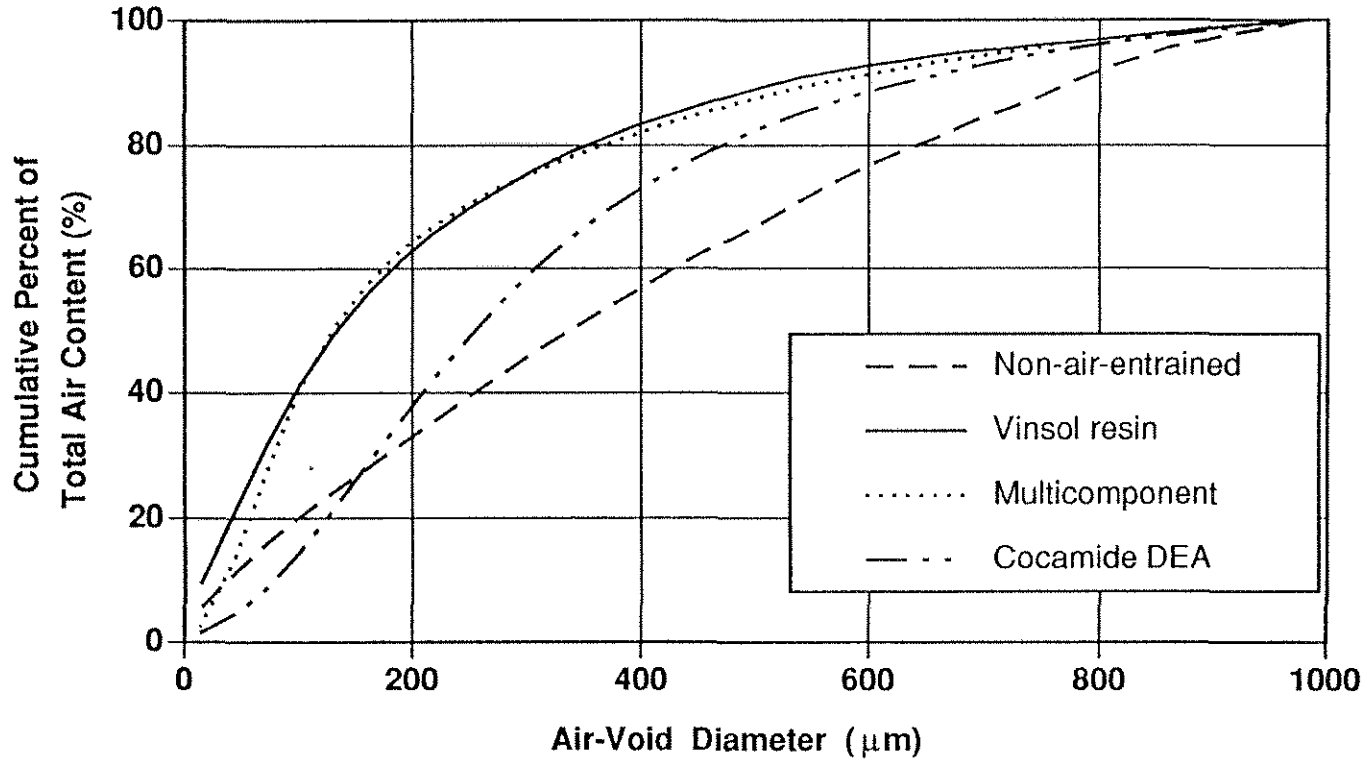

Figure 4.49 Cumulative percent of total air content versus chord length, averages for the different air-entraining agents

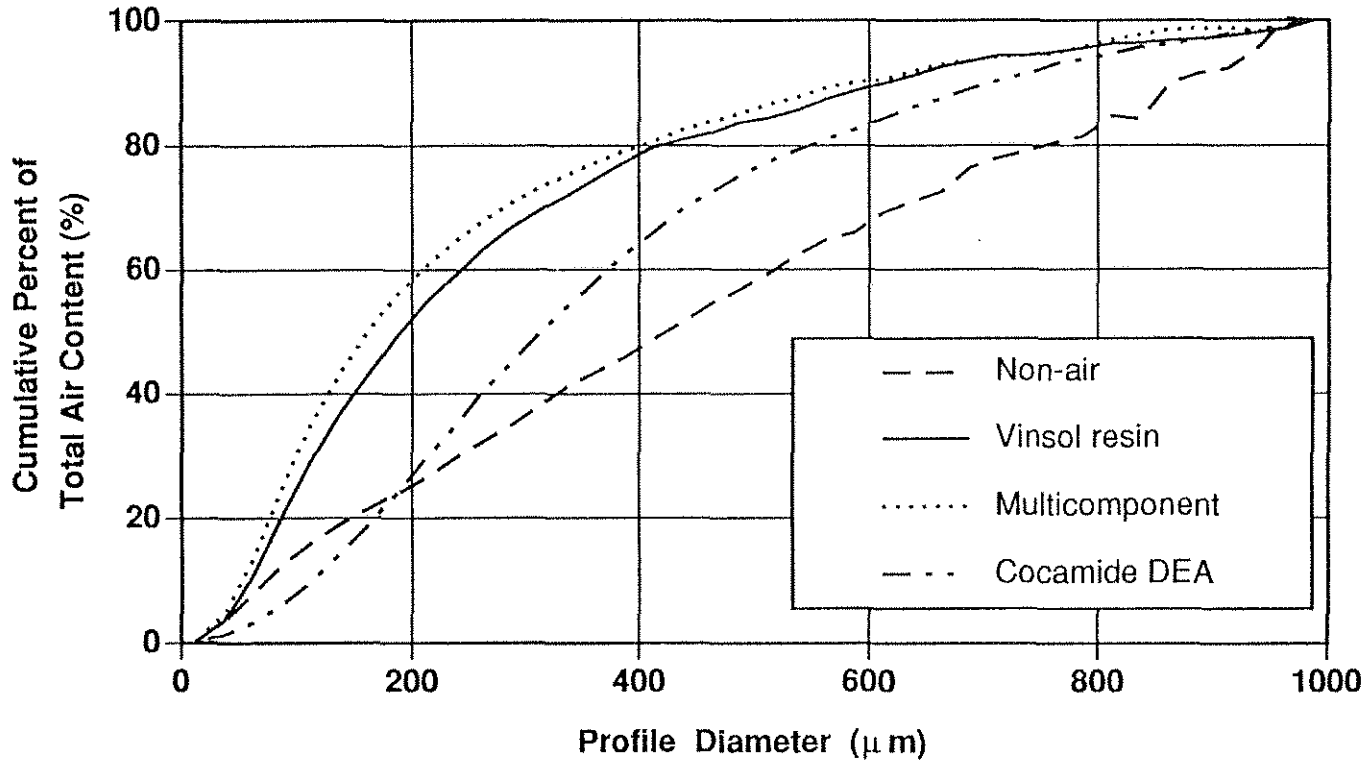

Figure 4.50 Cumulative percent of total air content versus profile diameter, averages for the different air-entraining agents

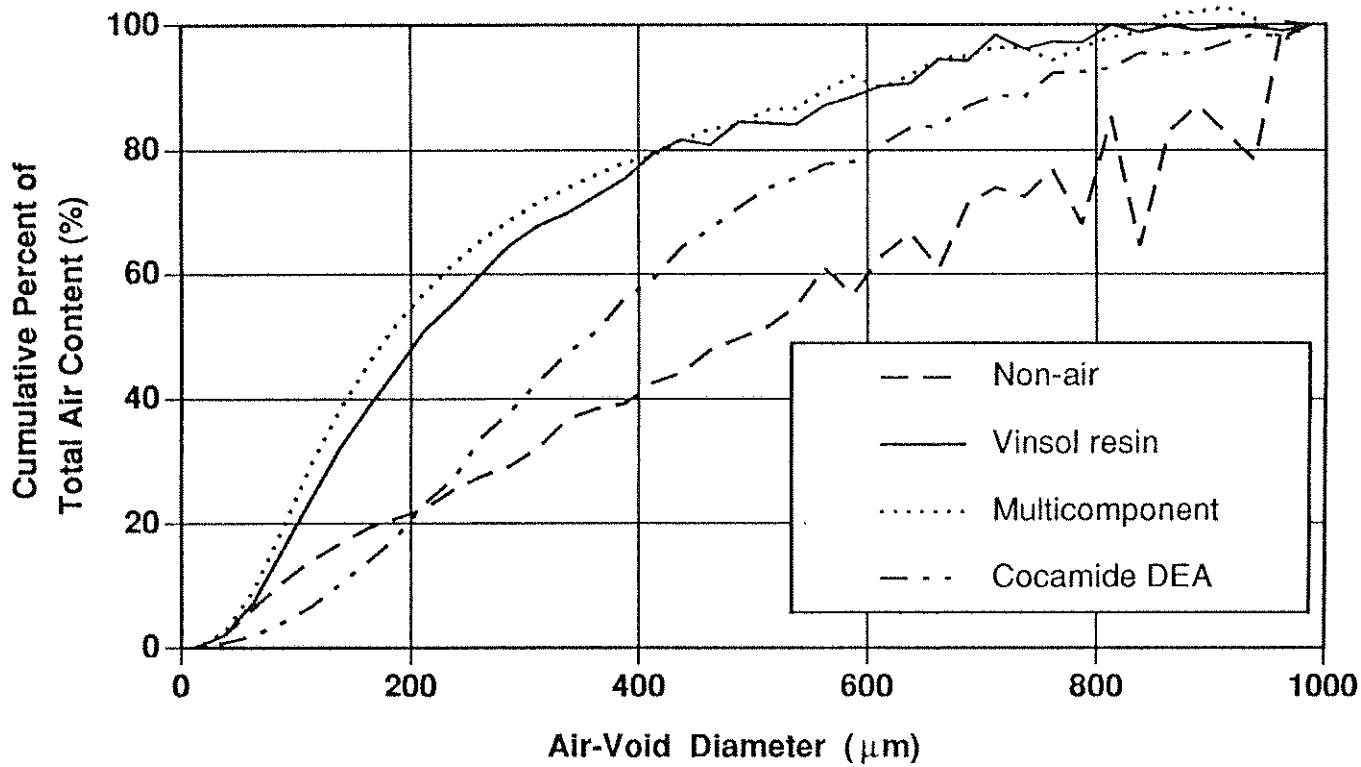

Figure 4.51 Cumulative percent of total air content versus air-void diameter, averages for the different air-entraining agents

APPENDIX A

Batching and Strength Test Results

The batching information and strength test results were provided by Professional Service Industries, Inc. All samples were mixed on 3/22/88 in a laboratory provided by Solvay Construction Materials. The samples were mixed in a nine cubic foot motorized mixer following the procedures in ASTM C 192. The 3 x 6 in. cylinder molds were manufactured by M. A. Industries. Inc. of Peachtree City, Ga. The compression tests were performed with an E.L.E. 400,000 lb. test machine.

Table A.1 Batching and compression test results for mix 1 and mix 2

Non-Air-Entrained

	Mix 1	Mix 2	
Cement	523	525	(lbs.)
Coarse Aggregate	1820	1828	(lbs.)
Fine Aggregate	1495	1501	(lbs.)
Water	318	307	(lbs.)
Air[1]	1.9	1.95	(%)
Slump[2]	3 1/2	3	(in.)
Unit Wt.[3]	151.3	151.5	(#/ft^3)
Water/Cement	0.61	0.58	

Compressive Strength

1 Day	1110	1175	(psi)
3 Days	2988	3091	(psi)
7 Days	4199	4493	(psi)
28 Days	6120	6419	(psi)

1. ASTM C 231
2. ASTM C 143
3. ASTM C 138

Table A.2 Batching and compression test results for mix 3 and mix 4

Vinsol Resin[1]

	Mix 3	Mix 4	
Cement	510	511	(lbs.)
Coarse Aggregate	1776	1780	(lbs.)
Fine Aggregate	1404	1407	(lbs.)
Water	278	270	(lbs.)
Air[2]	6.5	6.5	(%)
Slump[3]	4	3 3/4	(in.)
Unit Wt.[4]	144.5	144.5	(#/ft^3)
Water/Cement	0.55	0.53	
Compressive Strength			
1 Day	1113	1120	(psi)
3 Days	2576	2542	(psi)
7 Days	3713	3652	(psi)
28 Days	5347	5293	(psi)

1. Manufacured by Hercules Chemical
2. ASTM C 231
3. ASTM C 143
4. ASTM C 138

Table A.3 Batching and compression test results for mix 5 and mix 6

Micro-Air (Multi-Component)[1]

	Mix 5	Mix 6	
Cement	517	515	(lbs.)
Coarse Aggregate	1799	1792	(lbs.)
Fine Aggregate	1422	1417	(lbs.)
Water	273	272	(lbs.)
Air[2]	6.0	6.25	(%)
Slump[3]	3 3/4	3 3/4	(in.)
Unit Wt.[4]	146.1	145.5	(#/ft^3)
Water/Cement	0.53	0.53	
Compressive Strength			
1 Day	1130	1015	(psi)
3 Days	2636	2547	(psi)
7 Days	3708	3689	(psi)
28 Days	5117	4982	(psi)

1. Manufacured by Master Builders, Inc.
2. ASTM C 231
3. ASTM C 143
4. ASTM C 138

Table A.4 Batching and compression test results for mix 7 and mix 8

Catexol A.E. 260 (Cocamide DEA)[1]

	Mix 7	Mix 8	
Cement	512	513	(lbs.)
Coarse Aggregate	1783	1787	(lbs.)
Fine Aggregate	1409	1413	(lbs.)
Water	279	271	(lbs.)
Air[2]	7.0	6.8	(%)
Slump[3]	6 3/4	5 3/4	(in.)
Unit Wt.[4]	145.1	145.1	(#/ft^3)
Water/Cement	0.55	0.53	
Compressive Strength			
1 Day	1196	1295	(psi)
3 Days	2735	2957	(psi)
7 Days	3945	4100	(psi)
28 Days	5382	5756	(psi)

1. Manufacured by Solvay Construction Materials
2. ASTM C 231
3. ASTM C 143
4. ASTM C 138

Table A.5 Batching and compression test results for mix 9 and mix 10

Catexol A.E. 260 (Cocamide DEA)[1]

	Mix 9	Mix 10	
Cement	515	515	(lbs.)
Coarse Aggregate	1793	1793	(lbs.)
Fine Aggregate	1418	1418	(lbs.)
Water	260	260	(lbs.)
Air[2]	6.5	6.5	(%)
Slump[3]	3 1/2	3 1/4	(in.)
Unit Wt.[4]	145.31	145.3	(#/ft^3)
Water/Cement	0.51	0.51	
Compressive Strength			
1 Day	1420	1375	(psi)
3 Days	3189	3221	(psi)
7 Days	4482	4510	(psi)
28 Days	5954	6148	(psi)

1. Manufacured by Solvay Construction Materials
2. ASTM C 231
3. ASTM C 143
4. ASTM C 138

APPENDIX B

Modified Point Count Test Results

The ten mixes used in this study were sectioned, polished, and petrographically analyzed by Professional Service Industries, Inc. during April 1988. The results of the modified point count analyses provided in this appendix are as reported in their report dated 5/13/88.

Table B.1 Modified point count[1] results for mix 1 and mix 2

Mix 1

	Section			
	Longitudinal[2]	Top[3]	Middle[4]	
Air Content	3.3	1.3	1.9	(volume %)
Paste Content	26.8	36.5	23.5	(volume %)
Specific Surface	370.9	559.5	339.4	(in^2/in^3)
Powers Spacing Factor	0.016	0.017	0.021	(in.)
Paste-Air Ratio	8.1	26.8	12.3	
Traverse Length	104.3	100.4	100.0	(in.)
Area Traversed	13.8	7.1	7.1	($in.^2$)

Mix 2

	Section			
	Longitudinal[2]	Top[3]	Middle[4]	
Air Content	2.8	3.9	1.7	(volume %)
Paste Content	26.0	37.9	23.5	(volume %)
Specific Surface	446.4	333.3	335.8	(in^2/in^3)
Powers Spacing Factor	0.014	0.019	0.022	(in.)
Paste-Air Ratio	9.2	9.8	13.9	
Traverse Length	100.1	98.4	101.5	(in.)
Area Traversed	15.0	7.1	7.1	($in.^2$)

1. ASTM C 457-82a
2. Section through the center of the 3 x 6 in. cylinder
3. Transverse section at top of cylinder (top surface polished)
4. Transverse section at cylinder mid-height

Table B.2 Modified point count[1] results for mix 3 and mix 4

Mix 3

	Section			
	Longitudinal[2]	Top[3]	Middle[4]	
Air Content	7.6	10.0	6.4	(volume %)
Paste Content	23.5	39.0	23.9	(volume %)
Specific Surface	694.8	895.3	782.9	(in^2/in^3)
Powers Spacing Factor	0.005	0.004	0.005	(in.)
Paste-Air Ratio	3.1	3.9	3.7	
Traverse Length	100.5	100.2	99.6	(in.)
Area Traversed	15.0	7.1	7.1	($in.^2$)

Mix 4

	Section			
	Longitudinal[2]	Top[3]	Middle[4]	
Air Content	6.9	8.8	6.4	(volume %)
Paste Content	21.6	37.3	22.5	(volume %)
Specific Surface	670.0	925.3	828.8	(in^2/in^3)
Powers Spacing Factor	0.005	0.005	0.004	(in.)
Paste-Air Ratio	3.1	4.2	3.5	
Traverse Length	102.4	99.8	99.9	(in.)
Area Traversed	16.0	7.1	7.1	($in.^2$)

1. ASTM C 457-82a
2. Section through center of the 3 x 6 in. cylinder
3. Transverse section at cylinder top (top surface polished)
4. Transverse section at cylinder mid-height

Table B.3 Modified point count[1] results fo mix 5 and mix 6

Mix 5

	Section			
	Longitudinal[2]	Top[3]	Middle[4]	
Air Content	6.0	7.5	9.2	(volume %)
Paste Content	20.0	33.1	24.2	(volume %)
Specific Surface	720.9	806.3	654.3	(in^2/in^3)
Powers Spacing Factor	0.005	0.005	0.004	(in.)
Paste-Air Ratio	3.3	4.5	2.6	
Traverse Length	99.2	98.8	100.4	(in.)
Area Traversed	15.0	7.1	7.1	($in.^2$)

Mix 6

	Section			
	Longitudinal[2]	Top[3]	Middle[4]	
Air Content	7.2	7.7	9.0	(volume %)
Paste Content	19.9	31.9	27.1	(volume %)
Specific Surface	700.9	1048.2	694.4	(in^2/in^3)
Powers Spacing Factor	0.004	0.004	0.004	(in.)
Paste-Air Ratio	2.8	4.1	3.0	
Traverse Length	104.7	99.1	98.7	(in.)
Area Traversed	16.8	7.1	7.1	($in.^2$)

1. ASTM C 457-82a
2. Section through center of the 3 x 6 in. cylinder
3. Transverse section at cylinder top (top surface polished)
4. Transverse section at cylinder mid-height

Table B.4 Modified point count[1] results for mix 7 and mix 8

Mix 7

	Section			
	Longitudinal[2]	Top[3]	Middle[4]	
Air Content	7.2	6.7	6.9	(volume %)
Paste Content	21.6	31.3	21.9	(volume %)
Specific Surface	334.4	545.4	404.5	(in^2/in^3)
Powers Spacing Factor	0.008	0.008	0.008	(in.)
Paste-Air Ratio	3.0	4.7	3.2	
Traverse Length	103.1	99.5	99.8	(in.)
Area Traversed	16.2	7.1	7.1	($in.^2$)

Mix 8

	Section			
	Longitudinal[2]	Top[3]	Middle[4]	
Air Content	6.2	5.1	6.8	(volume %)
Paste Content	19.5	36.1	22.7	(volume %)
Specific Surface	410.6	710.0	429.2	(in^2/in^3)
Powers Spacing Factor	0.008	0.008	0.008	(in.)
Paste-Air Ratio	3.1	7.0	3.3	
Traverse Length	99.5	99.2	99.2	(in.)
Area Traversed	15.1	7.1	7.1	($in.^2$)

1. ASTM C 457-82a
2. Section through center of the 3 x 6 in. cylinder
3. Transverse section at cylinder top (top surface polished)
4. Transverse section at cylinder mid-height

Table B.5 Modified point count[1] results for mix 9 and mix 10

Mix 9

	Section			
	Longitudinal[2]	Top[3]	Middle[4]	
Air Content	6.1	5.0	6.5	(volume %)
Paste Content	20.1	37.0	21.1	(volume %)
Specific Surface	392.1	650.1	453.0	(in^2/in^3)
Powers Spacing Factor	0.008	0.008	0.007	(in.)
Paste-Air Ratio	3.3	7.4	3.3	
Traverse Length	99.9	99.9	98.7	(in.)
Area Traversed	15.6	7.1	7.1	($in.^2$)

Mix 10

	Section			
	Longitudinal[2]	Top[3]	Middle[4]	
Air Content	8.1	7.1	6.6	(volume %)
Paste Content	24.7	31.7	20.4	(volume %)
Specific Surface	369.7	551.0	405.3	(in^2/in^3)
Powers Spacing Factor	0.008	0.008	0.008	(in.)
Paste-Air Ratio	3.1	4.4	3.1	
Traverse Length	105.4	99.6	99.2	(in.)
Area Traversed	15.0	7.1	7.1	($in.^2$)

1. ASTM C 457-82a
2. Section through center of the 3 x 6 in. cylinder
3. Transverse section at cylinder top (top surface polished)
4. Transverse section at cylinder mid-height

APPENDIX C

Edge effect correction of 480 lines/frame lineal image analysis data

Table C.1 Analysis of mix 1, magnification 12x, lineal data using 85 classes of 29.41 μm width

			MEASURED		TRUE[1]	
CLASS	LIMITS (μm)		CHORDS	N_L (#/cm)	N_L (#/cm)	CHORDS
1	0	29.41	8636	0.1406	0.1344	8255
2	29.41	58.82	12923	0.2104	0.2065	12683
3	58.82	88.23	6139	0.0999	0.0969	5955
4	88.23	117.64	4707	0.0766	0.0744	4569
5	117.64	147.05	2776	0.0452	0.0431	2650
6	147.05	176.46	2143	0.0349	0.0331	2032
7	176.46	205.87	1889	0.0308	0.0292	1795
8	205.87	235.28	1713	0.0279	0.0266	1635
9	235.28	264.69	1537	0.0250	0.0240	1472
10	264.69	294.10	1278	0.0208	0.0199	1220
11	294.10	323.51	1077	0.0175	0.0167	1025
12	323.51	352.92	960	0.0156	0.0149	914
13	352.92	382.33	832	0.0135	0.0129	790
14	382.33	411.74	713	0.0116	0.0110	674
15	411.74	441.15	665	0.0108	0.0103	631
16	441.15	470.56	637	0.0104	0.0099	609
17	470.56	499.97	536	0.0087	0.0083	509
18	499.97	529.38	487	0.0079	0.0075	462
19	529.38	558.79	477	0.0078	0.0074	457
20	558.79	588.20	440	0.0072	0.0069	423
21	588.20	617.61	454	0.0074	0.0072	443
22	617.61	647.02	409	0.0067	0.0065	400
23	647.02	676.43	333	0.0054	0.0052	321
24	676.43	705.84	266	0.0043	0.0041	251
25	705.84	735.25	228	0.0037	0.0035	212
26	735.25	764.66	172	0.0028	0.0025	153
27	764.66	794.07	196	0.0032	0.0030	182
28	794.07	823.48	193	0.0031	0.0029	181
29	823.48	852.89	210	0.0034	0.0033	202
30	852.89	882.30	253	0.0041	0.0041	254
31	882.30	911.71	208	0.0034	0.0034	206
32	911.71	941.12	152	0.0025	0.0024	145
33	941.12	970.53	148	0.0024	0.0023	142
34	970.53	999.94	156	0.0025	0.0025	153
35	999.94	1029.35	153	0.0025	0.0025	152
36	1029.35	1058.76	158	0.0026	0.0026	160
37	1058.76	1088.17	111	0.0018	0.0017	107
38	1088.17	1117.58	114	0.0019	0.0018	112
39	1117.58	1146.99	117	0.0019	0.0019	117
40	1146.99	1176.40	113	0.0018	0.0018	114
41	1176.40	1205.81	117	0.0019	0.0020	120
42	1205.81	1235.22	135	0.0022	0.0023	143
43	1235.22	1264.63	136	0.0022	0.0024	146
44	1264.63	1294.04	108	0.0018	0.0019	115
45	1294.04	1323.45	97	0.0016	0.0017	103
46	1323.45	1352.86	75	0.0012	0.0013	78
47	1352.86	1382.27	57	0.0009	0.0009	57
48	1382.27	1411.68	37	0.0006	0.0005	33
49	1411.68	1441.09	25	0.0004	0.0003	18
50	1441.09	1470.50	27	0.0004	0.0003	21

Table C.1 continued

			MEASURED		TRUE[1]	
CLASS	LIMITS (μm)		CHORDS	N_L (#/cm)	N_L (#/cm)	CHORDS
51	1470.50	1499.91	35	0.0006	0.0005	31
52	1499.91	1529.32	30	0.0005	0.0004	26
53	1529.32	1558.73	40	0.0007	0.0006	39
54	1558.73	1588.14	45	0.0007	0.0007	45
55	1588.14	1617.55	55	0.0009	0.0010	59
56	1617.55	1646.96	37	0.0006	0.0006	37
57	1646.96	1676.37	37	0.0006	0.0006	37
58	1676.37	1705.78	52	0.0008	0.0009	57
59	1705.78	1735.19	32	0.0005	0.0005	32
60	1735.19	1764.60	28	0.0005	0.0004	27
61	1764.60	1794.01	37	0.0006	0.0006	40
62	1794.01	1823.42	33	0.0005	0.0006	35
63	1823.42	1852.83	45	0.0007	0.0008	51
64	1852.83	1882.24	48	0.0008	0.0009	56
65	1882.24	1911.65	44	0.0007	0.0008	52
66	1911.65	1941.06	27	0.0004	0.0005	30
67	1941.06	1970.47	45	0.0007	0.0009	55
68	1970.47	1999.88	43	0.0007	0.0009	53
69	1999.88	2029.29	36	0.0006	0.0007	44
70	2029.29	2058.70	26	0.0004	0.0005	31
71	2058.70	2088.11	22	0.0004	0.0004	26
72	2088.11	2117.52	28	0.0005	0.0006	35
73	2117.52	2146.93	26	0.0004	0.0005	32
74	2146.93	2176.34	27	0.0004	0.0006	34
75	2176.34	2205.75	25	0.0004	0.0005	32
76	2205.75	2235.16	27	0.0004	0.0006	35
77	2235.16	2264.57	23	0.0004	0.0005	30
78	2264.57	2293.98	24	0.0004	0.0005	32
79	2293.98	2323.39	25	0.0004	0.0006	34
80	2323.39	2352.80	23	0.0004	0.0005	32
81	2352.80	2382.21	16	0.0003	0.0004	22
82	2382.21	2411.62	23	0.0004	0.0005	33
83	2411.62	2441.03	15	0.0002	0.0004	22
84	2441.03	2470.44	15	0.0002	0.0004	22
85	2470.44	2499.85	12	0.0002	0.0003	18
Totals			56629	0.921	0.893	54873
Average Chord Length (μm)				233.2	240.7	
Air Content (%)				2.15	2.15	
Powers Spacing Factor (μm)				407	420	

1. Calculated using Eq. 3.14

Table C.2 Analysis of mix 2, magnification 12x, lineal data using 85 classes of 29.41 μm width

			MEASURED		TRUE[1]	
CLASS	LIMITS (μm)		CHORDS	N_L (#/cm)	N_L (#/cm)	CHORDS
1	0.00	29.41	7636	0.1242	0.1184	7275
2	29.41	58.82	12932	0.2104	0.2068	12709
3	58.82	88.23	5889	0.0958	0.0931	5719
4	88.23	117.64	4007	0.0652	0.0630	3872
5	117.64	147.05	2670	0.0434	0.0415	2552
6	147.05	176.46	2043	0.0332	0.0316	1939
7	176.46	205.87	1558	0.0253	0.0238	1463
8	205.87	235.28	1490	0.0242	0.0230	1411
9	235.28	264.69	1337	0.0218	0.0206	1269
10	264.69	294.10	1118	0.0182	0.0172	1056
11	294.10	323.51	957	0.0156	0.0146	900
12	323.51	352.92	860	0.0140	0.0132	809
13	352.92	382.33	732	0.0119	0.0111	684
14	382.33	411.74	713	0.0116	0.0109	673
15	411.74	441.15	665	0.0108	0.0103	630
16	441.15	470.56	637	0.0104	0.0099	608
17	470.56	499.97	536	0.0087	0.0083	507
18	499.97	529.38	487	0.0079	0.0075	461
19	529.38	558.79	477	0.0078	0.0074	456
20	558.79	588.20	440	0.0072	0.0069	421
21	588.20	617.61	454	0.0074	0.0072	442
22	617.61	647.02	409	0.0067	0.0065	398
23	647.02	676.43	333	0.0054	0.0052	320
24	676.43	705.84	266	0.0043	0.0041	250
25	705.84	735.25	228	0.0037	0.0034	211
26	735.25	764.66	172	0.0028	0.0025	151
27	764.66	794.07	196	0.0032	0.0029	180
28	794.07	823.48	193	0.0031	0.0029	179
29	823.48	852.89	210	0.0034	0.0033	201
30	852.89	882.30	253	0.0041	0.0041	252
31	882.30	911.71	208	0.0034	0.0033	204
32	911.71	941.12	152	0.0025	0.0023	143
33	941.12	970.53	148	0.0024	0.0023	140
34	970.53	999.94	156	0.0025	0.0025	151
35	999.94	1029.35	153	0.0025	0.0024	150
36	1029.35	1058.76	158	0.0026	0.0026	158
37	1058.76	1088.17	111	0.0018	0.0017	105
38	1088.17	1117.58	114	0.0019	0.0018	110
39	1117.58	1146.99	117	0.0019	0.0019	115
40	1146.99	1176.40	113	0.0018	0.0018	112
41	1176.40	1205.81	117	0.0019	0.0019	118
42	1205.81	1235.22	135	0.0022	0.0023	141
43	1235.22	1264.63	136	0.0022	0.0024	145
44	1264.63	1294.04	108	0.0018	0.0018	113
45	1294.04	1323.45	97	0.0016	0.0016	101
46	1323.45	1352.86	75	0.0012	0.0012	76
47	1352.86	1382.27	57	0.0009	0.0009	55
48	1382.27	1411.68	37	0.0006	0.0005	31
49	1411.68	1441.09	25	0.0004	0.0003	16
50	1441.09	1470.50	27	0.0004	0.0003	19

Table C.2 continued

			MEASURED		TRUE[1]	
CLASS	LIMITS (μm)		CHORDS	N_L (#/cm)	N_L (#/cm)	CHORDS
51	1470.50	1499.91	35	0.0006	0.0005	29
52	1499.91	1529.32	30	0.0005	0.0004	23
53	1529.32	1558.73	40	0.0007	0.0006	36
54	1558.73	1588.14	45	0.0007	0.0007	43
55	1588.14	1617.55	55	0.0009	0.0009	57
56	1617.55	1646.96	37	0.0006	0.0006	34
57	1646.96	1676.37	37	0.0006	0.0006	35
58	1676.37	1705.78	52	0.0008	0.0009	55
59	1705.78	1735.19	32	0.0005	0.0005	30
60	1735.19	1764.60	28	0.0005	0.0004	25
61	1764.60	1794.01	37	0.0006	0.0006	37
62	1794.01	1823.42	33	0.0005	0.0005	32
63	1823.42	1852.83	45	0.0007	0.0008	49
64	1852.83	1882.24	58	0.0009	0.0011	67
65	1882.24	1911.65	54	0.0009	0.0010	63
66	1911.65	1941.06	27	0.0004	0.0004	27
67	1941.06	1970.47	45	0.0007	0.0008	52
68	1970.47	1999.88	63	0.0010	0.0013	78
69	1999.88	2029.29	36	0.0006	0.0007	42
70	2029.29	2058.70	38	0.0006	0.0007	45
71	2058.70	2088.11	22	0.0004	0.0004	24
72	2088.11	2117.52	28	0.0005	0.0005	32
73	2117.52	2146.93	26	0.0004	0.0005	30
74	2146.93	2176.34	49	0.0008	0.0010	63
75	2176.34	2205.75	25	0.0004	0.0005	30
76	2205.75	2235.16	27	0.0004	0.0005	34
77	2235.16	2264.57	37	0.0006	0.0008	48
78	2264.57	2293.98	24	0.0004	0.0005	30
79	2293.98	2323.39	36	0.0006	0.0008	48
80	2323.39	2352.80	38	0.0006	0.0008	52
81	2352.80	2382.21	36	0.0006	0.0008	50
82	2382.21	2411.62	43	0.0007	0.0010	61
83	2411.62	2441.03	25	0.0004	0.0006	36
84	2441.03	2470.44	36	0.0006	0.0009	53
85	2470.44	2499.85	24	0.0004	0.0006	36
Totals			53445	0.870	8.841	51691
Average Chord Length (μm)				247.1	255.4	
Air Content (%)				2.15	2.15	
Powers Spacing Factor (μm)				426	441	

1. Calculated using Eq. 3.14

Table C.3 Analysis of mix 3, magnification 12x, lineal data using 85 classes of 29.41 μm width

			MEASURED		TRUE[1]	
CLASS	LIMITS (μm)		CHORDS	N_L (#/cm)	N_L (#/cm)	CHORDS
1	0	29.41	32686	0.6031	0.5798	31425
2	29.41	58.82	34613	0.6386	0.6226	33743
3	58.82	88.23	31138	0.5745	0.5650	30621
4	88.23	117.64	22341	0.4122	0.4065	22032
5	117.64	147.05	15540	0.2867	0.2831	15345
6	147.05	176.46	11126	0.2053	0.2030	11001
7	176.46	205.87	7798	0.1439	0.1422	7705
8	205.87	235.28	5938	0.1096	0.1084	5875
9	235.28	264.69	4500	0.0830	0.0822	4453
10	264.69	294.1	3319	0.0612	0.0604	3276
11	294.1	323.51	2810	0.0518	0.0513	2783
12	323.51	352.92	2149	0.0396	0.0392	2122
13	352.92	382.33	1744	0.0322	0.0318	1721
14	382.33	411.74	1435	0.0265	0.0261	1415
15	411.74	441.15	1197	0.0221	0.0218	1179
16	441.15	470.56	1004	0.0185	0.0182	988
17	470.56	499.97	785	0.0145	0.0141	765
18	499.97	529.38	772	0.0142	0.0140	761
19	529.38	558.79	586	0.0108	0.0105	569
20	558.79	588.2	514	0.0095	0.0092	498
21	588.2	617.61	468	0.0086	0.0084	454
22	617.61	647.02	417	0.0077	0.0075	404
23	647.02	676.43	393	0.0073	0.0071	383
24	676.43	705.84	370	0.0068	0.0067	362
25	705.84	735.25	370	0.0068	0.0068	367
26	735.25	764.66	344	0.0063	0.0063	343
27	764.66	794.07	359	0.0066	0.0067	364
28	794.07	823.48	286	0.0053	0.0053	287
29	823.48	852.89	254	0.0047	0.0047	255
30	852.89	882.3	183	0.0034	0.0033	177
31	882.3	911.71	215	0.0040	0.0040	216
32	911.71	941.12	188	0.0035	0.0035	188
33	941.12	970.53	173	0.0032	0.0032	173
34	970.53	999.94	163	0.0030	0.0030	164
35	999.94	1029.35	89	0.0016	0.0015	81
36	1029.35	1058.76	80	0.0015	0.0013	71
37	1058.76	1088.17	130	0.0024	0.0024	131
38	1088.17	1117.58	112	0.0021	0.0021	111
39	1117.58	1146.99	81	0.0015	0.0014	76
40	1146.99	1176.4	91	0.0017	0.0016	89
41	1176.4	1205.81	87	0.0016	0.0016	86
42	1205.81	1235.22	97	0.0018	0.0018	99
43	1235.22	1264.63	90	0.0017	0.0017	92
44	1264.63	1294.04	99	0.0018	0.0019	104
45	1294.04	1323.45	86	0.0016	0.0017	90
46	1323.45	1352.86	58	0.0011	0.0010	57
47	1352.86	1382.27	70	0.0013	0.0013	72
48	1382.27	1411.68	76	0.0014	0.0015	81
49	1411.68	1441.09	101	0.0019	0.0021	113
50	1441.09	1470.5	68	0.0013	0.0014	73

Table C.3 continued

			MEASURED		TRUE[1]	
CLASS	LIMITS (μm)		CHORDS	N_L (#/cm)	N_L (#/cm)	CHORDS
51	1470.50	1499.91	55	0.0010	0.0011	58
52	1499.91	1529.32	47	0.0009	0.0009	49
53	1529.32	1558.73	65	0.0012	0.0013	72
54	1558.73	1588.14	44	0.0008	0.0009	47
55	1588.14	1617.55	43	0.0008	0.0009	46
56	1617.55	1646.96	37	0.0007	0.0007	39
57	1646.96	1676.37	41	0.0008	0.0008	45
58	1676.37	1705.78	42	0.0008	0.0009	47
59	1705.78	1735.19	93	0.0017	0.0021	114
60	1735.19	1764.60	47	0.0009	0.0010	56
61	1764.60	1794.01	20	0.0004	0.0004	21
62	1794.01	1823.42	16	0.0003	0.0003	16
63	1823.42	1852.83	9	0.0002	0.0001	7
64	1852.83	1882.24	8	0.0001	0.0001	6
65	1882.24	1911.65	13	0.0002	0.0002	13
66	1911.65	1941.06	13	0.0002	0.0002	13
67	1941.06	1970.47	14	0.0003	0.0003	14
68	1970.47	1999.88	23	0.0004	0.0005	27
69	1999.88	2029.29	16	0.0003	0.0003	18
70	2029.29	2058.70	17	0.0003	0.0004	19
71	2058.70	2088.11	11	0.0002	0.0002	11
72	2088.11	2117.52	17	0.0003	0.0004	20
73	2117.52	2146.93	14	0.0003	0.0003	16
74	2146.93	2176.34	12	0.0002	0.0002	13
75	2176.34	2205.75	34	0.0006	0.0008	45
76	2205.75	2235.16	25	0.0005	0.0006	33
77	2235.16	2264.57	14	0.0003	0.0003	18
78	2264.57	2293.98	16	0.0003	0.0004	21
79	2293.98	2323.39	19	0.0004	0.0005	25
80	2323.39	2352.80	21	0.0004	0.0005	29
81	2352.80	2382.21	27	0.0005	0.0007	38
82	2382.21	2411.62	22	0.0004	0.0006	31
83	2411.62	2441.03	18	0.0003	0.0005	26
84	2441.03	2470.44	8	0.0001	0.0002	12
85	2470.44	2499.85	17	0.0003	0.0005	25
Totals			188531	3.478	3.412	184929
Average Chord Length (μm)				143.8	146.6	
Air Content (%)				5.00	5.00	
Powers Spacing Factor (μm)				162	165	

1. Calculated using Eq. 3.14

Table C.4 Analysis of mix 4, magnification 12x, lineal data using 85 classes of 29.41 μm width

			MEASURED		TRUE[1]	
CLASS	LIMITS (μm)		CHORDS	N_L (#/cm)	N_L (#/cm)	CHORDS
1	0.00	29.41	28465	0.4631	0.4253	26141
2	29.41	58.82	91004	1.4807	1.4580	89606
3	58.82	88.23	66440	1.0810	1.0701	65767
4	88.23	117.64	47039	0.7654	0.7615	46803
5	117.64	147.05	25945	0.4221	0.4199	25806
6	147.05	176.46	15955	0.2596	0.2582	15866
7	176.46	205.87	10616	0.1727	0.1718	10558
8	205.87	235.28	7121	0.1159	0.1150	7071
9	235.28	264.69	5427	0.0883	0.0878	5398
10	264.69	294.10	3864	0.0629	0.0624	3834
11	294.10	323.51	2928	0.0476	0.0472	2901
12	323.51	352.92	2338	0.0380	0.0377	2316
13	352.92	382.33	1963	0.0319	0.0317	1949
14	382.33	411.74	1628	0.0265	0.0263	1618
15	411.74	441.15	1170	0.0190	0.0187	1151
16	441.15	470.56	1130	0.0184	0.0183	1122
17	470.56	499.97	913	0.0149	0.0147	904
18	499.97	529.38	839	0.0137	0.0136	835
19	529.38	558.79	728	0.0118	0.0118	726
20	558.79	588.20	645	0.0105	0.0105	645
21	588.20	617.61	609	0.0099	0.0100	614
22	617.61	647.02	424	0.0069	0.0068	419
23	647.02	676.43	413	0.0067	0.0067	412
24	676.43	705.84	298	0.0048	0.0047	290
25	705.84	735.25	298	0.0048	0.0048	294
26	735.25	764.66	226	0.0037	0.0035	217
27	764.66	794.07	159	0.0026	0.0024	145
28	794.07	823.48	174	0.0028	0.0027	164
29	823.48	852.89	149	0.0024	0.0022	138
30	852.89	882.30	190	0.0031	0.0030	186
31	882.30	911.71	181	0.0029	0.0029	179
32	911.71	941.12	141	0.0023	0.0022	135
33	941.12	970.53	129	0.0021	0.0020	123
34	970.53	999.94	110	0.0018	0.0017	103
35	999.94	1029.35	137	0.0022	0.0022	136
36	1029.35	1058.76	136	0.0022	0.0022	136
37	1058.76	1088.17	122	0.0020	0.0020	122
38	1088.17	1117.58	120	0.0020	0.0020	121
39	1117.58	1146.99	95	0.0015	0.0015	93
40	1146.99	1176.40	41	0.0007	0.0005	30
41	1176.40	1205.81	46	0.0007	0.0006	37
42	1205.81	1235.22	46	0.0007	0.0006	37
43	1235.22	1264.63	51	0.0008	0.0007	44
44	1264.63	1294.04	34	0.0006	0.0004	24
45	1294.04	1323.45	46	0.0007	0.0006	39
46	1323.45	1352.86	30	0.0005	0.0003	20
47	1352.86	1382.27	29	0.0005	0.0003	19
48	1382.27	1411.68	34	0.0006	0.0004	25
49	1411.68	1441.09	25	0.0004	0.0002	14
50	1441.09	1470.50	42	0.0007	0.0006	36

Table C.4 continued

			MEASURED		TRUE[1]	
CLASS	LIMITS (μm)		CHORDS	N_L (#/cm)	N_L (#/cm)	CHORDS
51	1470.50	1499.91	28	0.0005	0.0003	19
52	1499.91	1529.32	22	0.0004	0.0002	12
53	1529.32	1558.73	36	0.0006	0.0005	29
54	1558.73	1588.14	44	0.0007	0.0007	40
55	1588.14	1617.55	29	0.0005	0.0003	22
56	1617.55	1646.96	32	0.0005	0.0004	26
57	1646.96	1676.37	29	0.0005	0.0004	22
58	1676.37	1705.78	38	0.0006	0.0006	34
59	1705.78	1735.19	42	0.0007	0.0006	40
60	1735.19	1764.60	54	0.0009	0.0009	56
61	1764.60	1794.01	44	0.0007	0.0007	44
62	1794.01	1823.42	68	0.0011	0.0012	76
63	1823.42	1852.83	45	0.0007	0.0008	47
64	1852.83	1882.24	43	0.0007	0.0007	45
65	1882.24	1911.65	64	0.0010	0.0012	74
66	1911.65	1941.06	48	0.0008	0.0009	54
67	1941.06	1970.47	33	0.0005	0.0006	34
68	1970.47	1999.88	43	0.0007	0.0008	48
69	1999.88	2029.29	49	0.0008	0.0009	57
70	2029.29	2058.70	68	0.0011	0.0014	84
71	2058.70	2088.11	60	0.0010	0.0012	75
72	2088.11	2117.52	45	0.0007	0.0009	55
73	2117.52	2146.93	25	0.0004	0.0005	28
74	2146.93	2176.34	43	0.0007	0.0009	54
75	2176.34	2205.75	29	0.0005	0.0006	35
76	2205.75	2235.16	44	0.0007	0.0009	57
77	2235.16	2264.57	35	0.0006	0.0007	45
78	2264.57	2293.98	16	0.0003	0.0003	18
79	2293.98	2323.39	22	0.0004	0.0004	27
80	2323.39	2352.80	48	0.0008	0.0011	65
81	2352.80	2382.21	43	0.0007	0.0010	59
82	2382.21	2411.62	47	0.0008	0.0011	66
83	2411.62	2441.03	34	0.0006	0.0008	48
84	2441.03	2470.44	54	0.0009	0.0013	79
85	2470.44	2499.85	55	0.0009	0.0013	82
Totals			322152	5.242	5.158	317021
Average Chord Length (μm)				119.9	121.8	
Air Content (%)				6.28	6.28	
Powers Spacing Factor (μm)				103	105	

1. Calculated using Eq. 3.14

Table C.5 Analysis of mix 5, magnification 12x, lineal data using 85 classes of 29.41 μm width

			MEASURED		TRUE[1]	
CLASS	LIMITS (μm)		CHORDS	N_L (#/cm)	N_L (#/cm)	CHORDS
1	0.00	29.41	22104	0.3596	0.3315	20371
2	29.41	58.82	66104	1.0756	1.0587	65068
3	58.82	88.23	48202	0.7843	0.7758	47682
4	88.23	117.64	35971	0.5853	0.5824	35795
5	117.64	147.05	20848	0.3392	0.3378	20761
6	147.05	176.46	12690	0.2065	0.2056	12636
7	176.46	205.87	8239	0.1341	0.1334	8201
8	205.87	235.28	5508	0.0896	0.0891	5474
9	235.28	264.69	3811	0.0620	0.0615	3778
10	264.69	294.10	2988	0.0486	0.0482	2965
11	294.10	323.51	2245	0.0365	0.0362	2223
12	323.51	352.92	1784	0.0290	0.0287	1766
13	352.92	382.33	1439	0.0234	0.0232	1423
14	382.33	411.74	1286	0.0209	0.0208	1279
15	411.74	441.15	1018	0.0166	0.0164	1009
16	441.15	470.56	798	0.0130	0.0128	787
17	470.56	499.97	637	0.0104	0.0101	624
18	499.97	529.38	578	0.0094	0.0092	568
19	529.38	558.79	541	0.0088	0.0087	535
20	558.79	588.20	426	0.0069	0.0068	417
21	588.20	617.61	323	0.0053	0.0050	310
22	617.61	647.02	361	0.0059	0.0058	355
23	647.02	676.43	361	0.0059	0.0059	360
24	676.43	705.84	315	0.0051	0.0051	314
25	705.84	735.25	248	0.0040	0.0040	243
26	735.25	764.66	276	0.0045	0.0045	278
27	764.66	794.07	255	0.0041	0.0042	258
28	794.07	823.48	171	0.0028	0.0027	167
29	823.48	852.89	189	0.0031	0.0031	189
30	852.89	882.30	175	0.0028	0.0029	176
31	882.30	911.71	187	0.0030	0.0031	192
32	911.71	941.12	185	0.0030	0.0031	192
33	941.12	970.53	102	0.0017	0.0016	99
34	970.53	999.94	127	0.0021	0.0021	129
35	999.94	1029.35	105	0.0017	0.0017	106
36	1029.35	1058.76	96	0.0016	0.0016	97
37	1058.76	1088.17	106	0.0017	0.0018	110
38	1088.17	1117.58	101	0.0016	0.0017	105
39	1117.58	1146.99	105	0.0017	0.0018	111
40	1146.99	1176.40	71	0.0012	0.0012	73
41	1176.40	1205.81	69	0.0011	0.0012	71
42	1205.81	1235.22	57	0.0009	0.0009	58
43	1235.22	1264.63	62	0.0010	0.0011	65
44	1264.63	1294.04	48	0.0008	0.0008	49
45	1294.04	1323.45	31	0.0005	0.0005	29
46	1323.45	1352.86	42	0.0007	0.0007	42
47	1352.86	1382.27	53	0.0009	0.0009	57
48	1382.27	1411.68	30	0.0005	0.0005	29
49	1411.68	1441.09	41	0.0007	0.0007	43
50	1441.09	1470.50	49	0.0008	0.0009	54

Table C.5 continued

			MEASURED		TRUE[1]	
CLASS	LIMITS (μm)		CHORDS	N_L (#/cm)	N_L (#/cm)	CHORDS
51	1470.50	1499.91	51	0.0008	0.0009	57
52	1499.91	1529.32	22	0.0004	0.0003	21
53	1529.32	1558.73	23	0.0004	0.0004	23
54	1558.73	1588.14	35	0.0006	0.0006	38
55	1588.14	1617.55	47	0.0008	0.0009	54
56	1617.55	1646.96	23	0.0004	0.0004	24
57	1646.96	1676.37	31	0.0005	0.0006	35
58	1676.37	1705.78	33	0.0005	0.0006	38
59	1705.78	1735.19	32	0.0005	0.0006	37
60	1735.19	1764.60	24	0.0004	0.0004	28
61	1764.60	1794.01	2	0.0000	0.0000	-1
62	1794.01	1823.42	3	0.0000	0.0000	0
63	1823.42	1852.83	3	0.0000	0.0000	0
64	1852.83	1882.24	10	0.0002	0.0002	10
65	1882.24	1911.65	14	0.0002	0.0002	15
66	1911.65	1941.06	23	0.0004	0.0004	28
67	1941.06	1970.47	16	0.0003	0.0003	19
68	1970.47	1999.88	11	0.0002	0.0002	12
69	1999.88	2029.29	22	0.0004	0.0004	27
70	2029.29	2058.70	20	0.0003	0.0004	25
71	2058.70	2088.11	17	0.0003	0.0003	21
72	2088.11	2117.52	7	0.0001	0.0001	8
73	2117.52	2146.93	6	0.0001	0.0001	6
74	2146.93	2176.34	6	0.0001	0.0001	6
75	2176.34	2205.75	13	0.0002	0.0003	17
76	2205.75	2235.16	11	0.0002	0.0002	14
77	2235.16	2264.57	8	0.0001	0.0002	10
78	2264.57	2293.98	5	0.0001	0.0001	6
79	2293.98	2323.39	15	0.0002	0.0003	20
80	2323.39	2352.80	16	0.0003	0.0004	22
81	2352.80	2382.21	16	0.0003	0.0004	22
82	2382.21	2411.62	8	0.0001	0.0002	11
83	2411.62	2441.03	9	0.0001	0.0002	13
84	2441.03	2470.44	18	0.0003	0.0004	26
85	2470.44	2499.85	9	0.0001	0.0002	13
Totals			242167	3.940	3.877	238310
Average Chord Length (μm)				119.9	121.8	
Air Content (%)				4.72	4.72	
Powers Spacing Factor (μm)				142	144	

1. Calculated using Eq. 3.14

Table C.6 Analysis of mix 6, magnification 12x, lineal data using 85 classes of 29.41 μm

			MEASURED		TRUE[1]	
CLASS	LIMITS (μm)		CHORDS	N_L (#/cm)	N_L (#/cm)	CHORDS
1	0	29.41	56913	0.9265	0.9001	55292
2	29.41	58.82	60465	0.9843	0.9691	59534
3	58.82	88.23	46731	0.7607	0.7540	46317
4	88.23	117.64	27802	0.4526	0.4493	27602
5	117.64	147.05	15903	0.2589	0.2568	15773
6	147.05	176.46	10025	0.1632	0.1617	9931
7	176.46	205.87	6666	0.1085	0.1073	6591
8	205.87	235.28	4705	0.0766	0.0756	4642
9	235.28	264.69	3519	0.0573	0.0564	3467
10	264.69	294.10	2594	0.0422	0.0414	2545
11	294.10	323.51	2264	0.0369	0.0363	2230
12	323.51	352.92	1833	0.0298	0.0294	1805
13	352.92	382.33	1474	0.0240	0.0236	1448
14	382.33	411.74	1271	0.0207	0.0204	1251
15	411.74	441.15	1090	0.0177	0.0175	1074
16	441.15	470.56	947	0.0154	0.0152	935
17	470.56	499.97	905	0.0147	0.0147	901
18	499.97	529.38	768	0.0125	0.0125	765
19	529.38	558.79	661	0.0108	0.0107	659
20	558.79	588.20	528	0.0086	0.0085	523
21	588.20	617.61	528	0.0086	0.0086	529
22	617.61	647.02	472	0.0077	0.0077	475
23	647.02	676.43	390	0.0063	0.0064	391
24	676.43	705.84	326	0.0053	0.0053	325
25	705.84	735.25	314	0.0051	0.0051	316
26	735.25	764.66	297	0.0048	0.0049	301
27	764.66	794.07	218	0.0035	0.0035	216
28	794.07	823.48	246	0.0040	0.0041	251
29	823.48	852.89	252	0.0041	0.0042	261
30	852.89	882.30	195	0.0032	0.0032	200
31	882.30	911.71	170	0.0028	0.0028	174
32	911.71	941.12	127	0.0021	0.0021	127
33	941.12	970.53	109	0.0018	0.0018	108
34	970.53	999.94	121	0.0020	0.0020	123
35	999.94	1029.35	84	0.0014	0.0013	82
36	1029.35	1058.76	122	0.0020	0.0021	127
37	1058.76	1088.17	78	0.0013	0.0013	77
38	1088.17	1117.58	94	0.0015	0.0016	97
39	1117.58	1146.99	102	0.0017	0.0018	108
40	1146.99	1176.40	65	0.0011	0.0011	66
41	1176.40	1205.81	89	0.0014	0.0016	95
42	1205.81	1235.22	71	0.0012	0.0012	75
43	1235.22	1264.63	57	0.0009	0.0010	59
44	1264.63	1294.04	65	0.0011	0.0011	70
45	1294.04	1323.45	42	0.0007	0.0007	43
46	1323.45	1352.86	55	0.0009	0.0010	59
47	1352.86	1382.27	38	0.0006	0.0006	39
48	1382.27	1411.68	32	0.0005	0.0005	32
49	1411.68	1441.09	46	0.0007	0.0008	50
50	1441.09	1470.50	37	0.0006	0.0006	40

Table C.6 continued

CLASS	LIMITS (μm)		MEASURED CHORDS	MEASURED N_L (#/cm)	TRUE[1] N_L (#/cm)	TRUE[1] CHORDS
51	1470.50	1499.91	25	0.0004	0.0004	25
52	1499.91	1529.32	32	0.0005	0.0006	35
53	1529.32	1558.73	73	0.0012	0.0014	87
54	1558.73	1588.14	74	0.0012	0.0015	89
55	1588.14	1617.55	72	0.0012	0.0014	88
56	1617.55	1646.96	28	0.0005	0.0005	33
57	1646.96	1676.37	24	0.0004	0.0005	28
58	1676.37	1705.78	17	0.0003	0.0003	20
59	1705.78	1735.19	15	0.0002	0.0003	17
60	1735.19	1764.60	9	0.0001	0.0002	10
61	1764.60	1794.01	11	0.0002	0.0002	13
62	1794.01	1823.42	4	0.0001	0.0001	4
63	1823.42	1852.83	1	0.0000	0.0000	0
64	1852.83	1882.24	4	0.0001	0.0001	4
65	1882.24	1911.65	8	0.0001	0.0001	9
66	1911.65	1941.06	3	0.0000	0.0000	2
67	1941.06	1970.47	4	0.0001	0.0001	4
68	1970.47	1999.88	5	0.0001	0.0001	5
69	1999.88	2029.29	1	0.0000	0.0000	0
70	2029.29	2058.70	1	0.0000	0.0000	0
71	2058.70	2088.11	4	0.0001	0.0001	4
72	2088.11	2117.52	14	0.0002	0.0003	18
73	2117.52	2146.93	19	0.0003	0.0004	25
74	2146.93	2176.34	8	0.0001	0.0002	10
75	2176.34	2205.75	3	0.0000	0.0001	3
76	2205.75	2235.16	9	0.0001	0.0002	12
77	2235.16	2264.57	13	0.0002	0.0003	18
78	2264.57	2293.98	6	0.0001	0.0001	8
79	2293.98	2323.39	5	0.0001	0.0001	7
80	2323.39	2352.80	4	0.0001	0.0001	5
81	2352.80	2382.21	6	0.0001	0.0001	9
82	2382.21	2411.62	1	0.0000	0.0000	1
83	2411.62	2441.03	1	0.0000	0.0000	1
84	2441.03	2470.44	6	0.0001	0.0001	9
85	2470.44	2499.85	4	0.0001	0.0001	6
Totals			252420	4.109	4.050	248810
Average Chord Length (μm)				107.7	109.2	
Air Content (%)				4.42	4.42	
Powers Spacing Factor (μm)				119	120	

1. Calculated using Eq. 3.14

Table C.7 Analysis of mix 7, magnification 12x, lineal data using 85 classes of 29.41 μm width

			MEASURED		TRUE[1]	
CLASS	LIMITS (μm)		CHORDS	N_L (#/cm)	N_L (#/cm)	CHORDS
1	0.00	29.41	27747	0.4517	0.1736	10663
2	29.41	58.82	24630	0.4009	0.4544	27913
3	58.82	88.23	23331	0.3798	0.3528	21670
4	88.23	117.64	21149	0.3443	0.3624	22265
5	117.64	147.05	17946	0.2921	0.3109	19100
6	147.05	176.46	15234	0.2480	0.2629	16152
7	176.46	205.87	12657	0.2060	0.2220	13638
8	205.87	235.28	10009	0.1629	0.1846	11343
9	235.28	264.69	8134	0.1324	0.1450	8906
10	264.69	294.10	6223	0.1013	0.1132	6956
11	294.10	323.51	5232	0.0852	0.0924	5677
12	323.51	352.92	4243	0.0691	0.0766	4704
13	352.92	382.33	3455	0.0562	0.0629	3863
14	382.33	411.74	2665	0.0434	0.0488	3000
15	411.74	441.15	2176	0.0354	0.0392	2405
16	441.15	470.56	1723	0.0280	0.0313	1921
17	470.56	499.97	1468	0.0239	0.0244	1502
18	499.97	529.38	1409	0.0229	0.0238	1464
19	529.38	558.79	1230	0.0200	0.0212	1302
20	558.79	588.20	1056	0.0172	0.0191	1171
21	588.20	617.61	966	0.0157	0.0167	1028
22	617.61	647.02	821	0.0134	0.0147	901
23	647.02	676.43	722	0.0118	0.0129	793
24	676.43	705.84	643	0.0105	0.0110	677
25	705.84	735.25	647	0.0105	0.0106	650
26	735.25	764.66	471	0.0077	0.0096	589
27	764.66	794.07	422	0.0069	0.0073	449
28	794.07	823.48	361	0.0059	0.0060	371
29	823.48	852.89	325	0.0053	0.0060	367
30	852.89	882.30	335	0.0055	0.0055	340
31	882.30	911.71	337	0.0055	0.0055	339
32	911.71	941.12	223	0.0036	0.0052	321
33	941.12	970.53	203	0.0033	0.0032	199
34	970.53	999.94	222	0.0036	0.0032	197
35	999.94	1029.35	154	0.0025	0.0036	222
36	1029.35	1058.76	130	0.0021	0.0024	149
37	1058.76	1088.17	130	0.0021	0.0018	109
38	1088.17	1117.58	99	0.0016	0.0019	114
39	1117.58	1146.99	108	0.0018	0.0019	116
40	1146.99	1176.40	68	0.0011	0.0014	86
41	1176.40	1205.81	98	0.0016	0.0011	70
42	1205.81	1235.22	88	0.0014	0.0016	98
43	1235.22	1264.63	99	0.0016	0.0015	91
44	1264.63	1294.04	95	0.0015	0.0019	119
45	1294.04	1323.45	52	0.0008	0.0010	64
46	1323.45	1352.86	55	0.0009	0.0008	51
47	1352.86	1382.27	39	0.0006	0.0009	54
48	1382.27	1411.68	41	0.0007	0.0004	27
49	1411.68	1441.09	59	0.0010	0.0008	52
50	1441.09	1470.50	44	0.0007	0.0007	45

Table C.7 continued

			MEASURED		TRUE[1]	
CLASS	LIMITS (μm)		CHORDS	N_L (#/cm)	N_L (#/cm)	CHORDS
51	1470.50	1499.91	63	0.0010	0.0010	60
52	1499.91	1529.32	102	0.0017	0.0016	101
53	1529.32	1558.73	46	0.0007	0.0013	82
54	1558.73	1588.14	64	0.0010	0.0009	56
55	1588.14	1617.55	56	0.0009	0.0011	66
56	1617.55	1646.96	39	0.0006	0.0008	52
57	1646.96	1676.37	47	0.0008	0.0008	50
58	1676.37	1705.78	54	0.0009	0.0010	60
59	1705.78	1735.19	56	0.0009	0.0010	63
60	1735.19	1764.60	59	0.0010	0.0007	45
61	1764.60	1794.01	42	0.0007	0.0014	88
62	1794.01	1823.42	33	0.0005	0.0006	39
63	1823.42	1852.83	28	0.0005	0.0006	37
64	1852.83	1882.24	28	0.0005	0.0005	33
65	1882.24	1911.65	36	0.0006	0.0007	40
66	1911.65	1941.06	29	0.0005	0.0008	49
67	1941.06	1970.47	28	0.0005	0.0004	24
68	1970.47	1999.88	23	0.0004	0.0004	26
69	1999.88	2029.29	15	0.0002	0.0005	32
70	2029.29	2058.70	13	0.0002	0.0003	17
71	2058.70	2088.11	15	0.0002	0.0003	16
72	2088.11	2117.52	16	0.0003	0.0004	26
73	2117.52	2146.93	7	0.0001	0.0002	12
74	2146.93	2176.34	5	0.0001	0.0001	4
75	2176.34	2205.75	8	0.0001	0.0001	6
76	2205.75	2235.16	12	0.0002	0.0003	16
77	2235.16	2264.57	7	0.0001	0.0001	9
78	2264.57	2293.98	2	0.0000	0.0001	9
79	2293.98	2323.39	8	0.0001	0.0000	0
80	2323.39	2352.80	9	0.0001	0.0002	15
81	2352.80	2382.21	20	0.0003	0.0004	24
82	2382.21	2411.62	10	0.0002	0.0004	22
83	2411.62	2441.03	6	0.0001	0.0001	9
84	2441.03	2470.44	5	0.0001	0.0001	7
85	2470.44	2499.85	18	0.0003	0.0002	12
Totals			200783	3.268	3.189	195895
Average Chord Length (μm)				183.2	187.8	
Air Content (%)				5.99	5.99	
Powers Spacing Factor (μm)				165	169	

1. Calculated using Eq. 3.14

Table C.8 Analysis of mix 8, magnification 12x, lineal data using 85 classes of 29.41 μm width

			MEASURED		TRUE[1]	
CLASS	LIMITS (μm)		CHORDS	N_L (#/cm)	N_L (#/cm)	CHORDS
1	0	29.41	27429	0.4465	0.4275	26261
2	29.41	58.82	19993	0.3255	0.3103	19063
3	58.82	88.23	18028	0.2935	0.2816	17297
4	88.23	117.64	16878	0.2748	0.2659	16333
5	117.64	147.05	14934	0.2431	0.2367	14542
6	147.05	176.46	12719	0.2070	0.2026	12444
7	176.46	205.87	10772	0.1754	0.1724	10589
8	205.87	235.28	8907	0.1450	0.1431	8788
9	235.28	264.69	7406	0.1206	0.1194	7336
10	264.69	294.10	5756	0.0937	0.0929	5706
11	294.10	323.51	4702	0.0765	0.0761	4672
12	323.51	352.92	4068	0.0662	0.0661	4063
13	352.92	382.33	3187	0.0519	0.0518	3183
14	382.33	411.74	2549	0.0415	0.0415	2547
15	411.74	441.15	2266	0.0369	0.0371	2277
16	441.15	470.56	1940	0.0316	0.0319	1957
17	470.56	499.97	1608	0.0262	0.0265	1625
18	499.97	529.38	1280	0.0208	0.0210	1292
19	529.38	558.79	1044	0.0170	0.0171	1053
20	558.79	588.20	839	0.0137	0.0137	844
21	588.20	617.61	695	0.0113	0.0114	697
22	617.61	647.02	604	0.0098	0.0099	607
23	647.02	676.43	532	0.0087	0.0087	535
24	676.43	705.84	482	0.0078	0.0079	487
25	705.84	735.25	418	0.0068	0.0069	422
26	735.25	764.66	403	0.0066	0.0067	411
27	764.66	794.07	299	0.0049	0.0049	300
28	794.07	823.48	290	0.0047	0.0048	294
29	823.48	852.89	241	0.0039	0.0039	242
30	852.89	882.30	224	0.0036	0.0037	226
31	882.30	911.71	174	0.0028	0.0028	172
32	911.71	941.12	210	0.0034	0.0035	216
33	941.12	970.53	143	0.0023	0.0023	141
34	970.53	999.94	119	0.0019	0.0019	116
35	999.94	1029.35	136	0.0022	0.0022	137
36	1029.35	1058.76	135	0.0022	0.0022	138
37	1058.76	1088.17	162	0.0026	0.0028	171
38	1088.17	1117.58	90	0.0015	0.0014	89
39	1117.58	1146.99	117	0.0019	0.0020	122
40	1146.99	1176.40	71	0.0012	0.0011	69
41	1176.40	1205.81	53	0.0009	0.0008	48
42	1205.81	1235.22	64	0.0010	0.0010	62
43	1235.22	1264.63	73	0.0012	0.0012	74
44	1264.63	1294.04	71	0.0012	0.0012	73
45	1294.04	1323.45	63	0.0010	0.0010	64
46	1323.45	1352.86	63	0.0010	0.0011	65
47	1352.86	1382.27	64	0.0010	0.0011	67
48	1382.27	1411.68	44	0.0007	0.0007	43
49	1411.68	1441.09	60	0.0010	0.0010	64
50	1441.09	1470.50	61	0.0010	0.0011	66

Table C.8 continued

			MEASURED		TRUE[1]	
CLASS	LIMITS (μm)		CHORDS	N_L (#/cm)	N_L (#/cm)	CHORDS
51	1470.50	1499.91	55	0.0009	0.0010	59
52	1499.91	1529.32	63	0.0010	0.0011	70
53	1529.32	1558.73	39	0.0006	0.0007	41
54	1558.73	1588.14	32	0.0005	0.0005	33
55	1588.14	1617.55	34	0.0006	0.0006	36
56	1617.55	1646.96	44	0.0007	0.0008	49
57	1646.96	1676.37	34	0.0006	0.0006	37
58	1676.37	1705.78	49	0.0008	0.0009	57
59	1705.78	1735.19	61	0.0010	0.0012	73
60	1735.19	1764.60	86	0.0014	0.0017	107
61	1764.60	1794.01	21	0.0003	0.0004	23
62	1794.01	1823.42	14	0.0002	0.0002	15
63	1823.42	1852.83	13	0.0002	0.0002	13
64	1852.83	1882.24	17	0.0003	0.0003	19
65	1882.24	1911.65	21	0.0003	0.0004	25
66	1911.65	1941.06	45	0.0007	0.0009	58
67	1941.06	1970.47	15	0.0002	0.0003	18
68	1970.47	1999.88	7	0.0001	0.0001	7
69	1999.88	2029.29	4	0.0001	0.0000	3
70	2029.29	2058.70	5	0.0001	0.0001	4
71	2058.70	2088.11	6	0.0001	0.0001	6
72	2088.11	2117.52	8	0.0001	0.0001	9
73	2117.52	2146.93	10	0.0002	0.0002	12
74	2146.93	2176.34	14	0.0002	0.0003	18
75	2176.34	2205.75	8	0.0001	0.0002	9
76	2205.75	2235.16	11	0.0002	0.0002	14
77	2235.16	2264.57	13	0.0002	0.0003	17
78	2264.57	2293.98	15	0.0002	0.0003	20
79	2293.98	2323.39	9	0.0001	0.0002	12
80	2323.39	2352.80	26	0.0004	0.0006	37
81	2352.80	2382.21	17	0.0003	0.0004	24
82	2382.21	2411.62	19	0.0003	0.0004	28
83	2411.62	2441.03	10	0.0002	0.0002	15
84	2441.03	2470.44	0	0.0000	0.0000	0
85	2470.44	2499.85	2	0.0000	0.0000	3
Totals			173293	2.821	2.752	169061
Average Chord Length (μm)				183.8	188.4	
Air Content (%)				5.19	5.18	
Powers Spacing Factor (μm)				173	177	

1. Calculated using Eq. 3.14

Table C.9 Analysis of mix 9, magnification 12x, lineal data using 85 classes of 29.41 μm width

			MEASURED		TRUE[1]	
CLASS	LIMITS (μm)		CHORDS	N_L (#/cm)	N_L (#/cm)	CHORDS
1	0	29.41	16238	0.2659	0.2487	15186
2	29.41	58.82	16194	0.2652	0.2509	15321
3	58.82	88.23	16754	0.2743	0.2632	16071
4	88.23	117.64	15975	0.2616	0.2533	15470
5	117.64	147.05	14451	0.2366	0.2308	14098
6	147.05	176.46	12522	0.2050	0.2012	12288
7	176.46	205.87	10630	0.1741	0.1717	10488
8	205.87	235.28	8626	0.1412	0.1399	8542
9	235.28	264.69	6885	0.1127	0.1120	6838
10	264.69	294.10	5685	0.0931	0.0928	5670
11	294.10	323.51	4458	0.0730	0.0729	4455
12	323.51	352.92	3502	0.0573	0.0574	3505
13	352.92	382.33	2794	0.0458	0.0459	2801
14	382.33	411.74	2230	0.0365	0.0366	2238
15	411.74	441.15	1820	0.0298	0.0299	1829
16	441.15	470.56	1510	0.0247	0.0249	1521
17	470.56	499.97	1326	0.0217	0.0220	1342
18	499.97	529.38	1103	0.0181	0.0183	1119
19	529.38	558.79	882	0.0144	0.0146	894
20	558.79	588.20	683	0.0112	0.0113	689
21	588.20	617.61	632	0.0103	0.0105	642
22	617.61	647.02	467	0.0076	0.0077	469
23	647.02	676.43	436	0.0071	0.0072	441
24	676.43	705.84	378	0.0062	0.0063	383
25	705.84	735.25	451	0.0074	0.0077	469
26	735.25	764.66	282	0.0046	0.0047	286
27	764.66	794.07	236	0.0039	0.0039	239
28	794.07	823.48	252	0.0041	0.0043	260
29	823.48	852.89	204	0.0033	0.0034	209
30	852.89	882.30	187	0.0031	0.0032	192
31	882.30	911.71	174	0.0028	0.0030	180
32	911.71	941.12	178	0.0029	0.0031	187
33	941.12	970.53	179	0.0029	0.0031	191
34	970.53	999.94	117	0.0019	0.0020	122
35	999.94	1029.35	85	0.0014	0.0014	86
36	1029.35	1058.76	82	0.0013	0.0014	84
37	1058.76	1088.17	82	0.0013	0.0014	85
38	1088.17	1117.58	65	0.0011	0.0011	66
39	1117.58	1146.99	56	0.0009	0.0009	57
40	1146.99	1176.40	45	0.0007	0.0007	44
41	1176.40	1205.81	60	0.0010	0.0010	63
42	1205.81	1235.22	42	0.0007	0.0007	42
43	1235.22	1264.63	15	0.0002	0.0002	10
44	1264.63	1294.04	22	0.0004	0.0003	19
45	1294.04	1323.45	21	0.0003	0.0003	18
46	1323.45	1352.86	20	0.0003	0.0003	17
47	1352.86	1382.27	34	0.0006	0.0006	34
48	1382.27	1411.68	34	0.0006	0.0006	35
49	1411.68	1441.09	18	0.0003	0.0003	16
50	1441.09	1470.50	15	0.0002	0.0002	12

Table C.9 continued

			MEASURED		TRUE[1]	
CLASS	LIMITS (μm)		CHORDS	N_L (#/cm)	N_L (#/cm)	CHORDS
51	1470.50	1499.91	16	0.0003	0.0002	13
52	1499.91	1529.32	19	0.0003	0.0003	17
53	1529.32	1558.73	12	0.0002	0.0001	9
54	1558.73	1588.14	22	0.0004	0.0004	22
55	1588.14	1617.55	17	0.0003	0.0003	16
56	1617.55	1646.96	60	0.0010	0.0012	71
57	1646.96	1676.37	37	0.0006	0.0007	42
58	1676.37	1705.78	44	0.0007	0.0009	52
59	1705.78	1735.19	32	0.0005	0.0006	37
60	1735.19	1764.60	20	0.0003	0.0004	22
61	1764.60	1794.01	9	0.0001	0.0001	8
62	1794.01	1823.42	7	0.0001	0.0001	6
63	1823.42	1852.83	2	0.0000	0.0000	-1
64	1852.83	1882.24	10	0.0002	0.0002	10
65	1882.24	1911.65	12	0.0002	0.0002	12
66	1911.65	1941.06	10	0.0002	0.0002	10
67	1941.06	1970.47	7	0.0001	0.0001	6
68	1970.47	1999.88	11	0.0002	0.0002	12
69	1999.88	2029.29	18	0.0003	0.0004	21
70	2029.29	2058.70	10	0.0002	0.0002	11
71	2058.70	2088.11	9	0.0001	0.0002	10
72	2088.11	2117.52	7	0.0001	0.0001	7
73	2117.52	2146.93	9	0.0001	0.0002	10
74	2146.93	2176.34	16	0.0003	0.0003	20
75	2176.34	2205.75	12	0.0002	0.0002	14
76	2205.75	2235.16	19	0.0003	0.0004	25
77	2235.16	2264.57	15	0.0002	0.0003	19
78	2264.57	2293.98	28	0.0005	0.0006	38
79	2293.98	2323.39	19	0.0003	0.0004	26
80	2323.39	2352.80	21	0.0003	0.0005	29
81	2352.80	2382.21	10	0.0002	0.0002	14
82	2382.21	2411.62	9	0.0001	0.0002	13
83	2411.62	2441.03	16	0.0003	0.0004	23
84	2441.03	2470.44	16	0.0003	0.0004	24
85	2470.44	2499.85	2	0.0000	0.0000	3
Totals			149720	2.452	2.391	145993
Average Chord Length (μm)				187.4	192.1	
Air Content (%)				4.59	4.59	
Powers Spacing Factor (μm)				204	209	

1. Calculated using Eq. 3.14

Table C.10 Analysis of mix 10, magnification 12x, lineal data using 85 classes of 29.41 μm width

			MEASURED		TRUE[1]	
CLASS	LIMITS (μm)		CHORDS	N_L (#/cm)	N_L (#/cm)	CHORDS
1	0	29.41	24333	0.3961	0.3697	22710
2	29.41	58.82	26480	0.4311	0.4094	25147
3	58.82	88.23	26381	0.4294	0.4126	25346
4	88.23	117.64	24224	0.3943	0.3818	23453
5	117.64	147.05	21703	0.3533	0.3444	21157
6	147.05	176.46	18734	0.3050	0.2990	18365
7	176.46	205.87	15716	0.2558	0.2520	15478
8	205.87	235.28	12700	0.2067	0.2042	12546
9	235.28	264.69	10277	0.1673	0.1658	10182
10	264.69	294.10	8511	0.1385	0.1378	8465
11	294.10	323.51	6861	0.1117	0.1114	6842
12	323.51	352.92	5597	0.0911	0.0911	5597
13	352.92	382.33	4476	0.0729	0.0730	4483
14	382.33	411.74	3669	0.0597	0.0600	3683
15	411.74	441.15	2865	0.0466	0.0468	2873
16	441.15	470.56	2357	0.0384	0.0385	2366
17	470.56	499.97	1989	0.0324	0.0326	2001
18	499.97	529.38	1586	0.0258	0.0259	1592
19	529.38	558.79	1431	0.0233	0.0235	1444
20	558.79	588.20	1277	0.0208	0.0211	1295
21	588.20	617.61	970	0.0158	0.0159	977
22	617.61	647.02	859	0.0140	0.0141	868
23	647.02	676.43	762	0.0124	0.0126	772
24	676.43	705.84	684	0.0111	0.0113	696
25	705.84	735.25	579	0.0094	0.0096	588
26	735.25	764.66	387	0.0063	0.0062	382
27	764.66	794.07	381	0.0062	0.0062	380
28	794.07	823.48	350	0.0057	0.0057	350
29	823.48	852.89	359	0.0058	0.0059	365
30	852.89	882.30	288	0.0047	0.0047	289
31	882.30	911.71	253	0.0041	0.0041	253
32	911.71	941.12	210	0.0034	0.0034	207
33	941.12	970.53	214	0.0035	0.0035	215
34	970.53	999.94	154	0.0025	0.0024	148
35	999.94	1029.35	155	0.0025	0.0025	151
36	1029.35	1058.76	125	0.0020	0.0019	119
37	1058.76	1088.17	109	0.0018	0.0017	101
38	1088.17	1117.58	90	0.0015	0.0013	80
39	1117.58	1146.99	81	0.0013	0.0012	71
40	1146.99	1176.40	111	0.0018	0.0018	108
41	1176.40	1205.81	103	0.0017	0.0016	100
42	1205.81	1235.22	132	0.0021	0.0022	136
43	1235.22	1264.63	77	0.0013	0.0012	71
44	1264.63	1294.04	81	0.0013	0.0013	77
45	1294.04	1323.45	72	0.0012	0.0011	67
46	1323.45	1352.86	74	0.0012	0.0012	71
47	1352.86	1382.27	75	0.0012	0.0012	73
48	1382.27	1411.68	92	0.0015	0.0015	95
49	1411.68	1441.09	70	0.0011	0.0011	69
500	1441.09	1470.50	106	0.0017	0.0019	115

Table C.10 continued

CLASS	LIMITS (μm)		MEASURED CHORDS	MEASURED N_L (#/cm)	TRUE[1] N_L (#/cm)	TRUE[1] CHORDS
51	1470.50	1499.91	108	0.0018	0.0019	119
52	1499.91	1529.32	117	0.0019	0.0022	132
53	1529.32	1558.73	95	0.0015	0.0017	106
54	1558.73	1588.14	91	0.0015	0.0017	103
55	1588.14	1617.55	72	0.0012	0.0013	80
56	1617.55	1646.96	98	0.0016	0.0019	115
57	1646.96	1676.37	70	0.0011	0.0013	80
58	1676.37	1705.78	76	0.0012	0.0015	89
59	1705.78	1735.19	63	0.0010	0.0012	74
60	1735.19	1764.60	70	0.0011	0.0014	84
61	1764.60	1794.01	54	0.0009	0.0010	64
62	1794.01	1823.42	57	0.0009	0.0011	69
63	1823.42	1852.83	57	0.0009	0.0011	70
64	1852.83	1882.24	39	0.0006	0.0008	47
65	1882.24	1911.65	34	0.0006	0.0007	41
66	1911.65	1941.06	31	0.0005	0.0006	38
67	1941.06	1970.47	41	0.0007	0.0009	52
68	1970.47	1999.88	24	0.0004	0.0005	30
69	1999.88	2029.29	17	0.0003	0.0003	21
70	2029.29	2058.70	16	0.0003	0.0003	20
71	2058.70	2088.11	11	0.0002	0.0002	13
72	2088.11	2117.52	18	0.0003	0.0004	23
73	2117.52	2146.93	16	0.0003	0.0003	21
74	2146.93	2176.34	16	0.0003	0.0003	21
75	2176.34	2205.75	16	0.0003	0.0003	21
76	2205.75	2235.16	23	0.0004	0.0005	32
77	2235.16	2264.57	14	0.0002	0.0003	19
78	2264.57	2293.98	13	0.0002	0.0003	18
79	2293.98	2323.39	12	0.0002	0.0003	17
80	2323.39	2352.80	2	0.0000	0.0000	3
81	2352.80	2382.21	1	0.0000	0.0000	1
82	2382.21	2411.62	2	0.0000	0.0000	3
83	2411.62	2441.03	3	0.0000	0.0001	4
84	2441.03	2470.44	2	0.0000	0.0000	3
85	2470.44	2499.85	0	0.0000	0.0000	0
Totals			230549	3.753	3.657	224659
Average Chord Length (μm)				192.3	197.3	
Air Content (%)				7.22	7.21	
Powers Spacing Factor (μm)				164	169	

1. Calculated using Eq. 3.14

Table C.11 Analysis of mix 1, magnification 30x, lineal data using 85 classes of 29.25 μm width

			MEASURED		TRUE[1]	
CLASS	LIMITS (μm)		CHORDS	N_L (#/cm)	N_L (#/cm)	CHORDS
1	0.00	29.25	107525	0.6969	0.6780	104618
2	29.25	58.50	35628	0.2309	0.2208	34063
3	58.50	87.75	17304	0.1121	0.1045	16124
4	87.75	117.00	10885	0.0705	0.0642	9904
5	117.00	146.25	8259	0.0535	0.0482	7436
6	146.25	175.50	6373	0.0413	0.0366	5655
7	175.50	204.75	5503	0.0357	0.0317	4895
8	204.75	234.00	4669	0.0303	0.0268	4142
9	234.00	263.25	4327	0.0280	0.0253	3898
10	263.25	292.50	3738	0.0242	0.0218	3369
11	292.50	321.75	3498	0.0227	0.0208	3210
12	321.75	351.00	2947	0.0191	0.0174	2690
13	351.00	380.25	2411	0.0156	0.0140	2163
14	380.25	409.50	2189	0.0142	0.0128	1978
15	409.50	438.75	1905	0.0123	0.0111	1712
16	438.75	468.00	1912	0.0124	0.0115	1780
17	468.00	497.25	1468	0.0095	0.0085	1307
18	497.25	526.50	1510	0.0098	0.0091	1406
19	526.50	555.75	1344	0.0087	0.0081	1251
20	555.75	585.00	1139	0.0074	0.0067	1041
21	585.00	614.25	979	0.0063	0.0057	877
22	614.25	643.50	877	0.0057	0.0050	779
23	643.50	672.75	887	0.0057	0.0053	822
24	672.75	702.00	854	0.0055	0.0052	810
25	702.00	731.25	788	0.0051	0.0049	754
26	731.25	760.50	784	0.0051	0.0050	778
27	760.50	789.75	783	0.0051	0.0052	808
28	789.75	819.00	566	0.0037	0.0035	540
29	819.00	848.25	365	0.0024	0.0018	280
30	848.25	877.50	365	0.0024	0.0019	292
31	877.50	906.75	341	0.0022	0.0017	269
32	906.75	936.00	468	0.0030	0.0030	467
33	936.00	965.25	333	0.0022	0.0019	287
34	965.25	994.50	388	0.0025	0.0025	382
35	994.50	1023.75	331	0.0021	0.0020	312
36	1023.75	1053.00	338	0.0022	0.0022	337
37	1053.00	1082.25	412	0.0027	0.0030	469
38	1082.25	1111.50	269	0.0017	0.0017	262
39	1111.50	1140.75	189	0.0012	0.0009	145
40	1140.75	1170.00	192	0.0012	0.0010	157
41	1170.00	1199.25	205	0.0013	0.0012	186
42	1199.25	1228.50	172	0.0011	0.0009	139
43	1228.50	1257.75	219	0.0014	0.0015	228
44	1257.75	1287.00	238	0.0015	0.0018	273
45	1287.00	1316.25	189	0.0012	0.0013	200
46	1316.25	1345.50	173	0.0011	0.0012	181
47	1345.50	1374.75	151	0.0010	0.0010	150
48	1374.75	1404.00	266	0.0017	0.0024	377
49	1404.00	1433.25	186	0.0012	0.0016	243
50	1433.25	1462.50	256	0.0017	0.0026	395

Table C.11 continued

CLASS	LIMITS (μm)		MEASURED CHORDS	MEASURED N_L (#/cm)	TRUE[1] N_L (#/cm)	TRUE[1] CHORDS
51	1462.50	1491.75	212	0.0014	0.0021	330
52	1491.75	1521.00	147	0.0010	0.0014	217
53	1521.00	1550.25	111	0.0007	0.0010	154
54	1550.25	1579.50	89	0.0006	0.0008	117
55	1579.50	1608.75	25	0.0002	-0.0001	-15
56	1608.75	1638.00	42	0.0003	0.0001	22
57	1638.00	1667.25	101	0.0007	0.0010	158
58	1667.25	1696.50	126	0.0008	0.0015	227
59	1696.50	1725.75	74	0.0005	0.0008	119
60	1725.75	1755.00	22	0.0001	0.0000	0
61	1755.00	1784.25	18	0.0001	-0.0001	-10
62	1784.25	1813.50	16	0.0001	-0.0001	-16
63	1813.50	1842.75	34	0.0002	0.0002	30
64	1842.75	1872.00	9	0.0001	-0.0002	-35
65	1872.00	1901.25	26	0.0002	0.0001	9
66	1901.25	1930.50	71	0.0005	0.0009	139
67	1930.50	1959.75	61	0.0004	0.0008	121
68	1959.75	1989.00	53	0.0003	0.0007	108
69	1989.00	2018.25	80	0.0005	0.0013	202
70	2018.25	2047.50	40	0.0003	0.0006	92
71	2047.50	2076.75	25	0.0002	0.0003	51
72	2076.75	2106.00	28	0.0002	0.0004	67
73	2106.00	2135.25	2	0.0000	-0.0001	-18
74	2135.25	2164.50	3	0.0000	-0.0001	-17
75	2164.50	2193.75	1	0.0000	-0.0002	-26
76	2193.75	2223.00	0	0.0000	-0.0002	-33
77	2223.00	2252.25	0	0.0000	-0.0002	-37
78	2252.25	2281.50	0	0.0000	-0.0003	-42
79	2281.50	2310.75	9	0.0001	0.0000	-7
80	2310.75	2340.00	23	0.0001	0.0004	57
81	2340.00	2369.25	17	0.0001	0.0002	36
82	2369.25	2398.50	5	0.0000	-0.0001	-20
83	2398.50	2427.75	13	0.0001	0.0001	20
84	2427.75	2457.00	30	0.0002	0.0008	121
85	2457.00	2486.25	62	0.0004	0.0022	336
Totals			238673	1.547	1.473	227296
Average Chord Length (μm)				143.1	150.2	
Air Content (%)				2.21	2.21	
Powers Spacing Factor (μm)				247	259	

1. Calculated using Eq. 3.14

Table C.12 Analysis of mix 2, magnification 30x, lineal data using 85 classes of 29.25 μm width

CLASS	LIMITS (μm)		MEASURED		TRUE[1]	
			CHORDS	N_L (#/cm)	N_L (#/cm)	CHORDS
1	0.00	29.25	67025	0.4439	0.4293	64819
2	29.25	58.50	24208	0.1603	0.1515	22877
3	58.50	87.75	14037	0.0930	0.0864	13040
4	87.75	117.00	8727	0.0578	0.0522	7886
5	117.00	146.25	6605	0.0437	0.0390	5888
6	146.25	175.50	5078	0.0336	0.0294	4441
7	175.50	204.75	4260	0.0282	0.0245	3699
8	204.75	234.00	3851	0.0255	0.0223	3371
9	234.00	263.25	3352	0.0222	0.0194	2930
10	263.25	292.50	2750	0.0182	0.0156	2355
11	292.50	321.75	2404	0.0159	0.0135	2043
12	321.75	351.00	1972	0.0131	0.0107	1619
13	351.00	380.25	2042	0.0135	0.0116	1754
14	380.25	409.50	1761	0.0117	0.0098	1487
15	409.50	438.75	1754	0.0116	0.0101	1530
16	438.75	468.00	1483	0.0098	0.0083	1260
17	468.00	497.25	1207	0.0080	0.0064	972
18	497.25	526.50	1252	0.0083	0.0070	1062
19	526.50	555.75	1402	0.0093	0.0085	1285
20	555.75	585.00	1292	0.0086	0.0079	1195
21	585.00	614.25	1120	0.0074	0.0068	1022
22	614.25	643.50	889	0.0059	0.0051	764
23	643.50	672.75	757	0.0050	0.0041	622
24	672.75	702.00	864	0.0057	0.0052	786
25	702.00	731.25	595	0.0039	0.0030	459
26	731.25	760.50	512	0.0034	0.0024	365
27	760.50	789.75	694	0.0046	0.0042	628
28	789.75	819.00	642	0.0043	0.0039	582
29	819.00	848.25	644	0.0043	0.0040	609
30	848.25	877.50	577	0.0038	0.0036	538
31	877.50	906.75	317	0.0021	0.0012	186
32	906.75	936.00	302	0.0020	0.0011	172
33	936.00	965.25	285	0.0019	0.0010	154
34	965.25	994.50	284	0.0019	0.0011	159
35	994.50	1023.75	275	0.0018	0.0010	153
36	1023.75	1053.00	273	0.0018	0.0010	156
37	1053.00	1082.25	253	0.0017	0.0009	132
38	1082.25	1111.50	382	0.0025	0.0023	345
39	1111.50	1140.75	253	0.0017	0.0010	152
40	1140.75	1170.00	324	0.0021	0.0018	276
41	1170.00	1199.25	303	0.0020	0.0017	255
42	1199.25	1228.50	314	0.0021	0.0019	286
43	1228.50	1257.75	222	0.0015	0.0009	141
44	1257.75	1287.00	275	0.0018	0.0016	242
45	1287.00	1316.25	266	0.0018	0.0016	238
46	1316.25	1345.50	298	0.0020	0.0021	310
47	1345.50	1374.75	159	0.0011	0.0004	67
48	1374.75	1404.00	176	0.0012	0.0007	104
49	1404.00	1433.25	144	0.0010	0.0003	47
50	1433.25	1462.50	195	0.0013	0.0010	151

TableC.12 continued

CLASS	LIMITS (μm)		MEASURED CHORDS	MEASURED N_L (#/cm)	TRUE[1] N_L (#/cm)	TRUE[1] CHORDS
51	1462.50	1491.75	281	0.0021	0.0030	397
52	1491.75	1521.00	211	0.0016	0.0021	277
53	1521.00	1550.25	155	0.0012	0.0013	177
54	1550.25	1579.50	166	0.0012	0.0016	212
55	1579.50	1608.75	74	0.0006	0.0002	24
56	1608.75	1638.00	85	0.0006	0.0004	50
57	1638.00	1667.25	64	0.0005	0.0000	6
58	1667.25	1696.50	87	0.0007	0.0005	60
59	1696.50	1725.75	112	0.0008	0.0009	124
60	1725.75	1755.00	137	0.0010	0.0015	194
61	1755.00	1784.25	240	0.0018	0.0035	466
62	1784.25	1813.50	188	0.0014	0.0028	367
63	1813.50	1842.75	81	0.0006	0.0009	114
64	1842.75	1872.00	81	0.0006	0.0009	123
65	1872.00	1901.25	44	0.0003	0.0002	30
66	1901.25	1930.50	98	0.0007	0.0014	187
67	1930.50	1959.75	110	0.0008	0.0018	238
68	1959.75	1989.00	37	0.0003	0.0003	39
69	1989.00	2018.25	61	0.0005	0.0009	117
70	2018.25	2047.50	54	0.0004	0.0008	106
71	2047.50	2076.75	52	0.0004	0.0008	109
72	2076.75	2106.00	40	0.0003	0.0006	79
73	2106.00	2135.25	27	0.0002	0.0003	41
74	2135.25	2164.50	43	0.0003	0.0008	104
75	2164.50	2193.75	48	0.0004	0.0010	135
76	2193.75	2223.00	20	0.0002	0.0003	40
77	2223.00	2252.25	21	0.0002	0.0004	49
78	2252.25	2281.50	30	0.0002	0.0007	94
79	2281.50	2310.75	12	0.0001	0.0002	25
80	2310.75	2340.00	16	0.0001	0.0004	48
81	2340.00	2369.25	15	0.0001	0.0004	50
82	2369.25	2398.50	15	0.0001	0.0004	57
83	2398.50	2427.75	22	0.0002	0.0008	104
84	2427.75	2457.00	2	0.0000	0.0001	7
85	2457.00	2486.25	6	0.0000	0.0002	33
Totals			523082	3.933	3.760	500129
Average Chord Length (μm)				131.7	137.7	
Air Content (%)				5.18	5.18	
Powers Spacing Factor (μm)				149	156	

1. Calculated using Eq. 3.14

Table C.13 Analysis of mix 3, magnification 30x, lineal data using 85 classes of 29.25 μm width

			MEASURED		TRUE[1]	
CLASS	LIMITS (μm)		CHORDS	N_L (#/cm)	N_L (#/cm)	CHORDS
1	0.00	29.25	122785	0.9232	0.8624	114696
2	29.25	58.50	92352	0.6944	0.6537	86946
3	58.50	87.75	81491	0.6127	0.5890	78338
4	87.75	117.00	58583	0.4405	0.4269	56778
5	117.00	146.25	39715	0.2986	0.2902	38597
6	146.25	175.50	27277	0.2051	0.1994	26524
7	175.50	204.75	19597	0.1473	0.1434	19075
8	204.75	234.00	14284	0.1074	0.1044	13891
9	234.00	263.25	10844	0.0815	0.0793	10547
10	263.25	292.50	8261	0.0621	0.0603	8014
11	292.50	321.75	6963	0.0524	0.0512	6816
12	321.75	351.00	5278	0.0397	0.0385	5124
13	351.00	380.25	4304	0.0324	0.0314	4175
14	380.25	409.50	3790	0.0285	0.0280	3719
15	409.50	438.75	2667	0.0201	0.0190	2524
16	438.75	468.00	2549	0.0192	0.0186	2471
17	468.00	497.25	2037	0.0153	0.0146	1941
18	497.25	526.50	1781	0.0134	0.0128	1698
19	526.50	555.75	1587	0.0119	0.0114	1520
20	555.75	585.00	1118	0.0084	0.0074	989
21	585.00	614.25	915	0.0069	0.0058	769
22	614.25	643.50	931	0.0070	0.0062	818
23	643.50	672.75	916	0.0069	0.0062	830
24	672.75	702.00	698	0.0052	0.0043	575
25	702.00	731.25	654	0.0049	0.0041	539
26	731.25	760.50	649	0.0049	0.0042	554
27	760.50	789.75	526	0.0040	0.0031	408
28	789.75	819.00	501	0.0038	0.0029	390
29	819.00	848.25	470	0.0035	0.0027	362
30	848.25	877.50	491	0.0037	0.0031	407
31	877.50	906.75	480	0.0036	0.0031	409
32	906.75	936.00	503	0.0038	0.0035	460
33	936.00	965.25	347	0.0026	0.0019	248
34	965.25	994.50	324	0.0024	0.0017	224
35	994.50	1023.75	311	0.0023	0.0016	214
36	1023.75	1053.00	351	0.0026	0.0022	286
37	1053.00	1082.25	355	0.0027	0.0023	306
38	1082.25	1111.50	348	0.0026	0.0023	309
39	1111.50	1140.75	335	0.0025	0.0023	303
40	1140.75	1170.00	295	0.0022	0.0019	251
41	1170.00	1199.25	367	0.0028	0.0029	384
42	1199.25	1228.50	263	0.0020	0.0017	226
43	1228.50	1257.75	224	0.0017	0.0013	170
44	1257.75	1287.00	268	0.0020	0.0019	256
45	1287.00	1316.25	291	0.0022	0.0023	311
46	1316.25	1345.50	219	0.0016	0.0015	196
47	1345.50	1374.75	289	0.0022	0.0025	337
48	1374.75	1404.00	262	0.0020	0.0023	305
49	1404.00	1433.25	213	0.0016	0.0017	227
50	1433.25	1462.50	288	0.0022	0.0029	388

Table C.13 continued

CLASS	LIMITS (μm)		MEASURED CHORDS	MEASURED N_L (#/cm)	TRUE[1] N_L (#/cm)	TRUE[1] CHORDS
51	1462.50	1491.75	281	0.0021	0.0030	397
52	1491.75	1521.00	211	0.0016	0.0021	277
53	1521.00	1550.25	155	0.0012	0.0013	177
54	1550.25	1579.50	166	0.0012	0.0016	212
55	1579.50	1608.75	74	0.0006	0.0002	24
56	1608.75	1638.00	85	0.0006	0.0004	50
57	1638.00	1667.25	64	0.0005	0.0000	6
58	1667.25	1696.50	87	0.0007	0.0005	60
59	1696.50	1725.75	112	0.0008	0.0009	124
60	1725.75	1755.00	137	0.0010	0.0015	194
61	1755.00	1784.25	240	0.0018	0.0035	466
62	1784.25	1813.50	188	0.0014	0.0028	367
63	1813.50	1842.75	81	0.0006	0.0009	114
64	1842.75	1872.00	81	0.0006	0.0009	123
65	1872.00	1901.25	44	0.0003	0.0002	30
66	1901.25	1930.50	98	0.0007	0.0014	187
67	1930.50	1959.75	110	0.0008	0.0018	238
68	1959.75	1989.00	37	0.0003	0.0003	39
69	1989.00	2018.25	61	0.0005	0.0009	117
70	2018.25	2047.50	54	0.0004	0.0008	106
71	2047.50	2076.75	52	0.0004	0.0008	109
72	2076.75	2106.00	40	0.0003	0.0006	79
73	2106.00	2135.25	27	0.0002	0.0003	41
74	2135.25	2164.50	43	0.0003	0.0008	104
75	2164.50	2193.75	48	0.0004	0.0010	135
76	2193.75	2223.00	20	0.0002	0.0003	40
77	2223.00	2252.25	21	0.0002	0.0004	49
78	2252.25	2281.50	30	0.0002	0.0007	94
79	2281.50	2310.75	12	0.0001	0.0002	25
80	2310.75	2340.00	16	0.0001	0.0004	48
81	2340.00	2369.25	15	0.0001	0.0004	50
82	2369.25	2398.50	15	0.0001	0.0004	57
83	2398.50	2427.75	22	0.0002	0.0008	104
84	2427.75	2457.00	2	0.0000	0.0001	7
85	2457.00	2486.25	6	0.0000	0.0002	33
Totals			523082	3.933	3.760	500129
Average Chord Length (μm)				131.7	137.7	
Air Content (%)				5.18	5.18	
Powers Spacing Factor (μm)				149	156	

1. Calculated using Eq. 3.14

Table C.14 Analysis of mix 4, magnification 30x, lineal data using 85 classes of 29.25 μm width

			MEASURED		TRUE[1]	
CLASS	LIMITS (μm)		CHORDS	N_L (#/cm)	N_L (#/cm)	CHORDS
1	0.00	29.25	28465	0.4631	0.3703	22756
2	29.25	58.50	91004	1.4807	1.4244	87544
3	58.50	87.75	66440	1.0810	1.0538	64766
4	87.75	117.00	47039	0.7654	0.7559	46458
5	117.00	146.25	25945	0.4221	0.4166	25605
6	146.25	175.50	15955	0.2596	0.2561	15739
7	175.50	204.75	10616	0.1727	0.1704	10476
8	204.75	234.00	7121	0.1159	0.1139	6999
9	234.00	263.25	5427	0.0883	0.0872	5358
10	263.25	292.50	3864	0.0629	0.0617	3791
11	292.50	321.75	2928	0.0476	0.0466	2862
12	321.75	351.00	2338	0.0380	0.0372	2285
13	351.00	380.25	1963	0.0319	0.0314	1931
14	380.25	409.50	1628	0.0265	0.0261	1606
15	409.50	438.75	1170	0.0190	0.0183	1122
16	438.75	468.00	1130	0.0184	0.0181	1113
17	468.00	497.25	913	0.0149	0.0145	891
18	497.25	526.50	839	0.0137	0.0135	833
19	526.50	555.75	728	0.0118	0.0118	726
20	555.75	585.00	645	0.0105	0.0105	648
21	585.00	614.25	609	0.0099	0.0102	627
22	614.25	643.50	424	0.0069	0.0067	413
23	643.50	672.75	413	0.0067	0.0067	415
24	672.75	702.00	298	0.0048	0.0045	280
25	702.00	731.25	298	0.0048	0.0047	290
26	731.25	760.50	226	0.0037	0.0033	205
27	760.50	789.75	159	0.0026	0.0020	121
28	789.75	819.00	174	0.0028	0.0024	147
29	819.00	848.25	149	0.0024	0.0019	118
30	848.25	877.50	190	0.0031	0.0030	181
31	877.50	906.75	181	0.0029	0.0029	176
32	906.75	936.00	141	0.0023	0.0020	125
33	936.00	965.25	129	0.0021	0.0018	113
34	965.25	994.50	110	0.0018	0.0014	89
35	994.50	1023.75	137	0.0022	0.0022	134
36	1023.75	1053.00	136	0.0022	0.0023	139
37	1053.00	1082.25	122	0.0020	0.0020	123
38	1082.25	1111.50	120	0.0020	0.0020	126
39	1111.50	1140.75	95	0.0015	0.0015	91
40	1140.75	1170.00	41	0.0007	0.0001	6
41	1170.00	1199.25	46	0.0007	0.0002	15
42	1199.25	1228.50	46	0.0007	0.0003	16
43	1228.50	1257.75	51	0.0008	0.0004	25
44	1257.75	1287.00	34	0.0006	-0.0001	-4
45	1287.00	1316.25	46	0.0007	0.0003	18
46	1316.25	1345.50	30	0.0005	-0.0002	-11
47	1345.50	1374.75	29	0.0005	-0.0002	-13
48	1374.75	1404.00	34	0.0006	-0.0001	-4
49	1404.00	1433.25	25	0.0004	-0.0004	-22
50	1433.25	1462.50	42	0.0007	0.0002	10

Table C.14 continued

			MEASURED		TRUE[1]	
CLASS	LIMITS (μm)		CHORDS	N_L (#/cm)	N_L (#/cm)	CHORDS
51	1462.50	1491.75	28	0.0005	-0.0003	-17
52	1491.75	1521.00	22	0.0004	-0.0005	-31
53	1521.00	1550.25	36	0.0006	-0.0001	-3
54	1550.25	1579.50	44	0.0007	0.0002	14
55	1579.50	1608.75	29	0.0005	-0.0003	-18
56	1608.75	1638.00	32	0.0005	-0.0002	-13
57	1638.00	1667.25	29	0.0005	-0.0003	-21
58	1667.25	1696.50	38	0.0006	0.0000	-1
59	1696.50	1725.75	42	0.0007	0.0001	9
60	1725.75	1755.00	54	0.0009	0.0006	38
61	1755.00	1784.25	44	0.0007	0.0003	16
62	1784.25	1813.50	68	0.0011	0.0013	79
63	1813.50	1842.75	45	0.0007	0.0004	25
64	1842.75	1872.00	43	0.0007	0.0003	21
65	1872.00	1901.25	64	0.0010	0.0013	81
66	1901.25	1930.50	48	0.0008	0.0007	42
67	1930.50	1959.75	33	0.0005	0.0000	2
68	1959.75	1989.00	43	0.0007	0.0005	32
69	1989.00	2018.25	49	0.0008	0.0009	54
70	2018.25	2047.50	68	0.0011	0.0020	120
71	2047.50	2076.75	60	0.0010	0.0017	105
72	2076.75	2106.00	45	0.0007	0.0010	64
73	2106.00	2135.25	25	0.0004	0.0000	0
74	2135.25	2164.50	43	0.0007	0.0011	66
75	2164.50	2193.75	29	0.0005	0.0003	20
76	2193.75	2223.00	44	0.0007	0.0013	82
77	2223.00	2252.25	35	0.0006	0.0009	55
78	2252.25	2281.50	16	0.0003	-0.0003	-20
79	2281.50	2310.75	22	0.0004	0.0001	5
80	2310.75	2340.00	48	0.0008	0.0021	127
81	2340.00	2369.25	43	0.0007	0.0020	121
82	2369.25	2398.50	47	0.0008	0.0026	159
83	2398.50	2427.75	34	0.0006	0.0019	114
84	2427.75	2457.00	54	0.0009	0.0040	248
85	2457.00	2486.25	55	0.0009	0.0049	298
Totals			322152	5.242	5.033	309333
Average Chord Length (μm)				119.4	124.3	
Air Content (%)				6.26	6.26	
Powers Spacing Factor (μm)				103	107	

1. Calculated using Eq. 3.14

Table C.15 Analysis of mix 5, magnification 30x, lineal data using 85 classes of 29.25 μm width

			MEASURED		TRUE[1]	
CLASS	LIMITS (μm)		CHORDS	N_L (#/cm)	N_L (#/cm)	CHORDS
1	0.00	29.25	154508	1.1617	1.0967	145856
2	29.25	58.50	131735	0.9905	0.9541	126894
3	58.50	87.75	100752	0.7575	0.7418	98664
4	87.75	117.00	61947	0.4658	0.4594	61098
5	117.00	146.25	34842	0.2620	0.2582	34347
6	146.25	175.50	21455	0.1613	0.1588	21127
7	175.50	204.75	14598	0.1098	0.1082	14396
8	204.75	234.00	9053	0.0681	0.0662	8809
9	234.00	263.25	6828	0.0513	0.0499	6641
10	263.25	292.50	5240	0.0394	0.0383	5088
11	292.50	321.75	3447	0.0259	0.0243	3236
12	321.75	351.00	3149	0.0237	0.0226	3005
13	351.00	380.25	2600	0.0195	0.0186	2474
14	380.25	409.50	2154	0.0162	0.0153	2038
15	409.50	438.75	2323	0.0175	0.0174	2308
16	438.75	468.00	1751	0.0132	0.0128	1707
17	468.00	497.25	1427	0.0107	0.0103	1376
18	497.25	526.50	1155	0.0087	0.0082	1093
19	526.50	555.75	1236	0.0093	0.0093	1233
20	555.75	585.00	891	0.0067	0.0064	847
21	585.00	614.25	588	0.0044	0.0037	495
22	614.25	643.50	604	0.0045	0.0040	534
23	643.50	672.75	757	0.0057	0.0057	753
24	672.75	702.00	503	0.0038	0.0034	448
25	702.00	731.25	586	0.0044	0.0043	576
26	731.25	760.50	589	0.0044	0.0045	603
27	760.50	789.75	570	0.0043	0.0045	601
28	789.75	819.00	249	0.0019	0.0014	180
29	819.00	848.25	215	0.0016	0.0011	140
30	848.25	877.50	261	0.0020	0.0016	211
31	877.50	906.75	309	0.0023	0.0022	290
32	906.75	936.00	333	0.0025	0.0025	337
33	936.00	965.25	169	0.0013	0.0008	108
34	965.25	994.50	278	0.0021	0.0021	277
35	994.50	1023.75	190	0.0014	0.0012	155
36	1023.75	1053.00	107	0.0008	0.0002	33
37	1053.00	1082.25	201	0.0015	0.0014	183
38	1082.25	1111.50	124	0.0009	0.0005	68
39	1111.50	1140.75	150	0.0011	0.0009	114
40	1140.75	1170.00	109	0.0008	0.0004	51
41	1170.00	1199.25	216	0.0016	0.0018	234
42	1199.25	1228.50	304	0.0023	0.0030	396
43	1228.50	1257.75	203	0.0015	0.0018	241
44	1257.75	1287.00	147	0.0011	0.0012	154
45	1287.00	1316.25	371	0.0028	0.0043	565
46	1316.25	1345.50	632	0.0048	0.0081	1074
47	1345.50	1374.75	82	0.0006	0.0008	107
48	1374.75	1404.00	73	0.0005	0.0007	95
49	1404.00	1433.25	66	0.0005	0.0007	87
50	1433.25	1462.50	82	0.0006	0.0009	124

Table C.15 continued

CLASS	LIMITS (μm)		MEASURED CHORDS	MEASURED N_L (#/cm)	TRUE[1] N_L (#/cm)	TRUE[1] CHORDS
51	1462.50	1491.75	23	0.0002	0.0001	13
52	1491.75	1521.00	21	0.0002	0.0001	9
53	1521.00	1550.25	33	0.0002	0.0003	35
54	1550.25	1579.50	36	0.0003	0.0003	44
55	1579.50	1608.75	46	0.0003	0.0005	68
56	1608.75	1638.00	52	0.0004	0.0006	86
57	1638.00	1667.25	22	0.0002	0.0002	23
58	1667.25	1696.50	34	0.0003	0.0004	53
59	1696.50	1725.75	47	0.0004	0.0007	88
60	1725.75	1755.00	15	0.0001	0.0001	16
61	1755.00	1784.25	34	0.0003	0.0005	64
62	1784.25	1813.50	11	0.0001	0.0001	10
63	1813.50	1842.75	19	0.0001	0.0002	32
64	1842.75	1872.00	18	0.0001	0.0002	32
65	1872.00	1901.25	19	0.0001	0.0003	37
66	1901.25	1930.50	3	0.0000	0.0000	-5
67	1930.50	1959.75	3	0.0000	0.0000	-6
68	1959.75	1989.00	17	0.0001	0.0003	36
69	1989.00	2018.25	4	0.0000	0.0000	-1
70	2018.25	2047.50	0	0.0000	-0.0001	-14
71	2047.50	2076.75	7	0.0001	0.0001	8
72	2076.75	2106.00	9	0.0001	0.0001	15
73	2106.00	2135.25	5	0.0000	0.0000	3
74	2135.25	2164.50	5	0.0000	0.0000	3
75	2164.50	2193.75	4	0.0000	0.0000	0
76	2193.75	2223.00	5	0.0000	0.0000	4
77	2223.00	2252.25	4	0.0000	0.0000	0
78	2252.25	2281.50	8	0.0001	0.0001	17
79	2281.50	2310.75	13	0.0001	0.0003	42
80	2310.75	2340.00	13	0.0001	0.0004	47
81	2340.00	2369.25	5	0.0000	0.0001	15
82	2369.25	2398.50	2	0.0000	0.0000	2
83	2398.50	2427.75	4	0.0000	0.0001	13
84	2427.75	2457.00	4	0.0000	0.0001	15
85	2457.00	2486.25	10	0.0001	0.0004	54
Totals			570714	4.291	4.153	552327
Average Chord Length (μm)				96.7	99.9	
Air Content (%)				4.15	4.15	
Powers Spacing Factor (μm)				110	114	

1. Calculated using Eq. 3.14

Table C.16 Analysis of mix 6, magnification 30x, lineal data using 85 classes of 29.25 μm width

CLASS	LIMITS (μm)		MEASURED		TRUE[1]	
			CHORDS	N_L (#/cm)	N_L (#/cm)	CHORDS
1	0.00	29.25	22108	0.3599	0.2866	17608
2	29.25	58.50	69061	1.1242	1.0787	66265
3	58.50	87.75	51651	0.8408	0.8180	50249
4	87.75	117.00	38471	0.6263	0.6186	38003
5	117.00	146.25	20734	0.3375	0.3327	20436
6	146.25	175.50	12722	0.2071	0.2038	12520
7	175.50	204.75	8095	0.1318	0.1290	7923
8	204.75	234.00	5436	0.0885	0.0859	5276
9	234.00	263.25	4164	0.0678	0.0658	4045
10	263.25	292.50	3092	0.0503	0.0485	2982
11	292.50	321.75	2381	0.0388	0.0371	2280
12	321.75	351.00	2131	0.0347	0.0337	2071
13	351.00	380.25	1629	0.0265	0.0254	1563
14	380.25	409.50	1390	0.0226	0.0218	1338
15	409.50	438.75	1190	0.0194	0.0187	1148
16	438.75	468.00	993	0.0162	0.0155	953
17	468.00	497.25	959	0.0156	0.0154	946
18	497.25	526.50	820	0.0133	0.0132	810
19	526.50	555.75	714	0.0116	0.0115	709
20	555.75	585.00	575	0.0094	0.0091	561
21	585.00	614.25	527	0.0086	0.0085	521
22	614.25	643.50	527	0.0086	0.0088	541
23	643.50	672.75	434	0.0071	0.0072	440
24	672.75	702.00	342	0.0056	0.0055	336
25	702.00	731.25	290	0.0047	0.0046	280
26	731.25	760.50	321	0.0052	0.0054	333
27	760.50	789.75	263	0.0043	0.0043	267
28	789.75	819.00	229	0.0037	0.0038	231
29	819.00	848.25	235	0.0038	0.0041	249
30	848.25	877.50	240	0.0039	0.0043	266
31	877.50	906.75	184	0.0030	0.0032	197
32	906.75	936.00	146	0.0024	0.0024	150
33	936.00	965.25	96	0.0016	0.0013	82
34	965.25	994.50	136	0.0022	0.0024	146
35	994.50	1023.75	85	0.0014	0.0012	74
36	1023.75	1053.00	102	0.0017	0.0017	104
37	1053.00	1082.25	98	0.0016	0.0017	102
38	1082.25	1111.50	93	0.0015	0.0016	99
39	1111.50	1140.75	98	0.0016	0.0018	112
40	1140.75	1170.00	60	0.0010	0.0009	55
41	1170.00	1199.25	86	0.0014	0.0016	101
42	1199.25	1228.50	70	0.0011	0.0013	79
43	1228.50	1257.75	58	0.0009	0.0010	62
44	1257.75	1287.00	59	0.0010	0.0011	67
45	1287.00	1316.25	49	0.0008	0.0009	52
46	1316.25	1345.50	52	0.0008	0.0010	61
47	1345.50	1374.75	45	0.0007	0.0008	51
48	1374.75	1404.00	32	0.0005	0.0005	29
49	1404.00	1433.25	25	0.0004	0.0003	17
50	1433.25	1462.50	34	0.0006	0.0006	36

Table C.16 continued

			MEASURED		TRUE[1]	
CLASS	LIMITS (μm)		CHORDS	N_L (#/cm)	N_L (#/cm)	CHORDS
51	1462.50	1491.75	31	0.0005	0.0005	32
52	1491.75	1521.00	24	0.0004	0.0003	20
53	1521.00	1550.25	46	0.0007	0.0011	67
54	1550.25	1579.50	58	0.0009	0.0016	97
55	1579.50	1608.75	68	0.0011	0.0020	125
56	1608.75	1638.00	37	0.0006	0.0010	64
57	1638.00	1667.25	25	0.0004	0.0007	41
58	1667.25	1696.50	22	0.0004	0.0006	37
59	1696.50	1725.75	8	0.0001	0.0001	6
60	1725.75	1755.00	17	0.0003	0.0005	28
61	1755.00	1784.25	11	0.0002	0.0002	15
62	1784.25	1813.50	9	0.0001	0.0002	11
63	1813.50	1842.75	0	0.0000	-0.0002	-12
64	1842.75	1872.00	2	0.0000	-0.0001	-7
65	1872.00	1901.25	5	0.0001	0.0000	1
66	1901.25	1930.50	6	0.0001	0.0001	3
67	1930.50	1959.75	4	0.0001	0.0000	-2
68	1959.75	1989.00	7	0.0001	0.0001	7
69	1989.00	2018.25	2	0.0000	-0.0001	-8
70	2018.25	2047.50	0	0.0000	-0.0003	-15
71	2047.50	2076.75	3	0.0000	-0.0001	-7
72	2076.75	2106.00	8	0.0001	0.0002	9
73	2106.00	2135.25	21	0.0003	0.0009	57
74	2135.25	2164.50	12	0.0002	0.0005	30
75	2164.50	2193.75	2	0.0000	-0.0001	-5
76	2193.75	2223.00	8	0.0001	0.0003	18
77	2223.00	2252.25	13	0.0002	0.0007	41
78	2252.25	2281.50	4	0.0001	0.0001	7
79	2281.50	2310.75	8	0.0001	0.0004	26
80	2310.75	2340.00	7	0.0001	0.0004	25
81	2340.00	2369.25	4	0.0001	0.0002	14
82	2369.25	2398.50	3	0.0000	0.0002	11
83	2398.50	2427.75	1	0.0000	0.0000	2
84	2427.75	2457.00	2	0.0000	0.0001	8
85	2457.00	2486.25	5	0.0001	0.0004	27
Totals			253815	4.132	3.965	243595
Average Chord Length (μm)				120.9	125.9	
Air Content (%)				4.99	4.99	
Powers Spacing Factor (μm)				121	126	

1. Calculated using Eq. 3.14

Table C.17 Analysis of mix 7, magnification 30x, lineal data using 85 classes of 29.25 μm width

			MEASURED		TRUE[1]	
CLASS	LIMITS (μm)		CHORDS	N_L (#/cm)	N_L (#/cm)	CHORDS
1	0.00	29.25	84203	0.5447	0.4897	75707
2	29.25	58.50	64130	0.4148	0.3713	57405
3	58.50	87.75	59404	0.3842	0.3509	54254
4	87.75	117.00	53016	0.3429	0.3185	49235
5	117.00	146.25	45569	0.2948	0.2774	42889
6	146.25	175.50	38317	0.2478	0.2360	36488
7	175.50	204.75	32399	0.2096	0.2022	31255
8	204.75	234.00	24824	0.1606	0.1552	23993
9	234.00	263.25	19612	0.1269	0.1230	19023
10	263.25	292.50	15681	0.1014	0.0987	15264
11	292.50	321.75	12643	0.0818	0.0799	12345
12	321.75	351.00	10290	0.0666	0.0652	10077
13	351.00	380.25	8421	0.0545	0.0535	8265
14	380.25	409.50	7008	0.0453	0.0446	6901
15	409.50	438.75	5572	0.0360	0.0352	5447
16	438.75	468.00	4454	0.0288	0.0278	4304
17	468.00	497.25	3782	0.0245	0.0236	3646
18	497.25	526.50	3393	0.0219	0.0214	3301
19	526.50	555.75	2903	0.0188	0.0182	2815
20	555.75	585.00	2843	0.0184	0.0184	2844
21	585.00	614.25	2518	0.0163	0.0164	2538
22	614.25	643.50	2186	0.0141	0.0143	2207
23	643.50	672.75	1859	0.0120	0.0121	1867
24	672.75	702.00	1564	0.0101	0.0100	1551
25	702.00	731.25	1495	0.0097	0.0098	1520
26	731.25	760.50	1250	0.0081	0.0081	1249
27	760.50	789.75	1079	0.0070	0.0069	1066
28	789.75	819.00	1058	0.0068	0.0070	1080
29	819.00	848.25	1024	0.0066	0.0070	1076
30	848.25	877.50	867	0.0056	0.0058	898
31	877.50	906.75	865	0.0056	0.0060	933
32	906.75	936.00	807	0.0052	0.0057	888
33	936.00	965.25	750	0.0049	0.0054	842
34	965.25	994.50	767	0.0050	0.0059	905
35	994.50	1023.75	599	0.0039	0.0045	688
36	1023.75	1053.00	464	0.0030	0.0033	510
37	1053.00	1082.25	421	0.0027	0.0030	465
38	1082.25	1111.50	403	0.0026	0.0030	458
39	1111.50	1140.75	423	0.0027	0.0033	513
40	1140.75	1170.00	334	0.0022	0.0025	390
41	1170.00	1199.25	349	0.0023	0.0028	435
42	1199.25	1228.50	289	0.0019	0.0023	354
43	1228.50	1257.75	188	0.0012	0.0013	196
44	1257.75	1287.00	170	0.0011	0.0011	175
45	1287.00	1316.25	110	0.0007	0.0005	76
46	1316.25	1345.50	148	0.0010	0.0010	150
47	1345.50	1374.75	247	0.0016	0.0022	343
48	1374.75	1404.00	196	0.0013	0.0017	265
49	1404.00	1433.25	223	0.0014	0.0021	332
50	1433.25	1462.50	272	0.0018	0.0029	448

Table C.17 continued

			MEASURED		TRUE[1]	
CLASS	LIMITS (μm)		CHORDS	N_L (#/cm)	N_L (#/cm)	CHORDS
51	1462.50	1491.75	175	0.0011	0.0018	279
52	1491.75	1521.00	191	0.0012	0.0021	329
53	1521.00	1550.25	101	0.0007	0.0010	160
54	1550.25	1579.50	77	0.0005	0.0008	119
55	1579.50	1608.75	69	0.0004	0.0007	109
56	1608.75	1638.00	61	0.0004	0.0006	99
57	1638.00	1667.25	32	0.0002	0.0003	39
58	1667.25	1696.50	9	0.0001	-0.0001	-12
59	1696.50	1725.75	7	0.0000	-0.0001	-17
60	1725.75	1755.00	15	0.0001	0.0000	1
61	1755.00	1784.25	20	0.0001	0.0001	13
62	1784.25	1813.50	27	0.0002	0.0002	32
63	1813.50	1842.75	17	0.0001	0.0001	9
64	1842.75	1872.00	28	0.0002	0.0003	39
65	1872.00	1901.25	12	0.0001	0.0000	-2
66	1901.25	1930.50	5	0.0000	-0.0001	-22
67	1930.50	1959.75	6	0.0000	-0.0001	-21
68	1959.75	1989.00	12	0.0001	0.0000	-5
69	1989.00	2018.25	12	0.0001	0.0000	-6
70	2018.25	2047.50	13	0.0001	0.0000	-3
71	2047.50	2076.75	4	0.0000	-0.0002	-33
72	2076.75	2106.00	6	0.0000	-0.0002	-30
73	2106.00	2135.25	9	0.0001	-0.0001	-22
74	2135.25	2164.50	17	0.0001	0.0000	5
75	2164.50	2193.75	13	0.0001	-0.0001	-10
76	2193.75	2223.00	17	0.0001	0.0000	5
77	2223.00	2252.25	9	0.0001	-0.0002	-27
78	2252.25	2281.50	25	0.0002	0.0002	38
79	2281.50	2310.75	16	0.0001	0.0000	3
80	2310.75	2340.00	42	0.0003	0.0008	124
81	2340.00	2369.25	49	0.0003	0.0011	177
82	2369.25	2398.50	63	0.0004	0.0018	275
83	2398.50	2427.75	17	0.0001	0.0005	70
84	2427.75	2457.00	19	0.0001	0.0006	93
85	2457.00	2486.25	9	0.0001	0.0003	49
Totals			522593	3.380	3.181	491730
Average Chord Length (μm)				177.2	188.3	
Air Content (%)				5.99	5.99	
Powers Spacing Factor (μm)				160	170	

1. Calculated using Eq. 3.14

Table C.18 Analysis of mix 8, magnification 30x, lineal data using 85 classes of 29.25 μm width

CLASS	LIMITS (μm)		MEASURED		TRUE[1]	
			CHORDS	N_L (#/cm)	N_L (#/cm)	CHORDS
1	0.00	29.25	117906	0.7656	0.7161	110276
2	29.25	58.50	57044	0.3704	0.3325	51202
3	58.50	87.75	48957	0.3179	0.2882	44382
4	87.75	117.00	44976	0.2921	0.2700	41579
5	117.00	146.25	38786	0.2519	0.2359	36325
6	146.25	175.50	32727	0.2125	0.2012	30991
7	175.50	204.75	27828	0.1807	0.1733	26685
8	204.75	234.00	23130	0.1502	0.1455	22414
9	234.00	263.25	18919	0.1229	0.1201	18497
10	263.25	292.50	14708	0.0955	0.0936	14408
11	292.50	321.75	12163	0.0790	0.0780	12017
12	321.75	351.00	9980	0.0648	0.0645	9931
13	351.00	380.25	8532	0.0554	0.0558	8599
14	380.25	409.50	6389	0.0415	0.0415	6396
15	409.50	438.75	5769	0.0375	0.0382	5886
16	438.75	468.00	4931	0.0320	0.0331	5092
17	468.00	497.25	4001	0.0260	0.0270	4151
18	497.25	526.50	3167	0.0206	0.0213	3281
19	526.50	555.75	2767	0.0180	0.0189	2906
20	555.75	585.00	2106	0.0137	0.0142	2186
21	585.00	614.25	1734	0.0113	0.0117	1796
22	614.25	643.50	1476	0.0096	0.0100	1533
23	643.50	672.75	1093	0.0071	0.0071	1094
24	672.75	702.00	949	0.0062	0.0061	947
25	702.00	731.25	906	0.0059	0.0060	926
26	731.25	760.50	782	0.0051	0.0052	796
27	760.50	789.75	649	0.0042	0.0042	646
28	789.75	819.00	549	0.0036	0.0035	533
29	819.00	848.25	477	0.0031	0.0029	454
30	848.25	877.50	430	0.0028	0.0026	406
31	877.50	906.75	548	0.0036	0.0039	594
32	906.75	936.00	531	0.0034	0.0039	594
33	936.00	965.25	357	0.0023	0.0023	362
34	965.25	994.50	229	0.0015	0.0012	185
35	994.50	1023.75	184	0.0012	0.0008	124
36	1023.75	1053.00	218	0.0014	0.0012	183
37	1053.00	1082.25	150	0.0010	0.0005	84
38	1082.25	1111.50	207	0.0013	0.0012	179
39	1111.50	1140.75	139	0.0009	0.0005	77
40	1140.75	1170.00	166	0.0011	0.0008	125
41	1170.00	1199.25	129	0.0008	0.0004	69
42	1199.25	1228.50	127	0.0008	0.0004	69
43	1228.50	1257.75	242	0.0016	0.0018	273
44	1257.75	1287.00	150	0.0010	0.0008	124
45	1287.00	1316.25	226	0.0015	0.0017	267
46	1316.25	1345.50	255	0.0017	0.0022	335
47	1345.50	1374.75	151	0.0010	0.0010	159
48	1374.75	1404.00	156	0.0010	0.0012	178
49	1404.00	1433.25	125	0.0008	0.0008	128
50	1433.25	1462.50	214	0.0014	0.0020	311

Table C.18 continued

CLASS	LIMITS (μm)		MEASURED CHORDS	MEASURED N_L (#/cm)	TRUE[1] N_L (#/cm)	TRUE[1] CHORDS
51	1462.50	1491.75	165	0.0011	0.0015	230
52	1491.75	1521.00	157	0.0010	0.0015	228
53	1521.00	1550.25	119	0.0008	0.0011	162
54	1550.25	1579.50	60	0.0004	0.0003	46
55	1579.50	1608.75	90	0.0006	0.0007	115
56	1608.75	1638.00	72	0.0005	0.0005	82
57	1638.00	1667.25	81	0.0005	0.0007	108
58	1667.25	1696.50	66	0.0004	0.0005	80
59	1696.50	1725.75	86	0.0006	0.0009	134
60	1725.75	1755.00	25	0.0002	0.0000	-6
61	1755.00	1784.25	31	0.0002	0.0001	9
62	1784.25	1813.50	24	0.0002	-0.0001	-8
63	1813.50	1842.75	27	0.0002	0.0000	-1
64	1842.75	1872.00	32	0.0002	0.0001	12
65	1872.00	1901.25	33	0.0002	0.0001	16
66	1901.25	1930.50	39	0.0003	0.0002	34
67	1930.50	1959.75	33	0.0002	0.0001	20
68	1959.75	1989.00	41	0.0003	0.0003	46
69	1989.00	2018.25	29	0.0002	0.0001	13
70	2018.25	2047.50	48	0.0003	0.0005	75
71	2047.50	2076.75	54	0.0004	0.0007	102
72	2076.75	2106.00	47	0.0003	0.0006	88
73	2106.00	2135.25	62	0.0004	0.0010	150
74	2135.25	2164.50	34	0.0002	0.0004	64
75	2164.50	2193.75	62	0.0004	0.0012	178
76	2193.75	2223.00	29	0.0002	0.0004	68
77	2223.00	2252.25	9	0.0001	0.0000	-7
78	2252.25	2281.50	9	0.0001	0.0000	-7
79	2281.50	2310.75	13	0.0001	0.0001	10
80	2310.75	2340.00	17	0.0001	0.0002	30
81	2340.00	2369.25	22	0.0001	0.0004	58
82	2369.25	2398.50	46	0.0003	0.0012	191
83	2398.50	2427.75	27	0.0002	0.0008	118
84	2427.75	2457.00	15	0.0001	0.0004	69
85	2457.00	2486.25	15	0.0001	0.0005	81
Totals			500054	3.247	3.074	473339
Average Chord Length (μm)				160.3	169.3	
Air Content (%)				5.21	5.20	
Powers Spacing Factor (μm)				150	158	

1. Calculated using Eq. 3.14

Table C.19 Analysis of mix 9, magnification 30x, lineal data using 85 classes of 29.25 μm width

			MEASURED		TRUE[1]	
CLASS	LIMITS (μm)		CHORDS	N_L (#/cm)	N_L (#/cm)	CHORDS
1	0.00	29.25	82777	0.5354	0.4896	75699
2	29.25	58.50	48748	0.3153	0.2787	43091
3	58.50	87.75	46561	0.3012	0.2725	42134
4	87.75	117.00	44251	0.2862	0.2653	41009
5	117.00	146.25	39007	0.2523	0.2376	36737
6	146.25	175.50	32979	0.2133	0.2034	31450
7	175.50	204.75	27647	0.1788	0.1726	26691
8	204.75	234.00	22281	0.1441	0.1403	21692
9	234.00	263.25	18096	0.1171	0.1150	17780
10	263.25	292.50	14425	0.0933	0.0923	14270
11	292.50	321.75	11569	0.0748	0.0745	11523
12	321.75	351.00	9071	0.0587	0.0586	9062
13	351.00	380.25	7065	0.0457	0.0457	7058
14	380.25	409.50	5873	0.0380	0.0382	5910
15	409.50	438.75	4596	0.0297	0.0298	4609
16	438.75	468.00	3685	0.0238	0.0238	3684
17	468.00	497.25	3394	0.0220	0.0224	3463
18	497.25	526.50	2608	0.0169	0.0170	2628
19	526.50	555.75	2235	0.0145	0.0146	2262
20	555.75	585.00	1957	0.0127	0.0129	1998
21	585.00	614.25	1554	0.0101	0.0101	1561
22	614.25	643.50	1131	0.0073	0.0070	1078
23	643.50	672.75	1144	0.0074	0.0073	1136
24	672.75	702.00	1224	0.0079	0.0083	1285
25	702.00	731.25	1069	0.0069	0.0073	1128
26	731.25	760.50	886	0.0057	0.0060	926
27	760.50	789.75	724	0.0047	0.0048	742
28	789.75	819.00	693	0.0045	0.0047	729
29	819.00	848.25	647	0.0042	0.0045	694
30	848.25	877.50	574	0.0037	0.0040	619
31	877.50	906.75	350	0.0023	0.0021	322
32	906.75	936.00	467	0.0030	0.0033	507
33	936.00	965.25	447	0.0029	0.0032	500
34	965.25	994.50	399	0.0026	0.0029	449
35	994.50	1023.75	254	0.0016	0.0016	247
36	1023.75	1053.00	218	0.0014	0.0013	203
37	1053.00	1082.25	138	0.0009	0.0006	86
38	1082.25	1111.50	119	0.0008	0.0004	60
39	1111.50	1140.75	188	0.0012	0.0011	175
40	1140.75	1170.00	203	0.0013	0.0013	208
41	1170.00	1199.25	232	0.0015	0.0017	267
42	1199.25	1228.50	135	0.0009	0.0007	115
43	1228.50	1257.75	105	0.0007	0.0004	68
44	1257.75	1287.00	115	0.0007	0.0006	89
45	1287.00	1316.25	128	0.0008	0.0008	118
46	1316.25	1345.50	153	0.0010	0.0011	170
47	1345.50	1374.75	168	0.0011	0.0013	207
48	1374.75	1404.00	149	0.0010	0.0012	182
49	1404.00	1433.25	104	0.0007	0.0007	106
50	1433.25	1462.50	89	0.0006	0.0005	82

Table C.19 continued

CLASS	LIMITS (μm)		MEASURED CHORDS	MEASURED N_L (#/cm)	TRUE[1] N_L (#/cm)	TRUE[1] CHORDS
51	1462.50	1491.75	124	0.0008	0.0010	157
52	1491.75	1521.00	131	0.0008	0.0012	181
53	1521.00	1550.25	129	0.0008	0.0012	188
54	1550.25	1579.50	132	0.0009	0.0013	206
55	1579.50	1608.75	74	0.0005	0.0006	93
56	1608.75	1638.00	113	0.0007	0.0012	186
57	1638.00	1667.25	86	0.0006	0.0009	137
58	1667.25	1696.50	34	0.0002	0.0002	25
59	1696.50	1725.75	84	0.0005	0.0009	146
60	1725.75	1755.00	130	0.0008	0.0017	269
61	1755.00	1784.25	54	0.0003	0.0006	98
62	1784.25	1813.50	29	0.0002	0.0003	41
63	1813.50	1842.75	8	0.0001	-0.0001	-11
64	1842.75	1872.00	14	0.0001	0.0000	5
65	1872.00	1901.25	16	0.0001	0.0001	11
66	1901.25	1930.50	22	0.0001	0.0002	29
67	1930.50	1959.75	28	0.0002	0.0003	49
68	1959.75	1989.00	8	0.0001	0.0000	-7
69	1989.00	2018.25	12	0.0001	0.0000	4
70	2018.25	2047.50	6	0.0000	-0.0001	-14
71	2047.50	2076.75	6	0.0000	-0.0001	-16
72	2076.75	2106.00	18	0.0001	0.0002	24
73	2106.00	2135.25	6	0.0000	-0.0001	-16
74	2135.25	2164.50	19	0.0001	0.0002	30
75	2164.50	2193.75	19	0.0001	0.0002	33
76	2193.75	2223.00	24	0.0002	0.0004	57
77	2223.00	2252.25	16	0.0001	0.0002	30
78	2252.25	2281.50	21	0.0001	0.0004	56
79	2281.50	2310.75	17	0.0001	0.0003	45
80	2310.75	2340.00	21	0.0001	0.0005	70
81	2340.00	2369.25	33	0.0002	0.0009	139
82	2369.25	2398.50	2	0.0000	0.0000	0
83	2398.50	2427.75	9	0.0001	0.0002	38
84	2427.75	2457.00	8	0.0001	0.0003	39
85	2457.00	2486.25	4	0.0000	0.0001	22
Totals			44089	2.873	2.711	419154
Average Chord Length (μm)				168.5	178.5	
Air Content (%)				4.84	4.84	
Powers Spacing Factor (μm)				175	185	

1. Calculated using Eq. 3.14

Table C.20 Analysis of mix10, magnification 30x, lineal data using 85 classes of 29.25 μm width

			MEASURED		TRUE[1]	
CLASS	LIMITS (μm)		CHORDS	N_L (#/cm)	N_L (#/cm)	CHORDS
1	0.00	29.25	88040	0.5695	0.4970	76832
2	29.25	58.50	76398	0.4942	0.4347	67206
3	58.50	87.75	67851	0.4389	0.3907	60396
4	87.75	117.00	64226	0.4154	0.3781	58455
5	117.00	146.25	60183	0.3893	0.3622	55992
6	146.25	175.50	51769	0.3349	0.3154	48760
7	175.50	204.75	40250	0.2603	0.2450	37872
8	204.75	234.00	37851	0.2448	0.2359	36466
9	234.00	263.25	32259	0.2087	0.2036	31480
10	263.25	292.50	28551	0.1847	0.1835	28376
11	292.50	321.75	25921	0.1677	0.1704	26350
12	321.75	351.00	17598	0.1138	0.1148	17749
13	351.00	380.25	15049	0.0973	0.0997	15412
14	380.25	409.50	11188	0.0724	0.0740	11440
15	409.50	438.75	9052	0.0586	0.0603	9318
16	438.75	468.00	7598	0.0491	0.0512	7910
17	468.00	497.25	6968	0.0451	0.0481	7429
18	497.25	526.50	5304	0.0343	0.0366	5664
19	526.50	555.75	4027	0.0260	0.0278	4292
20	555.75	585.00	3329	0.0215	0.0231	3576
21	585.00	614.25	2932	0.0190	0.0207	3206
22	614.25	643.50	2479	0.0160	0.0178	2746
23	643.50	672.75	2187	0.0141	0.0160	2471
24	672.75	702.00	1937	0.0125	0.0145	2238
25	702.00	731.25	1612	0.0104	0.0122	1893
26	731.25	760.50	1246	0.0081	0.0095	1474
27	760.50	789.75	1016	0.0066	0.0079	1218
28	789.75	819.00	803	0.0052	0.0063	972
29	819.00	848.25	594	0.0038	0.0046	719
30	848.25	877.50	389	0.0025	0.0030	457
31	877.50	906.75	305	0.0020	0.0023	355
32	906.75	936.00	246	0.0016	0.0018	284
33	936.00	965.25	198	0.0013	0.0015	225
34	965.25	994.50	181	0.0012	0.0014	209
35	994.50	1023.75	156	0.0010	0.0012	180
36	1023.75	1053.00	121	0.0008	0.0009	134
37	1053.00	1082.25	103	0.0007	0.0007	112
38	1082.25	1111.50	76	0.0005	0.0005	74
39	1111.50	1140.75	78	0.0005	0.0005	80
40	1140.75	1170.00	69	0.0004	0.0004	69
41	1170.00	1199.25	66	0.0004	0.0004	68
42	1199.25	1228.50	58	0.0004	0.0004	58
43	1228.50	1257.75	58	0.0004	0.0004	60
44	1257.75	1287.00	63	0.0004	0.0005	72
45	1287.00	1316.25	61	0.0004	0.0005	73
46	1316.25	1345.50	51	0.0003	0.0004	58
47	1345.50	1374.75	49	0.0003	0.0004	58
48	1374.75	1404.00	45	0.0003	0.0003	53
49	1404.00	1433.25	43	0.0003	0.0003	52
50	1433.25	1462.50	41	0.0003	0.0003	52

Table C.20 continued

CLASS	LIMITS (μm)		MEASURED CHORDS	MEASURED N_L (#/cm)	TRUE[1] N_L (#/cm)	TRUE[1] CHORDS
51	1462.50	1491.75	36	0.0002	0.0003	45
52	1491.75	1521.00	34	0.0002	0.0003	43
53	1521.00	1550.25	31	0.0002	0.0003	40
54	1550.25	1579.50	32	0.0002	0.0003	44
55	1579.50	1608.75	29	0.0002	0.0003	40
56	1608.75	1638.00	25	0.0002	0.0002	34
57	1638.00	1667.25	23	0.0001	0.0002	32
58	1667.25	1696.50	21	0.0001	0.0002	29
59	1696.50	1725.75	18	0.0001	0.0002	24
60	1725.75	1755.00	14	0.0001	0.0001	16
61	1755.00	1784.25	16	0.0001	0.0001	22
62	1784.25	1813.50	16	0.0001	0.0002	24
63	1813.50	1842.75	12	0.0001	0.0001	15
64	1842.75	1872.00	9	0.0001	0.0001	8
65	1872.00	1901.25	9	0.0001	0.0001	9
66	1901.25	1930.50	9	0.0001	0.0001	10
67	1930.50	1959.75	11	0.0001	0.0001	17
68	1959.75	1989.00	9	0.0001	0.0001	12
69	1989.00	2018.25	8	0.0001	0.0001	10
70	2018.25	2047.50	7	0.0000	0.0001	8
71	2047.50	2076.75	8	0.0001	0.0001	12
72	2076.75	2106.00	7	0.0000	0.0001	10
73	2106.00	2135.25	8	0.0001	0.0001	14
74	2135.25	2164.50	7	0.0000	0.0001	12
75	2164.50	2193.75	7	0.0000	0.0001	13
76	2193.75	2223.00	6	0.0000	0.0001	11
77	2223.00	2252.25	7	0.0000	0.0001	16
78	2252.25	2281.50	6	0.0000	0.0001	14
79	2281.50	2310.75	5	0.0000	0.0001	12
80	2310.75	2340.00	6	0.0000	0.0001	18
81	2340.00	2369.25	3	0.0000	0.0000	6
82	2369.25	2398.50	5	0.0000	0.0001	17
83	2398.50	2427.75	5	0.0000	0.0001	20
84	2427.75	2457.00	6	0.0000	0.0002	29
85	2457.00	2486.25	4	0.0000	0.0001	22
Totals			671134	4.341	4.084	631402
Average Chord Length (μm)				177.7	188.8	
Air Content (%)				7.71	7.71	
Powers Spacing Factor (μm)				142	151	

1. Calculated using Eq. 3.14

Table C.21 Chords not included in analysis of magnification 12x data

	Mix									
Class[1]	1	2	3	4	5	6	7	8	9	10
86	0	8	8	28	10	5	20	5	2	3
87	4	7	17	26	5	5	15	3	0	5
88	5	5	13	21	6	21	6	15	0	6
89	7	8	16	26	8	10	9	14	3	1
90	2	1	41	20	5	17	10	18	3	6
91	1	1	13	12	3	15	14	5	2	10
92	1	1	15	9	0	5	4	7	3	12
93	1	2	47	6	4	8	20	8	3	9
94	0	3	18	7	2	9	23	0	6	12
95	0	1	0	8	8	0	0	0	0	8
96	0	2	37	10	12	32	16	9	8	6
97	4	2	18	11	6	24	0	10	14	5
98	5	1	12	7	9	11	1	17	3	5
99	3	2	15	21	9	7	1	12	10	4
100	7	2	18	9	5	0	0	23	12	2
101	1	0	26	16	6	1	2	7	9	0
102	0	1	11	9	6	3	3	2	5	1
103	0	1	3	14	4	1	4	1	11	0
104	0	0	0	12	2	0	3	3	15	2
105	1	4	0	10	0	10	1	0	5	0
106	1	2	0	22	1	2	1	7	2	1
107	5	3	0	14	0	4	1	17	6	0
108	3	4	0	3	2	1	3	16	4	1
109	6	2	0	1	6	5	1	15	1	1
110	2	2	0	5	6	7	1	1	2	2
111	5	2	0	11	3	1	2	1	1	0
112	4	1	0	8	4	6	1	0	0	0
113	0	1	0	1	2	1	7	0	1	1
114	2	1	0	3	0	0	5	10	0	0
115	1	1	0	6	1	0	3	0	2	0
116	0	1	0	2	0	0	9	0	1	0
117	0	3	0	0	0	0	3	0	0	2
118	1	3	0	5	0	2	5	0	0	1
119	1	3	0	3	2	2	2	0	0	0
120	2	4	0	4	0	7	3	0	0	0
121	3	2	0	5	1	4	4	0	0	0
122	3	1	0	2	0	2	6	0	0	0
123	4	3	0	3	0	4	3	0	0	0
124	1	1	0	4	0	13	6	0	0	0

Table C.21 continued

	Mix									
Class[1]	1	2	3	4	5	6	7	8	9	10
125	2	3	0	4	0	9	3	0	0	0
126	3	5	0	1	0	12	5	0	0	0
127	1	10	0	7	0	3	4	0	0	0
128	0	10	0	1	0	1	8	0	0	0
129	0	5	0	3	0	1	3	0	0	0
130	1	3	0	3	0	1	6	0	0	0
131	1	5	0	9	0	3	10	0	0	0
132	0	7	0	2	0	1	3	0	0	0
133	0	4	0	3	0	0	21	0	0	0
134	1	8	0	2	0	0	13	0	0	0
135	1	2	0	2	0	2	12	0	0	0
136	2	8	0	2	0	3	11	0	0	0
137	2	5	0	2	0	2	2	0	0	0
138	4	1	0	2	0	0	0	0	0	0
139	3	5	0	2	0	0	0	0	0	0
140	3	1	0	1	0	0	1	0	0	0
141	1	0	0	2	0	0	0	0	0	0
142	0	0	0	0	0	0	0	0	0	0
143	0	0	0	1	0	0	0	0	0	0
144	0	0	0	2	0	0	0	0	0	0
145	0	0	0	1	0	0	0	0	0	0

1. Class size = 29.25 μm

Table C.22 Chords not included in analysis of magnification 30x data

	Mix									
Class[1]	1	2	3	4	5	6	7	8	9	10
86	0	0	4	13	16	36	14	9	0	22
87	0	0	6	35	16	36	20	13	0	24
88	0	0	4	0	37	43	6	10	0	50
89	0	0	28	0	30	57	8	22	0	58
90	0	0	21	0	31	75	0	13	0	36
91	0	0	45	0	27	52	7	11	0	27
92	0	0	87	0	26	67	4	20	0	27
93	0	0	29	0	29	22	10	18	0	134
94	0	0	55	2	19	31	1	45	0	52
95	0	0	3	21	5	40	13	30	0	16
96	0	0	4	0	14	37	11	22	0	11
97	0	0	9	0	30	26	5	0	0	40
98	0	0	0	0	92	25	13	0	0	16
99	0	0	0	0	42	57	21	0	0	23
100	0	0	2	0	14	31	1	0	0	2
101	0	0	6	0	26	46	5	0	0	0
102	0	0	0	0	0	30	35	0	0	13
103	0	0	0	0	99	500	679	0	0	311

1. Class size = 29.41 μm

APPENDIX D

Edge effect correction and area-to-volume conversion of areal image analysis data

Table D.1 Analysis of mix 1, magnification 12x, areal data using 85 classes of 25 μm width

CLASS	LIMITS (μm)		MEASURED[1]		TRUE[2]		
			FEATURES	N_A (#/cm^2)	N_A (#/cm^2)	FEATURES	N_V(#/cm^3)[3]
1	0	25	1349	18.598	17.849	1295	3592.90
2	25	50	2677	36.906	36.380	2639	10486.67
3	50	75	1102	15.193	14.912	1082	2745.23
4	75	100	595	8.203	8.037	583	1250.99
5	100	125	304	4.191	4.056	294	432.07
6	125	150	213	2.936	2.836	206	260.99
7	150	175	152	2.096	2.017	146	167.43
8	175	200	105	1.448	1.378	100	116.06
9	200	225	70	0.965	0.894	65	30.28
10	225	250	69	0.951	0.900	65	60.86
11	250	275	48	0.662	0.606	44	20.06
12	275	300	47	0.648	0.605	44	19.43
13	300	325	45	0.620	0.589	43	25.76
14	325	350	37	0.510	0.482	35	19.70
15	350	375	33	0.455	0.433	31	8.51
16	375	400	32	0.441	0.431	31	31.70
17	400	425	16	0.221	0.191	14	-5.95
18	425	450	23	0.317	0.307	22	15.60
19	450	475	16	0.221	0.204	15	2.11
20	475	500	17	0.234	0.226	16	10.71
21	500	525	11	0.152	0.136	10	3.55
22	525	550	11	0.152	0.139	10	-1.80
23	550	575	13	0.179	0.176	13	13.07
24	575	600	5	0.069	0.048	3	-7.61
25	600	625	12	0.165	0.167	12	7.02
26	625	650	9	0.124	0.122	9	0.87
27	650	675	9	0.124	0.127	9	10.14
28	675	700	1	0.014	-0.007	0	-2.22
29	700	725	3	0.041	0.026	2	-3.47
30	725	750	6	0.083	0.079	6	2.61
31	750	775	5	0.069	0.063	5	-1.75
32	775	800	7	0.097	0.101	7	4.81
33	800	825	4	0.055	0.051	4	-0.84
34	825	850	5	0.069	0.071	5	3.28
35	850	875	3	0.041	0.037	3	-1.43
36	875	900	5	0.069	0.075	5	2.30
37	900	925	3	0.041	0.042	3	3.72
38	925	950	0	0.000	-0.014	-1	-3.51
39	950	975	3	0.041	0.042	3	0.95
40	975	1000	3	0.041	0.043	3	-0.99
41	1000	1025	4	0.055	0.065	5	4.18
42	1025	1050	1	0.014	0.009	1	-2.10
43	1050	1075	3	0.041	0.049	4	2.65
44	1075	1100	1	0.014	0.011	1	-0.10
45	1100	1125	1	0.014	0.012	1	1.00
46	1125	1150	0	0.000	-0.008	-1	-0.82
47	1150	1175	1	0.014	0.011	1	-1.18
48	1175	1200	2	0.028	0.033	2	2.38
49	1200	1225	0	0.000	-0.007	-1	-1.13
50	1225	1250	1	0.014	0.013	1	0.17

Table D.1 Continued

			MEASURED[1]		TRUE[2]		
CLASS	LIMITS (μm)		FEATURES	N_A (#/cm^2)	N_A (#/cm^2)	FEATURES	N_V(#/cm^3)[3]
51	1250	1275	1	0.014	0.014	1	0.05
52	1275	1300	1	0.014	0.014	1	0.76
53	1300	1325	0	0.000	-0.007	-1	0.30
54	1325	1350	0	0.000	-0.008	-1	-2.66
55	1350	1375	2	0.028	0.036	3	2.92
56	1375	1400	0	0.000	-0.008	-1	-3.43
57	1400	1425	3	0.041	0.060	4	3.73
58	1425	1450	0	0.000	-0.005	0	-1.18
59	1450	1475	1	0.014	0.018	1	1.02
60	1475	1500	0	0.000	-0.005	0	-0.15
61	1500	1525	0	0.000	-0.006	0	-0.77
62	1525	1550	1	0.014	0.017	1	-0.99
63	1550	1575	2	0.028	0.043	3	2.26
64	1575	1600	0	0.000	-0.003	0	0.15
65	1600	1625	0	0.000	-0.004	0	-1.16
66	1625	1650	1	0.014	0.021	2	1.19
67	1650	1675	0	0.000	-0.003	0	-0.21
68	1675	1700	0	0.000	-0.003	0	0.15
69	1700	1725	0	0.000	-0.004	0	-1.27
70	1725	1750	1	0.014	0.022	2	1.27
71	1750	1775	0	0.000	-0.003	0	-0.93
72	1775	1800	1	0.014	0.023	2	0.12
73	1800	1825	1	0.014	0.024	2	1.24
74	1825	1850	0	0.000	-0.001	0	-0.02
75	1850	1875	0	0.000	-0.001	0	-0.02
76	1875	1900	0	0.000	-0.001	0	-0.04
77	1900	1925	0	0.000	-0.001	0	0.00
78	1925	1950	0	0.000	-0.001	0	-0.16
79	1950	1975	0	0.000	-0.001	0	0.20
80	1975	2000	0	0.000	-0.002	0	-1.16
81	2000	2025	1	0.014	0.027	2	1.29
82	2025	2050	0	0.000	0.000	0	0.00
83	2050	2075	0	0.000	0.000	0	0.00
84	2075	2100	0	0.000	0.000	0	0.00
85	2100	2125	0	0.000	0.000	0	0.00
Totals			7098	97.86	95.30	6913	19327.35
Average Feature Diameter (μm)				85.5	85.2		49.3
Air Content (%)				2.03	2.03		2.02
Powers Spacing Factor (μm)				435	448		451
Philleo Factor (μm)				--	--		212

1. Features not included in analysis include: 1 in class 97 and 1 in class 99
2. Calculated using Eq. 3.29
3. Calculated using Eq. 3.54

Table D.2 Analysis of mix 2, magnification 12x, areal data using 85 classes of 25 μm width

			MEASURED[1]		TRUE[2]		
CLASS	LIMITS (μm)		FEATURES	N_A (#/cm^2)	N_A (#/cm^2)	FEATURES	N_V(#/cm^3)[3]
1	0	25	1173	16.171	15.500	1124	3048.33
2	25	50	2357	32.494	32.007	2322	9027.70
3	50	75	1050	14.476	14.221	1032	2519.13
4	75	100	601	8.286	8.157	592	1351.48
5	100	125	271	3.736	3.628	263	374.67
6	125	150	194	2.675	2.602	189	271.14
7	150	175	119	1.641	1.576	114	143.56
8	175	200	75	1.034	0.969	70	68.77
9	200	225	59	0.813	0.754	55	16.11
10	225	250	64	0.882	0.845	61	57.38
11	250	275	48	0.662	0.627	45	12.21
12	275	300	49	0.676	0.659	48	60.61
13	300	325	22	0.303	0.266	19	-11.08
14	325	350	34	0.469	0.456	33	30.46
15	350	375	21	0.290	0.269	19	6.11
16	375	400	19	0.262	0.245	18	20.96
17	400	425	8	0.110	0.079	6	-10.42
18	425	450	17	0.234	0.222	16	11.46
19	450	475	11	0.152	0.133	10	4.28
20	475	500	9	0.124	0.104	8	2.03
21	500	525	9	0.124	0.106	8	-0.90
22	525	550	11	0.152	0.141	10	4.79
23	550	575	9	0.124	0.113	8	1.83
24	575	600	8	0.110	0.099	7	4.70
25	600	625	6	0.083	0.068	5	-5.29
26	625	650	11	0.152	0.154	11	7.88
27	650	675	6	0.083	0.074	5	-0.35
28	675	700	8	0.110	0.110	8	0.31
29	700	725	9	0.124	0.133	10	7.59
30	725	750	3	0.041	0.033	2	2.71
31	750	775	1	0.014	-0.003	0	-4.31
32	775	800	5	0.069	0.068	5	1.12
33	800	825	4	0.055	0.052	4	2.92
34	825	850	3	0.041	0.035	3	-5.31
35	850	875	8	0.110	0.129	9	8.66
36	875	900	1	0.014	0.005	0	-0.09
37	900	925	1	0.014	0.005	0	-1.51
38	925	950	3	0.041	0.042	3	-1.08
39	950	975	4	0.055	0.063	5	4.76
40	975	1000	0	0.000	-0.011	-1	-1.94
41	1000	1025	2	0.028	0.026	2	-0.90
42	1025	1050	3	0.041	0.047	3	2.41
43	1050	1075	1	0.014	0.010	1	0.09
44	1075	1100	1	0.014	0.010	1	-0.68
45	1100	1125	2	0.028	0.030	2	-0.02
46	1125	1150	2	0.028	0.032	2	2.45
47	1150	1175	0	0.000	-0.008	-1	-1.48
48	1175	1200	1	0.014	0.012	1	1.10
49	1200	1225	0	0.000	-0.009	-1	-1.92
50	1225	1250	2	0.028	0.032	2	-0.48

Table D.2 Continued

			MEASURED[1]		TRUE[2]		
CLASS	LIMITS (μm)		FEATURES	N_A (#/cm^2)	N_A (#/cm^2)	FEATURES	N_V(#/cm^3)[3]
51	1250	1275	3	0.041	0.055	4	1.45
52	1275	1300	2	0.028	0.037	3	2.21
53	1300	1325	0	0.000	-0.004	0	0.15
54	1325	1350	0	0.000	-0.005	0	-1.26
55	1350	1375	1	0.014	0.017	1	1.35
56	1375	1400	0	0.000	-0.004	0	-1.14
57	1400	1425	1	0.014	0.018	1	1.17
58	1425	1450	0	0.000	-0.004	0	-0.19
59	1450	1475	0	0.000	-0.004	0	0.12
60	1475	1500	0	0.000	-0.005	0	-1.12
61	1500	1525	1	0.014	0.019	1	1.01
62	1525	1550	0	0.000	-0.004	0	0.16
63	1550	1575	0	0.000	-0.004	0	-1.27
64	1575	1600	1	0.014	0.020	1	1.37
65	1600	1625	0	0.000	-0.004	0	-1.14
66	1625	1650	1	0.014	0.021	2	1.18
67	1650	1675	0	0.000	-0.003	0	-0.08
68	1675	1700	0	0.000	-0.003	0	-0.05
69	1700	1725	0	0.000	-0.004	0	-0.23
70	1725	1750	0	0.000	-0.004	0	0.15
71	1750	1775	0	0.000	-0.005	0	-1.34
72	1775	1800	1	0.014	0.021	2	1.39
73	1800	1825	0	0.000	-0.005	0	-1.32
74	1825	1850	1	0.014	0.022	2	1.29
75	1850	1875	0	0.000	-0.004	0	-1.09
76	1875	1900	1	0.014	0.023	2	0.32
77	1900	1925	1	0.014	0.024	2	0.13
78	1925	1950	1	0.014	0.026	2	1.28
79	1950	1975	0	0.000	0.000	0	0.00
80	1975	2000	0	0.000	0.000	0	0.00
81	2000	2025	0	0.000	0.000	0	0.00
82	2025	2050	0	0.000	0.000	0	0.00
83	2050	2075	0	0.000	0.000	0	0.00
84	2075	2100	0	0.000	0.000	0	0.00
85	2100	2125	0	0.000	0.000	0	0.00
Totals			6340	87.41	85.16	6177	17036.39
Average Feature Diameter (μm)				84.1	83.8		50.0
Air Content (%)				1.80	1.80		1.79
Powers Spacing Factor (μm)				457	471		474
Philleo Factor (μm)				--	--		224

1. Features not included in analysis include: 1 in class 90, 2 in class 95,1 in class 127, and 1 in class 135
2. Calculated using Eq. 3.29
3. Calculated using Eq. 3.54

Table D.3 Continued

CLASS	LIMITS (μm)		MEASURED[1] FEATURES	MEASURED[1] N_A (#/cm^2)	TRUE[2] N_A (#/cm^2)	TRUE[2] FEATURES	N_V(#/cm^3)[3]
51	1250	1275	3	0.047	0.058	4	1.88
52	1275	1300	2	0.031	0.037	2	0.08
53	1300	1325	2	0.031	0.039	2	1.90
54	1325	1350	1	0.016	0.016	1	-1.46
55	1350	1375	2	0.031	0.042	3	3.12
56	1375	1400	0	0.000	-0.007	0	-2.65
57	1400	1425	2	0.031	0.044	3	2.90
58	1425	1450	0	0.000	-0.005	0	-1.29
59	1450	1475	1	0.016	0.021	1	1.30
60	1475	1500	0	0.000	-0.004	0	-0.11
61	1500	1525	0	0.000	-0.005	0	-0.09
62	1525	1550	0	0.000	-0.005	0	-0.28
63	1550	1575	0	0.000	-0.006	0	0.09
64	1575	1600	0	0.000	-0.007	0	-1.46
65	1600	1625	1	0.016	0.020	1	1.19
66	1625	1650	0	0.000	-0.007	0	-0.85
67	1650	1675	1	0.016	0.020	1	-1.33
68	1675	1700	2	0.031	0.051	3	2.98
69	1700	1725	0	0.000	-0.004	0	-1.45
70	1725	1750	1	0.016	0.025	2	1.57
71	1750	1775	0	0.000	-0.004	0	-1.28
72	1775	1800	1	0.016	0.026	2	1.22
73	1800	1825	0	0.000	-0.002	0	0.20
74	1825	1850	0	0.000	-0.003	0	-1.32
75	1850	1875	1	0.016	0.028	2	1.42
76	1875	1900	0	0.000	-0.001	0	-0.18
77	1900	1925	0	0.000	-0.002	0	0.23
78	1925	1950	0	0.000	-0.002	0	-1.30
79	1950	1975	1	0.016	0.030	2	1.45
80	1975	2000	0	0.000	0.000	0	0.00
81	2000	2025	0	0.000	0.000	0	0.00
82	2025	2050	0	0.000	0.000	0	0.00
83	2050	2075	0	0.000	0.000	0	0.00
84	2075	2100	0	0.000	0.000	0	0.00
85	2100	2125	0	0.000	0.000	0	0.00
Totals			21622	337.83	328.10	20999	48209.48
Average Feature Diameter (μm)				93.8	94.7		68.1
Air Content (%)				5.04	5.04		5.01
Powers Spacing Factor (μm)				179	182		182
Philleo Factor (μm)				--	--		133

1. Features not included in analysis include: 1 in class 90, 1 in class 100, 1 in class 107, and 1 in class 121
2. Calculated using Eq. 3.29
3. Calculated using Eq. 3.54

Table D.4 Analysis of mix 4, magnification 12x, areal data using 85 classes of 25 μm width

			MEASURED[1]		TRUE[2]		
CLASS	LIMITS (μm)		FEATURES	N_A (#/cm^2)	N_A (#/cm^2)	FEATURES	N_V(#/cm^3)[3]
1	0	25	4047	55.793	51.564	3740	1446.13
2	25	50	10822	149.196	144.882	10509	30905.15
3	50	75	8562	118.039	115.314	8364	17466.38
4	75	100	6202	85.503	84.182	6106	12391.93
5	100	125	3509	48.376	47.620	3454	5217.88
6	125	150	2338	32.233	31.915	2315	3547.97
7	150	175	1338	18.446	18.217	1321	1515.38
8	175	200	942	12.987	12.906	936	1107.31
9	200	225	589	8.120	8.056	584	606.18
10	225	250	394	5.432	5.384	390	355.31
11	250	275	277	3.819	3.784	274	244.32
12	275	300	191	2.633	2.594	188	131.62
13	300	325	152	2.096	2.075	151	102.12
14	325	350	115	1.585	1.569	114	90.36
15	350	375	81	1.117	1.088	79	19.07
16	375	400	85	1.172	1.184	86	66.57
17	400	425	54	0.744	0.734	53	28.40
18	425	450	44	0.607	0.598	43	20.17
19	450	475	38	0.524	0.521	38	17.07
20	475	500	31	0.427	0.424	31	19.49
21	500	525	23	0.317	0.307	22	-0.95
22	525	550	28	0.386	0.400	29	20.26
23	550	575	16	0.221	0.215	16	7.69
24	575	600	13	0.179	0.172	12	-0.21
25	600	625	15	0.207	0.211	15	8.82
26	625	650	11	0.152	0.150	11	-0.40
27	650	675	13	0.179	0.190	14	9.74
28	675	700	7	0.097	0.094	7	1.09
29	700	725	7	0.097	0.097	7	3.79
30	725	750	5	0.069	0.066	5	0.38
31	750	775	5	0.069	0.068	5	3.78
32	775	800	2	0.028	0.017	1	-0.92
33	800	825	3	0.041	0.034	2	-1.25
34	825	850	4	0.055	0.053	4	1.52
35	850	875	4	0.055	0.054	4	-3.55
36	875	900	8	0.110	0.131	9	6.40
37	900	925	3	0.041	0.044	3	2.78
38	925	950	1	0.014	0.007	1	-2.07
39	950	975	3	0.041	0.045	3	1.49
40	975	1000	2	0.028	0.028	2	0.53
41	1000	1025	2	0.028	0.029	2	-0.02
42	1025	1050	2	0.028	0.031	2	2.35
43	1050	1075	0	0.000	-0.008	-1	-1.34
44	1075	1100	1	0.014	0.011	1	0.16
45	1100	1125	1	0.014	0.011	1	-1.03
46	1125	1150	2	0.028	0.032	2	0.66
47	1150	1175	2	0.028	0.033	2	-0.64
48	1175	1200	3	0.041	0.056	4	2.49
49	1200	1225	1	0.014	0.017	1	1.16
50	1225	1250	0	0.000	-0.003	0	-0.30

Table D.4 Continued

CLASS	LIMITS (μm)		MEASURED[1] FEATURES	MEASURED[1] N_A (#/cm^2)	TRUE[2] N_A (#/cm^2)	TRUE[2] FEATURES	N_V(#/cm^3)[3]
51	1250	1275	0	0.000	-0.003	0	0.22
52	1275	1300	0	0.000	-0.004	0	-1.96
53	1300	1325	2	0.028	0.039	3	1.34
54	1325	1350	1	0.014	0.020	1	1.20
55	1350	1375	0	0.000	-0.001	0	-0.02
56	1375	1400	0	0.000	-0.001	0	-0.02
57	1400	1425	0	0.000	-0.001	0	-0.03
58	1425	1450	0	0.000	-0.002	0	-0.03
59	1450	1475	0	0.000	-0.002	0	-0.05
60	1475	1500	0	0.000	-0.002	0	-0.02
61	1500	1525	0	0.000	-0.002	0	-0.16
62	1525	1550	0	0.000	-0.002	0	0.17
63	1550	1575	0	0.000	-0.003	0	-1.11
64	1575	1600	1	0.014	0.022	2	1.20
65	1600	1625	0	0.000	-0.001	0	-0.02
66	1625	1650	0	0.000	-0.002	0	-0.05
67	1650	1675	0	0.000	-0.002	0	-0.01
68	1675	1700	0	0.000	-0.002	0	-0.16
69	1700	1725	0	0.000	-0.002	0	0.18
70	1725	1750	0	0.000	-0.003	0	-1.13
71	1750	1775	1	0.014	0.023	2	1.23
72	1775	1800	0	0.000	-0.001	0	-0.02
73	1800	1825	0	0.000	-0.001	0	-0.03
74	1825	1850	0	0.000	-0.001	0	-0.03
75	1850	1875	0	0.000	-0.002	0	-0.05
76	1875	1900	0	0.000	-0.002	0	-0.02
77	1900	1925	0	0.000	-0.002	0	-0.19
78	1925	1950	0	0.000	-0.002	0	0.20
79	1950	1975	0	0.000	-0.003	0	-1.32
80	1975	2000	1	0.014	0.026	2	1.49
81	2000	2025	0	0.000	-0.002	0	-1.17
82	2025	2050	1	0.014	0.028	2	1.30
83	2050	2075	0	0.000	0.000	0	0.00
84	2075	2100	0	0.000	0.000	0	0.00
85	2100	2125	0	0.000	0.000	0	0.00
Totals			40005	551.5	537.3	38973	75362.17
Average Feature Diameter (μm)				83.8	84.7		71.3
Air Content (%)				5.78	5.78		5.72
Powers Spacing Factor (μm)				117	119		119
Philleo Factor (μm)				--	--		110

1. Features not included in analysis include: 1 in class 86, 1 in class 88, 1 in class 94, 1 in class 109, and 1 in class 118
2. Calculated using Eq. 3.29
3. Calculated using Eq. 3.54

Table D.5 Analysis of mix 5, magnification 12x, areal data using 85 classes of 25 μm width

			MEASURED[1]		TRUE[2]		
CLASS	LIMITS (μm)		FEATURES	N_A (#/cm^2)	N_A (#/cm^2)	FEATURES	N_V(#/cm^3)[3]
1	0	25	4621	63.707	60.380	4380	16668.89
2	25	50	8522	117.487	114.231	8286	25313.05
3	50	75	6372	87.847	85.768	6221	13168.26
4	75	100	4585	63.210	62.143	4508	8630.49
5	100	125	2822	38.905	38.361	2783	4367.68
6	125	150	1812	24.981	24.755	1796	2668.73
7	150	175	1067	14.710	14.582	1058	1370.03
8	175	200	668	9.209	9.133	662	720.69
9	200	225	452	6.231	6.200	450	508.67
10	225	250	274	3.777	3.728	270	239.10
11	250	275	201	2.771	2.739	199	149.63
12	275	300	155	2.137	2.123	154	131.13
13	300	325	108	1.489	1.470	107	61.36
14	325	350	91	1.255	1.253	91	73.49
15	350	375	59	0.813	0.796	58	35.03
16	375	400	48	0.662	0.647	47	16.02
17	400	425	46	0.634	0.635	46	31.48
18	425	450	33	0.455	0.449	33	10.86
19	450	475	30	0.414	0.416	30	23.50
20	475	500	19	0.262	0.251	18	-2.94
21	500	525	24	0.331	0.340	25	20.14
22	525	550	13	0.179	0.171	12	-2.15
23	550	575	18	0.248	0.259	19	8.70
24	575	600	14	0.193	0.203	15	11.02
25	600	625	7	0.097	0.092	7	2.89
26	625	650	6	0.083	0.078	6	-0.05
27	650	675	7	0.097	0.098	7	4.07
28	675	700	4	0.055	0.050	4	2.41
29	700	725	3	0.041	0.033	2	-3.87
30	725	750	7	0.097	0.105	8	4.53
31	750	775	4	0.055	0.056	4	2.64
32	775	800	2	0.028	0.022	2	0.40
33	800	825	2	0.028	0.023	2	-1.05
34	825	850	3	0.041	0.041	3	1.72
35	850	875	2	0.028	0.025	2	-0.85
36	875	900	3	0.041	0.044	3	1.56
37	900	925	2	0.028	0.027	2	0.30
38	925	950	2	0.028	0.028	2	0.46
39	950	975	2	0.028	0.029	2	0.25
40	975	1000	2	0.028	0.030	2	1.45
41	1000	1025	1	0.014	0.012	1	0.01
42	1025	1050	1	0.014	0.013	1	0.93
43	1050	1075	0	0.000	-0.006	0	-0.08
44	1075	1100	0	0.000	-0.007	-1	-1.31
45	1100	1125	1	0.014	0.012	1	0.31
46	1125	1150	1	0.014	0.012	1	-1.11
47	1150	1175	2	0.028	0.033	2	1.64
48	1175	1200	1	0.014	0.014	1	-1.10
49	1200	1225	2	0.028	0.036	3	2.28
50	1225	1250	0	0.000	-0.005	0	-0.72

Table D.5 Continued

CLASS	LIMITS (μm)		MEASURED[1] FEATURES	MEASURED[1] N_A (#/cm^2)	TRUE[2] N_A (#/cm^2)	TRUE[2] FEATURES	N_V(#/cm^3)[3]
51	1250	1275	1	0.014	0.016	1	-1.09
52	1275	1300	2	0.028	0.039	3	2.59
53	1300	1325	0	0.000	-0.003	0	-1.10
54	1325	1350	1	0.014	0.019	1	1.19
55	1350	1375	0	0.000	-0.002	0	-0.05
56	1375	1400	0	0.000	-0.002	0	-0.02
57	1400	1425	0	0.000	-0.002	0	-0.16
58	1425	1450	0	0.000	-0.002	0	0.17
59	1450	1475	0	0.000	-0.003	0	-1.10
60	1475	1500	1	0.014	0.021	1	1.19
61	1500	1525	0	0.000	-0.002	0	-0.02
62	1525	1550	0	0.000	-0.002	0	-0.03
63	1550	1575	0	0.000	-0.002	0	-0.04
64	1575	1600	0	0.000	-0.002	0	-0.04
65	1600	1625	0	0.000	-0.002	0	-0.08
66	1625	1650	0	0.000	-0.002	0	-0.01
67	1650	1675	0	0.000	-0.003	0	-0.31
68	1675	1700	0	0.000	-0.003	0	0.37
69	1700	1725	0	0.000	-0.004	0	-2.22
70	1725	1750	2	0.028	0.048	3	2.47
71	1750	1775	0	0.000	-0.001	0	-0.01
72	1775	1800	0	0.000	-0.001	0	-0.01
73	1800	1825	0	0.000	-0.001	0	-0.02
74	1825	1850	0	0.000	-0.001	0	-0.02
75	1850	1875	0	0.000	-0.001	0	-0.03
76	1875	1900	0	0.000	-0.001	0	-0.03
77	1900	1925	0	0.000	-0.002	0	-0.05
78	1925	1950	0	0.000	-0.002	0	-0.02
79	1950	1975	0	0.000	-0.002	0	-0.18
80	1975	2000	0	0.000	-0.002	0	0.16
81	2000	2025	0	0.000	-0.003	0	-1.17
82	2025	2050	1	0.014	0.026	2	1.14
83	2050	2075	0	0.000	-0.002	0	0.21
84	2075	2100	0	0.000	-0.002	0	-1.19
85	2100	2125	1	0.014	0.028	2	1.32
Totals			32130	442.96	432.07	31340	74242.34
Average Feature Diameter (μm)				79.9	80.7		58.2
Air Content (%)				4.41	4.41		4.36
Powers Spacing Factor (μm)				138	140		140
Philleo Factor (μm)				--	--		114

1. Features not included in analysis include: 1 in class 100, 1 in class 147, and 1 in class 166
2. Calculated using Eq. 3.29
3. Calculated using Eq. 3.54

Table D.6 Analysis of mix 6, magnification 12x, areal data using 85 classes of 25 μm width

			MEASURED [1]		TRUE[2]		
CLASS	LIMITS (μm)		FEATURES	N_A (#/cm^2)	N_A (#/cm^2)	FEATURES	N_V(#/cm^3)[3]
1	0	25	4330	59.695	55.910	4055	8453.84
2	25	50	9764	134.610	130.834	9490	28988.52
3	50	75	7337	101.150	98.714	7160	14675.39
4	75	100	5497	75.784	74.594	5411	10288.34
5	100	125	3398	46.846	46.318	3360	5593.30
6	125	150	2011	27.724	27.494	1994	3082.74
7	150	175	1115	15.372	15.201	1103	1436.98
8	175	200	695	9.582	9.455	686	692.73
9	200	225	506	6.976	6.924	502	530.10
10	225	250	334	4.605	4.561	331	290.13
11	250	275	244	3.364	3.343	242	215.34
12	275	300	165	2.275	2.248	163	140.63
13	300	325	114	1.572	1.536	111	55.70
14	325	350	103	1.420	1.412	102	76.08
15	350	375	74	1.020	1.006	73	43.25
16	375	400	57	0.786	0.772	56	44.23
17	400	425	37	0.510	0.480	35	4.36
18	425	450	43	0.593	0.589	43	19.06
19	450	475	35	0.483	0.481	35	31.72
20	475	500	17	0.234	0.205	15	-4.29
21	500	525	23	0.317	0.307	22	8.95
22	525	550	21	0.290	0.283	21	2.42
23	550	575	23	0.317	0.326	24	14.03
24	575	600	15	0.207	0.204	15	7.94
25	600	625	11	0.152	0.143	10	0.42
26	625	650	13	0.179	0.181	13	3.40
27	650	675	12	0.165	0.171	12	7.46
28	675	700	8	0.110	0.108	8	0.12
29	700	725	9	0.124	0.129	9	5.52
30	725	750	6	0.083	0.082	6	0.12
31	750	775	7	0.097	0.103	7	4.10
32	775	800	4	0.055	0.053	4	3.15
33	800	825	2	0.028	0.019	1	-2.33
34	825	850	4	0.055	0.056	4	3.03
35	850	875	2	0.028	0.021	2	-1.71
36	875	900	4	0.055	0.059	4	1.68
37	900	925	3	0.041	0.043	3	2.20
38	925	950	1	0.014	0.007	1	0.94
39	950	975	0	0.000	-0.012	-1	-1.69
40	975	1000	1	0.014	0.005	0	-0.29
41	1000	1025	2	0.028	0.024	2	-3.41
42	1025	1050	5	0.069	0.084	6	5.46
43	1050	1075	1	0.014	0.008	1	-2.81
44	1075	1100	4	0.055	0.069	5	2.63
45	1100	1125	2	0.028	0.032	2	2.31
46	1125	1150	0	0.000	-0.007	0	-0.28
47	1150	1175	0	0.000	-0.007	-1	-0.07
48	1175	1200	0	0.000	-0.008	-1	-1.17
49	1200	1225	1	0.014	0.012	1	0.19
50	1225	1250	1	0.014	0.013	1	-0.16

Table D.6 Continued

CLASS	LIMITS (μm)		MEASURED[1] FEATURES	MEASURED[1] N_A (#/cm^2)	TRUE[2] N_A (#/cm^2)	TRUE[2] FEATURES	N_V(#/cm^3)[3]
51	1250	1275	1	0.014	0.013	1	1.13
52	1275	1300	0	0.000	-0.008	-1	-1.29
53	1300	1325	1	0.014	0.013	1	0.26
54	1325	1350	1	0.014	0.013	1	-0.98
55	1350	1375	2	0.028	0.036	3	1.31
56	1375	1400	1	0.014	0.015	1	0.11
57	1400	1425	1	0.014	0.016	1	0.13
58	1425	1450	1	0.014	0.016	1	0.13
59	1450	1475	1	0.014	0.017	1	0.25
60	1475	1500	1	0.014	0.018	1	0.08
61	1500	1525	1	0.014	0.019	1	1.02
62	1525	1550	0	0.000	-0.003	0	0.03
63	1550	1575	0	0.000	-0.004	0	-1.05
64	1575	1600	1	0.014	0.020	1	0.31
65	1600	1625	1	0.014	0.021	2	0.12
66	1625	1650	1	0.014	0.023	2	1.22
67	1650	1675	0	0.000	-0.001	0	-0.01
68	1675	1700	0	0.000	-0.001	0	-0.02
69	1700	1725	0	0.000	-0.001	0	-0.02
70	1725	1750	0	0.000	-0.001	0	-0.02
71	1750	1775	0	0.000	-0.001	0	-0.02
72	1775	1800	0	0.000	-0.001	0	-0.05
73	1800	1825	0	0.000	-0.002	0	-0.01
74	1825	1850	0	0.000	-0.002	0	-0.16
75	1850	1875	0	0.000	-0.002	0	0.19
76	1875	1900	0	0.000	-0.003	0	-1.16
77	1900	1925	1	0.014	0.025	2	1.25
78	1925	1950	0	0.000	-0.001	0	-0.04
79	1950	1975	0	0.000	-0.001	0	0.00
80	1975	2000	0	0.000	-0.001	0	-0.16
81	2000	2025	0	0.000	-0.001	0	0.20
82	2025	2050	0	0.000	-0.002	0	-1.18
83	2050	2075	1	0.014	0.028	2	1.30
84	2075	2100	0	0.000	0.000	0	0.00
85	2100	2125	0	0.000	0.000	0	0.00
Totals			36077	497.37	484.84	35168.11	74723.15
Average Feature Diameter (μm)				81.9	82.7		64.9
Air Content (%)				5.26	5.26		5.21
Powers Spacing Factor (μm)				122	124		125
Philleo Factor (μm)				--	--		110

1. Features not included in analysis include: 1 in class 115 and 1 in class 217
2. Calculated using Eq. 3.29
3. Calculated using Eq. 3.54

Table D.7 Analysis of mix 7, magnification 12x, areal data using 85 classes of 25 μm width

			MEASURED[1]		TRUE[2]		
CLASS	LIMITS (μm)		FEATURES	N_A (#/cm^2)	N_A (#/cm^2)	FEATURES	N_V(#/cm^3)[3]
1	0	25	2074	28.593	26.962	1956	7950.74
2	25	50	3580	49.355	47.650	3456	11780.45
3	50	75	2279	31.419	29.997	2176	3840.90
4	75	100	1954	26.939	25.867	1876	3210.72
5	100	125	1413	19.480	18.626	1351	1509.66
6	125	150	1212	16.709	16.114	1169	1500.05
7	150	175	862	11.884	11.392	826	709.23
8	175	200	754	10.395	10.074	731	661.91
9	200	225	591	8.148	7.922	575	544.96
10	225	250	438	6.038	5.851	424	262.47
11	250	275	386	5.322	5.228	379	344.06
12	275	300	267	3.681	3.576	259	134.94
13	300	325	240	3.309	3.265	237	190.50
14	325	350	164	2.261	2.193	159	87.80
15	350	375	143	1.971	1.929	140	56.29
16	375	400	135	1.861	1.863	135	89.91
17	400	425	97	1.337	1.324	96	59.29
18	425	450	73	1.006	0.985	71	31.71
19	450	475	62	0.855	0.839	61	34.61
20	475	500	47	0.648	0.623	45	11.72
21	500	525	48	0.662	0.657	48	15.22
22	525	550	44	0.607	0.614	45	27.16
23	550	575	30	0.414	0.402	29	6.98
24	575	600	30	0.414	0.415	30	9.91
25	600	625	28	0.386	0.396	29	10.25
26	625	650	25	0.345	0.360	26	13.70
27	650	675	16	0.221	0.220	16	14.02
28	675	700	6	0.083	0.054	4	-6.12
29	700	725	13	0.179	0.176	13	-1.11
30	725	750	16	0.221	0.235	17	9.87
31	750	775	10	0.138	0.138	10	3.03
32	775	800	8	0.110	0.107	8	4.96
33	800	825	5	0.069	0.056	4	-3.77
34	825	850	9	0.124	0.130	9	4.07
35	850	875	7	0.097	0.099	7	1.21
36	875	900	6	0.083	0.085	6	5.35
37	900	925	2	0.028	0.012	1	-4.73
38	925	950	7	0.097	0.106	8	1.17
39	950	975	7	0.097	0.111	8	4.49
40	975	1000	3	0.041	0.039	3	2.75
41	1000	1025	1	0.014	0.000	0	-5.00
42	1025	1050	6	0.083	0.097	7	1.64
43	1050	1075	6	0.083	0.102	7	1.79
44	1075	1100	5	0.069	0.088	6	5.33
45	1100	1125	1	0.014	0.012	1	-1.15
46	1125	1150	2	0.028	0.033	2	2.39
47	1150	1175	0	0.000	-0.007	0	-0.99
48	1175	1200	1	0.014	0.013	1	0.00
49	1200	1225	1	0.014	0.014	1	1.09
50	1225	1250	0	0.000	-0.006	0	-0.38

Table D.7 Continued

CLASS	LIMITS (μm)		MEASURED[1] FEATURES	MEASURED[1] N_A (#/cm^2)	TRUE[2] N_A (#/cm^2)	TRUE[2] FEATURES	N_V(#/cm^3)[3]
51	1250	1275	0	0.000	-0.007	-1	0.03
52	1275	1300	0	0.000	-0.008	-1	-1.98
53	1300	1325	2	0.028	0.034	3	0.43
54	1325	1350	2	0.028	0.037	3	1.16
55	1350	1375	1	0.014	0.017	1	1.33
56	1375	1400	0	0.000	-0.005	0	-1.11
57	1400	1425	1	0.014	0.018	1	1.03
58	1425	1450	0	0.000	-0.004	0	0.14
59	1450	1475	0	0.000	-0.005	0	-1.13
60	1475	1500	1	0.014	0.018	1	1.15
61	1500	1525	0	0.000	-0.004	0	-0.07
62	1525	1550	0	0.000	-0.004	0	-0.10
63	1550	1575	0	0.000	-0.005	0	-0.09
64	1575	1600	0	0.000	-0.005	0	-0.23
65	1600	1625	0	0.000	-0.006	0	-0.01
66	1625	1650	0	0.000	-0.007	0	-1.13
67	1650	1675	1	0.014	0.018	1	0.26
68	1675	1700	1	0.014	0.019	1	-0.05
69	1700	1725	1	0.014	0.020	1	1.25
70	1725	1750	0	0.000	-0.005	0	-0.96
71	1750	1775	1	0.014	0.021	1	0.08
72	1775	1800	1	0.014	0.022	2	1.20
73	1800	1825	0	0.000	-0.003	0	-0.09
74	1825	1850	0	0.000	-0.003	0	-0.03
75	1850	1875	0	0.000	-0.004	0	-0.34
76	1875	1900	0	0.000	-0.004	0	0.35
77	1900	1925	0	0.000	-0.005	0	-2.31
78	1925	1950	2	0.028	0.051	4	2.38
79	1950	1975	0	0.000	-0.002	0	0.16
80	1975	2000	0	0.000	-0.003	0	-1.17
81	2000	2025	1	0.014	0.026	2	1.13
82	2025	2050	0	0.000	-0.002	0	0.20
83	2050	2075	0	0.000	-0.002	0	-1.18
84	2075	2100	1	0.014	0.028	2	1.31
85	2100	2125	0	0.000	0.000	0	0.00
Totals			17013	236.16	227.27	16485.14	33136.65
Average Feature Diameter (μm)				122.8	124.3		68.6
Air Content (%)				6.12	6.11		6.09
Powers Spacing Factor (μm)				186	191		192
Philleo Factor (μm)				--	--		142

1. Features not included in analysis include: 1 in class 97, 1 in class 102, 1 in class 112, and 1 in class 126
2. Calculated using Eq. 3.29
3. Calculated using Eq. 3.54

Table D.8 Analysis of mix 8, magnification 12x, areal data using 85 classes of 25 μm width

			MEASURED[1]		TRUE[2]		
CLASS	LIMITS (μm)		FEATURES	N_A (#/cm^2)	N_A (#/cm^2)	FEATURES	N_V(#/cm^3)[3]
1	0	25	2141	29.517	28.138	2041	10153.25
2	25	50	3207	44.213	42.849	3108	11121.98
3	50	75	1824	25.146	24.020	1742	3357.29
4	75	100	1454	20.045	19.157	1390	2279.36
5	100	125	1095	15.096	14.377	1043	1164.67
6	125	150	947	13.056	12.533	909	1090.48
7	150	175	707	9.747	9.324	676	652.02
8	175	200	577	7.955	7.633	554	454.00
9	200	225	478	6.590	6.355	461	415.21
10	225	250	375	5.170	4.979	361	166.58
11	250	275	367	5.060	4.992	362	349.04
12	275	300	234	3.226	3.124	227	139.34
13	300	325	198	2.730	2.660	193	118.23
14	325	350	162	2.233	2.182	158	93.88
15	350	375	138	1.903	1.872	136	51.89
16	375	400	127	1.751	1.759	128	109.83
17	400	425	76	1.048	1.010	73	7.27
18	425	450	87	1.199	1.215	88	56.16
19	450	475	61	0.841	0.839	61	34.55
20	475	500	46	0.634	0.623	45	16.58
21	500	525	43	0.593	0.594	43	14.04
22	525	550	40	0.551	0.565	41	23.80
23	550	575	27	0.372	0.370	27	14.30
24	575	600	20	0.276	0.265	19	1.46
25	600	625	22	0.303	0.306	22	7.18
26	625	650	22	0.303	0.316	23	1.22
27	650	675	24	0.331	0.363	26	22.61
28	675	700	10	0.138	0.136	10	-3.02
29	700	725	13	0.179	0.193	14	14.49
30	725	750	3	0.041	0.025	2	-7.16
31	750	775	10	0.138	0.149	11	5.71
32	775	800	6	0.083	0.084	6	4.56
33	800	825	3	0.041	0.033	2	-2.17
34	825	850	5	0.069	0.070	5	3.10
35	850	875	3	0.041	0.035	3	-1.18
36	875	900	4	0.055	0.055	4	2.27
37	900	925	3	0.041	0.038	3	-2.82
38	925	950	6	0.083	0.096	7	4.43
39	950	975	3	0.041	0.043	3	0.74
40	975	1000	2	0.028	0.026	2	2.91
41	1000	1025	0	0.000	-0.012	-1	-4.77
42	1025	1050	4	0.055	0.065	5	4.07
43	1050	1075	1	0.014	0.008	1	-2.27
44	1075	1100	3	0.041	0.048	4	2.22
45	1100	1125	2	0.028	0.030	2	-1.92
46	1125	1150	4	0.055	0.073	5	4.80
47	1150	1175	0	0.000	-0.005	0	-0.12
48	1175	1200	0	0.000	-0.005	0	-0.11
49	1200	1225	0	0.000	-0.005	0	-0.25
50	1225	1250	0	0.000	-0.006	0	-0.05

Table D.8 Continued

CLASS	LIMITS (μm)		MEASURED[1] FEATURES	MEASURED[1] N_A (#/cm^2)	TRUE[2] N_A (#/cm^2)	TRUE[2] FEATURES	N_V(#/cm^3)[3]
51	1250	1275	0	0.000	-0.007	0	-1.12
52	1275	1300	1	0.014	0.014	1	0.19
53	1300	1325	1	0.014	0.015	1	0.05
54	1325	1350	1	0.014	0.015	1	0.80
55	1350	1375	0	0.000	-0.006	0	0.27
56	1375	1400	0	0.000	-0.007	-1	-2.47
57	1400	1425	2	0.028	0.038	3	2.47
58	1425	1450	0	0.000	-0.007	0	-1.83
59	1450	1475	2	0.028	0.039	3	0.25
60	1475	1500	2	0.028	0.042	3	2.26
61	1500	1525	0	0.000	-0.003	0	0.16
62	1525	1550	0	0.000	-0.003	0	-1.12
63	1550	1575	1	0.014	0.021	2	1.18
64	1575	1600	0	0.000	-0.002	0	-0.06
65	1600	1625	0	0.000	-0.002	0	-0.05
66	1625	1650	0	0.000	-0.003	0	-0.17
67	1650	1675	0	0.000	-0.003	0	0.03
68	1675	1700	0	0.000	-0.004	0	-0.93
69	1700	1725	1	0.014	0.021	2	0.11
70	1725	1750	1	0.014	0.023	2	1.22
71	1750	1775	0	0.000	-0.001	0	-0.03
72	1775	1800	0	0.000	-0.001	0	-0.03
73	1800	1825	0	0.000	-0.002	0	-0.05
74	1825	1850	0	0.000	-0.002	0	-0.04
75	1850	1875	0	0.000	-0.002	0	-0.16
76	1875	1900	0	0.000	-0.002	0	0.04
77	1900	1925	0	0.000	-0.003	0	-0.95
78	1925	1950	1	0.014	0.025	2	0.12
79	1950	1975	1	0.014	0.027	2	1.28
80	1975	2000	0	0.000	0.000	0	0.00
81	2000	2025	0	0.000	0.000	0	0.00
82	2025	2050	0	0.000	0.000	0	0.00
83	2050	2075	0	0.000	0.000	0	0.00
84	2075	2100	0	0.000	0.000	0	0.00
85	2100	2125	0	0.000	0.000	0	0.00
Totals			14598	201.25	193.81	14058	31941.08
Average Feature Diameter (μm)				120.7	122.1		60.7
Air Content (%)				5.11	5.11		5.09
Powers Spacing Factor (μm)				201	206		207
Philleo Factor (μm)				--	--		146

1. Features not included in analysis include: 1 in class 97, 1 in class 101, and 1 in class 102
2. Calculated using Eq. 3.29
3. Calculated using Eq. 3.54

Table D.9 Analysis of mix 9, magnification 12x, areal data using 85 classes of 25 μm width

			MEASURED[1]		TRUE[2]		
CLASS	LIMITS (μm)		FEATURES	N_A (#/cm^2)	N_A (#/cm^2)	FEATURES	N_V(#/cm^3)[3]
1	0	25	1463	19.706	18.570	1379	7249.44
2	25	50	2106	28.367	27.088	2011	6116.69
3	50	75	1551	20.891	19.757	1467	2513.03
4	75	100	1357	18.278	17.345	1288	1813.42
5	100	125	1130	15.220	14.475	1075	1239.44
6	125	150	953	12.836	12.266	911	921.16
7	150	175	791	10.654	10.232	760	741.23
8	175	200	629	8.472	8.150	605	487.13
9	200	225	527	7.098	6.877	511	417.86
10	225	250	425	5.725	5.569	413	268.92
11	250	275	363	4.889	4.811	357	306.01
12	275	300	255	3.435	3.351	249	139.78
13	300	325	223	3.004	2.967	220	142.96
14	325	350	177	2.384	2.364	175	101.92
15	350	375	148	1.993	1.997	148	82.30
16	375	400	119	1.603	1.619	120	92.04
17	400	425	75	1.010	0.994	74	33.91
18	425	450	65	0.876	0.869	65	28.83
19	450	475	55	0.741	0.740	55	28.06
20	475	500	45	0.606	0.605	45	11.82
21	500	525	45	0.606	0.625	46	25.08
22	525	550	33	0.444	0.455	34	18.48
23	550	575	24	0.323	0.326	24	9.27
24	575	600	21	0.283	0.288	21	8.39
25	600	625	18	0.242	0.249	19	8.56
26	625	650	14	0.189	0.193	14	7.48
27	650	675	9	0.121	0.117	9	6.86
28	675	700	3	0.040	0.019	1	-1.25
29	700	725	6	0.081	0.068	5	-9.27
30	725	750	15	0.202	0.225	17	13.41
31	750	775	5	0.067	0.061	5	1.37
32	775	800	4	0.054	0.045	3	0.08
33	800	825	5	0.067	0.064	5	-2.35
34	825	850	8	0.108	0.120	9	4.85
35	850	875	5	0.067	0.071	5	1.84
36	875	900	3	0.040	0.038	3	4.15
37	900	925	0	0.000	-0.016	-1	-6.45
38	925	950	6	0.081	0.093	7	4.13
39	950	975	3	0.040	0.042	3	1.06
40	975	1000	2	0.027	0.025	2	1.39
41	1000	1025	1	0.013	0.006	0	-1.87
42	1025	1050	2	0.027	0.025	2	2.19
43	1050	1075	1	0.013	0.005	0	-6.06
44	1075	1100	7	0.094	0.122	9	6.05
45	1100	1125	2	0.027	0.031	2	1.51
46	1125	1150	1	0.013	0.012	1	-1.20
47	1150	1175	2	0.027	0.032	2	1.82
48	1175	1200	1	0.013	0.013	1	-2.04
49	1200	1225	3	0.040	0.055	4	3.47
50	1225	1250	0	0.000	-0.003	0	-0.20

Table D.9 Continued

CLASS	LIMITS (μm)		MEASURED[1] FEATURES	MEASURED[1] N_A (#/cm^2)	TRUE[2] N_A (#/cm^2)	TRUE[2] FEATURES	N_V(#/cm^3)[3]
51	1250	1275	0	0.000	-0.004	0	-0.06
52	1275	1300	0	0.000	-0.005	0	-0.90
53	1300	1325	1	0.013	0.016	1	-0.20
54	1325	1350	1	0.013	0.017	1	1.52
55	1350	1375	0	0.000	-0.004	0	-2.27
56	1375	1400	2	0.027	0.039	3	2.50
57	1400	1425	0	0.000	-0.003	0	-1.09
58	1425	1450	1	0.013	0.020	1	1.04
59	1450	1475	0	0.000	-0.002	0	0.04
60	1475	1500	0	0.000	-0.002	0	-0.87
61	1500	1525	1	0.013	0.020	2	0.13
62	1525	1550	1	0.013	0.022	2	1.19
63	1550	1575	0	0.000	0.000	0	0.00
64	1575	1600	0	0.000	0.000	0	0.00
65	1600	1625	0	0.000	0.000	0	0.00
66	1625	1650	0	0.000	0.000	0	0.00
67	1650	1675	0	0.000	0.000	0	0.00
68	1675	1700	0	0.000	0.000	0	0.00
69	1700	1725	0	0.000	0.000	0	0.00
70	1725	1750	0	0.000	0.000	0	0.00
71	1750	1775	0	0.000	0.000	0	0.00
72	1775	1800	0	0.000	0.000	0	0.00
73	1800	1825	0	0.000	0.000	0	0.00
74	1825	1850	0	0.000	0.000	0	0.00
75	1850	1875	0	0.000	0.000	0	0.00
76	1875	1900	0	0.000	0.000	0	0.00
77	1900	1925	0	0.000	0.000	0	0.00
78	1925	1950	0	0.000	0.000	0	0.00
79	1950	1975	0	0.000	0.000	0	0.00
80	1975	2000	0	0.000	0.000	0	0.00
81	2000	2025	0	0.000	0.000	0	0.00
82	2025	2050	0	0.000	0.000	0	0.00
83	2050	2075	0	0.000	0.000	0	0.00
84	2075	2100	0	0.000	0.000	0	0.00
85	2100	2125	0	0.000	0.000	0	0.00
Totals			12713	171.24	164.17	12188	22837.73
Average Feature Diameter (μm)				134.7	137.0		71.9
Air Content (%)				4.76	4.76		4.75
Powers Spacing Factor (μm)				218	224		224
Philleo Factor (μm)				--	--		167

1. Features not included in analysis include: 1 in class 88 and 1 in class 115
2. Calculated using Eq. 3.29
3. Calculated using Eq. 3.54

Table D.10 Analysis of mix 10, magnification 12x, areal data using 85 classes of 25 μm width

			MEASURED[1]		TRUE[2]		
CLASS	LIMITS (μm)		FEATURES	N_A (#/cm^2)	N_A (#/cm^2)	FEATURES	N_V(#/cm^3)[3]
1	0	25	1321	18.212	16.671	1209	3061.17
2	25	50	2798	38.574	36.787	2668	8078.97
3	50	75	2156	29.723	28.147	2042	3492.49
4	75	100	1915	26.401	25.134	1823	2803.02
5	100	125	1512	20.845	19.823	1438	1735.53
6	125	150	1254	17.288	16.494	1196	1250.27
7	150	175	1039	14.324	13.725	996	963.25
8	175	200	840	11.581	11.127	807	706.00
9	200	225	683	9.416	9.078	658	521.70
10	225	250	561	7.734	7.491	543	408.07
11	250	275	456	6.287	6.114	443	314.43
12	275	300	369	5.087	4.965	360	243.74
13	300	325	295	4.067	3.976	288	186.83
14	325	350	240	3.309	3.244	235	118.02
15	350	375	211	2.909	2.891	210	141.13
16	375	400	157	2.164	2.136	155	77.56
17	400	425	134	1.847	1.839	133	74.14
18	425	450	104	1.434	1.420	103	57.67
19	450	475	85	1.172	1.159	84	15.12
20	475	500	90	1.241	1.278	93	64.03
21	500	525	57	0.786	0.786	57	24.95
22	525	550	47	0.648	0.648	47	22.27
23	550	575	38	0.524	0.519	38	9.31
24	575	600	38	0.524	0.536	39	15.27
25	600	625	31	0.427	0.438	32	18.18
26	625	650	22	0.303	0.300	22	-0.31
27	650	675	27	0.372	0.396	29	12.61
28	675	700	20	0.276	0.291	21	14.28
29	700	725	11	0.152	0.144	10	-0.75
30	725	750	14	0.193	0.202	15	3.56
31	750	775	13	0.179	0.192	14	7.74
32	775	800	8	0.110	0.110	8	2.14
33	800	825	8	0.110	0.114	8	-0.01
34	825	850	9	0.124	0.137	10	7.08
35	850	875	4	0.055	0.051	4	0.08
36	875	900	4	0.055	0.053	4	2.18
37	900	925	3	0.041	0.036	3	-2.59
38	925	950	5	0.069	0.074	5	5.00
39	950	975	2	0.028	0.020	1	-5.32
40	975	1000	7	0.097	0.117	8	7.16
41	1000	1025	1	0.014	0.006	0	0.23
42	1025	1050	1	0.014	0.006	0	-2.09
43	1050	1075	3	0.041	0.045	3	1.45
44	1075	1100	2	0.028	0.027	2	0.38
45	1100	1125	2	0.028	0.028	2	0.10
46	1125	1150	2	0.028	0.030	2	1.34
47	1150	1175	1	0.014	0.010	1	-0.66
48	1175	1200	2	0.028	0.031	2	0.06
49	1200	1225	2	0.028	0.033	2	2.37
50	1225	1250	0	0.000	-0.007	-1	-1.02

Table D.10 continued

CLASS	LIMITS (μm)		MEASURED[1] FEATURES	MEASURED[1] N_A (#/cm^2)	TRUE[2] N_A (#/cm^2)	TRUE[2] FEATURES	N_V(#/cm^3)[3]
51	1250	1275	1	0.014	0.013	1	0.01
52	1275	1300	1	0.014	0.014	1	0.94
53	1300	1325	0	0.000	-0.007	0	-0.08
54	1325	1350	0	0.000	-0.008	-1	-1.16
55	1350	1375	1	0.014	0.013	1	0.08
56	1375	1400	1	0.014	0.014	1	0.00
57	1400	1425	1	0.014	0.014	1	0.19
58	1425	1450	1	0.014	0.015	1	-0.60
59	1450	1475	2	0.028	0.038	3	0.23
60	1475	1500	2	0.028	0.041	3	2.38
61	1500	1525	0	0.000	-0.003	0	-0.06
62	1525	1550	0	0.000	-0.003	0	-0.09
63	1550	1575	0	0.000	-0.004	0	-0.06
64	1575	1600	0	0.000	-0.004	0	-0.24
65	1600	1625	0	0.000	-0.005	0	0.15
66	1625	1650	0	0.000	-0.005	0	-1.43
67	1650	1675	1	0.014	0.019	1	1.57
68	1675	1700	0	0.000	-0.005	0	-2.26
69	1700	1725	2	0.028	0.046	3	2.42
70	1725	1750	0	0.000	-0.003	0	-0.10
71	1750	1775	0	0.000	-0.003	0	-0.04
72	1775	1800	0	0.000	-0.004	0	-0.34
73	1800	1825	0	0.000	-0.004	0	0.34
74	1825	1850	0	0.000	-0.005	0	-2.30
75	1850	1875	2	0.028	0.049	4	2.36
76	1875	1900	0	0.000	-0.002	0	0.04
77	1900	1925	0	0.000	-0.003	0	-0.95
78	1925	1950	1	0.014	0.025	2	0.12
79	1950	1975	1	0.014	0.027	2	1.28
80	1975	2000	0	0.000	0.000	0	0.00
81	2000	2025	0	0.000	0.000	0	0.00
82	2025	2050	0	0.000	0.000	0	0.00
83	2050	2075	0	0.000	0.000	0	0.00
84	2075	2100	0	0.000	0.000	0	0.00
85	2100	2125	0	0.000	0.000	0	0.00
Totals			16621	229.14	219.13	15895	24460.59
Average Feature Diameter (μm)				142.6	145.2		89.6
Air Content (%)				7.13	7.13		7.12
Powers Spacing Factor (μm)				189	194		195
Philleo Factor (μm)				--	--		157

1. Features not included in analysis include: 1 in class 86, 1 in class 97, 1 in class 104, and 1 in class 133
2. Calculated using Eq. 3.29
3. Calculated using Eq. 3.54

Table D.11 Analysis of mix 1, magnification 30x, areal data using 85 classes of 25 μm width

			MEASURED[1]		TRUE[2]		
CLASS	LIMITS (μm)		FEATURES	N_A (#/cm^2)	N_A (#/cm^2)	FEATURES	N_V(#/cm^3)[3]
1	0	25	4056	55.916	53.381	3872	32180.79
2	25	50	2840	39.153	37.386	2712	9257.52
3	50	75	1689	23.285	22.469	1630	4415.81
4	75	100	803	11.07	10.626	771	1643.74
5	100	125	412	5.68	5.366	389	673.34
6	125	150	238	3.281	3.021	219	292.20
7	150	175	160	2.206	1.987	144	181.93
8	175	200	107	1.475	1.262	92	69.30
9	200	225	94	1.296	1.128	82	60.35
10	225	250	80	1.103	0.972	70	55.54
11	250	275	62	0.855	0.734	53	45.66
12	275	300	46	0.634	0.505	37	11.58
13	300	325	47	0.648	0.556	40	13.98
14	325	350	46	0.634	0.582	42	27.41
15	350	375	35	0.483	0.427	31	24.76
16	375	400	25	0.345	0.270	20	0.70
17	400	425	27	0.372	0.330	24	12.81
18	425	450	23	0.317	0.278	20	3.92
19	450	475	23	0.317	0.305	22	14.16
20	475	500	17	0.234	0.210	15	6.24
21	500	525	15	0.207	0.188	14	6.69
22	525	550	12	0.165	0.143	10	7.44
23	550	575	7	0.097	0.044	3	4.21
24	575	600	6	0.083	0.019	1	-14.40
25	600	625	14	0.193	0.210	15	14.56
26	625	650	7	0.097	0.062	5	-5.99
27	650	675	11	0.152	0.169	12	6.97
28	675	700	8	0.11	0.115	8	3.08
29	700	725	6	0.083	0.078	6	6.85
30	725	750	3	0.041	0.005	0	-6.66
31	750	775	6	0.083	0.090	7	8.81
32	775	800	2	0.028	-0.015	-1	-8.41
33	800	825	6	0.083	0.101	7	8.47
34	825	850	2	0.028	-0.009	-1	-6.01
35	850	875	5	0.069	0.083	6	4.47
36	875	900	3	0.041	0.030	2	-1.86
37	900	925	4	0.055	0.068	5	2.51
38	925	950	3	0.041	0.045	3	0.08
39	950	975	3	0.041	0.054	4	2.71
40	975	1000	1	0.014	-0.011	-1	2.24
41	1000	1025	1	0.014	-0.020	-1	-11.64
42	1025	1050	6	0.083	0.176	13	13.69
43	1050	1075	0	0	-0.032	-2	-4.51
44	1075	1100	2	0.028	0.045	3	2.29
45	1100	1125	1	0.014	0.011	1	0.25
46	1125	1150	1	0.014	0.014	1	-0.17
47	1150	1175	1	0.014	0.019	1	1.97
48	1175	1200	0	0	-0.024	-2	0.23
49	1200	1225	0	0	-0.031	-2	-2.83
50	1225	1250	1	0.014	0.014	1	1.58

Table D.11 continued

CLASS	LIMITS (μm)		MEASURED[1]		TRUE[2]		
			FEATURES	N_A (#/cm^2)	N_A (#/cm^2)	FEATURES	N_V(#/cm^3)[3]
51	1250	1275	0	0	-0.039	-3	0.44
52	1275	1300	0	0	-0.058	-4	-7.03
53	1300	1325	3	0.041	0.101	7	-1.07
54	1325	1350	3	0.041	0.134	10	9.30
55	1350	1375	0	0	-0.022	-2	-3.65
56	1375	1400	1	0.014	0.041	3	3.69
57	1400	1425	0	0	-0.020	-1	-3.47
58	1425	1450	1	0.014	0.050	4	3.10
59	1450	1475	0	0	-0.010	-1	0.13
60	1475	1500	0	0	-0.014	-1	-0.99
61	1500	1525	0	0	-0.021	-2	1.73
62	1525	1550	0	0	-0.039	-3	-8.47
63	1550	1575	2	0.028	0.143	10	7.69
64	1575	1600	0	0	0	0	0
65	1600	1625	0	0	0	0	0
66	1625	1650	0	0	0	0	0
67	1650	1675	0	0	0	0	0
68	1675	1700	0	0	0	0	0
69	1700	1725	0	0	0	0	0
70	1725	1750	0	0	0	0	0
71	1750	1775	0	0	0	0	0
72	1775	1800	0	0	0	0	0
73	1800	1825	0	0	0	0	0
74	1825	1850	0	0	0	0	0
75	1850	1875	0	0	0	0	0
76	1875	1900	0	0	0	0	0
77	1900	1925	0	0	0	0	0
78	1925	1950	0	0	0	0	0
79	1950	1975	0	0	0	0	0
80	1975	2000	0	0	0	0	0
81	2000	2025	0	0	0	0	0
82	2025	2050	0	0	0	0	0
83	2050	2075	0	0	0	0	0
84	2075	2100	0	0	0	0	0
85	2100	2125	0	0	0	0	0
Totals			10977	151.33	143.68	10422	49029.75
Average Feature Diameter (μm)				66.6	65.8		29.3
Air Content (%)				1.97	1.97		1.95
Powers Spacing Factor (μm)				355	378		383
Philleo Factor (μm)				--	--		156

1. Features not included in the analysis include: 1 in class 90 and 1 in class 104
2. Calculated using Eq. 3.29
3. Calculated using Eq. 3.54

Table D.12 Analysis of mix 2, magnification 30x, areal data using 85 classes of 25 μm width

			MEASURED[1]		TRUE[2]		
CLASS	LIMITS (μm)		FEATURES	N_A (#/cm^2)	N_A (#/cm^2)	FEATURES	N_V(#/cm^3)[3]
1	0	25	3346	46.171	44.059	3193	46097.42
2	25	50	2460	33.945	32.525	2357	20690.97
3	50	75	1364	18.822	18.181	1318	10960.56
4	75	100	643	8.873	8.532	618	7068.72
5	100	125	323	4.457	4.216	306	3412.81
6	125	150	175	2.415	2.199	159	2027.07
7	150	175	116	1.601	1.408	102	1013.10
8	175	200	84	1.159	0.980	71	676.91
9	200	225	68	0.938	0.776	56	486.75
10	225	250	71	0.980	0.877	64	314.05
11	250	275	50	0.690	0.580	42	164.81
12	275	300	48	0.662	0.586	42	183.67
13	300	325	43	0.593	0.544	39	68.39
14	325	350	31	0.428	0.371	27	60.65
15	350	375	19	0.262	0.175	13	53.89
16	375	400	23	0.317	0.263	19	34.47
17	400	425	21	0.290	0.247	18	68.49
18	425	450	16	0.221	0.168	12	27.32
19	450	475	15	0.207	0.162	12	-11.78
20	475	500	13	0.179	0.133	10	25.47
21	500	525	13	0.179	0.142	10	-10.18
22	525	550	15	0.207	0.200	14	1.89
23	550	575	14	0.193	0.201	15	14.67
24	575	600	8	0.110	0.085	6	10.17
25	600	625	8	0.110	0.094	7	1.27
26	625	650	7	0.097	0.082	6	1.15
27	650	675	2	0.028	-0.038	-3	13.73
28	675	700	10	0.138	0.162	12	-2.48
29	700	725	4	0.055	0.025	2	15.59
30	725	750	5	0.069	0.055	4	-5.37
31	750	775	3	0.041	0.004	0	3.67
32	775	800	5	0.069	0.060	4	-7.55
33	800	825	5	0.069	0.069	5	10.44
34	825	850	2	0.028	-0.017	-1	-4.57
35	850	875	8	0.110	0.170	12	-4.18
36	875	900	3	0.041	0.037	3	-0.07
37	900	925	1	0.014	-0.027	-2	2.49
38	925	950	4	0.055	0.069	5	-1.19
39	950	975	5	0.069	0.120	9	-1.50
40	975	1000	1	0.014	-0.004	0	5.31
41	1000	1025	2	0.028	0.034	2	4.81
42	1025	1050	1	0.014	0.003	0	2.49
43	1050	1075	0	0	-0.038	-3	-0.89
44	1075	1100	1	0.014	-0.005	0	0.81
45	1100	1125	2	0.028	0.039	3	-6.06
46	1125	1150	1	0.014	0.005	0	5.25
47	1150	1175	0	0	-0.041	-3	-2.38
48	1175	1200	0	0	-0.055	-4	-2.76
49	1200	1225	2	0.028	0.029	2	2.35
50	1225	1250	3	0.041	0.091	7	2.66

Table D.12 continued

CLASS	LIMITS (μm)		MEASURED[1] FEATURES	MEASURED[1] N_A (#/cm^2)	TRUE[2] N_A (#/cm^2)	TRUE[2] FEATURES	N_V(#/cm^3)[3]
51	1250	1275	1	0.014	0.007	0	-0.60
52	1275	1300	1	0.014	0.010	1	2.59
53	1300	1325	0	0	-0.048	-4	-2.62
54	1325	1350	1	0.014	-0.004	0	-2.20
55	1350	1375	2	0.028	0.059	4	-0.48
56	1375	1400	2	0.028	0.083	6	5.60
57	1400	1425	0	0	-0.031	-2	0.68
58	1425	1450	0	0	-0.042	-3	-4.02
59	1450	1475	1	0.014	0.025	2	3.63
60	1475	1500	0	0	-0.05	-4	-3.17
61	1500	1525	1	0.014	0.019	1	-0.50
62	1525	1550	1	0.014	0.032	2	3.22
63	1550	1575	0	0	-0.049	-4	0.26
64	1575	1600	0	0	-0.074	-5	-3.82
65	1600	1625	1	0.014	-0.001	0	-1.59
66	1625	1650	1	0.014	-0.007	0	3.02
67	1650	1675	1	0.014	-0.027	-2	-13.07
68	1675	1700	3	0.041	0.231	17	17.01
69	1700	1725	0	0	-0.081	-6	-12.77
70	1725	1750	2	0.028	0.182	13	11.92
71	1750	1775	0	0	-0.043	-3	-6.79
72	1775	1800	1	0.014	0.112	8	5.70
73	1800	1825	0	0	-0.002	0	0.01
74	1825	1850	0	0	-0.002	0	0.01
75	1850	1875	0	0	-0.002	0	0.01
76	1875	1900	0	0	-0.002	0	0.04
77	1900	1925	0	0	-0.003	0	0.03
78	1925	1950	0	0	-0.005	0	0.15
79	1950	1975	0	0	-0.007	0	-0.16
80	1975	2000	0	0	-0.011	-1	0.87
81	2000	2025	0	0	-0.019	-1	-2.07
82	2025	2050	0	0	-0.039	-3	7.05
83	2050	2075	0	0	-0.180	-13	-19.20
84	2075	2100	1	0.014	0.280	20	13.04
85	2100	2125	0	0	0	0	0
Totals			9084	125.35	118.84	8612	40457.25
Average Feature Diameter (μm)				68.9	67.0		29.4
Air Content (%)				2.09	2.09		2.08
Powers Spacing Factor (μm)				423	458		465
Philleo Factor (μm)				--	--		164

1. Features not included in the analysis include: 1 in class 86 and 1 in class 100
2. Calculated using Eq. 3.29
3. Calculated using Eq. 3.54

Table D.13 Analysis of mix 3, magnification 30x, areal data using 85 classes of 25 μm width

			MEASURED[1]		TRUE[2]		
CLASS	LIMITS (μm)		FEATURES	N_A (#/cm^2)	N_A (#/cm^2)	FEATURES	N_V(#/cm^3)[3]
1	0	25	6082	97.549	90.019	5612	46097.42
2	25	50	6278	100.693	93.692	5841	20690.97
3	50	75	4685	75.143	70.603	4402	10960.56
4	75	100	3292	52.800	50.296	3136	7068.72
5	100	125	1989	31.902	30.374	1894	3412.81
6	125	150	1293	20.738	19.816	1235	2027.07
7	150	175	825	13.232	12.566	783	1013.10
8	175	200	600	9.623	9.229	575	676.91
9	200	225	436	6.993	6.775	422	486.75
10	225	250	302	4.844	4.681	292	314.05
11	250	275	216	3.464	3.333	208	164.81
12	275	300	173	2.775	2.731	170	183.67
13	300	325	112	1.796	1.688	105	68.39
14	325	350	96	1.540	1.486	93	60.65
15	350	375	80	1.283	1.266	79	53.89
16	375	400	67	1.075	1.093	68	34.47
17	400	425	58	0.930	1.001	62	68.49
18	425	450	28	0.449	0.405	25	27.32
19	450	475	18	0.289	0.201	13	-11.78
20	475	500	24	0.385	0.365	23	25.47
21	500	525	13	0.209	0.121	8	-10.18
22	525	550	20	0.321	0.305	19	1.89
23	550	575	21	0.337	0.365	23	14.67
24	575	600	15	0.241	0.245	15	10.17
25	600	625	11	0.176	0.161	10	1.27
26	625	650	12	0.192	0.206	13	1.15
27	650	675	12	0.192	0.233	15	13.73
28	675	700	7	0.112	0.115	7	-2.48
29	700	725	8	0.128	0.165	10	15.59
30	725	750	1	0.016	-0.034	-2	-5.37
31	750	775	3	0.048	0.025	2	3.67
32	775	800	2	0.032	-0.007	0	-7.55
33	800	825	5	0.080	0.097	6	10.44
34	825	850	0	0	-0.067	-4	-4.57
35	850	875	2	0.032	-0.009	-1	-4.18
36	875	900	4	0.064	0.061	4	-0.07
37	900	925	4	0.064	0.070	4	2.49
38	925	950	3	0.048	0.039	2	-1.19
39	950	975	4	0.064	0.083	5	-1.50
40	975	1000	5	0.080	0.143	9	5.31
41	1000	1025	3	0.048	0.086	5	4.81
42	1025	1050	1	0.016	0.014	1	2.49
43	1050	1075	0	0	-0.029	-2	-0.89
44	1075	1100	0	0	-0.035	-2	0.81
45	1100	1125	0	0	-0.045	-3	-6.06
46	1125	1150	2	0.032	0.052	3	5.25
47	1150	1175	0	0	-0.046	-3	-2.38
48	1175	1200	1	0.016	-0.003	0	-2.76
49	1200	1225	2	0.032	0.056	4	2.35
50	1225	1250	1	0.016	0.012	1	2.66

Table D.13 continued

CLASS	LIMITS (μm)		MEASURED[1] FEATURES	MEASURED[1] N_A (#/cm^2)	TRUE[2] N_A (#/cm^2)	TRUE[2] FEATURES	N_V(#/cm^3)[3]
51	1250	1275	0	0	-0.052	-3	-2.41
52	1275	1300	1	0.016	-0.004	0	-3.93
53	1300	1325	2	0.032	0.065	4	4.39
54	1325	1350	1	0.016	0.008	1	-4.37
55	1350	1375	2	0.032	0.090	6	7.23
56	1375	1400	0	0	-0.042	-3	-3.60
57	1400	1425	1	0.016	0.026	2	0.46
58	1425	1450	1	0.016	0.034	2	-0.48
59	1450	1475	1	0.016	0.051	3	3.98
60	1475	1500	0	0	-0.024	-2	-0.63
61	1500	1525	0	0	-0.033	-2	1.04
62	1525	1550	0	0	-0.049	-3	-5.42
63	1550	1575	1	0.016	0.048	3	4.98
64	1575	1600	0	0	-0.055	-3	-4.14
65	1600	1625	1	0.016	0.046	3	-0.91
66	1625	1650	1	0.016	0.074	5	5.25
67	1650	1675	0	0	-0.029	-2	-0.83
68	1675	1700	0	0	-0.041	-3	1.85
69	1700	1725	0	0	-0.069	-4	-7.90
70	1725	1750	1	0.016	0.075	5	8.14
71	1750	1775	0	0	-0.075	-5	-8.79
72	1775	1800	1	0.016	0.091	6	8.96
73	1800	1825	0	0	-0.078	-5	-8.98
74	1825	1850	1	0.016	0.121	8	7.80
75	1850	1875	0	0	-0.042	-3	-0.85
76	1875	1900	0	0	-0.071	-4	2.69
77	1900	1925	0	0	-0.155	-10	-9.95
78	1925	1950	1	0.016	0.041	3	1.21
79	1950	1975	1	0.016	0.072	5	-6.27
80	1975	2000	1	0.016	0.184	11	16.64
81	2000	2025	0	0	-0.153	-10	-17.73
82	2025	2050	1	0.016	0.269	17	12.67
83	050	2075	0	0	0	0	0
84	2075	2100	0	0	0	0	0
85	2100	2125	0	0	0	0	0
Totals			26835	430.41	404.32	25209	93473.47
Average Feature Diameter (μm)				79.4	80.5		43.3
Air Content (%)				5.17	5.16		5.12
Powers Spacing Factor (μm)				168	176		177
Philleo Factor (μm)				--	--		106

1. Features not included in the analysis include: 1 in class 86 and 1 in class 99
2. Calculated using Eq. 3.29
3. Calculated using Eq. 3.54

Table D.14 Analysis of mix 4, magnification 30x, areal data using 85 classes of 25 μm width

			MEASURED[1]		TRUE[2]		
CLASS	LIMITS (μm)		FEATURES	N_A (#/cm^2)	N_A (#/cm^2)	FEATURES	N_V(#/cm^3)[3]
1	0	25	8707	120.259	106.926	7742	34386.20
2	25	50	14505	200.340	187.839	13600	39431.93
3	50	75	11367	156.999	150.318	10883	25680.85
4	75	100	6974	96.323	93.505	6770	14044.34
5	100	125	3736	51.601	50.301	3642	6308.52
6	125	150	2097	28.963	28.318	2050	3056.32
7	150	175	1234	17.044	16.682	1208	1554.89
8	175	200	778	10.746	10.553	764	846.25
9	200	225	511	7.058	6.965	504	595.88
10	225	250	309	4.268	4.109	297	193.55
11	250	275	262	3.619	3.633	263	266.79
12	275	300	162	2.238	2.185	158	118.21
13	300	325	119	1.644	1.601	116	104.92
14	325	350	78	1.077	0.983	71	23.39
15	350	375	77	1.064	1.047	76	43.26
16	375	400	62	0.856	0.858	62	46.25
17	400	425	42	0.580	0.548	40	24.89
18	425	450	31	0.428	0.377	27	13.35
19	450	475	28	0.387	0.346	25	-2.48
20	475	500	32	0.442	0.467	34	27.04
21	500	525	18	0.249	0.214	15	8.80
22	525	550	15	0.207	0.165	12	-5.34
23	550	575	19	0.262	0.272	20	12.30
24	575	600	14	0.193	0.185	13	-0.21
25	600	625	15	0.207	0.230	17	11.28
26	625	650	10	0.138	0.135	10	0.90
27	650	675	10	0.138	0.153	11	7.95
28	675	700	6	0.083	0.070	5	1.45
29	700	725	5	0.069	0.051	4	2.29
30	725	750	4	0.055	0.026	2	-3.98
31	750	775	7	0.097	0.111	8	0.06
32	775	800	7	0.097	0.129	9	8.37
33	800	825	3	0.041	0.028	2	-2.53
34	825	850	5	0.069	0.094	7	1.68
35	850	875	4	0.055	0.081	6	7.60
36	875	900	0	0	-0.035	-3	-1.84
37	900	925	1	0.014	-0.010	-1	-2.11
38	925	950	2	0.028	0.023	2	1.43
39	950	975	1	0.014	-0.009	-1	0.55
40	975	1000	1	0.014	-0.014	-1	-4.44
41	1000	1025	3	0.041	0.059	4	3.19
42	1025	1050	2	0.028	0.030	2	-2.33
43	1050	1075	3	0.041	0.081	6	6.03
44	1075	1100	0	0	-0.028	-2	0.80
45	1100	1125	0	0	-0.036	-3	-5.26
46	1125	1150	2	0.028	0.049	4	5.08
47	1150	1175	0	0	-0.034	-2	-2.96
48	1175	1200	1	0.014	0.008	1	2.28
49	1200	1225	0	0	-0.043	-3	-2.34
50	1225	1250	1	0.014	-0.004	0	-2.21

Table D.14 Continued

CLASS	LIMITS (μm)		MEASURED[1] FEATURES	MEASURED[1] N_A (#/cm^2)	TRUE[2] N_A (#/cm^2)	TRUE[2] FEATURES	N_V(#/cm^3)[3]
51	1250	1275	2	0.028	0.049	4	0.21
52	1275	1300	2	0.028	0.064	5	2.47
53	1300	1325	1	0.014	0.026	2	2.75
54	1325	1350	0	0	-0.026	-2	-0.40
55	1350	1375	0	0	-0.033	-2	0.15
56	1375	1400	0	0	-0.045	-3	-2.78
57	1400	1425	1	0.014	0.012	1	-0.67
58	1425	1450	1	0.014	0.018	1	3.00
59	1450	1475	0	0	-0.057	-4	-2.18
60	1475	1500	1	0.014	0.001	0	-4.87
61	1500	1525	2	0.028	0.093	7	7.71
62	1525	1550	0	0	-0.057	-4	-4.35
63	1550	1575	1	0.014	0.014	1	1.31
64	1575	1600	1	0.014	0.014	1	-5.15
65	1600	1625	2	0.028	0.137	10	7.75
66	1625	1650	0	0	-0.027	-2	1.22
67	1650	1675	0	0	-0.044	-3	-5.35
68	1675	1700	1	0.014	0.072	5	4.71
69	1700	1725	0	0	-0.024	-2	0.15
70	1725	1750	0	0	-0.033	-2	-0.48
71	1750	1775	0	0	-0.049	-4	0.89
72	1775	1800	0	0	-0.088	-6	-5.00
73	1800	1825	1	0.014	0.042	3	-2.54
74	1825	1850	1	0.014	0.084	6	8.76
75	1850	1875	0	0	-0.089	-6	-8.71
76	1875	1900	1	0.014	0.103	7	7.00
77	1900	1925	0	0	-0.073	-5	0.65
78	1925	1950	0	0	-0.165	-12	-3.31
79	1950	1975	1	0.014	-0.038	-3	-17.90
80	1975	2000	2	0.028	0.354	26	23.65
81	2000	2025	0	0	-0.132	-10	-15.27
82	2025	2050	1	0.014	0.232	17	10.91
83	2050	2075	0	0	0	0	0
84	2075	2100	0	0	0	0	0
85	2100	2125	0	0	0	0	0
Totals			51292	708.43	669.88	48501	126815.16
Average Feature Diameter (μm)				71.0	72.3		52.8
Air Content (%)				5.86	5.85		5.79
Powers Spacing Factor (μm)				107	111		113
Philleo Factor (μm)				--	--		92

1. Features not included in the analysis include: 1 in class 94 and 1 in class 98
2. Calculated using Eq. 3.29
3. Calculated using Eq. 3.54

Table D.15 Analysis of mix 5, magnification 30x, areal data using 85 classes of 25 μm width

			MEASURED[1]		TRUE[2]		
CLASS	LIMITS (μm)		FEATURES	N_A (#/cm^2)	N_A (#/cm^2)	FEATURES	N_V(#/cm^3)[3]
1	0	25	8251	114.067	102.755	7433	35144.61
2	25	50	12941	178.905	168.908	12218	39158.25
3	50	75	8858	122.459	116.987	8462	19779.37
4	75	100	5540	76.589	74.162	5364	10842.61
5	100	125	3118	43.105	42.050	3042	5137.09
6	125	150	1803	24.926	24.522	1774	2785.31
7	150	175	990	13.686	13.413	970	1240.87
8	175	200	625	8.640	8.509	615	713.46
9	200	225	398	5.502	5.420	392	432.35
10	225	250	253	3.498	3.404	246	211.11
11	250	275	187	2.585	2.541	184	157.96
12	275	300	136	1.880	1.856	134	92.63
13	300	325	103	1.424	1.427	103	109.84
14	325	350	57	0.788	0.705	51	11.19
15	350	375	59	0.816	0.802	58	38.69
16	375	400	43	0.594	0.568	41	30.60
17	400	425	32	0.442	0.402	29	0.92
18	425	450	34	0.470	0.481	35	31.78
19	450	475	20	0.276	0.240	17	-2.57
20	475	500	23	0.318	0.327	24	19.78
21	500	525	13	0.180	0.145	10	2.79
22	525	550	13	0.180	0.157	11	-1.18
23	550	575	15	0.207	0.219	16	9.22
24	575	600	10	0.138	0.129	9	8.12
25	600	625	6	0.083	0.045	3	-5.01
26	625	650	10	0.138	0.145	10	0.81
27	650	675	10	0.138	0.165	12	10.07
28	675	700	5	0.069	0.057	4	0.03
29	700	725	5	0.069	0.065	5	3.59
30	725	750	3	0.041	0.018	1	-0.48
31	750	775	3	0.041	0.017	1	-0.64
32	775	800	4	0.055	0.044	3	-4.73
33	800	825	7	0.097	0.140	10	5.79
34	825	850	4	0.055	0.072	5	4.60
35	850	875	2	0.028	0.020	1	-2.03
36	875	900	3	0.041	0.056	4	3.83
37	900	925	1	0.014	-0.002	0	-0.21
38	925	950	1	0.014	-0.004	0	-1.03
39	950	975	2	0.028	0.030	2	-2.54
40	975	1000	3	0.041	0.074	5	6.60
41	1000	1025	0	0	-0.026	-2	-2.60
42	1025	1050	1	0.014	0.009	1	1.74
43	1050	1075	0	0	-0.033	-2	-1.70
44	1075	1100	1	0.014	-0.002	0	-3.85
45	1100	1125	3	0.041	0.085	6	1.85
46	1125	1150	2	0.028	0.062	4	5.27
47	1150	1175	0	0	-0.019	-1	-2.87
48	1175	1200	1	0.014	0.027	2	2.98
49	1200	1225	0	0	-0.018	-1	-2.68
50	1225	1250	1	0.014	0.032	2	2.56

Table D.15 continued

CLASS	LIMITS (μm)		MEASURED[1] FEATURES	MEASURED[1] N_A (#/cm^2)	TRUE[2] N_A (#/cm^2)	TRUE[2] FEATURES	N_V(#/cm^3)[3]
51	1250	1275	0	0	-0.013	-1	0.02
52	1275	1300	0	0	-0.015	-1	-0.38
53	1300	1325	0	0	-0.019	-1	0.53
54	1325	1350	0	0	-0.026	-2	-3.08
55	1350	1375	1	0.014	0.034	2	2.56
56	1375	1400	0	0	-0.022	-2	0.65
57	1400	1425	0	0	-0.030	-2	-3.47
58	1425	1450	1	0.014	0.039	3	3.10
59	1450	1475	0	0	-0.024	-2	0.13
60	1475	1500	0	0	-0.031	-2	-1.05
61	1500	1525	0	0	-0.041	-3	1.75
62	1525	1550	0	0	-0.065	-5	-8.94
63	1550	1575	2	0.028	0.109	8	8.15
64	1575	1600	0	0	-0.054	-4	-3.66
65	1600	1625	1	0.014	0.031	2	-0.74
66	1625	1650	1	0.014	0.051	4	3.99
67	1650	1675	0	0	-0.046	-3	-0.01
68	1675	1700	0	0	-0.076	-6	-3.05
69	1700	1725	1	0.014	0.012	1	-6.93
70	1725	1750	2	0.028	0.182	13	9.63
71	1750	1775	0	0	-0.032	-2	1.69
72	1775	1800	0	0	-0.060	-4	-6.96
73	1800	1825	1	0.014	0.099	7	5.19
74	1825	1850	0	0	-0.036	-3	2.25
75	1850	1875	0	0	-0.077	-6	-8.45
76	1875	1900	1	0.014	0.122	9	5.88
77	1900	1925	0	0	-0.042	-3	3.81
78	1925	1950	0	0	-0.106	-8	-12.82
79	1950	1975	1	0.014	0.146	11	12.98
80	1975	2000	0	0	-0.114	-8	-13.78
81	2000	2025	1	0.014	0.213	15	10.07
82	2025	2050	0	0	0	0	0
83	2050	2075	0	0	0	0	0
84	2075	2100	0	0	0	0	0
85	2100	2125	0	0	0	0	0
Totals			43613	602.94	571.30	41325	115973.17
Average Feature Diameter (μm)				68.5	69.7		49.3
Air Content (%)				4.68	4.67		4.62
Powers Spacing Factor (μm)				121	126		127
Philleo Factor (μm)				--	--		98

1. Features not included in the analysis include: 1 in class 94 and 1 in class 110
2. Calculated using Eq. 3.29
3. Calculated using Eq. 3.54

Table D.16 Analysis of mix 6, magnification 30x, areal data using 85 classes of 25 μm width

			MEASURED		TRUE[1]		
CLASS	LIMITS (μm)		FEATURES	N_A (#/cm^2)	N_A (#/cm^2)	FEATURES	N_V(#/cm^3)[2]
1	0	25	7631	109.267	98.815	6901	40057.78
2	25	50	10675	152.854	143.130	9996	29976.29
3	50	75	8415	120.493	115.177	8044	19303.96
4	75	100	5332	76.348	74.139	5178	10940.36
5	100	125	2910	41.668	40.763	2847	5424.52
6	125	150	1501	21.493	20.903	1460	2116.63
7	150	175	951	13.617	13.366	933	1295.40
8	175	200	566	8.104	7.916	553	677.01
9	200	225	362	5.183	5.030	351	335.86
10	225	250	264	3.780	3.715	259	275.59
11	250	275	170	2.434	2.341	163	137.96
12	275	300	124	1.776	1.694	118	101.71
13	300	325	91	1.303	1.218	85	37.62
14	325	350	83	1.188	1.170	82	71.92
15	350	375	54	0.773	0.710	50	27.16
16	375	400	46	0.659	0.610	43	18.24
17	400	425	41	0.587	0.562	39	22.46
18	425	450	34	0.487	0.468	33	10.65
19	450	475	30	0.430	0.429	30	26.93
20	475	500	19	0.272	0.228	16	-9.51
21	500	525	26	0.372	0.407	28	21.41
22	525	550	17	0.243	0.245	17	2.83
23	550	575	17	0.243	0.273	19	13.49
24	575	600	10	0.143	0.137	10	7.73
25	600	625	7	0.100	0.075	5	-6.02
26	625	650	11	0.158	0.185	13	8.48
27	650	675	7	0.100	0.105	7	4.28
28	675	700	5	0.072	0.065	5	1.94
29	700	725	4	0.057	0.046	3	1.42
30	725	750	3	0.043	0.021	1	-0.15
31	750	775	4	0.057	0.049	3	-5.69
32	775	800	7	0.100	0.147	10	9.95
33	800	825	2	0.029	0.016	1	-0.63
34	825	850	3	0.043	0.048	3	-2.37
35	850	875	4	0.057	0.091	6	8.33
36	875	900	0	0	-0.028	-2	-2.63
37	900	925	1	0.014	0.002	0	1.58
38	925	950	0	0	-0.036	-2	-2.21
39	950	975	1	0.014	-0.010	-1	-3.08
40	975	1000	3	0.043	0.062	4	-2.21
41	1000	1025	4	0.057	0.116	8	7.12
42	1025	1050	1	0.014	0.017	1	-0.33
43	1050	1075	1	0.014	0.021	1	2.45
44	1075	1100	0	0	-0.019	-1	-2.00
45	1100	1125	1	0.014	0.022	2	-0.09
46	1125	1150	1	0.014	0.029	2	2.44
47	1150	1175	0	0	-0.011	-1	-0.05
48	1175	1200	0	0	-0.013	-1	-0.08
49	1200	1225	0	0	-0.015	-1	-0.12
50	1225	1250	0	0	-0.018	-1	-0.18

Table D.16 continued

			MEASURED		TRUE[1]		
CLASS	LIMITS (μm)		FEATURES	N_A (#/cm^2)	N_A (#/cm^2)	FEATURES	N_V(#/cm^3)[2]
51	1250	1275	0	0	-0.022	-2	-0.30
52	1275	1300	0	0	-0.029	-2	-0.61
53	1300	1325	0	0	-0.041	-3	-1.30
54	1325	1350	1	0.014	0.006	0	-6.73
55	1350	1375	3	0.043	0.149	10	9.23
56	1375	1400	0	0	-0.014	-1	-0.16
57	1400	1425	0	0	-0.018	-1	0.10
58	1425	1450	0	0	-0.023	-2	-0.99
59	1450	1475	0	0	-0.031	-2	1.61
60	1475	1500	0	0	-0.049	-3	-8.24
61	1500	1525	2	0.029	0.118	8	7.59
62	1525	1550	0	0	-0.024	-2	-1.10
63	1550	1575	0	0	-0.035	-2	1.95
64	1575	1600	0	0	-0.06	-4	-9.61
65	1600	1625	2	0.029	0.145	10	8.13
66	1625	1650	0	0	-0.027	-2	0.57
67	1650	1675	0	0	-0.049	-3	-4.29
68	1675	1700	1	0.014	0.059	4	-1.01
69	1700	1725	1	0.014	0.096	7	5.11
70	1725	1750	0	0	-0.005	0	0.05
71	1750	1775	0	0	-0.007	0	-0.09
72	1775	1800	0	0	-0.010	-1	0.28
73	1800	1825	0	0	-0.015	-1	-0.95
74	1825	1850	0	0	-0.026	-2	2.40
75	1850	1875	0	0	-0.064	-4	-9.27
76	1875	1900	1	0.014	0.151	11	7.38
77	1900	1925	0	0	0	0	0
78	1925	1950	0	0	0	0	0
79	1950	1975	0	0	0	0	0
80	1975	2000	0	0	0	0	0
81	2000	2025	0	0	0	0	0
82	2025	2050	0	0	0	0	0
83	2050	2075	0	0	0	0	0
84	2075	2100	0	0	0	0	0
85	2100	2125	0	0	0	0	0
Totals			39450	564.88	534.59	37335	110913.91
Average Feature Diameter (μm)				70.0	71.3		48.2
Air Content (%)				4.50	4.49		4.44
Powers Spacing Factor (μm)				125	129		130
Philleo Factor (μm)				--	--		100

1. Calculated using Eq. 3.29
2. Calculated using Eq. 3.54

Table D.17 Analysis of mix 7, magnification 30x, areal data using 85 classes of 25 μm width

			MEASURED[1]		TRUE[2]		
CLASS	LIMITS (μm)		FEATURES	N_A (#/cm^2)	N_A (#/cm^2)	FEATURES	N_V(#/cm^3)[3]
1	0	25	4891	69.033	64.016	4536	34616.61
2	25	50	4435	62.597	57.927	4104	14655.71
3	50	75	2698	38.080	34.360	2434	4868.09
4	75	100	2129	30.049	27.268	1932	3233.92
5	100	125	1588	22.414	20.319	1440	1934.69
6	125	150	1221	17.234	15.679	1111	1347.00
7	150	175	931	13.140	11.955	847	786.24
8	175	200	777	10.967	10.196	722	693.74
9	200	225	593	8.370	7.816	554	528.00
10	225	250	448	6.323	5.889	417	256.27
11	250	275	393	5.547	5.375	381	355.99
12	275	300	270	3.811	3.603	255	165.47
13	300	325	223	3.148	3.037	215	153.89
14	325	350	168	2.371	2.266	161	115.27
15	350	375	129	1.821	1.708	121	41.46
16	375	400	125	1.764	1.781	126	76.06
17	400	425	97	1.369	1.394	99	73.28
18	425	450	65	0.917	0.875	62	38.36
19	450	475	49	0.692	0.619	44	15.50
20	475	500	48	0.677	0.653	46	3.63
21	500	525	49	0.692	0.749	53	50.48
22	525	550	24	0.339	0.264	19	-0.78
23	550	575	27	0.381	0.357	25	5.81
24	575	600	25	0.353	0.349	25	16.66
25	600	625	17	0.240	0.191	14	0.32
26	625	650	18	0.254	0.233	17	2.36
27	650	675	18	0.254	0.258	18	5.02
28	675	700	17	0.240	0.263	19	4.74
29	700	725	15	0.212	0.244	17	12.07
30	725	750	10	0.141	0.137	10	-2.18
31	750	775	11	0.155	0.186	13	12.81
32	775	800	5	0.071	0.034	2	-5.61
33	800	825	8	0.113	0.128	9	5.99
34	825	850	5	0.071	0.053	4	0.55
35	850	875	5	0.071	0.059	4	-1.08
36	875	900	6	0.085	0.100	7	1.72
37	900	925	5	0.071	0.085	6	5.72
38	925	950	2	0.028	-0.009	-1	-1.54
39	950	975	3	0.042	0.021	1	-3.95
40	975	1000	5	0.071	0.098	7	2.72
41	1000	1025	4	0.056	0.077	5	1.02
42	1025	1050	4	0.056	0.093	7	1.67
43	1050	1075	3	0.042	0.074	5	6.89
44	1075	1100	0	0	-0.040	-3	-2.71
45	1100	1125	1	0.014	-0.005	0	0.32
46	1125	1150	1	0.014	-0.007	-1	-2.37
47	1150	1175	2	0.028	0.040	3	1.76
48	1175	1200	1	0.014	0	0	2.12
49	1200	1225	0	0	-0.056	-4	-3.48
50	1225	1250	2	0.028	0.032	2	-5.93

Table D.17 continued

CLASS	LIMITS (μm)		MEASURED[1] FEATURES	MEASURED[1] N_A (#/cm^2)	TRUE[2] N_A (#/cm^2)	TRUE[2] FEATURES	N_V(#/cm^3)[3]
51	1250	1275	4	0.056	0.159	11	10.45
52	1275	1300	0	0	-0.029	-2	0.49
53	1300	1325	0	0	-0.038	-3	-3.50
54	1325	1350	1	0.014	0.017	1	3.00
55	1350	1375	0	0	-0.046	-3	-2.65
56	1375	1400	1	0.014	0.010	1	-1.21
57	1400	1425	1	0.014	0.015	1	4.22
58	1425	1450	0	0	-0.063	-4	-7.11
59	1450	1475	2	0.028	0.077	5	3.68
60	1475	1500	1	0.014	0.021	1	-0.45
61	1500	1525	1	0.014	0.032	2	2.77
62	1525	1550	0	0	-0.049	-3	0.76
63	1550	1575	0	0	-0.080	-6	-7.05
64	1575	1600	2	0.028	0.091	6	-1.57
65	1600	1625	2	0.028	0.139	10	8.88
66	1625	1650	0	0	-0.031	-2	-1.93
67	1650	1675	0	0	-0.049	-3	3.88
68	1675	1700	0	0	-0.098	-7	-17.48
69	1700	1725	3	0.042	0.292	21	15.12
70	1725	1750	0	0	-0.002	0	0.01
71	1750	1775	0	0	-0.003	0	0.02
72	1775	1800	0	0	-0.004	0	0.01
73	1800	1825	0	0	-0.005	0	0.07
74	1825	1850	0	0	-0.007	0	-0.10
75	1850	1875	0	0	-0.010	-1	0.41
76	1875	1900	0	0	-0.017	-1	-1.17
77	1900	1925	0	0	-0.032	-2	3.35
78	1925	1950	0	0	-0.090	-6	-11.66
79	1950	1975	1	0.014	0.185	13	8.86
80	1975	2000	0	0	0	0	0
81	2000	2025	0	0	0	0	0
82	2025	2050	0	0	0	0	0
83	2050	2075	0	0	0	0	0
84	2075	2100	0	0	0	0	0
85	2100	2125	0	0	0	0	0
Totals			21590	304.73	281.13	19918	64080.38
Average Feature Diameter (μm)				102.0	103.9		43.9
Air Content (%)				6.02	6.01		5.99
Powers Spacing Factor (μm)				174	185		186
Philleo Factor (μm)				--	--		115

1. Features not included in analysis include: 2 in class 88, 1 in class 98, and 1 in class 110
2. Calculated using Eq. 3.29
3. Calculated using Eq. 3.54

Table D.18 Analysis of mix 8, magnification 30x, areal data using 85 classes of 25 μm width

			MEASURED[1]		TRUE[2]		
CLASS	LIMITS (μm)		FEATURES	N_A (#/cm^2)	N_A (#/cm^2)	FEATURES	N_V(#/cm^3)[3]
1	0	25	8379	118.264	112.905	7999	70396.81
2	25	50	5105	72.054	68.006	4818	19079.18
3	50	75	2386	33.677	30.571	2166	4844.77
4	75	100	1681	23.726	21.273	1507	2454.61
5	100	125	1294	18.264	16.353	1159	1453.18
6	125	150	1051	14.834	13.426	951	1129.04
7	150	175	797	11.249	10.143	719	779.30
8	175	200	626	8.836	7.962	564	345.09
9	200	225	578	8.158	7.699	545	609.01
10	225	250	389	5.490	5.013	355	176.78
11	250	275	363	5.124	4.938	350	347.50
12	275	300	236	3.331	3.057	217	139.33
13	300	325	194	2.738	2.526	179	116.25
14	325	350	159	2.244	2.069	147	60.90
15	350	375	148	2.089	2.030	144	81.86
16	375	400	119	1.680	1.642	116	75.68
17	400	425	95	1.341	1.306	93	16.46
18	425	450	97	1.369	1.477	105	82.97
19	450	475	60	0.847	0.853	60	33.94
20	475	500	45	0.635	0.615	44	26.75
21	500	525	36	0.508	0.474	34	-4.34
22	525	550	41	0.579	0.639	45	36.68
23	550	575	22	0.311	0.268	19	6.29
24	575	600	22	0.311	0.288	20	-10.78
25	600	625	30	0.423	0.517	37	25.34
26	625	650	18	0.254	0.280	20	7.55
27	650	675	16	0.226	0.263	19	4.03
28	675	700	15	0.212	0.274	19	14.13
29	700	725	7	0.099	0.095	7	7.99
30	725	750	4	0.056	0.019	1	-11.95
31	750	775	11	0.155	0.223	16	11.31
32	775	800	5	0.071	0.081	6	6.71
33	800	825	2	0.028	0.001	0	-4.53
34	825	850	4	0.056	0.064	5	5.75
35	850	875	1	0.014	-0.024	-2	-3.32
36	875	900	3	0.042	0.035	2	-2.31
37	900	925	4	0.056	0.075	5	4.64
38	925	950	2	0.028	0.016	1	-2.36
39	950	975	3	0.042	0.054	4	2.90
40	975	1000	2	0.028	0.025	2	-2.50
41	1000	1025	3	0.042	0.069	5	4.66
42	1025	1050	1	0.014	0	0	-2.10
43	1050	1075	2	0.028	0.041	3	0.75
44	1075	1100	2	0.028	0.049	3	-0.15
45	1100	1125	2	0.028	0.063	4	4.67
46	1125	1150	0	0	-0.015	-1	-0.04
47	1150	1175	0	0	-0.017	-1	-0.46
48	1175	1200	0	0	-0.021	-1	0.43
49	1200	1225	0	0	-0.028	-2	-3.16
50	1225	1250	1	0.014	0.020	1	2.82

Table D.18 continued

CLASS	LIMITS (μm)		MEASURED[1] FEATURES	MEASURED[1] N_A (#/cm^2)	TRUE[2] N_A (#/cm^2)	TRUE[2] FEATURES	N_V(#/cm^3)[3]
51	1250	1275	0	0	-0.032	-2	-2.80
52	1275	1300	1	0.014	0.016	1	0.34
53	1300	1325	1	0.014	0.021	1	-0.59
54	1325	1350	1	0.014	0.028	2	3.10
55	1350	1375	0	0	-0.032	-2	-2.66
56	1375	1400	1	0.014	0.026	2	-0.67
57	1400	1425	1	0.014	0.037	3	3.50
58	1425	1450	0	0	-0.031	-2	-2.91
59	1450	1475	1	0.014	0.038	3	-0.40
60	1475	1500	1	0.014	0.056	4	3.55
61	1500	1525	0	0	-0.010	-1	-0.01
62	1525	1550	0	0	-0.012	-1	0.01
63	1550	1575	0	0	-0.015	-1	-0.10
64	1575	1600	0	0	-0.019	-1	0.14
65	1600	1625	0	0	-0.025	-2	-0.78
66	1625	1650	0	0	-0.036	-3	1.48
67	1650	1675	0	0	-0.059	-4	-6.82
68	1675	1700	1	0.014	0.047	3	7.43
69	1700	1725	0	0	-0.087	-6	-11.94
70	1725	1750	2	0.028	0.182	13	8.98
71	1750	1775	0	0	-0.042	-3	3.55
72	1775	1800	0	0	-0.093	-7	-14.81
73	1800	1825	2	0.028	0.246	17	12.27
74	1825	1850	0	0	0	0	0
75	1850	1875	0	0	0	0	0
76	1875	1900	0	0	0	0	0
77	1900	1925	0	0	0	0	0
78	1925	1950	0	0	0	0	0
79	1950	1975	0	0	0	0	0
80	1975	2000	0	0	0	0	0
81	2000	2025	0	0	0	0	0
82	2025	2050	0	0	0	0	0
83	2050	2075	0	0	0	0	0
84	2075	2100	0	0	0	0	0
85	2100	2125	0	0	0	0	0
Totals			24073	339.77	317.89	22522	102347.91
Average Feature Diameter (μm)				84.7	85.3		31.1
Air Content (%)				5.30	5.29		5.26
Powers Spacing Factor (μm)				169	180		182
Philleo Factor (μm)				--	--		99

1. Features not included in analysis include: 1 in class 98, 1 in class 99, and 1 in class 104
2. Calculated using Eq. 3.29
3. Calculated using Eq. 3.54

Table D.19 Analysis of mix 9, magnification 30x, areal data using 85 classes of 25 μm width

			MEASURED[1]		TRUE[2]		
CLASS	LIMITS (μm)		FEATURES	N_A (#/cm^2)	N_A (#/cm^2)	FEATURES	N_V(#/cm^3)[3]
1	0	25	4680	66.055	62.293	4413	39542.73
2	25	50	2832	39.972	36.429	2581	8656.87
3	50	75	1918	27.071	24.13	1710	3504.26
4	75	100	1499	21.157	18.786	1331	1951.02
5	100	125	1249	17.629	15.835	1122	1427.15
6	125	150	1006	14.199	12.884	913	1076.11
7	150	175	764	10.783	9.767	692	772.83
8	175	200	585	8.257	7.431	526	320.42
9	200	225	548	7.735	7.311	518	525.00
10	225	250	391	5.519	5.154	365	260.18
11	250	275	319	4.502	4.283	303	283.32
12	275	300	224	3.162	2.908	206	82.34
13	300	325	219	3.091	3.047	216	142.83
14	325	350	169	2.385	2.379	169	148.58
15	350	375	113	1.595	1.512	107	26.69
16	375	400	112	1.581	1.629	115	92.35
17	400	425	76	1.073	1.062	75	25.49
18	425	450	69	0.974	1.024	73	61.60
19	450	475	43	0.607	0.580	41	5.38
20	475	500	45	0.635	0.685	48	35.16
21	500	525	27	0.381	0.364	26	24.80
22	525	550	16	0.226	0.148	11	-13.25
23	550	575	25	0.353	0.370	26	16.19
24	575	600	18	0.254	0.247	18	7.00
25	600	625	15	0.212	0.204	14	9.63
26	625	650	10	0.141	0.102	7	2.75
27	650	675	9	0.127	0.086	6	-1.52
28	675	700	9	0.127	0.093	7	5.63
29	700	725	8	0.113	0.070	5	-15.15
30	725	750	16	0.226	0.304	22	21.63
31	750	775	5	0.071	0.031	2	-3.94
32	775	800	7	0.099	0.090	6	1.54
33	800	825	7	0.099	0.098	7	-3.13
34	825	850	9	0.127	0.175	12	6.94
35	850	875	6	0.085	0.107	8	2.16
36	875	900	5	0.071	0.091	6	4.28
37	900	925	3	0.042	0.037	3	0.01
38	925	950	3	0.042	0.042	3	0.69
39	950	975	3	0.042	0.048	3	-0.81
40	975	1000	3	0.042	0.057	4	4.97
41	1000	1025	1	0.014	-0.014	-1	-5.65
42	1025	1050	4	0.056	0.103	7	1.86
43	1050	1075	3	0.042	0.086	6	6.61
44	1075	1100	0	0	-0.027	-2	-1.54
45	1100	1125	1	0.014	0.010	1	-2.95
46	1125	1150	2	0.028	0.061	4	5.29
47	1150	1175	0	0	-0.022	-2	-2.98
48	1175	1200	1	0.014	0.023	2	2.71
49	1200	1225	0	0	-0.025	-2	-2.59
50	1225	1250	1	0.014	0.022	2	0.37

Table D.19 continued

CLASS	LIMITS (μm)		MEASURED[1] FEATURES	MEASURED[1] N_A (#/cm^2)	TRUE[2] N_A (#/cm^2)	TRUE[2] FEATURES	N_V(#/cm^3)[3]
51	1250	1275	1	0.014	0.027	2	-0.21
52	1275	1300	1	0.014	0.037	3	2.76
53	1300	1325	0	0	-0.013	-1	-0.15
54	1325	1350	0	0	-0.016	-1	-0.01
55	1350	1375	0	0	-0.020	-1	-0.81
56	1375	1400	0	0	-0.028	-2	0.87
57	1400	1425	0	0	-0.044	-3	-6.30
58	1425	1450	2	0.028	0.094	7	2.50
59	1450	1475	1	0.014	0.049	3	4.22
60	1475	1500	0	0	-0.022	-2	-3.97
61	1500	1525	1	0.014	0.062	4	3.60
62	1525	1550	0	0	-0.007	-1	0.10
63	1550	1575	0	0	-0.010	-1	-0.56
64	1575	1600	0	0	-0.015	-1	1.08
65	1600	1625	0	0	-0.027	-2	-4.97
66	1625	1650	1	0.014	0.082	6	4.43
67	1650	1675	0	0	-0.002	0	0.03
68	1675	1700	0	0	-0.003	0	0.01
69	1700	1725	0	0	-0.003	0	0.02
70	1725	1750	0	0	-0.004	0	0.02
71	1750	1775	0	0	-0.004	0	0.03
72	1775	1800	0	0	-0.005	0	0.03
73	1800	1825	0	0	-0.007	0	0.09
74	1825	1850	0	0	-0.009	-1	-0.08
75	1850	1875	0	0	-0.013	-1	0.42
76	1875	1900	0	0	-0.019	-1	-1.13
77	1900	1925	0	0	-0.035	-2	3.38
78	1925	1950	0	0	-0.095	-7	-11.51
79	1950	1975	1	0.014	0.178	13	8.70
80	1975	2000	0	0	-0.011	-1	0.89
81	2000	2025	0	0	-0.020	-1	-2.12
82	2025	2050	0	0	-0.040	-3	7.22
83	2050	2075	0	0	-0.184	-13	-19.64
84	2075	2100	1	0.014	0.287	20	13.34
85	2100	2125	0	0	0	0	0
Totals			17087	241.17	222.27	15748	59014.08
Average Feature Diameter (μm)				103.2	105.2		37.7
Air Content (%)				4.84	4.84		4.82
Powers Spacing Factor (μm)				202	215		217
Philleo Factor (μm)				--	--		121

1. Features not included in analysis include: 1 in class 88
2. Calculated using Eq. 3.29
3. Calculated using Eq. 3.54

Table D.20 Analysis of mix 10, magnification 30x, areal data using 85 classes of 25 μm width

			MEASURED[1]		TRUE[2]		
CLASS	LIMITS (μm)		FEATURES	N_A (#/cm^2)	N_A (#/cm^2)	FEATURES	N_V(#/cm^3)[3]
1	0	25	6435	88.714	83.116	6029	50390.41
2	25	50	4482	61.789	56.459	4095	13847.92
3	50	75	2933	40.435	35.983	2610	4689.97
4	75	100	2479	34.176	30.789	2233	3698.72
5	100	125	1828	25.201	22.521	1634	2104.84
6	125	150	1439	19.838	17.755	1288	1381.36
7	150	175	1173	16.171	14.617	1060	987.14
8	175	200	953	13.138	12.018	872	860.58
9	200	225	720	9.926	8.997	653	444.05
10	225	250	632	8.713	8.147	591	432.77
11	250	275	519	7.155	6.827	495	361.29
12	275	300	407	5.611	5.415	393	312.30
13	300	325	295	4.067	3.856	280	179.72
14	325	350	240	3.309	3.167	230	114.20
15	350	375	209	2.881	2.864	208	136.97
16	375	400	156	2.151	2.112	153	96.20
17	400	425	118	1.627	1.559	113	54.02
18	425	450	103	1.420	1.398	101	28.92
19	450	475	100	1.379	1.476	107	61.30
20	475	500	73	1.006	1.069	78	59.96
21	500	525	45	0.620	0.578	42	10.68
22	525	550	43	0.593	0.594	43	20.05
23	550	575	33	0.455	0.431	31	20.12
24	575	600	24	0.331	0.261	19	-8.58
25	600	625	33	0.455	0.499	36	5.53
26	625	650	31	0.427	0.514	37	32.73
27	650	675	15	0.207	0.175	13	-6.88
28	675	700	21	0.290	0.350	25	10.13
29	700	725	15	0.207	0.242	18	19.57
30	725	750	6	0.083	0.024	2	-14.71
31	750	775	14	0.193	0.251	18	15.24
32	775	800	7	0.097	0.085	6	-3.65
33	800	825	9	0.124	0.159	12	9.92
34	825	850	4	0.055	0.031	2	-0.61
35	850	875	4	0.055	0.034	2	1.83
36	875	900	3	0.041	0.002	0	-3.77
37	900	925	6	0.083	0.098	7	-4.04
38	925	950	8	0.110	0.189	14	12.73
39	950	975	2	0.028	0.011	1	-0.72
40	975	1000	2	0.028	0.014	1	2.76
41	1000	1025	1	0.014	-0.024	-2	-4.74
42	1025	1050	3	0.041	0.051	4	4.28
43	1050	1075	1	0.014	-0.020	-1	-1.71
44	1075	1100	2	0.028	0.017	1	-1.27
45	1100	1125	2	0.028	0.023	2	5.20
46	1125	1150	0	0	-0.067	-5	-7.35
47	1150	1175	3	0.041	0.057	4	2.67
48	1175	1200	2	0.028	0.022	2	-0.63
49	1200	1225	2	0.028	0.028	2	2.67
50	1225	1250	1	0.014	-0.021	-2	-3.03

Table D.20 continued

CLASS	LIMITS (μm)		MEASURED[1] FEATURES	MEASURED[1] N_A (#/cm^2)	TRUE[2] N_A (#/cm^2)	TRUE[2] FEATURES	N_V(#/cm^3)[3]
51	1250	1275	2	0.028	0.026	2	0.86
52	1275	1300	2	0.028	0.029	2	-3.28
53	1300	1325	3	0.041	0.098	7	5.64
54	1325	1350	1	0.014	0.002	0	-0.81
55	1350	1375	1	0.014	0	0	1.24
56	1375	1400	1	0.014	-0.006	0	-6.39
57	1400	1425	3	0.041	0.137	10	6.02
58	1425	1450	1	0.014	0.037	3	2.63
59	1450	1475	0	0	-0.028	-2	0.90
60	1475	1500	0	0	-0.041	-3	-4.96
61	1500	1525	1	0.014	0.032	2	5.39
62	1525	1550	0	0	-0.055	-4	-9.08
63	1550	1575	2	0.028	0.120	9	8.75
64	1575	1600	0	0	-0.037	-3	-5.21
65	1600	1625	1	0.014	0.057	4	5.17
66	1625	1650	0	0	-0.036	-3	-4.98
67	1650	1675	1	0.014	0.073	5	3.85
68	1675	1700	0	0	-0.021	-2	1.39
69	1700	1725	0	0	-0.040	-3	-6.10
70	1725	1750	1	0.014	0.093	7	5.37
71	1750	1775	0	0	-0.013	-1	-0.81
72	1775	1800	0	0	-0.022	-2	1.90
73	1800	1825	0	0	-0.050	-4	-7.73
74	1825	1850	1	0.014	0.128	9	6.33
75	1850	1875	0	0	0	0	0
76	1875	1900	0	0	0	0	0
77	1900	1925	0	0	0	0	0
78	1925	1950	0	0	0	0	0
79	1950	1975	0	0	0	0	0
80	1975	2000	0	0	0	0	0
81	2000	2025	0	0	0	0	0
82	2025	2050	0	0	0	0	0
83	2050	2075	0	0	0	0	0
84	2075	2100	0	0	0	0	0
85	2100	2125	0	0	0	0	0
Totals			25657	353.71	325.23	23591	80363.11
Average Feature Diameter (μm)				106.0	108.3		40.5
Air Content (%)				7.35	7.35		7.32
Powers Spacing Factor (μm)				165	175		177
Philleo Factor (μm)				--	--		105

1. Features not included in analysis include: 1 in class 99, 1 in class 105, and 1 in class 112
2. Calculated using Eq. 3.29
3. Calculated using Eq. 3.54

APPENDIX E

CALCULATION OF AREA A_{ij}

E.1 Introduction

When using finite fields of view to measure a distribution of circular features, frame edge effects cause the measured size of some features to be smaller than the true size. "Frame edge effects" refers to the intersection of features by the edge or edges of the viewing field, with only that portion falling within the viewing field being measured. It was noted in Section 3.3 that, due to frame edge effects, a given size class i of measured features will include contributions from features of all size classes, j, greater than or equal to i. Stated another way, each size class of features, j, will contribute measured features to all size classes, i, smaller than or equal to j. The probability that a feature of diameter y_j will be intersected by a frame edge and have a resulting area equivalent diameter, AED, within the size limits of class i is equal to the ratio of the area in which the center of a diameter y_j feature can be located and have a measured AED within the size limits of class i to the total area in which the center of a diameter y_j feature can be located and be at least partially visible in the field of view. The former area is referred to as A_{ij}. Procedures for calculating A_{ij} for a rectangular field of view, L x H, are presented in this appendix.

For each size class j, containing features of diameter $y_j \pm \Delta y_j/2$, there is a region extending a distance $y_j/2$ on either side of the edges of the viewing frame in which a diameter y_j feature can be located and be intersected by a frame edge or edges. This region is called the intersection zone for features of diameter y_j, and is shown in Fig. E.1. Equations are developed for calculating the AED of the measured

portion of features with their centers inside this intersection zone. Procedures are also developed for calculating the individual areas, A_{ij}, within the intersection zone.

E.2 Equations for AED

The intersection zone can be divided into two distinct regions, as shown in Fig. E.2, based on whether a diameter y_j feature is intersected by one or two frame edges. If the center of a diameter y_j feature is located within an edge region, it will be intersected by a single edge, whereas if the feature center falls within a corner region, it will be intersected by two adjacent frame edges. Features with their center located within an edge or corner region are referred to as edge features or corner features, respectively. Separate equations are required to calculate the AED of edge and corner features.

Edge Feature.– A typical edge feature is shown in Fig. E.3. The x'-z' coordinate system is located at the feature center and is parallel to the frame edges, which represent the X-Z coordinate system. The position of a diameter y_j edge feature is given by z, which represents the distance in the direction of the Z axis, from the intersecting frame edge to the feature center. The range of values for z is plus or minus the feature radius, R_j. The visible area of an edge feature, A_e, is obtained by integrating, with respect to the x'-z' coordinate system, that portion of the intersected feature within the field of view

$$A_e = \int_{-z}^{R_j} 2\sqrt{R_j^2 - z'^2}\, dz' \qquad \text{(E.1a)}$$

$$A_e = \frac{\pi R_j^2}{2} + z\sqrt{R_j^2 - z^2} + R_j^2 \sin^{-1}(z/R_j) \qquad \text{(E.1b)}$$

Using Eq. 3.15, the AED of an edge feature, AED_e, is given as

$$AED_e = \sqrt{\frac{4}{\pi}}\sqrt{\frac{\pi R_j^2}{2} + z\sqrt{R_j^2 - z^2} + R_j^2 \sin^{-1}(z/R_j)} \qquad \text{(E.2)}$$

Corner Feature.–A single expression for the AED of a corner feature is not possible, because the visible shape of a corner feature differs, depending on the location of the feature center within a corner region. A symmetric half of a typical corner region, shown in Fig. E.4, can be divided into the sub-regions, segment 1 and segment 2, based on the visible shape of the resulting corner feature. A corner feature of diameter y_j, with its center located in either segment 1 or segment 2 of a corner region, is shown in Fig. E.5 or Fig. E.6, respectively. In both cases, the x'-z' coordinate system is located at the feature center and is parallel to the frame edges, which represent the X-Z coordinate system. The position of a diameter y_j corner feature is given by x and z, which represent the distances in the direction of the X and Z axes, respectively, from the frame corner to the feature center.

The range of values of x and z, within segment 1 of the symmetric half of a corner region, are $-\sqrt{0.5}\ R_j$ to $+R_j$ and $-Rj$ to $+Rj$, respectively. But, in no case can $\sqrt{x^2 + z^2}$ be greater than R_j. The visible area of a segment 1 corner feature, A_{c1}, is obtained by integrating, with respect to the x'–z' coordinate system, that portion of the intersected feature within the field of view. When z is positive this yields

$$A_{c1} = \pi R_j^2/4 + xz + \int_{-x}^{0}\left(\sqrt{R_j^2-x^2}\right)dx' + \int_{-z}^{0}\left(\sqrt{R_j^2-z^2}\right)dz' \qquad \text{(E.3a)}$$

$$A_{c1} = (1/2)\left[z\sqrt{R_j^2-z^2} + 2xz + x\sqrt{R_j^2-x^2} + R_j^2\left(\sin^{-1}(z/R_j) + \sin^{-1}(x/R_j) + \frac{\pi}{2}\right)\right] \qquad \text{(E.3b)}$$

When z is negative, for a segment 1 corner feature, A_{c1} becomes

$$A_{c1} = \int_{-x}^{\sqrt{R_i^2-z^2}}\left(\sqrt{R_j^2-z^2} + z\right)dx' \qquad \text{(E.4a)}$$

$$A_{c1} = (1/2)\left[z\sqrt{R_j^2-z^2} + 2xz + x\sqrt{R_j^2-x^2} + R_j^2\left\{\sin^{-1}\left(\sqrt{R_j^2-z^2}/R_j\right) + \sin^{-1}(x/R_j)\right\}\right] \qquad \text{(E.4b)}$$

Recognizing, that with z negative, $\sin^{-1}\left(\sqrt{R_j^2-z^2}/R_j\right) = (\sin^{-1}(z/R_j) + \pi/2)$, Eq. E.4b simplifies to Eq. E.3b.

Eq. E.3b provides an expression for the visible area of an intersected corner feature of diameter y_j, when its center lies anywhere within segment 1 of a corner region.

Using Eq. 3.15, the AED of a segment 1 corner feature is

$$AED_{c1} = \sqrt{4/\pi}\left\{(1/2)\left[z\sqrt{R_j^2-z^2} + 2xz + x\sqrt{R_j^2-x^2} + R_j^2\left(\sin^{-1}(z/R_j) + \sin^{-1}(x/R_j) + \frac{\pi}{2}\right)\right]\right\}^{\frac{1}{2}} \quad \text{(E.5)}$$

Within segment 2 of the symmetric half of a corner region, the positions of the intersected feature center, x and z, can range from $+\sqrt{0.5}\ R_j$ to $+R_j$ and from 0 to $+R_j$, respectively. But, $\sqrt{x^2+z^2}$ must always be greater than R_j. The calculation of the visible area of a segment 2 corner feature differs from that of a segment 1 corner feature because the frame corner is outside of the intersected feature, as shown in Fig.E.6. The corner area not occupied by the feature, A_p, is subtracted from Eq. E.3b to give an expression for the visible area of a segment 2 corner feature. Integrating with respect to the x'–y' coordinate system, A_p, is

$$A_p = \int_{-x}^{-\sqrt{R_j^2-z^2}} \left(z - \sqrt{R_j^2-x'^2}\right) dx' \quad \text{(E.6a)}$$

$$A_p = \left[-z\sqrt{R_j^2-z^2} + 2xz - x\sqrt{R_j^2-x^2} + R_j^2\left\{\sin^{-1}\left(\sqrt{R_j^2-z^2}/R_j\right) - \sin^{-1}(x/R_j)\right\}\right] \quad \text{(E.6b)}$$

Recognizing that with z always positive, $\sin^{-1}\left(\sqrt{R_j^2-z^2}/R_j\right) = (\pi/2 - \sin^{-1}(z/R_j))$, Eq. E.6b simplifies to

$$A_p = -z\sqrt{R_j^2-z^2} + 2xz - x\sqrt{R_j^2-x^2} - R_j^2\left(\sin^{-1}(z/R_j) + \sin^{-1}(x/R_j) - \pi/2\right) \qquad (E.7)$$

Subtracting Eq. E.7 from Eq. E.3a gives an expression for the visible area, A_{c2}, of a diameter y_j feature, with its center located in segment 2 of a corner region

$$A_{c2} = z\sqrt{R_j^2-z^2} + x\sqrt{R_j^2-x^2} + R_j^2\left\{\sin^{-1}(z/R_j) + \sin^{-1}(x/R_j)\right\} \qquad (E.8)$$

Using Eq. 3.15, the AED of a segment 2 corner feature, AED_{c2}, is

$$AED_{c2} = \sqrt{4/\pi}\ \sqrt{z\sqrt{R_j^2-z^2} + x\sqrt{R_j^2-x^2} + R_j^2\left\{\sin^{-1}(z/R_j) + \sin^{-1}(x/R_j)\right\}} \qquad (E.9)$$

E.3 Determination of A_{ij}

The intersection zones can be divided into j subregions, A_{ij}, each representing the area in which the center of a y_j feature can be located and result in a measured feature with an AED within the size limits of class i, in which $1 \leq i \leq j$. These A_{ij} areas correspond to the A_{ij} terms in column j of the matrix of coefficients, $[M_{ij}]$, in Eq. 3.28. Fig. E.7 shows a typical quadrant of an intersection zone, for a diameter y_j feature, divided into the j subregions, A_{ij}. Because of geometric differences, between the edge and corner regions, separate procedures are developed for calculating that portion of A_{ij} within each.

Edge Region.–As shown in Fig. E.8, the portion of A_{ij} located within a quadrant of an edge region is equal to the sum of the two rectangular strips $\Delta z_i L/2$ and $\Delta z_i H/2$ minus that part, A_o, of each rectangular strip within the corner region. The term Δz_i represents the range of values for z (see Fig. E.3), perpendicular to the intersec-

ting frame edge, over which the center of a diameter y_j edge feature can be located and produce a measured feature with an AED within the size limits of class i. Δz_i is equal to $z_i - z_{i-1}$, in which z_i and z_{i-1} correspond to the positions, z, of the intersected feature center that will produce a measured feature with an AED equal to the upper limits of class i and class i–1, respectively. The upper AED size limit for each class, 1 to j–i, can be substituted for AED_e in Eq. E.2. and the corresponding value of z calculated. The calculation of z can be accomplished by rearranging Eq. E.2 to be of the form f(z) = 0. The root, z, is then obtained by iteration. A special case exists for the inner and outer boundaries of the edge region, $+R_j$ and $-R_j$, which correspond to the upper limit of z for class j and the lower limit of z for class 1, z_j and z_0, respectively.

The determination of A_o, the extension of the rectangular strip of each edge region portion of A_{ij} into a corner region, depends on the sign of z_i and z_{i-1}. If the calculated values of z_i and z_{i-1} are both positive, then that part of each rectangular strip inside a corner region, A_o, is equal to

$$A_o = R_j \Delta z_i \qquad \text{(E.10)}$$

When the calculated values of z_i and z_{i-1}, are both negative, then that part of each rectangular strip inside a corner region, A_o, is equal to

$$A_o = \int_{z_{i-1}}^{z_i} \sqrt{R_j^2 - z^2}\, dz \qquad \text{(E.11a)}$$

$$A_o = \frac{1}{2}\left[z_i\sqrt{R_j^2 - z_i^2} - z_{i-1}\sqrt{R_j^2 - z_{i-1}^2} + R_j^2\left\{\sin^{-1}(z_i/R_j) - \sin^{-1}(z_{i-1}/R_j)\right\}\right] \quad \text{(E.11b)}$$

When the calculated value of z_i is positive and the valve of z_{i-1} is negative then that part of each rectangular strip inside a corner region, A_o, is equal to

$$A_o = z_i R_j + \int_{z_{i-1}}^{0} \sqrt{R_j^2 - z^2}\, dz \quad \text{(E.12a)}$$

$$A_o = z_i R_j - z_{i-1}\sqrt{R_j^2 - z_{i-1}^2} + R_j^2\left(\sin^{-1}(z_{i-1}/R_j)\right) \quad \text{(E.12b)}$$

The portion of each A_{ij} in the entire edge region of the intersection zone $(A_{ij})_{edge}$, is equal to $(2\Delta z_i(L+H) - A_o)$. For the three different possible expressions for A_o, depending on the sign of z_i and z_{i-1}, this yields

$$(A_{ij})_{edge} = \begin{cases} 2\Delta z_i(L+H-4R_j) & \begin{pmatrix} z_i \text{ and } z_{i-1} \\ \text{positive} \end{pmatrix} \\ 2\Delta z_i(L+H) - 4\left[z_i\sqrt{R_j^2 - z_i^2} - z_{i-1}\sqrt{R_j^2 - z_{i-1}^2} + R_j^2\left\{\sin^{-1}(z_i/R_j) - \sin^{-1}(z_{i-1}/R_j)\right\}\right] & \begin{pmatrix} z_i \text{ and } z_{i-1} \\ \text{negative} \end{pmatrix} \\ 2\Delta z_i(L+H) - 4\left[z_i R_j - z_{i-1}\sqrt{R_j^2 - z_{i-1}^2} + R_j^2\sin^{-1}(z_{i-1}/R_j)\right] & \begin{pmatrix} z_i \text{ positive} \\ z_{i-1} \text{negative} \end{pmatrix} \end{cases} \quad \text{(E.13)}$$

A check on the accuracy of the $(A_{ij})_{edge}$ calculations may be made by com-

paring the summation of all $(A_{ij})_{edge}$ values, in a class j intersection zone, to the actual area of the edge region, $4R_j(L+H-4R_j) + (R_j^2/2)(1-\pi/4)$.

Corner Region.– A symmetric half of a typical corner region is shown in Fig. E.9. As a result of its nonlinear shape, the calculation of that portion of each A_{ij} within the corner region, $(A_{ij})_{corner}$, is not as straightforward as that for the edge region. This calculation can be performed incrementally by dividing the symmetric half of the corner region into discrete intervals, Δx, in the X direction. For each Δx interval, the values of Δz_i are calculated. As with the edge region, Δz_i is equal to $z_i - z_{i-1}$, in which z_i and z_{i-1} correspond to the positions, z, of a diameter y_j feature center that will produce a measured feature with an AED equal to the upper size limit of class i and class i-1, respectively. The summation of the areas of these individual pieces of each $(A_{ij})_{edge}$, $(\Sigma \Delta x \Delta z_i)$, will approximate the true area of corner region contribution to A_{ij}. By keeping Δx small, this approximation will approach the true solution.

The process of calculating Δz_i within each Δx interval is similar to the procedure presented for an edge region. A major difference is that all classes (i = 1 to j) are not present in each Δx interval. The smallest class, in each Δx interval, can be established by substituting the value of z at lower boundary of the edge region ($z = \sqrt{R_j^2 + x^2}$) into Eq E.5 and solving for the corresponding AED. The largest class, in each Δx interval, can be established by substituting the value of z at the upper boundary of the symmetric half of the edge region (z = x) into Eq. E.5 (when $x < \sqrt{0.5}\, R_j$) or Eq. E.9 (when $x > \sqrt{0.5}\, R_j$), and solving for the corresponding AED. The upper AED size limit for each class, in each Δx interval, is substituted into the

appropriate of Eq. E.5 or Eq. E.9, and the corresponding values of z calculated. The upper limit of the largest class is equal to x, and the lower limit of the smallest class is equal to $\sqrt{R_j^2 + x^2}$.

Once the limits, z_i, for each class in the Δx interval are established, the Δz_i values can be calculated. The summation of the areas $\Delta x \Delta z_i$, for all of the Δx intervals, is equal to the contribution to A_{ij} from one half of a corner region. The total edge region portion of A_{ij} is

$$(A_{ij})_{corner} = 8 \sum \Delta z_i \Delta x \qquad (E.14)$$

A check on the accuracy of the $(A_{ij})_{corner}$ may be made by comparing the result of Eq. E.14 with the actual total corner region area, $(R_j^2/4)(1 + 3\pi/4)$.

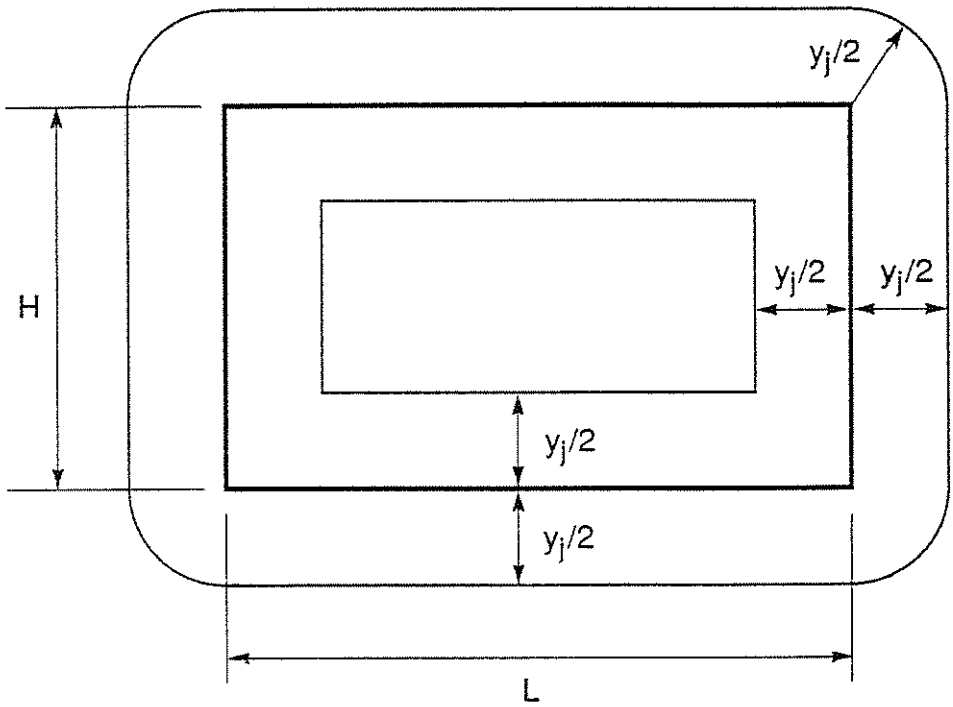

Figure E.1 Intersection zone for a diameter y_j feature

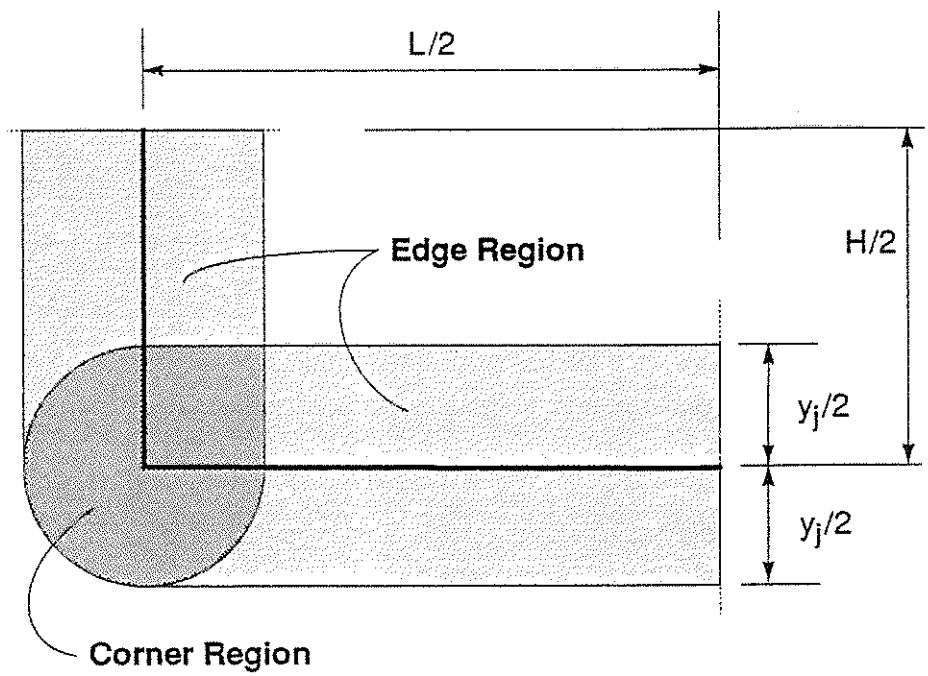

Figure E.2 Lower left quadrant of an intersection zone showing edge and corner regions

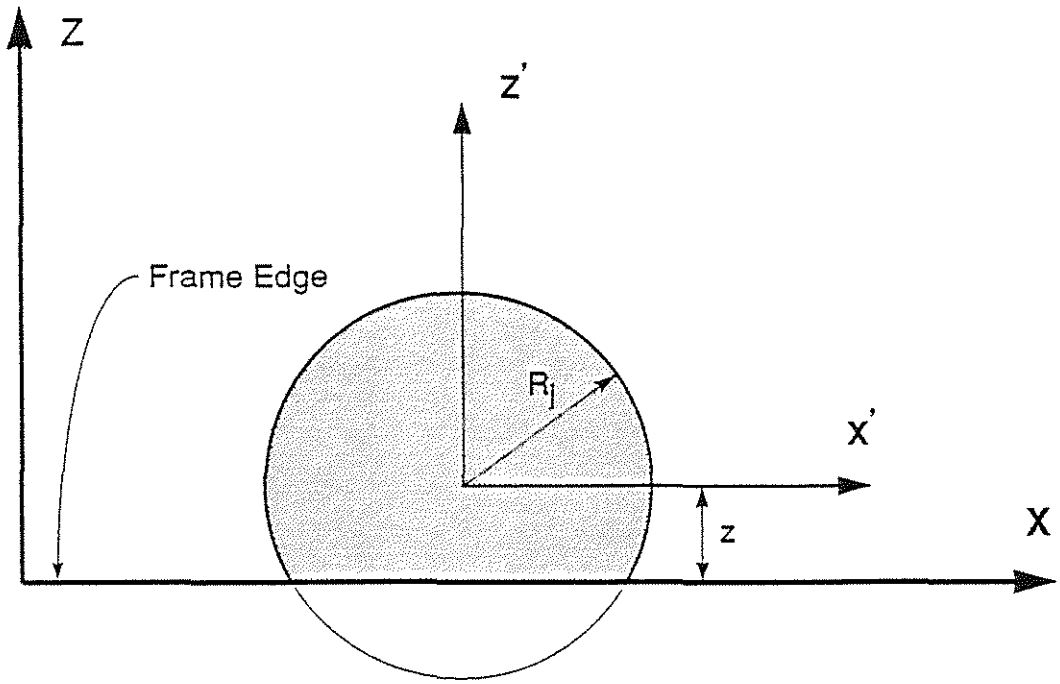

Figure E.3 Typical edge feature

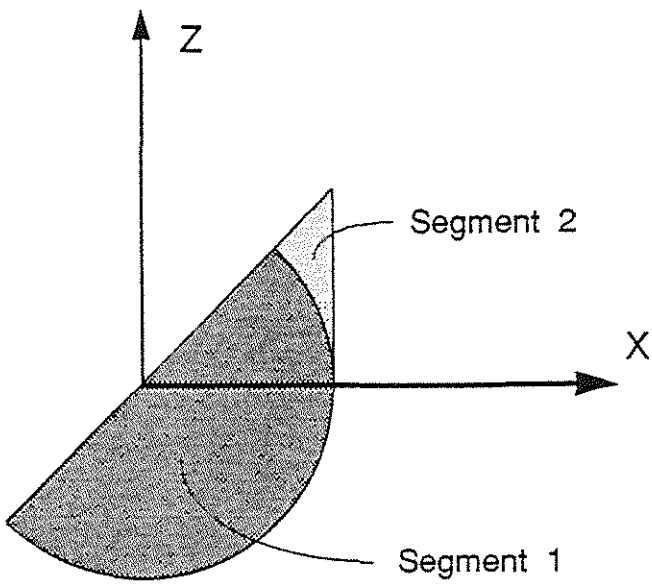

Figure E.4 Symmetric half of a typical corner region

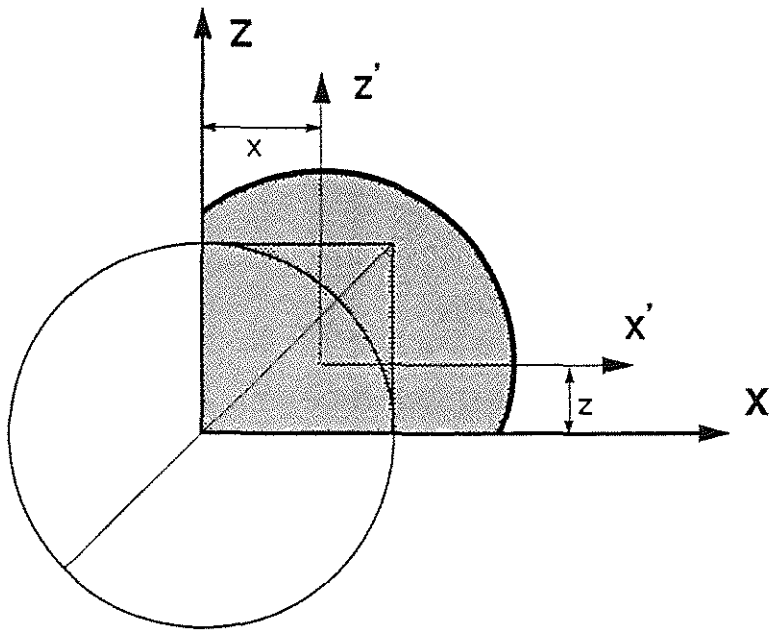

Figure E.5 Segment 1 corner feature

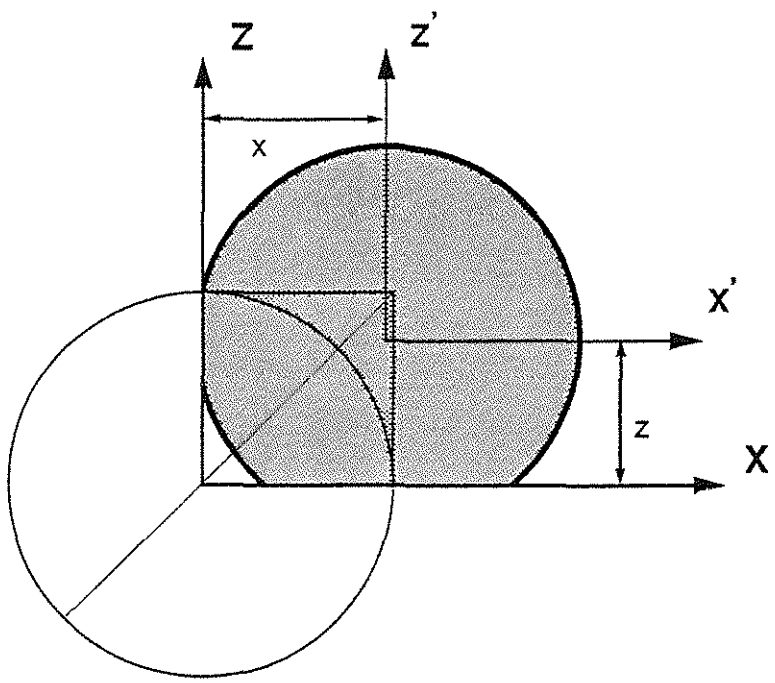

Figure E.6 Segment 2 corner feature

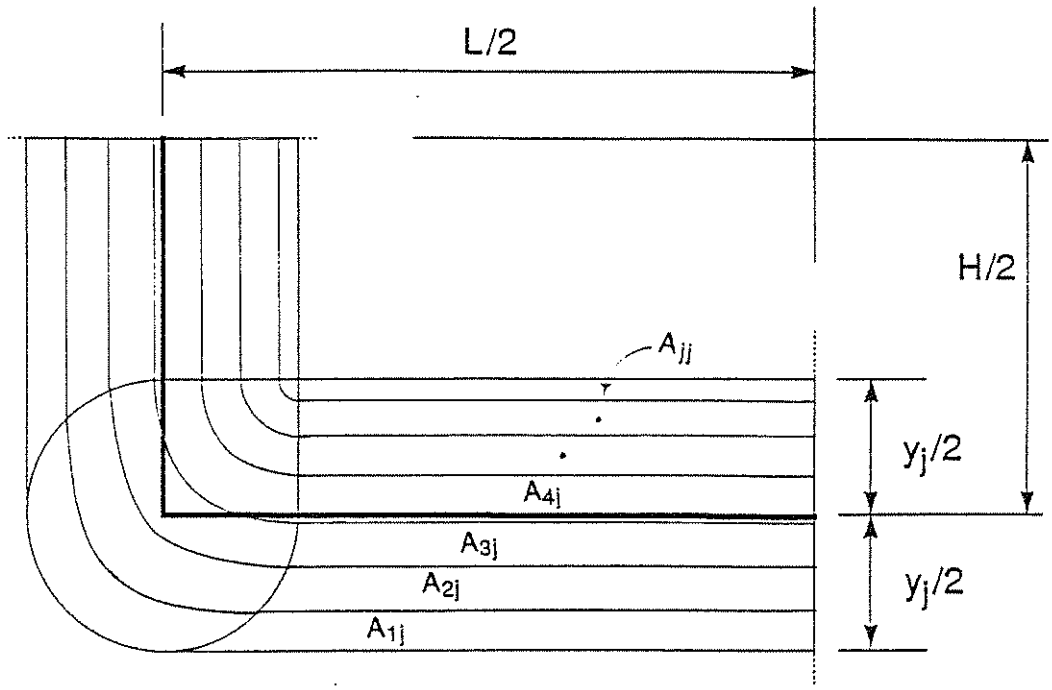

Figure D.7 Intersection zone quadrant showing A_{ij} subareas

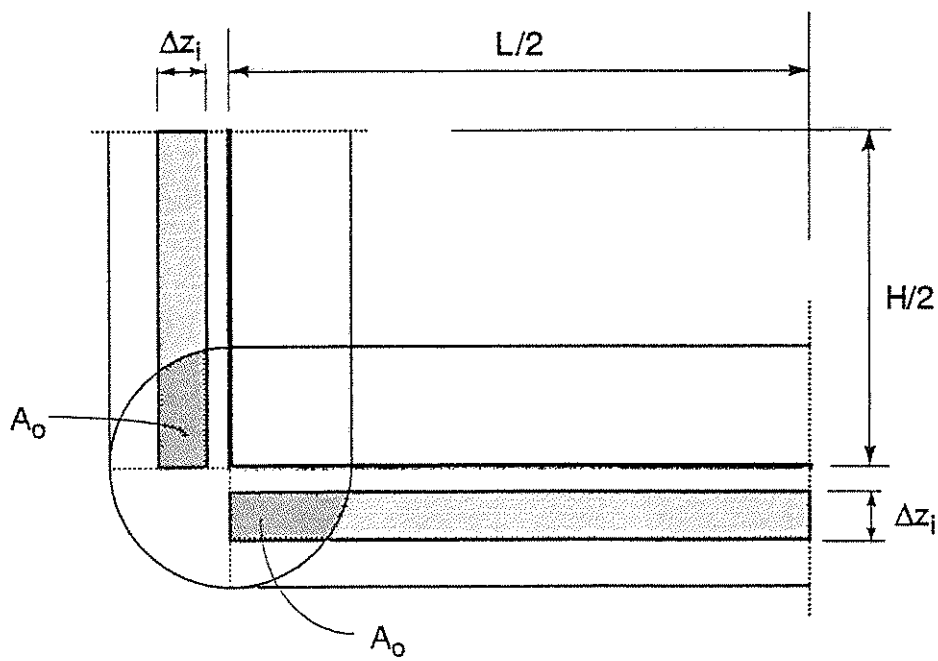

Figure D.8 Edge region portion of A_{ij} showing rectangular extensions in a corner region

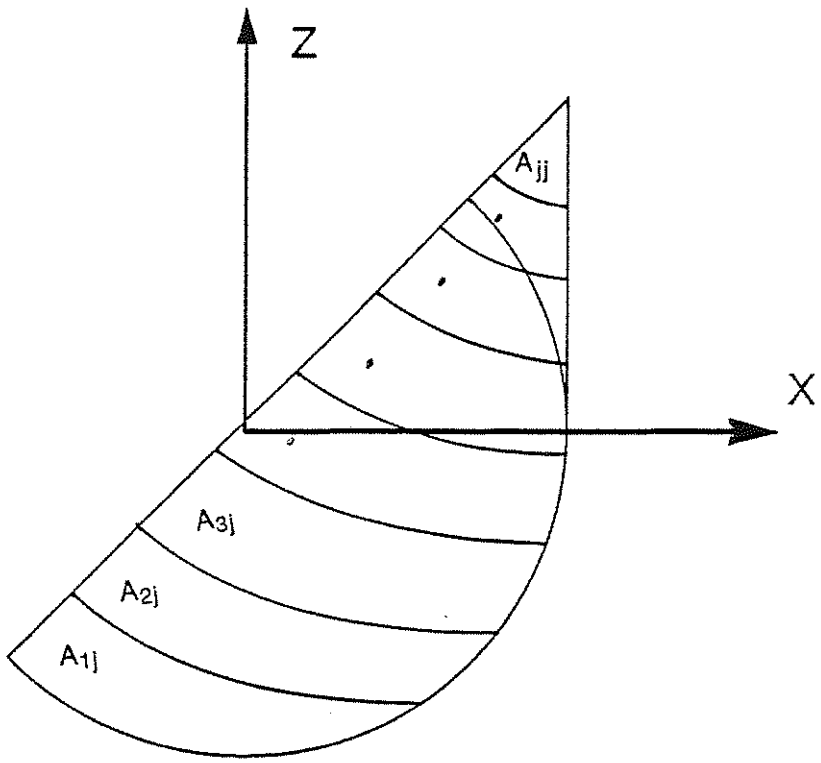

Figure D.9 Symmetric half of corner region showing A_{ij} subregions